CHARACTERIZATION OF IRRADIATION POSITIONS IN KAMINI & FBTR AND RADIOCHEMICAL PURIFICATION STUDIES

By

G. V. S. ASHOK KUMAR

Enrolment No: CHEM02201004015

Indira Gandhi Centre for Atomic Research
Kalpakkam

A thesis submitted to the
Board of Studies in Chemical Sciences
in partial fulfillment of requirements
for the Degree of

DOCTOR OF PHILOSOPHY

of

HOMI BHABHA NATIONAL INSTITUTE

August, 2017

Homi Bhabha National Institute

Recommendations of the Viva Voce Committee

As members of the Viva Voce Committee, we certify that we have read the dissertation prepared by G. V. S. Ashok Kumar entitled "**Characterization of Irradiation Positions in KAMINI & FBTR and Radiochemical Purification Studies**" and recommend that it may be accepted as fulfilling the thesis requirement for the award of Degree of Doctor of Philosophy.

Chairman - Dr. S. Anthonysamy	S. AnthonySamy	**Date:** 18.05.2018
Guide / Convener – Dr. M. Joseph		**Date:** 18.05.2018
Examiner - Dr. Moumita Maiti		**Date:** 18.05.2018
Member 1- Dr. K. Devan		**Date:** 18.05.2018
Member 2- Dr. S. Sivakumar		**Date:** 18.05.2018
Technology Adviser- Dr. R. Kumar	R. Kumar	**Date:** 18.05.2018

Final approval and acceptance of this thesis is contingent upon the candidate's submission of the final copies of the thesis to HBNI.

I hereby certify that I have read this thesis prepared under my direction and recommend that it may be accepted as fulfilling the thesis requirement.

Date: 18/5/18

Place: Kalpakkam,

Guide

STATEMENT BY AUTHOR

This dissertation has been submitted in partial fulfilment of requirements for an advanced degree at Homi Bhabha National Institute (HBNI) and is deposited in the Library to be made available to borrowers under rules of the HBNI.

Brief quotations from this dissertation are allowable without special permission, provided that accurate acknowledgement of source is made. Requests for permission for extended quotation from or reproduction of this manuscript in whole or in part may be granted by the Competent Authority of HBNI when in his or her judgment the proposed use of the material is in the interests of scholarship. In all other instances, however, permission must be obtained from the author.

G.V.S. 16/05/2018

G. V. S. Ashok Kumar

DECLARATION

I, hereby declare that the investigation presented in the thesis has been carried out by me. The work is original and has not been submitted earlier as a whole or in part for a degree/diploma at this or any other Institution/University.

G.V.S. 18/05/2018

G. V. S. Ashok Kumar

List of Publications arising from the thesis

Journal

1. “Studies on neutron spectrum characterization for the Pneumatic Fast Transfer System (PFTS) of KAMINI reactor”, **G. V. S. Ashok Kumar**, Sujoy Sen, E. Radha, J. S. Brahmaji Rao, R. Acharya, R. Kumar, C. R. Venkatasubramani, A. V. R. Reddy, M. Joseph, Appl. Radiat. Isot. 124 (2017) 49-55.

2. “Purification of ^{89}Sr source obtained from ^{89}Y(n, p) ^{89}Sr by ion-exchange chromatography using tri-sodium tri-meta phosphate (SMP) as eluant”, **G. V. S. Ashok Kumar,** J. Vithya, B. Siva Kumar, Debasish Saha, R. Kumar, C. R. Venkata Subramani, J. Radioanal. Nucl. Chem. 302 (2014) 803-808.

3. “Development of a Flow-sheet for the Radiochemical Processing of Irradiated Sulphate Targets for the Production of Carrier-free ^{32}P”, **G. V. S. Ashok Kumar**, J. Vithya, R. Kumar, C. R. Venkata Subramani; J. Radioanal. Nucl. Chem. (2014) 302:939–945.

4. “Radiochemical separation studies of ^{144}Ce-^{144}Pr from fission products from FBTR to establish secular equilibrium”, **G. V. S. Ashok Kumar**, R. Kumar, K. Ananthasivan, M. Joseph, U. Kamachi Mudali, Manuscript communicated to J. Chem. Educ.

5. “Design, installation & neutron flux measurement studies at Fast Flux Experimental Facility (FFEF) in Fast Breeder Test Reactor”, **G. V. S. Ashok Kumar**, R. Kumar, S. Murugan, K. Ananthasivan, C. R. Venkatasubramani, S. Varadarajan, K. V. Suresh Kumar, M. Joseph, Manuscript under preparation.

Conferences

1. “Neutron spectrum characterization at Pneumatic Fast Transfer System (PFTS) of KAMINI reactor”, **G. V. S. Ashok Kumar**, J. S. Brahmaji Rao, Sujoy Sen, E. Radha, R. Acharya, R. Kumar, C. R. Venkatasubramani, A.V.R. Reddy, Proc. Nucl. Radiochem. Symp. (NUCAR-2015), Mumbai, INDIA, 365-366.
2. “Rapid separation of pure ^{144}Ce fraction from fuel dissolver solution for demonstration experiment on secular equilibrium”, **G. V. S. Ashok Kumar**, R. Kumar, C. R. Venkatasubramani, Proc. First DAE-BRNS Symp. Current Trends in Anal. Chem. (CTAC) May 26-29 (2015) Mumbai, INDIA, 212.
3. “Separation profiles of Sr from irradiated yttrium matrix using different eluants by ion-exchange chromatography”, **G. V. S. Ashok Kumar**, J. Vithya, R. Kumar, C. R. Venkatasubramani, Proc. Int. Conf. on Application of Radiotracers and energetic beams in Sciences, (ARCEBS-2014), SINP, Kolkatta, INDIA, 207-208.
4. “Dose computation of Ti activated products for its qualification as a material for the sample holder in FBTR”, **G. V. S. Ashok Kumar**, R. Acharya, R. Kumar, C. R. Venkatasubramani, A.V.R. Reddy, Proc. Fourth Intl. Symp. Nucl. Anal. Chem. (NAC-2014), BARC, MUMBAI, INDIA, 298-299.
5. “Redetermination of f and α at PFTS position in KAMINI reactor”, J. S. Brahmaji Rao, **G. V. S. Ashok Kumar**, N. P. Seshadreesan, R. Acharya, R. Kumar, C. R. Venkatasubramani, A.V.R. Reddy, Proc. Nucl. Radiochem. Symp. (NUCAR-2013), Jabalpur, INDIA, 487-488.

6. “Study of the interference of Na & anionic moiety of trisodiumtrimetaphosphate (SMP) during the purification of ^{89}Sr by ion exchange chromatography”, **G. V. S. Ashok Kumar,** B. Siva Kumar, J. Vithya, K. Swaminathan, R. Kumar, C. R. Venkatasubramani, Proc. in Symp. Emerg. Trends in Sep. Sci. Technol., Feb 27-March 1 (2012) SVKM’s Mithibai College, Mumbai, INDIA, 222.
7. Purification of ^{89}Sr from bulk Y and other radioactive impurities using trisodium trimetaphosphate (SMP) in ion-exchange chromatography, **G.V.S. Ashok Kumar**, J. Vithya, B. Sivakumar, Debasish Saha, K. Swaminathan, R. Kumar, C. R. Venkatasubramani, Proc. Nucl. Radiochem. Symp. (NUCAR-11), Visakhapatnam, INDIA, 507–508 (Best Poster Award).
8. Feasibility studies on the production of ^{32}P using Sulphur powder as the target, **G.V.S. Ashok Kumar**, R. Senthilvadivu, J.S. Brahmaji Rao, R. Kumar and M.Joseph; Proc. VII DAE-BRNS Bienn. Symp. Emerg. Trends in Sep. Sci. Technol. (SESTEC-2016), May 17-20, IIT-Guwahati, INDIA; 196
9. Flow sheet development for the production of ^{32}P in KAMINI reactor using strontium sulphate target, **G.V.S. Ashok Kumar**, J. Vithya, R. Kumar and C.R. Venkatasubramani, Proc. Int. Conf. on Application of Radiotracers and energetic beams in Sciences, (ARCEBS-2014), SINP, Kolkata, INDIA, 205-206.
10. Developing a flow sheet for the production of ^{32}P using magnesium sulphate target in KAMINI reactor, **G.V.S. Ashok Kumar**, J. Vithya, R. Kumar, C.R. Venkatasubramani, Proc. Nucl. Radiochem. Symp. (NUCAR-2013), Mumbai, INDIA, 529-530.

G.V.S. 18/05/2018

G. V. S. Ashok Kumar

Dedicated to my beloved Family

No power is costlier than 'no power'

…… Dr. Homi J. Bhabha

Acknowledgement

I, at the outset, express my sincere thanks to my Ph.D supervisor **Dr. M. Joseph,** Director, MC&MFCG, IGCAR for his guidance, constant support, continuous evaluation and valuable suggestions to improve the quality of work throughout my tenure. His critical comments and guidance throughout the course of work made the thesis to this shape. I owe my deep sense of gratitude for his unimaginable support and inspiration.

I take immense pleasure in thanking my Technology Advisor **Dr. R. Kumar,** Head, NRCS, MC&MFCG for his keen assessment of work and strong support in all the time. His guidance, valuable suggestions, constant encouragement and motivation are unforgettable forever. His encouragement, immense knowledge and experience helped me in overcoming all the hurdles, not only during the course of my Ph.D but in all spheres of life.

I express my profound thanks to **Shri. C. R. Venkatasubramani**, Former Head, NRCS and RRF, IGCAR who was instrumental for setting-up the irradiation facility at FBTR and also for his technical support and guidance. I also express my sincere thanks to **Dr. A. V. R. Reddy**, my former Ph.D supervisor and former Head, Analytical Chemistry Division, BARC, Mumbai for his valuable inputs and suggestions towards my thesis work.

I am extremely grateful to the former directors **Dr. P. R. Vasudeva Rao** and **Dr. S. A. V. Satya Murty** and present director, IGCAR, **Dr. Arun Kumar Bhaduri** for permitting and made the IGCAR facilities available for my Ph.D. I also thank **Dr. K. Ananthasivan**, Head, FChD, IGCAR for permitting me to carry out Ph.D by providing various experimental facilities, and for his constant support and encouragement. I am pleased to express my deep sense of gratitude to my doctoral committee chairman, **Dr. S. Anthonysamy**, Associate Director, MFRG for his valuable suggestions and critical evaluation of the work progress. I thank my other doctoral committee members **Dr. K. Devan**, and **Dr. S. Siva Kumar** for their continuous support and valuable suggestions. I thank **Dr. N. Sivaraman**, Dean, Chemical Sciences, HBNI-IGCAR for his support and encouragement during my thesis submission.

I wish to record my sincere thanks to my colleagues in my section **Shri. J. S. Brahmaji Rao and Mrs. R. Senthilvadivu** for their kind help and support to carry out experiments, analyses during my thesis preparation. I thank my other colleagues in my section **Shri. M. Bootharajan, Shri. Debasish Saha, Shri. Manish Chand and Mrs. J. Vithya** for their kind support and valuable technical discussions. I thank my project students **Ms. K. L. Dhanya, Ms. A. Surya, Mr. J. Vasantha Kumar, Mr. Rahul, Mr. Shammem** and all others for their help in carrying out various experiments.

I wish to express my sincere thanks to **Dr. M. P. Antony, Dr. K. Sankaran, Dr. R. Sudha, Mrs. D. Sai Subhalakshmi, Shri. R. Raja Madhavan, Shri. S. Sriram, Shri. T. Kalaiyarasu** and **Mrs. S. Annapoorni**, for their kind help and technical support to accomplish my research work. I wish to express my sincere gratitude to all the members of Radiochemistry laboratory, IGCAR, for their excellent co-operation, kind support and provision of supportive environment.

I express my hearty thanks to **Shri. K. V. Suresh Kumar**, Director, RFG and **Shri, S. Varatharajan**, AD, TT&QAG for extending the reactor facilities in KAMINI and FBTR, constant technical supports and excellent cooperation. The technical and

logistical support from other engineers, officers and other supporting staffs in the reactor facilities as well as the radiation safety department for carrying out various irradiation experiments were also greatly acknowledged. I also thank **Shri. Sujoy Sen** and **Mrs. E. Radha** from Reactor Physics Section, RFG for their help in neutron spectrum characterization studies. I also thank **Dr. S. Murugan**, Head, RI&MMD, **Dr. Sunil Kumar**, Head, RSS and **Shri. Juby Abraham,** RDG for their help in heat release calculations that were required for the clearance of irradiation proposal in FBTR.

I also thank my training school batch mates, **Shri. B. Siva Kumar, Shri. P. Srijan, Shri. A. Venkatesh, Dr. Satendra Kumar, Shri. Suranjan Bera, Dr. Binoy Kumar Maji** and all other friends for providing healthy and friendly ambience during the course of work.

Finally, I am wordless to express my deepest gratitude to my parents **Shri. G. Eswara Rao** and **Smt. G. Bangaramma**, my brothers **Shri. G. Satya Suresh** and **Shri. G. A. Narasimham** who always encourage and support me from my childhood to the current position. I also would like to express my heartiest appreciation to my better-half, **G. Saipriya** and my son, **G. Satya Bhuvanyu** who went through all the inconvenience during my course of study and I am thankful for their love, affection, encouragement and strong support which are the source of my strength always.

Finally last but not the least, I owe all my small achievements in my life to the blessing of the great Almighty!

CONTENTS

Chapter 1: Introduction

Chapter 2: Experimental

Chapter 3: Studies on the Characterisation of Neutron Spectrum at Pneumatic Fast Transfer System (PFTS) of KAMINI Reactor

Chapter 4: Design and Installation of Fast Flux Experimental Facility (FFEF) at FBTR and neutron flux Measurement

Chapter 5: Measurement of Relative Fission Yields for Actinide Targets at KAMINI and FBTR

Chapter 6: Radiochemical Separation Studies of ^{144}Ce-^{144}Pr from fission products

Chapter 7: Studies on Radiochemical Separation of Sr from fission products and from irradiated yttria dissolver solution using tri-Sodium tri-Meta Phosphate

Chapter 8: Radiochemical Processing of ^{32}P Produced via ^{32}S(n,p)^{32}P in KAMINI reactor

Chapter 9: Summary and Conclusions

Chapter 10: Scope of future studies

SYNOPSIS

The discovery of radioactivity by Becquerel in 1896 during his studies of the fluorescence of uranium compounds is the beginning of nuclear sciences [1]. Subsequently, Rutherford has proposed the existence of the nucleus of an atom at its center on the basis of scattering of alpha particles from thin metallic foils [2]. He has also discovered the first nuclear reaction in which nitrogen target was bombarded with alpha particles and protons were observed as a result [3]. The most interesting breakthrough in nuclear sciences has taken place in 1932 with the discovery of neutron by Chadwick [4]. After the discovery of neutron, several groups of scientists were working on production of trans-uranium elements by bombarding uranium with neutrons [5]. During the course, Otto Hahn and Strassmann discovered the nuclear fission phenomenon in 1938 in which a heavy nucleus splits into two smaller fragments of comparable masses [6, 7]. Total kinetic energy associated in fission was estimated to be around 200 MeV by Meitner and Frisch who experimentally measured the high energy released in this reaction [8, 9]. It was established from that 2-3 neutrons were released in the process which unfolded a method for the production of immense energy through the construction of nuclear reactors [10].

Nuclear reactors as a neutron source with high fluxes, made feasible the production of a wide variety of radioactive nuclides, either by nuclear reactions ((n, γ), (n, p) etc.) or as fission products. The type and extent of the nuclear reactions that occur during the irradiation depend on the neutron energy spectrum of a particular irradiation facility very much [11]. Nuclear reaction cross-sections are very sensitive to the variations of neutron energy. Therefore, neutron spectrum characterization of a nuclear reactor is a mandatory requirement in evaluating the experimental results obtained from the irradiation studies of various materials. Neutron spectrum can be generated by irradiation of various activation foils having different threshold energies, covering a range of neutron energies of interest, followed by the application of spectrum unfolding methods [12]. Characterization of neutron spectrum along with the determination of the reactor parameters such as 'sub-cadmium to epithermal neutron flux ratio' (*f*) and 'epithermal neutron flux shape factor' (α) is required for the single-comparator (Au) based k_0-NAA, a radio-analytical technique for the estimation of the elemental concentrations of a sample [13]. Kalpakkam mini (KAMINI) and Fast Breeder Test Reactor (FBTR) are the two nuclear test reactors under operation at Kalpakkam, and characterization of the irradiation positions in them is being accomplished to carry on irradiation studies corresponding to their respective neutron spectra [14, 15].

The neutrons from the nuclear reactors are useful as projectiles for the production of wide variety of radioisotopes through nuclear reactions. The radioisotopes produced by the irradiation of various targets in the reactors need to be purified for their application. Similarly, the fission process taking place in the nuclear reactor itself has the potential of producing large number of fission products from the fission of heavy nuclides [16]. Radiochemical purifications methods play an important role for the separation of these radioisotopes from the neutron irradiated target or from the other fission products. The radiochemical separations of the fission products (^{137}Cs, ^{144}Ce-^{144}Pr, ^{90}Sr-^{90}Y, ^{99}Mo-^{99m}Tc etc.) and the radioisotopes produced with neutron irradiation (^{89}Sr, ^{32}P, ^{153}Sm etc) have potential applications in various fields like radio-pharmacy, tracer chemistry, biochemistry, industries, food processing, agriculture etc. [17, 18]. Suitable radiochemical methods are chosen for the separation of a given fission product element or a group of fission product elements produced during the fission process followed by their assay by beta or gamma counting. The commonly used radiochemical separation and purification methods are solvent extraction, ion-exchange chromatography, distillation, precipitation, electro-deposition etc.

The work discussed in the present thesis includes (i) Characterization of neutron spectrum at KAMINI reactor, (ii) Installation of fast flux experimental facility (FFEF) at FBTR and n-flux measurement (iii) Fission product assay of irradiated actinide targets at KAMINI and FBTR and (iv) Radiochemical purification studies of ^{90}Sr, ^{144}Ce-^{144}Pr and ^{32}P produced from FBTR and KAMINI irradiations. The thesis is divided into 10 chapters and their respective contents are briefed in the following sections.

Chapter 1

This chapter includes a brief introduction on the evaluation of nuclear sciences from the discovery of radioactivity to nuclear fission. The various types of neutron sources, its applications and different types of nuclear reactors were presented. This chapter also discusses the overview of neutron spectrum characterization methods and radiochemical purification studies of radioisotopes from fission products and reactor irradiated targets. Further, a brief description about the applications of some of the fission products and reactor produced radioisotopes in various fields was also presented. This chapter further outlines the reactor facilities available at Kalpakkam i.e. FBTR and KAMINI reactors and their utilization towards the irradiation studies [14, 15].

Chapter 2

This chapter discusses the various experimental methodologies adapted during the course of the study. It deals with the descriptions of various activation foils, chemicals, extractants, instruments and analytical techniques used for the neutron spectrum characterization studies and radiochemical purification studies of fission products reactor produced radioisotopes. The experimental methods adapted for these studies such as foil activation method, liquid-liquid extraction, impregnated resin, extraction chromatography, ion exchange chromatography etc. are discussed extensively. The radiometric techniques such as gamma ray spectrometry using high purity germanium (HPGe) and NaI(Tl) detector, Liquid Scintillation Counter (LSC) along with Cerenkov counting technique etc. used for the analysis of activation foils and fission products employed in the above studies are explained. Experimental details on the neutron spectrum unfolding technique, neutron activation analysis, fission product yield measurements and radiochemical separation studies of fission products are also presented.

Chapter 3

This chapter deals with the characterization of pneumatic fast transfer system (PFTS) facility at KAMINI reactor. The characterization studies of the irradiation facilities includes the determination of reactor parameters like ‘thermal to epithermal flux ratio’ (f), ‘epithermal neutron flux shape factor’ (α) and characteristic neutron spectrum determination associated with the irradiation facility. The parameters f and α are essential, especially for k_0 (a composite nuclear constant) based neutron activation analysis, a radioanalytical technique being used for the elemental analysis of various samples. The determination of f and α was carried out by cadmium ratio method as well as cadmium covered method using Au, Zr & Zn as flux monitors [19, 20]. The neutron spectrum facilitates the evaluation of the various reactor parameters like reactivity, burn-up, nuclear reaction rates, temperature distribution etc. The neutron spectrum characterization has been accomplished by foil activation method to determine the reaction rates by assaying the activated products of irradiated foils by high resolution gamma-ray spectrometry using HPGe detector [21, 22]. It was followed by the generation of computed guess spectrum to unfold the neutron spectrum using least square minimization approach. The f and α values were measured and reported along with neutron spectrum at PFTS position of KAMINI reactor.

Chapter 4

This chapter deals with the various experimental details and calculations involved in the design and installation of Fast Flux Experimental Facility (FFEF) at FBTR [15]. Development of this facility with a sample holder has been envisaged to carry out the studies on neutron spectrum characterization, fission systematics, determination of nuclear reaction cross sections, fast neutron activation analysis and minor actinide transmutation studies. The facility has modified the auxiliary shield plug of the central canal plug by attaching a long titanium rod along with a sample holder to the bottom of the shield plug. Samples that are thermally stable at FBTR operating temperature are suitable and allowed for irradiation in this facility. The present chapter details the modified FFEF facility, impurity analysis of titanium by neutron activation analysis (NAA) using relative NAA as well as Internal Monostandard - NAA (IM-NAA) methods and also computation of the radiation dose generated due to the irradiation of titanium rod inside FBTR. This chapter also presents the determination of gold (Au) equivalent neutron flux at FFEF of FBTR (25kWt) using foil activation method.

Chapter 5

This Chapter discusses the irradiation studies of uranium foil and PuO_2-ZrO_2 targets at KAMINI and FBTR respectively. Catcher foil technique using aluminum was carried out for the irradiation studies of uranium at KAMINI reactor [23]. The catcher foils after the irradiation with an actinide were assayed by high resolution gamma ray spectrometry using HPGe detector. The activities were employed for the determination of various fission yields which are normalized to the yield of one of the fission products. The fission yields were determined using calculated reaction rates in case of Pu irradiated at FBTR.

Chapter 6

This chapter describes the radiochemical separation studies of ^{144}Ce-^{144}Pr pair from fission product solution of FBTR. The separated ^{144}Ce-^{144}Pr pair has been used for the demonstration of the phenomenon called ‘radioactive secular equilibrium’. Separation of ^{144}Ce-^{144}Pr pair from other fission products as well as activation products were established by ion-exchange chromatography followed by further separation of pure parent (^{144}Ce) from the ^{144}Ce-^{144}Pr pair by solvent extraction technique using the extractant, di-(2-ethylhexyl)phosphoric acid. Assay of the separated fraction of pure ^{144}Ce was carried out using NaI(Tl) scintillation detector and the variation of the total activity due to both parent (^{144}Ce) and the in-grown daughter (^{144}Pr) was profiled as a function of time for the demonstration of the phenomenon of radioactive secular equilibrium. The secular equilibrium plot obtained from the above experiment was further resolved into its individual decay or growth profiles, i.e. parent decay, daughter growth in parent and daughter decay. The half-life of ^{144}Pr was also determined from the plot. Extraction chromatographic studies were also applied to achieve the separation of pure ^{144}Pr fraction from ^{144}Ce using 40% w/w HDEHP/XAD7 resin with 1M $KBrO_3$/9M HNO_3 as eluent [24]. The pure ^{144}Pr fraction obtained from the above experiment was assayed continuously using HPGe detector to evaluate its half-life experimentally and the same was found to be in good agreement with that of the reported value.

Chapter 7

This chapter deals with the radiochemical separation studies of Sr from the fission product solution of FBTR as well as FBTR irradiated yttria target. A radiochemical separation study of Sr has several applications in various fields. This chapter deals with the separation of the fission product, ^{90}Sr from the other fission products and the extended application of the method for the separation of ^{89}Sr from FBTR irradiated yttria target as well. ^{89}Sr as $SrCl_2$ in dilute HCl medium is being used in pain palliative care for metastatic bone cancer patients. A novel eluting agent tri-sodium tri-metaphosphate (SMP) was employed for the separation of ^{90}Sr and ^{137}Cs from the rest of the fission products by ion-exchange chromatography [25]. The distribution ratio (D_M) values for the various radionuclides present in the FBTR irradiated yttria dissolver solution were measured. The SMP concentration was optimized based on D_M data for the purification of ^{89}Sr source from the other radionuclidic impurities like ^{88}Y, ^{65}Zn, ^{54}Mn, ^{60}Co, ^{86}Rb, ^{192}Ir, ^{103}Ru, ^{113}Sn, ^{139}Ce ^{160}Tb,^{154}Eu etc. produced during the irradiation of yttria in FBTR. Cross contamination of the pure ^{89}Sr source from the complexing agent SMP itself was also evaluated to rule out such possibility. The yields of ^{89}Sr per gram of yttria were estimated based on radiometric assay using liquid scintillation counting, Cerenkov and HPGe counting which are summarized in this chapter.

Chapter 8

This chapter describes the radiochemical purification of carrier free ^{32}P which was produced in KAMINI reactor via $^{32}S(n,p)^{32}P$ using various sulphur targets. This study resulted in establishing the flow-sheet for the production of ^{32}P from the sulphur powder as well as sulphate targets such as magnesium sulphate and strontium sulphate [26, 27]. The PFTS and thimble positions were used for the irradiation of these targets based on their availability. The radiochemical processing involved (i) struvite precipitation method for magnesium sulphate target, (ii) co-precipitation with ferric hydroxide method for strontium sulphate target and (iii) Leaching of ^{32}P into acetic acid and (iv) distillation of ^{32}P from irradiated sulphur powder target. In all these processes, the final purification of the source was accomplished by a cation-exchange chromatographic technique. The yields of pure ^{32}P were established by Cerenkov technique using HIDEX LSC for its quantification.

Chapter 9

This chapter summarizes the results and conclusions obtained from the present thesis work. The various studies carried out i.e. characterization of PFTS position of KAMINI reactor, installation of FFEF at FBTR, flux measurement studies at FFEF, fission yields of U and Pu, radiochemical purification studies of ^{144}Ce-^{144}Pr, ^{89}Sr and ^{32}P were summarized.

Chapter 10

This chapter discusses the scope for future work in this field of work.

References

1. H. Becquerel, Emissions of the new radiations by metallic uranium. Comp. Rend. Acad. Sci. 122 (1896) 1086.
2. E. Rutherford, The scattering of α and β particles by matter and the structure of the atom, Phil. Mag. 21 (1911) 669.
3. E. Rutherford, Collision of α particles with light atoms IV, An anomalous effect in nitrogen, Phil. Mag. 37 (1919) 581.
4. J. Chadwick, The existence of a neutron, Proc. Roy. Soc. A (Lond) 136 (1932) 692.
5. E. Fermi, Possible production of elements of atomic number higher than 92, Nature 133 (1934) 898-899.
6. O. Hahn and F. Strassmann, Concerning the existence of alkaline earth metals resulting from neutron irradiation of uranium, Naturwiss 27 (1939) 11.
7. O. Hahn and F. Strassmann, Verification of the creation of radioactive barium isotopes from uranium and thorium by neutron irradiation; identification of additional radioactive fragments from uranium fission, Naturwiss 27 (1939) 89.
8. L. Meitner and O.R. Frisch, Disintegration of uranium by neutrons: a new type of nuclear reaction, Nature 143 (1939) 239-240.
9. L. Meitner and O.R. Frisch, Products of the fission of the uranium nucleus, Nature 143 (1939) 471-472.
10. S. Flugge, Can the energy content of atomic nuclei be made technically usable?, Die Naturwissenschaften 27 (1939) 403.
11. J. Graham, S. Landsberger, P. J. Ferreira, J. Ihlefeld, G. Brennecka, Neutron flux characterization techniques for radiation effects studies, J. Radioanal. Nucl. Chem. 291 (2012) 503–507.

12. D. K. Mohapatra, P. Mohanakrishnan, Measurement and prediction of neutron spectra in the Kalpakkam mini reactor (KAMINI), Appl. Radiat. Isot. 57 (2002) 25-33.
13. F. De Corte, A. Simonits, A. De Wispelaere, J. Hoste, Accuracy and applicability of the k_0-standardization method, J. Radioanal. Nucl. Chem. 113 (1987) 145-161.
14. S. Usha, R. R. Ramanarayanan, P. Mohanakrishnan, R. P. Kapoor, Research reactor KAMINI, Nucl. Eng. Des. 236 (2006) 872-880.
15. K. V. Suresh Kumar, A. Babu, B. Anandapadmanaban, G. Srinivasan, Twenty five years of operating experience with the Fast Breeder Test Reactor, Energy Procedia 7 (2011) 323-332.
16. J. E. Gindler, J. R. Huizenga, Nuclear Chemistry, Vol-II, Nuclear Fission; edited by L. Yaffe (Academic Press, New York, 1968).
17. Usha Pandey, Atchana Mukherjee, P. R. Chaudhary, M. R. A. Pillai, Meera Venkatesh, Preparation and studies with ^{90}Y-labelled particles for use in radiation synovectomy, Appl. Radiat. Isot. 55 (2001) 471-475.
18. Valéry Olivier Zilio, Om Parkash Joneja, Youri Popowski, François Oswald Bochud, Rakesh Chawla, ^{144}Ce as a potential candidate for interstitial and intravascular brachytherapy, Int. J. Radiation Oncology Biol. Phys. 62 (2005) 585-594.
19. F. De Corte, A. Simonits, A. De Wispelaere, J. Hoste, Accuracy and applicability of the k_0-standardization method, J. Radioanal. Nucl. Chem. 113 (1987) 145-161.
20. Ho. M. Dung, F. Sasajima, Determination of α and f for k_0-NAA in irradiation sites with high thermalized neutrons, J. Radioanal. Nucl. Chem. 257 (2003) 509.

21. A. Seghour, F. Z. Seghour, Neutron energy spectra unfolding from foil activation detector measurements with MINUIT, Nucl. Instrum. Methods. Phys. Res. A 555 (2005) 347-355.
22. L. Yuan-Hao, N. Sander, L. Hong-Ming, M. Ray, J. Shiang-Huei, Monte Carlo determined self-shielded group-wise cross-sections for the activation foil stack applied in the epithermal neutron spectrum adjustment, Nucl. Instrum. Methods. Phys. Res. A 602 (2009) 557-563.
23. H. Naik, G. N. Kim, R. Schwengner, K. Kim, R. John, R. Massarczyk, A. Junghans, A. Wagner, A. Goswami, Fission product yield distribution in the 12, 14, and 16 MeV bremsstrahlung-induced fission of ^{232}Th, Eur. Phys. J. A 51 (2015) 150.
24. A. R. Landgrebe, R. H. Rodriguez - Pasques, F. J. Schima, The Rapid Radiochemical separation of Radioactive Praseodymium from Radioactive Cerium, Int. J. Appl. Radiat. Isot. 19 (1968) 147-149.
25. A. Akseli, S. Kutun, Separation and determination of various elements by cation-exchange chromatography with sodium trimetaphosphate as the eluent, J. Chromatogr. A 847 (1999) 245–250.
26. F. W. Lima, A. B Rao, Production of Carrier-free Phosphorous-32 by using sulphates as material for irradiation, Third Inter-American Symp Peac Appl Nucl Energ Petrópolis, Brazil, July 16-23 (1960) I.E.A Publicação, NO. 37.
27. A. A. Razbash, N. A. Nerozin, M. V. Panarin, Y. G. Sevast'yanov, O. N. Polyakov, D.V. Podsoblyaev, W. Y. Smetanin, T. A. Dubinkina, M. P. Nikulin, Winning ^{32}P in the BR-10 Reactor, At. Energ. 70 (1991) 333-335.

List of figures

List of tables

CHAPTER 1

Chapter 1: Introduction

1.1. Evolution of nuclear sciences

1.1.1. Discovery of radioactivity

The accidental discovery of radioactivity by Becquerel in 1896 is the beginning of nuclear sciences [1]. The intention of the study was to establish a relation between fluorescence and emission of X-rays and discovered that uranium salt crystals emit highly penetrating rays similar to X-rays. Based on the subsequent experiments, it was observed that uranium salts spontaneously emitted these rays and the intensity of the rays was proportional to the amount of uranium present in these salts. These rays were called uranic rays. Subsequently, Marie and Pierre Curie had also started working on this phenomenon and named it as 'Radioactivity' [2]. During the course of the study, they observed that the uranium ores were more radioactive than pure uranium metal. Subsequently, this observation led to the discovery of new elements, polonium and radium [3,4]. In 1911, Rutherford proposed the existence of the nucleus of an atom at its centre on the basis of his experiment on scattering of alpha particles by thin metallic foils [5]. He proposed that the alpha particles scattered from the metallic foil because of the strong repulsion of a massive and positively charged centre in the atom which was responsible for producing an intense electric field of repulsion. He suggested that the positive charge and entire mass are concentrated in the nucleus, surrounded by the orbital electrons. In 1919, he also discovered the first nuclear reaction during his investigation on the possibility of an α induced transmutation on various targets [6]. He bombarded the nitrogen target with alpha particles that resulted into the production of proton, corresponding to the nuclear reaction

$$^{4}He + ^{14}N \longrightarrow ^{1}H + ^{17}O \qquad (1.1)$$

1.1.2. Discovery of neutron

It was initially believed that the nucleus contained only protons and electrons, but this theory had problems due to the ambiguity in mass balance [7]. This was resolved in 1932 by Chadwick who proposed the existence of a neutral particle (neutron) inside the nucleus [8]. Chadwick postulated that the emitted radiation from beryllium, when exposed to α particles of ^{210}Po was neutrons.

$$^{9}Be + ^{4}He \longrightarrow ^{12}C + ^{1}n \tag{1.2}$$

The discovery of neutron encouraged the nuclear chemist and physicist to use nuclear reactions involving neutrons for the production of artificial radioactivity, as the production of neutrons was not complicated and did not require expensive accelerators. A simple neutron source with the yields of 10^6 n/sec could be prepared by mixing beryllium powder with an α emitter (^{210}Po). When a neutron is captured by a nucleus, an isotope with one unit higher mass number is produced. The nucleus so formed is usually unstable and undergoes β^- decay forming the daughter nucleus with the next higher atomic number.

The availability of neutron sources had opened up an innovative field for the production of radioisotopes of most elements in the periodic table. Fermi and his co-workers established the production of artificial radioisotopes by the bombardment of all available elements with neutrons emitted by a radium-beryllium source [9,10]. Subsequently, several groups of scientists were working on the production of trans-uranium elements by bombarding uranium with neutrons [11]. It was presumed that uranium after capturing a neutron, undergoes a beta decay (β^-) to produce the next element i.e. neptunium (Z=93). The study led to the production of so many other radioactive nuclides when uranium was bombarded with neutrons. Different investigators started isolating these radionuclides but were unable to conclude the results about the production of transuranic elements.

In 1938, Hahn and Strassmann separated different radionuclides by precipitating them using barium and lanthanum carriers [12]. Subsequently, they proposed that the uranium nucleus bombarded with neutrons underwent division into two nuclei such as barium and krypton, rather than transmute to higher Z elements [13,14]. They also noticed that the division was not same every time because of which large number of radioactive nuclei were produced. This mysterious phenomenon drew the attention of many scientists for a plausible explanation. In due course, Meitner and Frisch were the first to explain this observation linking it to the division of a liquid drop and the phenomenon was named as “Nuclear Fission” analogous to the process of division in the biological cells [15,16]. They also estimated the total kinetic energy in the fission was around 200 MeV as these fission fragments needed to fly off with high velocity due to mutual coulombic repulsions. Immediately after the discovery, a comprehensive theoretical model for nuclear fission was proposed by Bohr and Wheeler on the basis of liquid drop model [17].

Since then, neutrons became an important experimental probe for various irradiation studies through nuclear fission for radioisotope production. Neutron sources have wide applications in scientific research, medicine, agriculture as well in industry. The important characteristics of the neutron sources are (i) neutron yield, (ii) distribution of their energy and (iii) their emission type (steady-state or pulsed type), which make them versatile analytical tools with applications in numerous fields [18].

1.2. Neutron sources

Different types of neutron sources are presently in practice, differing mutually in their properties and characteristic parameters. The classification of neutron sources is based on the method of their production. Accordingly, neutron sources are divided into four classes based on the type of nuclear reactions from which they are produced.

(i) (α, n) reactions: An energetic alpha particle from an external radiation source interacts with a target to produce a spectrum of neutrons.

(ii) (γ, n) reactions: Neutrons are emitted from a target nucleus by absorbing gamma radiations from a radioisotope.

(iii) Charged particle induced reactions: Neutrons are yielded from interaction of accelerated charged particles (protons, deuterons or ions) with target nucleus.

(iv) Fission reactions: Spontaneous or induced fission of heavy nucleus releases high amount of energy as well as two to three neutrons.

The yield i.e. number of neutrons emitted per second, is the most important characteristic parameter of a neutron source. Most reactions in a neutron source produce fast neutrons and their energy depends upon the energetics of the reaction, the energy of the projectile and the angle of emission of the neutron with respect to the angle of incidence of the projectile. By providing appropriate moderator and thickness, the neutron could be slowed down, but during the process the yields would decrease tremendously [18]. The characteristics of various neutron sources that are presently under use are discussed below in detail.

1.2.1. Alpha-neutron (α, n) sources

The (α, n) sources were prepared using an alpha emitter such as ^{210}Po, ^{241}Am etc. mixed with light elements such as beryllium, boron etc. [19]. The alpha particle was absorbed by the light elements which then decayed by neutron emission. The neutron yields from these sources depend on alpha emitter as well as the light element.

$$^{241}Am \longrightarrow {}^{237}Np + {}^{4}He \tag{1.3}$$

$$^{9}Be + {}^{4}He \longrightarrow {}^{12}C + n \tag{1.4}$$

$$^{19}F + {}^{4}He \longrightarrow {}^{22}Na + n \tag{1.5}$$

The alpha emitter is chosen based on the alpha energy, its half-life, cost and availability. Long-lived trans-actinides such as ^{241}Am ($t_{1/2}$ = 432.6 y) are chosen as alpha sources due to their long time availability. Beryllium is usually preferred over the other light elements as it provides substantially higher neutron yields. The ^{241}Am-Be source furnishes a neutron yield of 10^{6}-10^{8} n.s^{-1}.g^{-1} and is compact which does not require much gamma-ray shielding compared to the other (α, n) sources [20].

1.2.2. Gamma-neutron (γ, n) sources

The (γ, n) reactions produce neutrons in any element if the gamma energy is sufficiently high. When the γ energy is more than the binding energy of the neutron in the nucleus, a (γ, n) reaction can take place which are called as photonuclear reactions. The incident gamma photon energy and binding energy of the neutron dictates the energy of the emitted neutron. The typical minimum threshold energy (~ 8 MeV) is much higher than the gamma energies emitted from radioactive nuclides. However, the (γ, n) threshold energies for beryllium and deuterium are quite low i.e. 1.66 MeV and 2.22 MeV, respectively thus making the photonuclear reaction feasible. In practice, only ^{124}Sb with half-life of 60.2 d is being used as a gamma source as it emits sufficiently high gamma energies of 1.69 MeV and 2.09 MeV [21].

$$^{124}Sb \longrightarrow {}^{124}Te + \gamma \tag{1.6}$$

$$^{9}Be + \gamma \longrightarrow 2\,{}^{4}He + n \tag{1.7}$$

One curie of ^{124}Sb added with beryllium yields about 3x10^{6} n.sec^{-1} [20]. The gamma dose rate from the radioactive nuclide is quite high i.e. about 10 mGy/h at distance of 1 m and can thus cause serious radiation dose exposure problems to the researchers.

1.2.3. D-T source

Relatively higher neutron yields are produced by using neutron generators. Neutron generators are charged-particle accelerators operating at high energies which lead to neutron yielding reactions in a target. A neutron generator generally consists of a target such as ^{3}H or ^{2}H, which is bombarded with ^{2}H to produce high energy neutrons.

$$^{2}H+^{3}H \longrightarrow {}^{4}He+n+17.6\ \ MeV \qquad \text{(D-T reaction)} \qquad (1.8)$$

$$^{2}H+^{2}H \longrightarrow {}^{3}He+n+3.2\ \ MeV \qquad \text{(D-D reaction)} \qquad (1.9)$$

Presently, compact portable neutron sources are commercially available and are commonly based on the ‘D-T’ reaction. The energy (17.6 MeV) released is shared between ^{4}He and neutron. The neutron emitted from D-T reaction is fast neutrons of 14.1 MeV energy, and are widely used for industrial and security applications, based on fast neutron radiography and prompt gamma neutron activation analysis [19]. The typical yields in D-T generator are in the order of 10^{11} n.sec^{-1}.

1.2.4. Spontaneous fission sources

Nuclear fission, either spontaneous or induced is the most important and effective neutron producing source. Several transuranium elements not only undergo alpha decay, but also disintegrate through spontaneous fission to release several neutrons in the process. The most commonly used spontaneous fission neutron source is ^{252}Cf with its half-life of 2.65 y. Small quantities of ^{252}Cf source provides a strong source of neutrons with an yield of ~2.3x10^{12} n/s-Ci [18]. Induced fission as a neutron source is only feasible in nuclear reactors with higher neutron fluxes. Even though the neutron yields are several orders higher in a nuclear reactor, the limitations are their availability and high cost of construction and operation.

1.2.5. Induced fission sources - Nuclear reactor

Among the neutron sources, nuclear reactors using induced fission are the powerful neutron sources. Nuclear reactor is a device in which the controlled fission chain reaction takes place with emission of neutrons, for the production of energy. The neutrons released in fission are responsible for self-sustained chain reaction and thus forms a strong source of neutrons. The neutron fluxes vary with reactors and depend on the various characteristic features of a reactor like core size, fissile content etc. The typical fluxes can be in the range of ~10^7 – 10^{15} n.cm^{-2}.sec^{-1} [22].

1.3. Applications of neutron sources

Neutron sources of all types have a wide variety of applications in research, medicine, industry etc. The main applications of neutron sources are as follows [18]:

(i) Power generation
(ii) Radioisotope production
(iii) Industrial quality control
(iv) Fissile material assay
(v) Chemical analysis
(vi) Geophysical exploration
(vii) Radiation effects studies

(viii) Oil well logging

(ix) Medical therapy and

(x) Research and education

Even though the prime objective of the nuclear reactor is the production of electricity, they offer several other spin-off benefits. The neutrons in the reactor are useful for the production of various tailor-made radioisotopes which find applications in the field of agriculture, medicine, industry, physics and chemistry. The neutrons from reactor are also being used for various irradiation studies such as neutron radiography, neutron activation analysis, neutron shielding experiments, radiation effects on materials etc.

1.4. Nuclear reactors

As mentioned in the previous section, nuclear fission is a source of enormous energy along with an emission of 2 - 3 neutrons per fission [23]. These are known as prompt neutrons and if only one neutron is used to propagate further fission, then this reaction is called controlled chain reaction. This methodology forms the basis of nuclear reactors. The fissile material used in the reactor is called nuclear fuel. The energy liberated in the reactor can be used to generate electrical energy in a nuclear power station.

1.4.1. Basic components of nuclear reactor

A reactor consists of essential components such as fuel, coolant, moderator (in case of a thermal reactor, coolant can be a moderator too) and control rods. Figure 1.1 illustrates schematically the basic components of a nuclear reactor [23]. Generally, the nuclear fuel is made of pellets of uranium (natural or enriched) or plutonium or both; these elements are made in the form of metallic alloys, oxide or carbide and loaded into a clad. The cladding ensures the retention of fission products within the fuel and prevents coolant from its chemical interaction with the fuel. The prompt neutrons having energy upto 10 MeV are called as fast neutrons. As the slow (thermal) neutrons cause more fissions than that of the fast ones, moderators are used to slow down the speed of the neutrons. The commonly used moderators are liquid (e.g. light water or heavy water) or a solid (e.g. graphite).

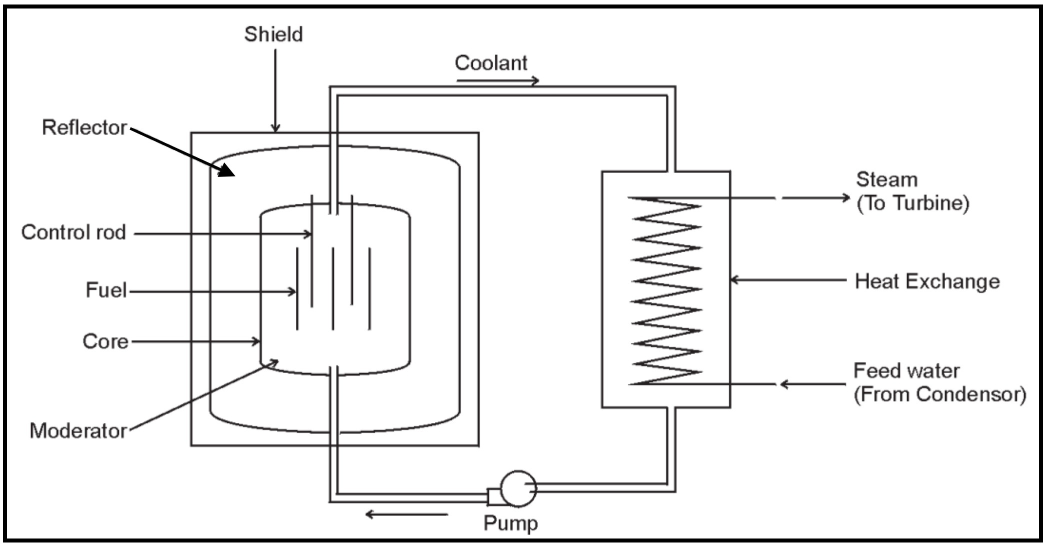

Figure 1.1. Schematic of nuclear reactor [23].

The materials such as cadmium or boron which absorb neutrons are used as control rods for controlling the fission chain reaction by moving them in and out of the core in the reactor. The heat energy released during the operation of the reactor is extracted by a coolant like light water, heavy water, liquid metal, gas etc. The coolant is cooled in a suitable heat exchanger outside the core and returned back to the reactor. The reactor core and reflector are surrounded by thick concrete shields which absorb neutrons, beta rays and gamma rays that are coming through the core-reflector; thus to protect personnel from radiation exposure. The entire reactor is accommodated in a leak tight containment to prevent the leakage of radioactivity into the environment, in the event of an unusual radiation leakage occur in the reactor.

1.4.2. Characteristics of neutrons from nuclear reactor

The natural composition of uranium is ^{234}U - 0.0054%, ^{235}U - 0.7204 and ^{238}U - 99.2742%. Among them, the only fissile nuclide, ^{235}U is responsible for fission in all uranium fuelled reactors. This is because, the excitation energy of compound nucleus (^{236}U) gained due to the absorption of neutron is higher than the fission barrier which results into the fission of ^{235}U. Thus, fission of ^{235}U is possible by bombarding with neutrons of all energies and such nuclei are called fissile nuclei. However, the compound nucleus formed by the ^{238}U due to the absorption of thermal neutron attains excitation energy less than its fission barrier by about 1 MeV. Thus, ^{238}U is fissionable only with neutron energies higher than 1 MeV. The excitation functions which explain the probability of fission for ^{235}U and ^{238}U nuclei are shown in Figure 1.2. The thermal neutron induced fission cross section of ^{235}U is about 580 b, and becomes 1.2 b at 2.5 MeV of neutron energy; whereas, the fission cross section of ^{238}U is negligible for thermal neutrons and is 0.6 b at 2.5 MeV of neutron energy.

The prompt neutrons produced in the nuclear fission are of high energy and mostly vary between 0.1 MeV and 10 MeV or more [24]. The fission neutron spectrum obtained by plotting the fraction of neutrons per MeV as a function of neutron energy is shown in Figure 1.3 [25]. The figure presents the neutron energy spectrum for thermal neutron in ^{235}U. It is understood that the most probable and the average neutron energies are about 0.7 MeV and 2 MeV, respectively. The energy distribution of the neutrons from nuclear fission is represented by the Watt Distribution as shown in the eqn 1.10. [24].

$$N(E) = e^{-E} \sinh(\sqrt{2E}) \qquad (1.10)$$

where N(E) represents the number neutrons per unit energy interval.

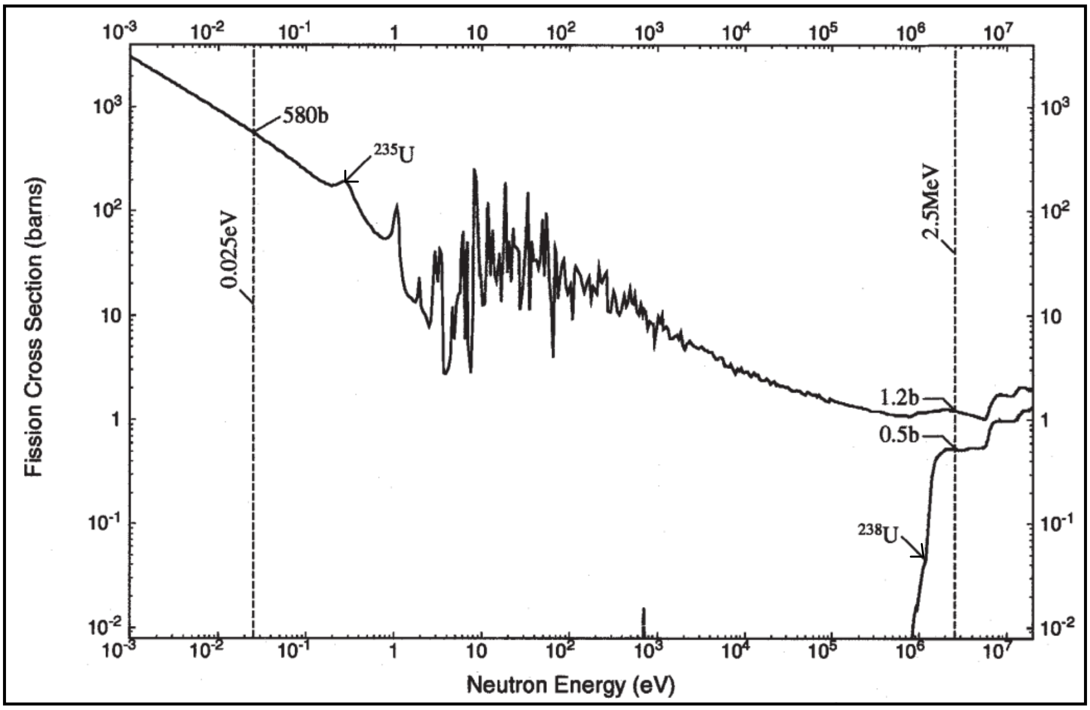

Figure 1.2. Neutron induced fission cross-sections of fissile ^{235}U & fertile ^{238}U nuclei in 640-group presentation [23].

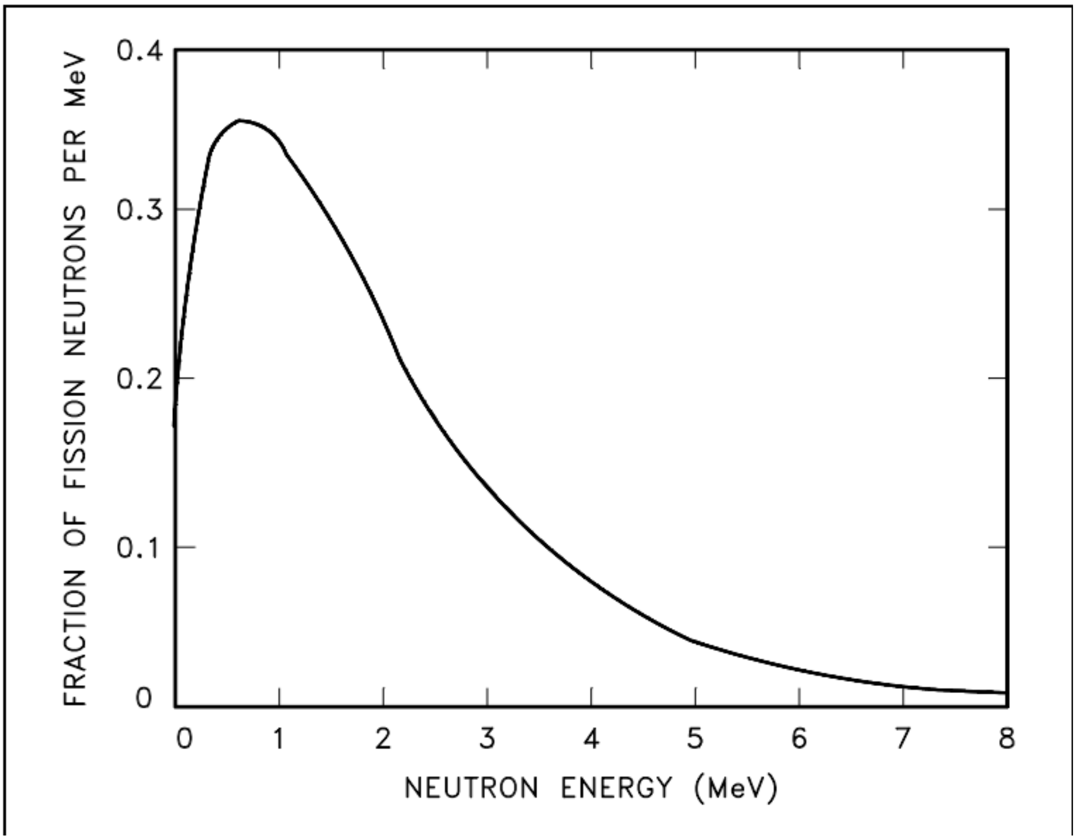

Figure 1.3. Prompt neutron energy distribution in the thermal fission of ^{235}U [25].

1.4.3. Classification of reactors according to neutron flux spectrum

The neutron energy spectrum from nuclear fission greatly differs from the spectrum that exists in a nuclear reactor. The neutron energy distribution in the nuclear reactor varies as function of the moderation and other slowing effects that exist inside the core. Based on the existence of neutron spectra, nuclear reactors are classified as either ‘thermal reactors’ or ‘fast reactors’. The typical neutron energy spectra existing in a thermal and fast reactor are shown in Figure 1.4 [25].

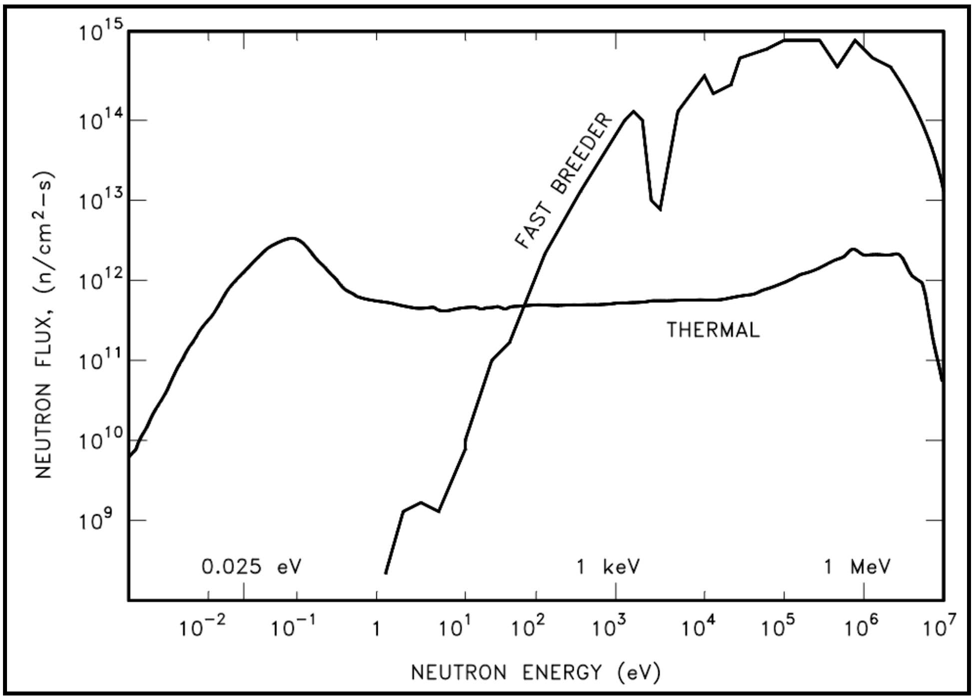

Figure 1.4. Comparison of typical neutron spectra at thermal and fast reactors [25].

In a fast reactor, a very fewer number of thermal neutrons exist due to absence of any moderator to thermalize the neutrons. The existence of the small fraction of these thermal neutrons in fast reactor is due to the collisions with the structural material present inside the reactor. The distribution of neutrons in the fast region (> 100 keV) has a similar shape to that of the fission neutron spectrum.

In a thermal reactor, the neutron energy spectrum has two prominent peaks, one in the thermal energy region and another in the fast region at energies where the neutrons are produced. The neutrons produced from fission undergo collisions with the atoms of the moderator material and achieve thermal equilibrium with them. These neutrons are known as thermal neutrons (~0.025 eV) with Maxwell energy distribution. The neutrons in the intermediate energy region (1 eV to 0.1 MeV) have 1/E dependence and are called as epithermal neutrons. The neutrons with the energy > 0.1 MeV in the neutron spectrum have a similar shape to that of the spectrum of neutrons released in the fission process and are known as fast neutrons.

1.4.4. Types of nuclear reactors

Several types of nuclear reactors are evolved and are classified based on the combination of coolant, moderator and fuel element materials. However, the reactors can also be divided based on their utilities i.e. power reactors and research reactors. While, the former is used mainly for the production of electricity, the latter is used for material research, testing, training and other neutron irradiation studies.

1.4.4.1. Power reactors

The power reactors are classified into the following categories [26].

1.4.4.1.1. Light Water Reactors (LWR): This type of reactors includes both pressurized water reactors (PWR) and boiling water reactors (BWR) in which light water acts as the coolant as well as moderator. This demands the fuel enrichment to about 3% fissile content, as water has high thermal neutron capture cross-section. Enriched uranium oxide (UO_2) is used as the fuel in these reactors [22].

1.4.4.1.2. Heavy Water Reactors (HWR): In these reactors, the generally used coolant is heavy water and sometimes by light water also. The need for enriched uranium can be overcome as the heavy water's neutron capture cross section is very small. The pressurized heavy water reactors (PHWRs) use natural UO_2 as the fuel and heavy water as moderator and coolant [22].

1.4.4.1.3. Gas Cooled Reactors (GCR): In these reactors, gas is used as the coolant and graphite is mostly used as the moderator. In 'Magnox' type GCRs, the coolant is CO_2 at a pressure of 20 bars. The reactor core consists of natural uranium metallic bars clad with magnesium alloy, known by the trade name "Magnox" [27]. The advanced gas cooled reactors (AGR) uses CO_2 as coolant at higher pressures (40 bars) and enriched UO_2 fuel with stainless steel as clad and graphite as moderator. The major drawback of GCRs is that the CO_2 might react with graphite under high temperatures in the reactor to produce CO, which corrodes graphite to reduce its strength. The high temperature gas cooled reactors (HTGR) uses helium as coolant & graphite as moderator. The reactor powers are in the range of 300 to 680 MWe.

1.4.4.1.4. Boiling Water Graphite Moderated Reactors (RBMK): The RBMK type reactors are developed by Russia. The reactor consists of graphite core with holes through which zirconium pressure tubes pass. Enriched UO_2 is the fuel and is loaded in the pressure tubes which are cooled by passing over light water [27].

1.4.4.1.5. Fast Breeder Reactors (FBR): In fast reactors, the chain reaction is sustained by fast neutrons and hence moderator is not required. The breeding ratio is high for the fast flux because of more number of neutrons produced per neutron absorbed in the fissile isotope. The fission cross-sections for fast neutrons are smaller in comparison with that of thermal neutrons which necessitates the use of high enrichment fuel in the core from criticality consideration. Natural uranium or thorium are used as blankets to capture the neutrons leaking from the core and thus to produce fissile material, namely, ^{239}Pu or ^{233}U, respectively as shown below.

$$^{238}_{92}U+^{1}_{0}n \longrightarrow ^{239}_{92}U \xrightarrow{\beta^-} ^{239}_{93}Np \xrightarrow{\beta^-} ^{239}_{94}Pu \qquad (1.11)$$

$$^{232}_{90}Th+^{1}_{0}n \longrightarrow ^{233}_{90}Th \xrightarrow{\beta^-} ^{233}_{91}Pa \xrightarrow{\beta^-} ^{233}_{92}U \qquad (1.12)$$

Liquid sodium is used as coolant in fast reactors due to its efficient heat transfer characteristics and can cope with high volumetric power densities. The Fast Breeder Test Reactor (FBTR) is under operation in India and uses Pu-U carbide as fuel and liquid sodium as coolant [28].

1.4.4.2. Research reactors

Unlike power reactors, the major purpose of research reactors is the production of neutrons and their utilisation for various research oriented programs. These reactors are extensively used for neutron irradiation studies like activation analysis, radiography and shielding experiments and importantly for the production of tailor-made radioisotopes which find applications in many fields. Currently, 245 research reactors are operating in the world [29].

The first nuclear research reactor, ‘Chicago Pile’ was constructed in 1942 by Fermi in University of Chicago [30]. The reactor used uranium oxide as fuel and graphite as moderator. APSARA, the first reactor built in India, in 1956, was a swimming pool type reactor, located at Bhabha Atomic Research Centre (BARC), Trombay [31]. 93% enriched U-Al alloy plates with Al cladding were used as the fuel and light water as the coolant as well as the moderator. The reactor was operated at 1 MWt power with a flux of 10^{12} n.cm^{-2}.s^{-1} and was extensively used for the production of radioisotopes, basic research, shielding experiments, activation analysis, radiography and testing of neutron detectors. The CIRUS reactor with natural uranium metal rods as fuel was commissioned in 1960. This reactor operated at a maximum power of 40 MWt with a neutron flux of 6.5×10^{13} $cm^{-2}.s^{-1}$ [32]. CIRUS reactor was used for condensed matter research, material irradiation, fuel testing, neutron activation analysis and production of radioisotopes for application in the fields of medicine, agriculture and industry. Both the APSARA and CIRUS reactors were permanently shut-down in the year 2010. DHRUVA, a high flux research reactor with 100 MWt power was set up at BARC in 1985 [33]. This is a natural uranium metal fuelled and heavy water moderated research reactor. The reactor provides a maximum neutron flux of 1.4×10^{14} $cm^{-2}.s^{-1}$ and is utilized for basic research, isotope production, activation analysis, testing of neutron detectors etc. Two more important research reactors in India under operation are Kalpakkam-Mini (KAMINI) reactor and Fast Breeder Test Reactor (FBTR) located at Indira Gandhi Centre for Atomic Research, Kalpakkam [28,34]. The description of these reactors is elaborated in the following sections.

1.5. Indian nuclear power programme

Natural uranium reserves in India are limited and estimated to be ~1,72,000 tons of U_3O_8 while thorium is estimated as ~6,50,000 tons [35,36]. The amount of uranium available in India could set a limitation to the growth of nuclear energy as in the case of fossil fuels. However, the generation of ^{239}Pu and ^{233}U in breeder reactors overcomes this limitation. ^{239}Pu can be generated using natural uranium containing ^{238}U as fuel and ^{233}U can be generated by bombarding fertile ^{232}Th with neutrons. Keeping this in view, a three-stage programme has been envisaged and implemented in our country by the visionary Dr. H. J. Bhabha in 1950's [37]. This was initiated for the effective utilization of uranium and enormous thorium reserves for the production of energy to secure the country's long term energy requirement. It is based on a closed fuel cycle concept, which demands the reprocessing of spent fuel from every reactor. A schematic of Indian three stage nuclear programme is depicted in Figure 1.5.

1.5.1. Stage-1: Thermal reactors

In the first stage of the programme, ^{235}U from the domestic natural uranium undergoes fission in a thermal reactor, and produces ^{239}Pu from fertile ^{238}U. At present all operating thermal reactors in India are based on the use of either natural uranium (0.7% ^{235}U) or low enriched uranium (3-4% ^{235}U). Currently, there are eighteen PHWRs, two BWR, and two PWR (VVER), operating with a total capacity of 6780 MWe [38]. The spent fuel from PHWR contains small quantities of fissile ^{239}Pu, along with residual uranium (known as depleted uranium, which predominantly contains ^{238}U). The product obtained in the first stage, namely, plutonium and depleted uranium is used for fuelling in fast breeder reactors (FBRs) in the second stage.

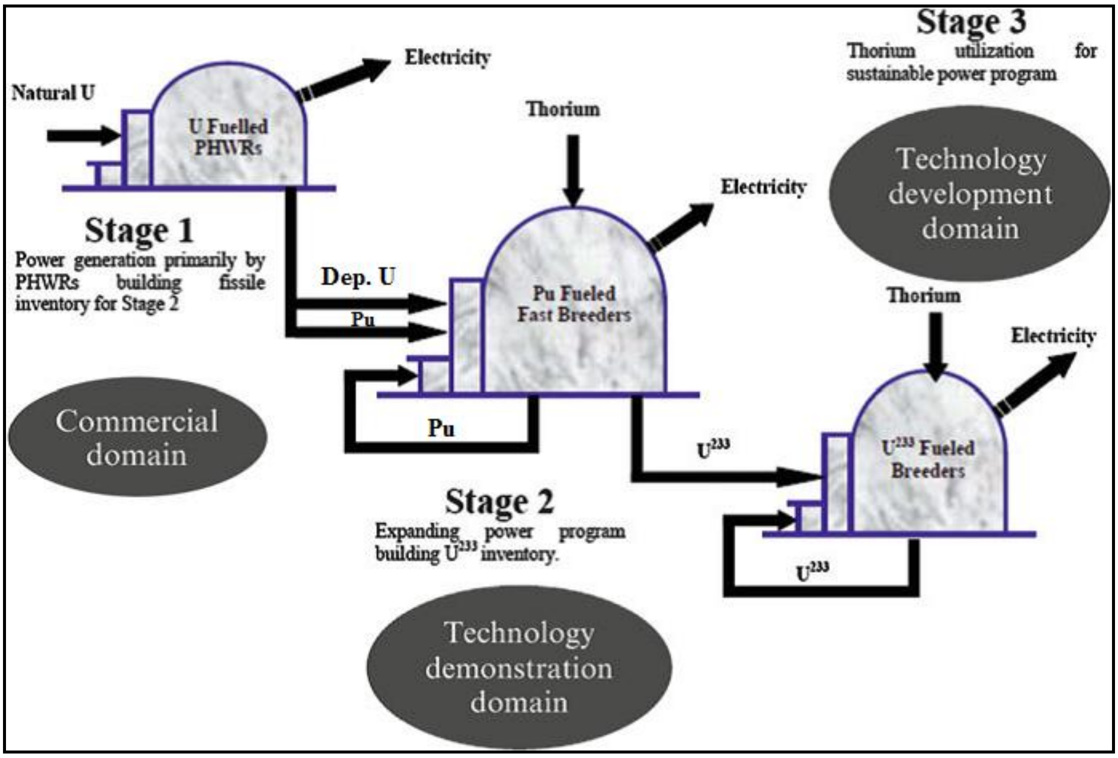

Figure 1.5. Schematic diagram of Indian nuclear power programme [39].

1.5.2. Stage-2: Fast breeder reactors

The second stage is based on the setting up of Fast Breeder Reactors (FBRs) which are fuelled by mixed oxide of ^{238}U and ^{239}Pu, recovered by reprocessing of the spent fuel from the first stage reactors. A 40 MWt Fast Breeder Test Reactor (FBTR) is in operation at Kalpakkam since 1985 [40] to demonstrate the second stage with indigenously developed mixed carbide ($U_{0.3}Pu_{0.7}$) as the fuel. India's first commercial fast reactor, the 500 MWe Prototype Fast Breeder Reactor (PFBR) is in the advanced stage of completion at Kalpakkam. In FBRs, ^{239}Pu undergoes fission, producing energy as well as ^{239}Pu, from the transmutation of ^{238}U. Thus the FBRs produce energy and fuel, & hence termed Breeders. FBRs are capable of generating more fuel than they consume and thus are technically capable of growing the nuclear capacity to a very high level. In the second stage nuclear power reactors, thorium (Th) is kept as blanket material for converting the fertile ^{232}Th into fissile ^{233}U, which will form fuel input for the third stage of the programme [41]. The major driving force behind the development of fast reactor is to breed fissile material from fertile material. This provides the key to utilising the uranium resources and the vast amount of thorium resources available in India.

1.5.3. Stage-3: Thermal breeders

In the third stage, the fissile ^{233}U will be used in thermal or fast breeders to produce electricity as well as to further breed ^{233}U from thorium. Thus the third stage of Indian nuclear power programme is purely based on the exploitation of plentiful resources of thorium available in India. A 30 kWt reactor, KAMINI at Kalpakkam, India is the only reactor in the world, which uses ^{233}U as fuel [34]. In addition to this, Advanced Heavy Water Reactors (AHWRs) are also conceptualized to employ ^{233}U as fuel. According to the three-stage programme, Indian nuclear energy could grow to about 10 GW through PHWRs fuelled by domestic uranium and the growth expected to come from FBRs will be about 50 GW. The third stage will be deployed only after the successful achievement of 2nd stage [42].

1.6. Nuclear reactors in India - Overview

The first commercial nuclear power plant (BWR) in India was set up at Tarapur, Maharashtra. This reactor became operational in 1969 which is the first in Asia and among a few countries in the world, which demonstrated the safe and reliable operation of a nuclear power plant [41]. Subsequently, construction and commercialization of several PHWRs was accomplished at various parts of India. Considering the growing energy demands, a second line of light water reactors has been added to the current indigenous programme of PHWRs. Recently, two Light Water Reactors of 1000 MWe “Voda Voda Energo Reactor” (VVER) units were installed and commercialized at Kudankulam, Tamil Nadu in collaboration with the Russian Federation [43]. Currently, a total of 22 thermal reactors are in operation which includes 18 PHWRs, 2 BWRs and 2 PWRs at various locations in India. Various nuclear power plants under operation with their power output are shown in Table 1.1.

Several research reactors were constructed and commissioned in India, out of which, presently, only three are in operation. They are (i) 100 MWt Dhruva reactor at BARC, Mumbai, (ii) 30 kWt KAMINI reactor and (iii) 40 MWt FBTR both at Kalpakkam.

Table 1.1. The nuclear power plants under operation in India [38]

Plant	**Location**	**Type**	**Capacity of each reactor (MWe)**
Tarapur Atomic Power Station, TAPS - 1 & 2	Tarapur, Maharashtra	BWR	160
Tarapur Atomic Power Station, TAPS - 3 & 4	Tarapur, Maharashtra	PHWR	540
Rajasthan Atomic Power Station, RAPS - 1 to 6	Rawatbhata, Rajasthan	PHWR	RAPS-1 = 100 RAPS-2 = 200 RAPS 3 to 6 = 220
Madras Atomic Power Station, MAPS - 1 & 2	Kalpakkam, Tamilnadu	PHWR	220
Kaiga Generating Station, KGS - 1 to 4	Kaiga, Karnataka	PHWR	220
Kudankulam Nuclear Power Station, KKNPS - 1 & 2	Kudankulam, Tamilnadu	VVER (PWR)	1000
Narora Atomic Power Station NAPS - 1 & 2	Narora, Uttarpradesh	PHWR	220
Kakrapar Atomic Power Station KAPS - 1 & 2	Kakrapar, Gujarat	PHWR	220

1.7. Nuclear reactors in Kalpakkam

Kalpakkam is a unique place for hosting reactors belonging to all three stages of India's nuclear power programme as envisioned by Dr. Homi Bhabha. The two PHWRs that use natural uranium as fuel represents the first stage, the FBTR and PFBR the second stage, and the KAMINI reactor represents the third stage. Among them, KAMINI and FBTR are the research reactors under Indira Gandhi Centre for

Atomic Research (IGCAR) which was established in 1971 as Reactor Research Centre. The details of KAMINI and FBTR are discussed below.

1.7.1. KAMINI reactor

KAMINI is a 30 kWt powered research reactor with ^{233}U-Al alloy fuel, demineralized light water is being used as moderator, coolant and biological shield. BeO and Cd plates are used as reflector and absorber material in the safety control plates, respectively. The reactor has a peak neutron flux of 10^{12} cm^{-2}.s^{-1} at the core centre and makes itself available as a neutron source for neutron radiography, neutron shielding experiments, neutron activation analysis, radiation physics research and testing of neutron detectors [34]. The reactor houses three beam tubes, two thimble irradiation locations and one special irradiation location named as “pneumatic fast transfer system” (PFTS) for carrying out irradiation experiments. The neutron spectra for these beam tubes and the thimble locations were characterized and reported elsewhere [44-46]. Recently, two new locations are installed inside the reactor called ‘dry tube-1’ and ‘dry tube-2’ (Figure 1.6) which have potential features to carry out Large Sample Neutron Activation Analysis (LS-NAA). The Horizontal cross-section view of the KAMINI reactor along with the irradiation positions is shown in Figure 1.6. The special irradiation position nearest to the core is PFTS and is used for producing and studying short and long lived isotopes in various irradiation experiments. The distance between the sample loading terminal and PFTS position is around 14 m while the sample transit time is less than 3 s. The sample with a maximum weight of 1.7 g in a polypropylene container of 20 mm diameter and 30 mm length is transported pneumatically into the irradiation site during reactor operation and retrieved immediately after the irradiation [34]. The irradiation of samples can be carried out in this location without the need for shutting down the reactor. An activation analysis lab adjacent to the KAMINI reactor with a fume hood facility is used for sample loading, sample preparation and pre or post-irradiation treatment. It also houses a well shielded high resolution gamma spectrometry system for the assay of short lived isotopes immediately after the irradiation. Recently, KAMINI reactor core was modified i.e. one of the ^{233}U-Al fuel was replaced with ^{239}Pu-Al fuel subassembly.

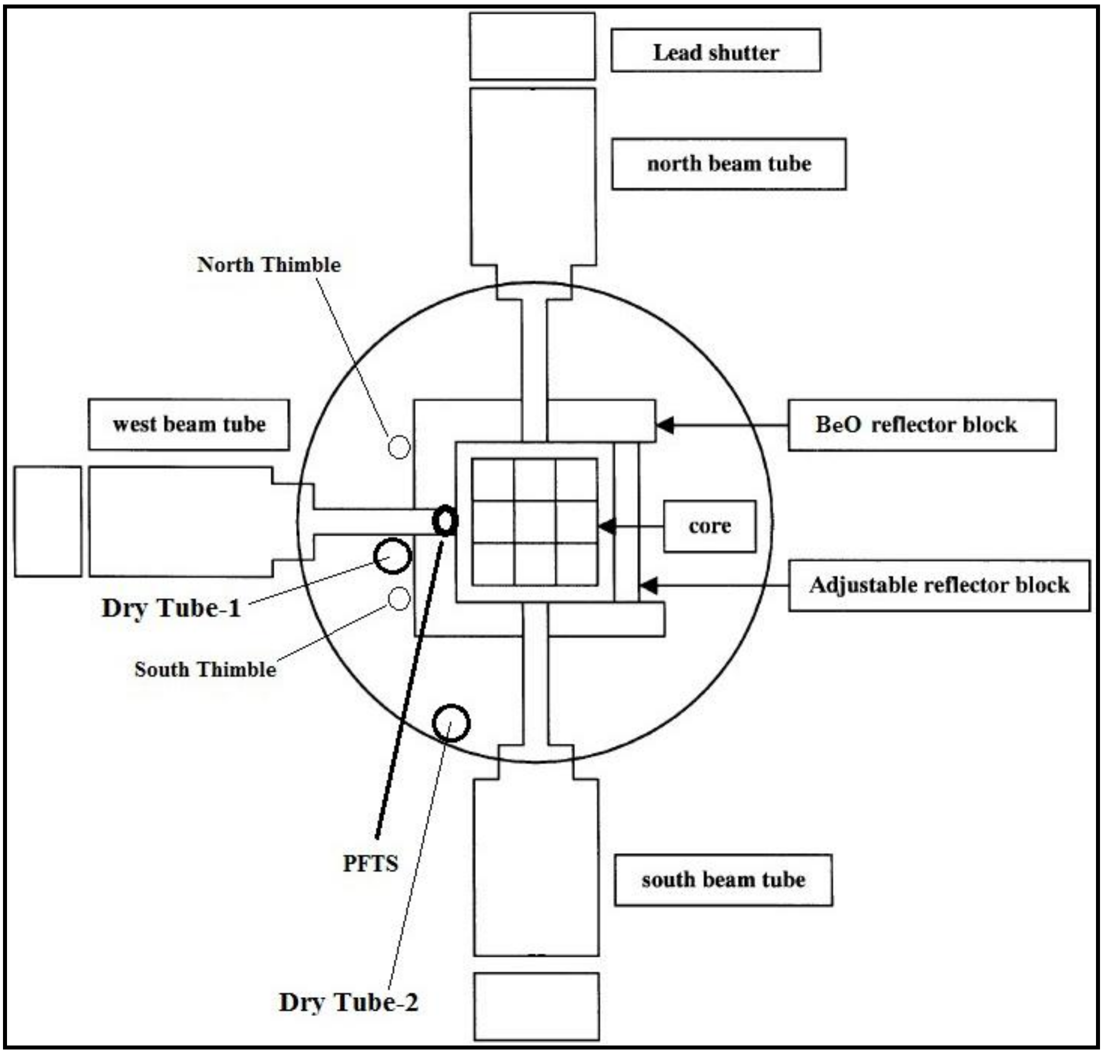

Figure 1.6. Horizontal cross-section view of the KAMINI reactor indicating various irradiation positions.

1.7.2. Fast Breeder Test Reactor (FBTR)

The second stage of India's three-stage nuclear energy programme constitutes the operation of sodium cooled fast breeder reactors for the effective utilization of uranium and exploitation of large reserves of thorium. FBTR is a 40 MWt test reactor located at Indira Gandhi Centre for Atomic Research (IGCAR), Kalpakkam. It is a sodium cooled, loop type fast reactor and operates with unique plutonium rich mixed carbide fuel. The main purpose of FBTR is to provide experience in operation of fast reactor, handling of large scale sodium and to serve as a test bed for the irradiation of fast reactor fuels & materials. FBTR was built in similar line of French Rapsodie-Fortissimo reactor and became critical on 18th October, 1985 [28]. The fuel of reactor consists of two types, i.e. Mark-I (70% PuC + 30% UC fuel) and Mark-II (55% PuC + 45% UC fuel) which was necessitated to attain the neutron flux flattening in the core. One of the current missions of FBTR is to irradiate and test the MOX fuel of commercial power reactor composition planned for the 500 MWe Prototype Fast Breeder Reactor (PFBR) being built at Kalpakkam.

The cross-sectional view of the FBTR assembly is shown in Figure 1.7. The top of the FBTR core was provided with sodium pool, argon cover gas and rotating plug. The rotating plug consists of layers of stainless steel, borated graphite and carbon steel and serves to reduce the dose rate to acceptable levels in the Reactor Containment Building (RCB) [47]. The temperature of the sodium that emerges out from each subassembly is monitored using thermocouples. For the temperature monitoring of the central subassembly outlet, four thermocouples are provided as an integral part of central canal plug (CCP) in the control plug of the reactor [48]. A central cavity of 18.5 mm dia was available in the CCP and this extends up to -6160 mm elevation ie. 57 mm above head of the central subassembly. The cavity was envisaged as a potential irradiation location above the core with fast neutrons. This cavity is enclosed with a supplementary shielding plug for axial shielding which extended up to -3050 mm elevation. The shielding provided by CCP and its shield plug ensures that the radiation dose due to neutron and gamma streaming is within the regulatory limits at the top of the plug.

The supplementary shielding plug was later modified to have a foil holder attached to a 3 m long titanium (Ti) rod. The foil holder which is 50 mm long and closed with a threaded plug is screwed to the Ti rod. This foil holder assembly with the cavity in this CCP serves as the Fast Flux Experimental Facility (FFEF) in FBTR. Introduction and withdrawal of samples is from the top of the reactor and the samples are not in contact with liquid sodium.

The outlet temperature of the sodium from the central subassembly is expected to be around 540 ^{o}C at full power of FBTR. Hence, it is necessary that the samples to be irradiated should be stable at a temperature of about 600 ^{o}C. This rules out the irradiation studies for materials such as organic samples, metallic or other samples with low melting point and samples that have high vapour pressure. Thus, the samples which can be studied by the irradiation can only be metals or ceramics of high melting points and low vapour pressures, withstanding the adverse thermal conditions.

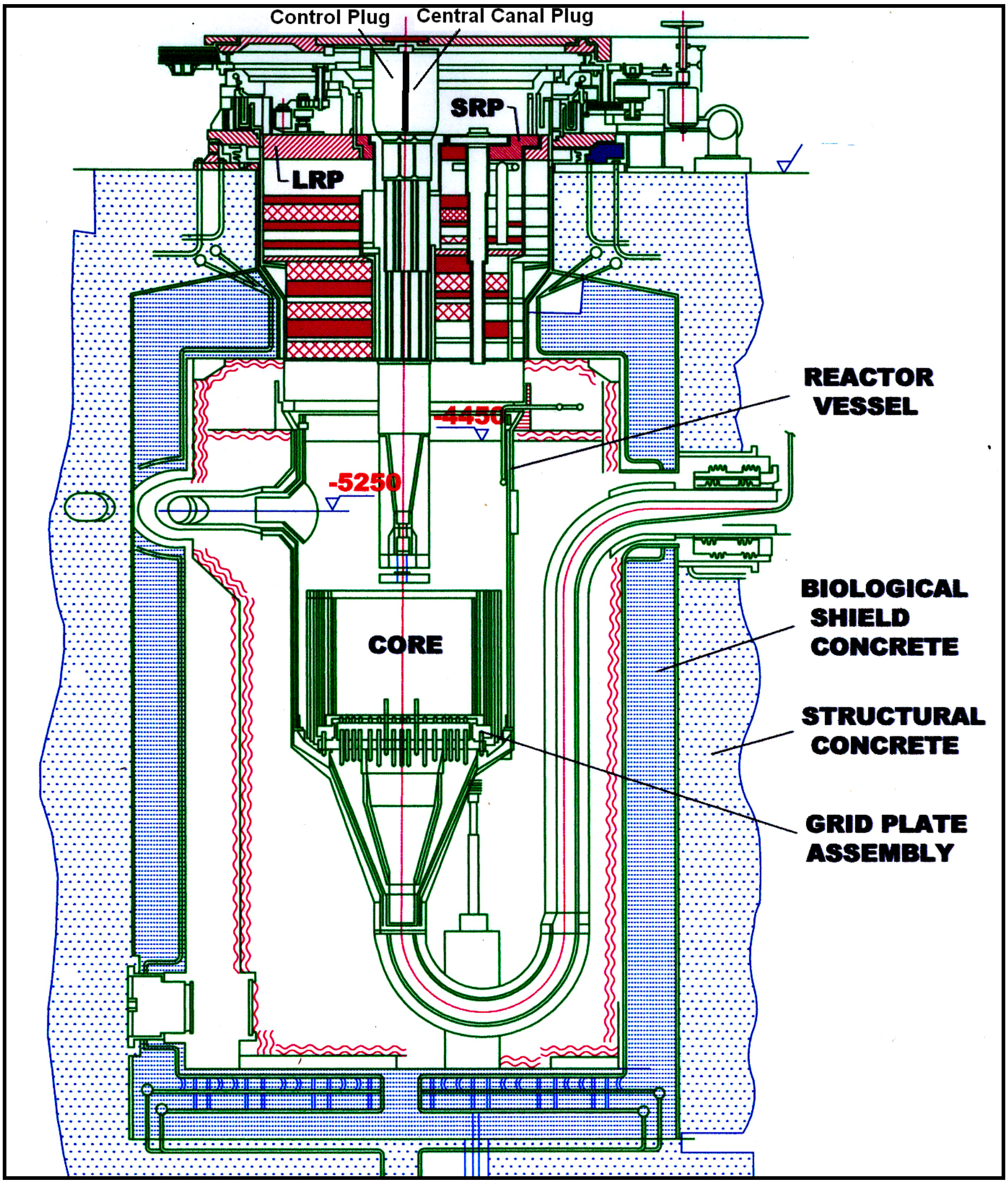

Figure 1.7. FBTR Assembly Cross Section.

1.8. Applications of KAMINI and FBTR

KAMINI reactor as a neutron source is being used extensively for various irradiation studies. It is used for the neutron activation analysis (NAA) of several samples towards routine analysis and research works. It is also used for studies on neutron shielding and neutron radiography of irradiated fuel from the FBTR. KAMINI also renders the necessary and crucial analytical support to the Indian space mission through the neutron radiography of pyro-device based components for all space missions of the Indian Space Research Organisation (ISRO) [49]. Furthermore, the reactor is also being used for the calibration of neutron detectors and characterization of materials.

The FFEF of FBTR is designed for the use in the fission studies of actinides, fast neutron activation analysis and minor actinide transmutation. Further, the reactor is also being used for the production of radioisotopes for the societal applications [50]. ^{89}Sr, a pain palliative care for bone metastasis is being produced in FBTR, and several other radioisotopes (^{32}P, ^{60}Co, ^{117m}Sn etc.) are also envisaged for the investigation towards their production feasibility.

The principles of the important applications of KAMINI and FBTR that are focused in the present thesis are summarized below.

1.8.1. Neutron activation analysis

Neutron activation analysis (NAA) is a radioanalytical technique used to determine the concentrations of elements in materials of different fields. The NAA technique is based on the conversion of a stable element of interest present in the sample into a radioactive element which is also known as “activation” and is accomplished through induced nuclear reaction using neutrons from a nuclear reactor

(Figure 1.8) [51]. The activated element of the sample emits radiation, especially gamma radiation, with its own characteristic energy and intensity which are correlated to the original element and its amount in the sample, thus enabling its qualitative and quantitative analysis. The technique offers many advantages such as simultaneous determination of various elements in the sample, very low detection limit for many elements, better sensitivity, accuracy and significantly matrix independence.

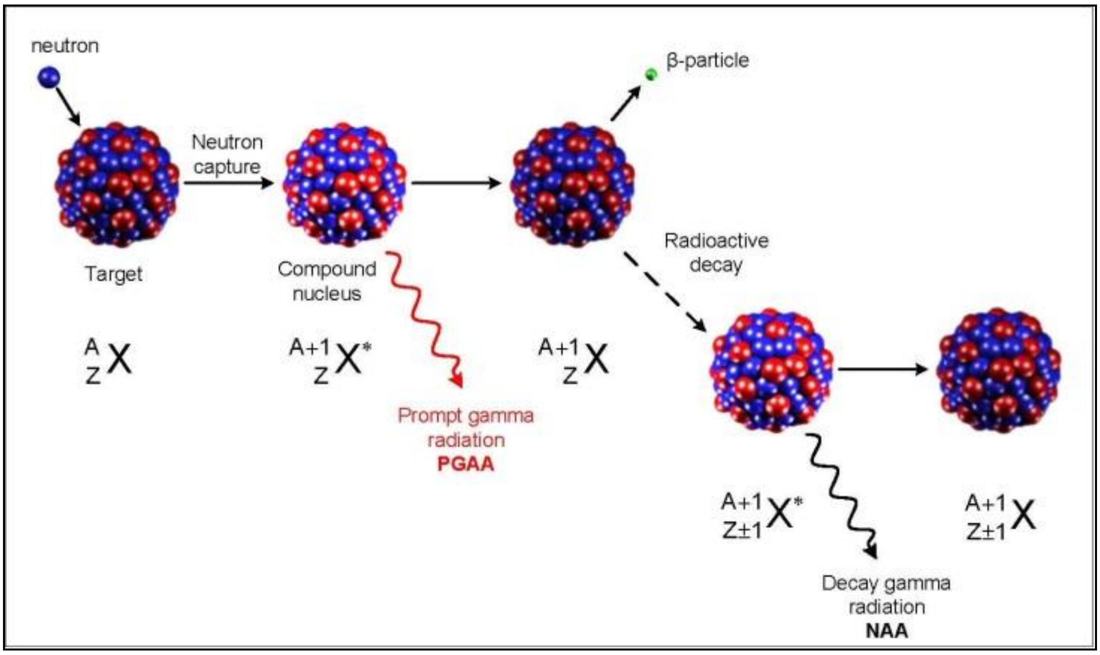

Figure 1.8. Basic Principle of Neutron Activation Analysis [51].

The activity (A) formed at the end of irradiation when a sample is irradiated in a neutron flux (ϕ) for a period of time (t_i), is given by eqn 1.13.

$$A = \frac{N_A.\theta.w}{M}.\sigma.\phi.[1-e^{-\lambda t_i}] \tag{1.13}$$

where, $[1-e^{-\lambda t_i}]$ is the saturation factor (S), λ is the decay constant, σ is the thermal neutron activation cross section, N_A is the Avogadro number, θ is isotopic abundance, w is mass of the element and M is atomic weight. The activity after a cooling period of T_d & for a counting period of 'LT' is given by

$$A = \frac{N_A.\theta.w}{M}.\sigma.\phi.[1-e^{-\lambda t_i}].e^{-\lambda t_d}.\left[\frac{1-e^{-\lambda LT}}{\lambda LT}\right] \qquad (1.14)$$

where, $e^{-\lambda t_d}$ and $\left[\frac{1-e^{-\lambda LT}}{\lambda LT}\right]$ are decay (D) and counting (C) correction terms. There are three standardization methods of NAA as described below.

1.8.1.1. Absolute method

The mass of the element (m) can be determined directly from measured activity by employing the nuclear and reactor based data using the eqn. 1.15.

$$m = \frac{Cp/LT}{S.D.C}.\frac{M}{N_A.\theta}.\frac{1}{\sigma.\phi}.\frac{1}{a_\gamma.\varepsilon} \qquad (1.15)$$

where, C_p is the photo peak area, a_γ is the gamma abundance and ε is the absolute detector efficiency. However, this method is not in use much, because of the difficulty in obtaining the absolute values of σ and ϕ since both vary with neutron energy.

1.8.1.2. Relative method

In this method, the sample irradiated along with an elemental standard and activities from both are measured in identical conditions with respect to the detector. This method is simple and faster to arrive at the results, since it does not need the nuclear and reactor based input parameters. Mass of the element in standard ($m_{x,std}$) and activities of standard ($[Cp]_{x,std}$) and sample ($[Cp]_{x,sample}$) are used to determine the mass of the element in the sample ($m_{x,sample}$) for the same counting time as given by eqn 1.16.

$$m_{x,sample} = m_{x,std} \; . \; \frac{[Cp]_{x,sample}}{[Cp]_{x,std}} \; . \; \frac{D_{std}}{D_{sample}} \qquad (1.16)$$

Even though the relative method is simple and precise, a priori knowledge of the elements present in the sample is necessary to prepare multi-elemental standards or certified reference materials (CRMs) of similar matrices.

1.8.1.3. Single comparator or 'k_0-NAA' method

The possibility of using a single element as comparator for multi-element NAA (k_0-NAA) involves the simultaneous irradiation of a sample and a neutron flux monitor (gold), and the use of a composite nuclear constant (k_0). It eliminates the standard preparation for each element and a priori knowledge of constituents of sample is not necessary. The concentration of an element, C_i (µg.g^{-1}) in k_0-NAA method is calculated using the following eqn [52,53].

$$C_i = \frac{\dfrac{C_p/LT}{S.D.C.W}}{\left(\dfrac{C_p/LT}{S.D.C.w}\right)^{\#}} \cdot \frac{1}{k_0} \cdot \frac{f + Q_0(\alpha)^{\#}}{f + Q_0(\alpha)} \cdot \frac{\varepsilon^{\#}}{\varepsilon} \qquad (1.17)$$

where, W and w are the masses of the sample and comparator respectively, k_0 is the literature reported $k_{0,Au}$-factor [54], $Q_o(\alpha)$ is the ratio of $I_o(\alpha)$ to σ_0, where, $I_o(\alpha)$ is infinitely dilute resonance integral corrected for α, σ_0 is the (n,γ) cross-section at 2,200 ms^{-1} (thermal neutron velocity) and the symbol '#' refers to the corresponding parameters of the gold.

1.8.2. Production of radioisotopes

Production of radioisotopes is possible by altering the neutron-proton (N/Z) ratio in a stable isotope. The N/Z ratio can be altered by bombarding the suitable target with neutrons or charged particles. Neutron irradiation produces "neutron rich" isotopes which usually decay by negatron (β^-) emission, whereas energised charged particle bombardment from an accelerator yields “neutron deficient” isotopes which decay by either positron (β^+) emission or electron capture (EC).

The use of alpha or beta emitting radionuclides is in high demand for the treatment of bone pain palliation caused by metastatic bone cancer [55]. Over the past 60 years, several bone-seeking radiopharmaceuticals are used to treat bone pain caused by metastases. However, US Food and Drug Administration (US FDA) approved [56] only three of them for the treatment of bone pain palliation, namely ^{32}P-Orthophosphate, ^{89}Sr-Strontium chloride and ^{153}Sm-EDTMP (Ethylene Diamine Tetra Methylene Phosphonic acid). Among them, ^{89}Sr and ^{32}P can be produced in FBTR with high specific activity using the nuclear reactions ^{89}Y(n,p)^{89}Sr and ^{32}S(n,p)^{32}P, respectively.

1.9. Characterization of nuclear reactor as a source of neutrons

Neutron spectrum characterization of a neutron source like nuclear reactor is a mandatory requirement for the evaluation of experimental results involving the irradiation of materials. The type and extent of reaction that takes place during the irradiation highly depend on the neutron energy spectrum of the particular facility. Characterization of a neutron facility requires the determination of thermal to epithermal neutron flux ratio (f), epithermal neutron flux shape factor (α) and the neutron spectrum. The importance of these reactor parameters and the methodology being used for their determination are described below.

1.9.1. Determination of reactor parameters ‘f’ and ‘α’

Determination of f and α is an important requirement for the single comparator based k_0-NAA, a radioanalytical technique to estimate the elemental profile of a sample [53]. Evaluation of reactor based parameters (f and α), detector based parameters (absolute efficiency) and a composite nuclear constant (k_0) are the pre-requisites for the k_0-NAA method to determine the elemental concentrations accurately.

The reactor parameters *f* and *α* are the characteristics of an irradiation location in a reactor and need to be evaluated either a priori or simultaneously with the samples during irradiation. For a given ideal neutron energy spectrum, the epithermal neutron energy flux variation is always proportional to 1/E which is not practically observed in real cases. Generally, it is rather proportional to $1/E^{1+\alpha}$ [52], where *α* is a measure of epithermal neutron energy deviation. Although the observed deviation between these two shapes for most of the irradiation positions is small or insignificant, α is introduced [53,57] still to account for the same towards a better accuracy in the related studies. The sign of the α value can be either positive or negative indicating whether epithermal neutron spectrum is 'softened' or 'hardened', respectively [53]. The α value is being used in the subsequent calculation of $Q_o(\alpha)$ [58,59] using eqn 1.18.

$$Q_0(\alpha) = \frac{Q_0 - 0.429}{\overline{E}_\gamma^\alpha} + \frac{0.429}{(2\alpha+1)E_{Cd}^\alpha} \qquad (1.18)$$

where $\bar{E}_r$ is the effective resonance energy in eV. The α value can be determined by several methods such as bare, Cd-ratio and Cd-cover methods using dual or multi monitors [60,61].

1.9.2. Neutron spectrum characterization

Theoretical calculation for the determination of neutron energy distribution depends on the interaction cross sections, numerical procedure adopted for the calculation and other reactor parameters such as fuel burn-up, material composition, geometry and operating conditions [62]. Inaccuracies associated with any of these parameters are difficult to estimate and they naturally propagate to result into an introduction of an element of inaccuracy in the estimation of neutron spectrum. A generally adopted method to bypass rigorous procedure involving the determination of accurate reactor parameters is to perform foil activation measurements [63]. Various foils with their associated characteristics and distinct activation energies as the threshold values and sensitive to different energy regions are selected. The foils are irradiated with the neutrons, at the irradiation location with its characteristic neutron spectrum to obtain reaction rates in the energy region of interest. These reaction rates can thus be obtained from the induced activity of the activation foils from their irradiation which needs data on number of target atoms, irradiation time, counting time, decay time, efficiency of the counting system etc. Thus the exact determination of the neutron flux is possible from the foil activation studies [64].

All the activation foils need to be irradiated in the reactor under identical conditions i.e. in the same position as well as under similar operational conditions such as power level, positions of control rods, moderator temperature etc. to obtain the reaction rates accurately [64,65]. The reaction rates with respect to the threshold energies are generally unfolded using codes like SAND-II, SANDBP and SPECTRA [46,66,67]. Spectrum unfolding uses an approximate solution to flux spectrum which is derived from a theoretical calculation with an optimization procedure for spectral adjustment based on these measured activities. The optimized spectrum should enable the reproduction of the measured reaction rates within the experimental tolerances as well as result into a proximity, continuity and shape with respect to the calculated spectrum. Generally an initial guess spectrum is generated by reactor physics codes and its associated libraries. The unfolding codes translate the guess spectrum into the best fit spectrum using iterative procedures which are adjusted by the minimum deviation between experimental and calculated saturated activities of the different irradiated foils [68].

1.9.3. Yields of fission products

In the neutron induced fission of a heavy nucleus (^{235}U, ^{239}Pu, ^{233}U etc), fission fragments are produced which decay into their corresponding fission products. The fission products are still neutron rich and undergo successive beta decay along an isobaric chain to reach stability. As an example, let us look at an isobaric chain given below corresponding to the mass A=135 for the thermal neutron induced fission of ^{235}U [69].

$$^{94}Br \xrightarrow{0.11s} {}^{94}Kr \xrightarrow{0.21s} {}^{94}Rb \xrightarrow{2.73s} {}^{94}Sr \xrightarrow{1.25m} {}^{94}Y \xrightarrow{18.7m} {}^{94}Zr(Stable)$$

INY:	$1.66*10^{-4}$	0.0868	1.57	4.51	0.39	0.0195
CUMY:	$1.66*10^{-4}$	0.087	1.65	6.06	6.45	6.47

where, INY refers ‘Independent Yield’ and CUMY refers ‘Cumulative Yield’.

In the above isobaric chain, all the fission products are formed as a consequence of the direct fission and due to the decay from the precursor. The yield of the fission products formed directly from the fission without precursor decay is known as ‘independent yield’ whereas with precursor decay, it is ‘cumulative yield’. The cumulative yield of the last product is known as the chain yield for the isobaric chain of the specific mass number. The determination of chain yields is necessary for the mass distribution studies, whereas estimation of independent and cumulative yields of various isobaric chains lead to charge distribution data. Furthermore, yields data are very important towards the fuel burn-up determinations, calculations of fission product inventory in spent fuel, reprocessing of spent fuel and management of nuclear waste [70].

1.9.4. Determination of fission yields

1.9.4.1. Absolute fission yield method

The yield of a fission product in absolute method was determined using the following eqn [71] and termed as absolute yields (Y).

$$Y = \frac{A}{N.\sigma.\phi.(1-e^{-\lambda T_i}).e^{-\lambda T_d}} \tag{1.19}$$

where N is the number of atoms of target fissile nuclide, σ is its fission cross-section (cm^2), ϕ is the flux (n.cm^{-2}.sec^{-1}), λ is the decay constant of the fission product of interest (s^{-1}) with yields Y (% fission), T_i is the time of irradiation and T_d is the time of cooling. Determination of absolute fission yields required the knowledge of all these terms which is practically difficult. Since the direct measurement of absolute yields was difficult, in general, yields were determined relative to a reference mass number and the relative yield curve obtained was then normalized to 200 per cent to give absolute yields [72].

1.9.4.2. Relative yield method

In relative method, fission products yields are determined relative to any one of the products which is determined using absolute method. Absolute yields of fission products viz. ^{99}Mo and ^{140}Ba are used as standard yields and the yields of other fission products are determined relative to these standard yields. The activities of the individual and standard fission products are assayed by a beta or gamma counting system for each irradiation and are related to the respective yields with the following eqn.

$$Y_i = Y_s . \frac{A_i}{A_s} . \frac{[(1-e^{-\lambda_s T_{irr}})e^{-\lambda_s T_d}]}{[(1-e^{-\lambda_i T_{irr}})e^{-\lambda_i T_d}]} \qquad (1.20)$$

where suffix 'i' refers to the fission product of interest and 's' stands for the standard fission product while all other symbols refers to the ones described in eqn 1.19.

1.9.4.3. Comparison method

The comparison method is sort of an extension of the relative method. In this method, a fission product yield in a fissioning system is determined relative to other standard fissioning nuclei in which the yields of fission products were known accurately. The standard fissioning nuclei are chosen depending upon the availability of accurate fission yield data and more often ^{235}U(n$_{th}$, f) is picked, as most exhaustive data available for this system. In this method, fissile nuclide of interest and ^{235}U are irradiated and activities of the fission products are assayed by identical techniques. The experimental parameter 'R-value' is calculated using the activities of fission products in two fissioning system and related to their yield ratios with the following eqn.

$$R = \left(\frac{A_x}{A_{Mo}} \right)_I \left(\frac{A_{Mo}}{A_x} \right)_S \qquad (1.21)$$

$$[Y_x]_I = R.(Y_{Mo})_I \left(\frac{Y_x}{Y_{Mo}} \right)_S \qquad (1.22)$$

where 'I' refers to the fissioning nuclide for which yields are to be determined and 'S' stands for the fission of ^{235}U which is taken as standard. A_x, A_{Mo} are the activities of fission product X and ^{99}Mo (internal standard), Y_X and Y_{Mo} are the respective yields. A large number of mass distribution data was evaluated using this technique [73].

1.10. Application of radioisotopes

Radioisotopes play a major role in a variety of fields such as nuclear medicine, industry, agriculture, sterilization, life sciences and research. The radioisotopes have provided a great or at times, an exclusive tool to resolve many problems associated with chemical, biological and medical fields. Applications of radioactive tracers in chemical research enable the understanding of the reaction mechanism, kinetics, exchange processes and analytical applications such as radiometric titrations, solubility product estimation, isotope dilution analysis and autoradiography [74]. Identification of leaks in buried pipelines and dams was possible only by employing radioisotopes. Process parameters such as mixing efficiency, residence time, flow rate, material inventory and silt movement in harbours are monitored using radioisotopes. Ionising radiation has been employed for the sterilization of medical products and devices. In agriculture, radioisotopes are used to improve the quality, productivity and for optimum utilisation of pesticides, fertilisers and insecticides without or negligible harmful effects to plants and mankind [75].

In the field of nuclear medicine, several diagnostic and therapeutic applications have been standardized using radioisotopes and being routinely employed to patients as per the need. The therapeutic applications of radioisotopes include both curative as well as palliative treatment. The therapeutic treatment involves using implanted or external sealed sources of radioisotopes or by administration of appropriate radiopharmaceuticals [76]. For many applications, the naturally occurring radioisotopes are not sufficient but need tailor-made radioisotopes satisfying requirements of certain radiation characteristics. This necessitates the artificial production of radioisotopes with the required radiation characteristics.

1.11. Production routes of radioisotopes

The schematic production routes of radioisotopes in reactor and cyclotron is shown in Figure 1.9 [23]. Even though the yields of radioisotopes are low in cyclotron, high specific activities can be obtained. Similarly, using nuclear reactions (n,p) and (n,α), production of high specific active radioisotopes is feasible by irradiating appropriate targets in fast reactor which is not possible in thermal reactor due to the difficulty in separating the isotope produced from (n,γ) reaction from the target isotope of the same element. Useful radioisotopes also can be obtained from fission products which are formed during nuclear fission.

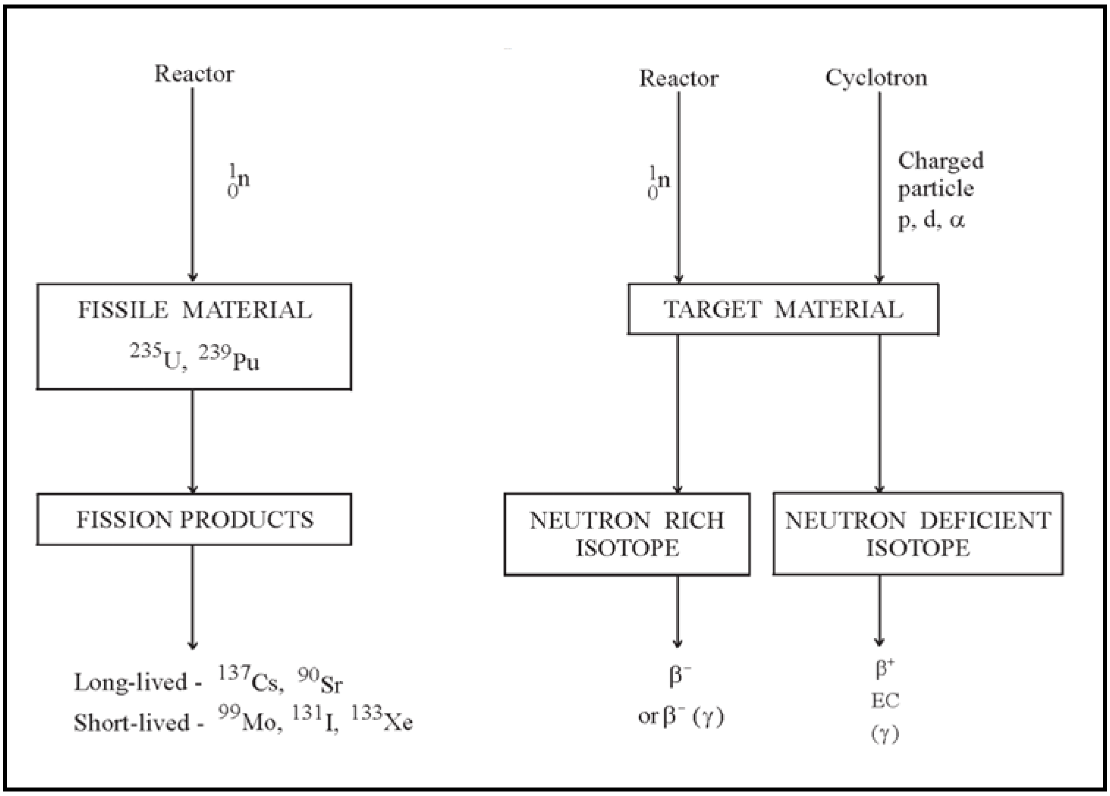

Figure 1.9. Production routes of radioisotopes [23].

1.11.1. Radioisotopes from fission products produced in nuclear fission

Nuclear fission offers a host of several fission products with great significance. Some of the most important fission products which serve in many useful applications are, short lived fission products such as ^{99}Mo and ^{131}I and long lived fission products such as ^{90}Sr, ^{137}Cs and ^{144}Ce [77]. The most important medical radioisotope ^{99m}Tc is a daughter product of ^{99}Mo and is also known as the work horse of nuclear medicine. It is widely being used in Single Photon Emission Computed Tomography (SPECT), a diagnostic technique to obtain and evaluate tomographic images of various organs (brain, lungs, liver, heart etc.) of human body for the evaluation of their functioning [78]. ^{131}I ($t_{1/2}$=8 days) is separated in the form of sodium iodide (NaI) from the fission products and is being administered for both diagnostic as well as therapeutic applications [79] especially in the case of thyroid patients i.e. measurement of thyroid uptake and thyroid imaging after oral administration and the treatment of thyroid diseases such as thyroid carcinoma and hyperthyroidism [80]. ^{90}Y ($t_{1/2}$ = 64.1 h, $E_{\beta\text{max}}$= 2.28 MeV) is a pure β^- particle emitter that can be obtained from the decay of ^{90}Sr ($t_{1/2}$ = 28.8 years) which itself is again a fission product. It is used as a therapeutic isotope for the selective destruction of cancer cells using the radio-immunotherapy approach and also is being used in radiation synovectomy for the treatment of rheumatoid arthritis [81]. ^{137}Cs ($t_{1/2}$ = 30 y) is one of the abundant fission products, recommended for low-dose-rate brachytherapy treatment of gynaecologic cancers through intra-cavitary implants [82]. It is also being used in food preservation by gamma irradiation, sterilization of medical supplies and treatment of municipal sewage sludge by irradiation [83].

Another fission product, ^{144}Ce ($t_{1/2}$ = 285 d) has several applications in various fields of research. The only viable source for this isotope is from nuclear fission which is in secular equilibrium with ^{144}Pr ($t_{1/2}$=17.29 min). The ^{144}Ce-^{144}Pr pair is widely used practically for the demonstration of radioactive equilibrium concept in general and secular equilibrium in particular for pedagogical activities in educational institutions [84]. It is also being evaluated as a potential candidate for the interstitial and intravascular brachytherapy applications due to its long half-life [85]. The ^{144}Ce is also used as a radioactive tracer in chemical and biochemical studies to track the path of cerium [86]. It is further used as energy & efficiency calibration source for gamma spectrometric studies using HPGe detector [87].

1.11.2. Radioisotopes production in cyclotron

The cyclotron produced radionuclides are often neutron deficient and hence decay mainly either by electron capture (EC) or positron (β^+) emission. These radioisotopes are especially suitable for diagnostic studies. Cyclotron produced isotopes such as ^{67}Ga, ^{111}In, ^{123}I and ^{201}Tl decay by EC and are extensively used in nuclear medicine. Positron emitting isotopes such as ^{11}C, ^{13}N, ^{15}O and ^{18}F are short lived and their production in cyclotron is followed by rapid radiochemical processing to yield labeled molecules. Even though, radioisotopes produced in cyclotron are highly expensive, many important neutron deficient isotopes with high specific activity need to be produced only through cyclotron.

1.11.3. Radioisotopes production in nuclear reactor

Most of the artificial radioisotopes are being produced by neutron in a nuclear reactor. The general nuclear reactions include neutron radiative capture i.e. (n,γ) and neutron capture followed by particle emission i.e. (n,n'), (n,p) and (n,α). The most widely encountered reaction is (n,γ) with thermal neutrons. The isotopes like ^{153}Sm, ^{186}Re, ^{188}Re, ^{64}Cu etc. are produced by using this route. The advantage of this route is its simplicity and high production yields owing to the high absorption cross-section. However, the specific activity of source is low in this case, due to difficulty in the isotopic separation of the radioisotope from the target. Higher specific active radioisotopes (^{89}Sr, ^{32}P, ^{67}Cu etc.) are produced through (n,p) and (n,α) reactions which are of threshold in nature and are feasible with fast neutrons in fast reactors. These radioisotopes are neutron rich and hence generally decay by β^- emission.

1.11.3.1 Radioisotopes production in FBTR

1.11.3.1.1. Production of ^{89}Sr

^{89}Sr, a pure beta emitter with half-life of 50.53 d is used in its chloride form for pain palliation of bone metastasis. ^{89}Sr can be produced either by irradiating enriched Sr targets in thermal reactors using ^{88}Sr(n,γ)^{89}Sr reaction [88] or by irradiating yttrium targets in fast reactor using ^{89}Y(n,p)^{89}Sr reaction [89]. However, the later route is preferred over the former as it leads the ^{89}Sr source with high specific activities due to the possible separation of Sr from the chemically different yttrium target. Yttria is the most suitable target for the production of ^{89}Sr in a fast reactor and the same was chosen for the production of ^{89}Sr in FBTR. A flow-sheet for the radiochemical processing of ^{89}Sr from the irradiated yttria target was standardized.

1.11.3.1.2. Production of ^{32}P

Radiochemical processing of ^{32}P was standardized for various sulphur targets irradiated in KAMINI reactor owing to the limited availability of FBTR. ^{32}P is a pure beta emitter with a half-life of 14.3 d and a whole body biological half-life of 39.2 days [90]. ^{32}P is intravenously injected to the cancer patients as orthophosphate in dilute hydrochloric acid medium [91]. ^{32}P as a tracer has also a variety of other applications in the field of plant physiology and soil chemistry. Research has also been carried out on the mechanism of nutrient uptake in the plants by using the isotope ^{32}P [92].

^{32}P can be produced through various nuclear reactions, either from particle irradiation using an accelerator or from thermal or fast neutron irradiation using a nuclear reactor. These methods have their own advantages and disadvantages. One method is preferred over the other based on many factors like cost, availability, end-use etc. Nuclear reaction using fast neutron irradiation of sulphur target through $^{32}S(n, p)^{32}P$ yields ^{32}P of high specific activity as the radionuclide produced from the matrix is different from target element and hence its separation is possible by simple chemical means unlike in the case of thermal neutron irradiation, which requires challenging isotope separation [77]. The associated radiochemical purification methods are simple and faster in the case of sulphur irradiation in fast reactor. Development of flow sheet for the production and purification of ^{32}P from the irradiated sulphur targets using small fast flux available at KAMINI reactor is very useful which can be applied to the FBTR irradiated sulphur targets.

1.12. Radiochemical purifications

The radiochemical separation methods are similar to the conventional separation methods for separating, collecting and detecting radionuclides. However, the decay properties of radionuclides give challenges to the radiochemist to find a suitable separation method for isolation of a pure isotope. The separation technique should be fast enough for radionuclides with short half-life, else they decay before their separation. The solvents should withstand the radiation dose associated with the radionuclides that cause damage and affect the process. In addition, the radiochemical separation method should also be concerned about the type and quantity of the waste generated, because of the difficulties associated with the disposal of radioactive waste.

Radiochemical purifications play an important role in the processing of irradiated targets in order to obtain the radioisotope with the desired level of purity. High pure radioisotopes are required for the radiopharmaceuticals as well as to the study the decay kinetics. The radiochemical purifications utilise one or more conventional separation methods like solvent extraction, ion-exchange, extraction chromatography, adsorption, co-precipitation, distillation, electrochemical methods etc. Some of the important radiochemical purification methods which are often used to purify radioisotopes are discussed below.

1.12.1. Solvent extraction

Solvent extraction is a versatile technique for the separation of desired elements or compounds from a complex mixture of other components present in the aqueous medium. It plays an important role in various fields like nuclear, metallurgical, pharmaceutical, chemical, petrochemical, biochemical, catalysis, polymers, etc, [93].

Solvent extraction essentially depends on the distribution of a solute (eg. a metal ion, M) between two immiscible/partially miscible liquids generally aqueous and organic liquids in mutual contact. The metal ion M, dissolved in one liquid distributes into another immiscible liquid until its chemical potential becomes equal in both the phases which is referred as equilibrium. The distribution of metal ion into the organic phase depends upon the complexing ability of the extractant present in organic phase. The distribution ratio of a solute M (D_M) is defined as the ratio of its concentration in the organic phase ($[M]_{org}$) to that in the aqueous phase ($[M]_{aq}$) at equilibrium as shown in eqn 1.23.

$$D_M = \frac{[M]_{org}}{[M]_{aq}} \qquad (1.23)$$

The distribution ratio of a solute is a constant for a given pair of liquids at constant temperature. In metal recovery operations, the valuable component is a metal ion or a metal complex contained in aqueous solution. This aqueous solution is mixed with an immiscible organic phase containing the extractant for the metal ion in the aqueous phase. The extractant transfers metal ion from aqueous phase into organic phase by a series of chemical interactions which is referred as ‘extraction’. The organic phase loaded with the metal ion after its equilibration with the aqueous phase is now separated from the aqueous phase. The metal ion present in the organic phase is recycled or extracted back to aqueous phase by treating with suitable reagent required for the metal recovery which is referred as ‘stripping’. The ‘stripped organic’ is called lean organic phase, which is recycled and reused in subsequent extractions and the aqueous phase containing metal now goes to the final metal recovery.

If ‘V’ mL of aqueous solution containing ‘x_{aq}’ g of solute is extracted ‘n’ times with ‘v’ mL portions of organic solvent, then the weight of solute remaining in the aqueous phase (x_n) is represented by [94]

$$x_n = x_{aq}\left(\frac{DV}{DV+v}\right)^n \qquad (1.24)$$

The significance of this equation is that the more number of extractions for the given amount of solvent leads to a better extraction efficiency.

1.12.2. Ion-exchange chromatography

Ion-exchange chromatography is a separation technique that is based on the unequal distribution of substances between a solid and a liquid (mobile) phase. The solid phase consists of an insoluble, but permeable inert polymeric matrix that contains fixed charged groups called exchange sites associated with mobile counter-ions of opposite charge. These counter-ions are exchanged with the ions in the mobile phase. Resins are either naturally occurring substances i.e. zeolites (inorganic silicate polymers) or synthetic polymers (organic ion-exchangers). Organic ion-exchanger is a cross-linked polymer matrix, made up of hydrocarbon chains, which carries functional groups. The synthesis of ion exchange resins involves (i) preparation of polymer matrix, and (ii) incorporation of desirable functional groups. The polymer matrix can be prepared either by a process called condensation or addition polymerization. Addition polymers are chemically more stable than condensation polymers. The addition polymer based on styrene and divinylbenzene (DVB) is being widely used in most of the applications. The degree of cross-linking can be controlled by the ratio of DVB to styrene. Ion-exchange resins are generally used in two modes i.e. batch operations and column processes. The amount of material to be processed dictates the column dimensions based on the ease of separation of that particular study. The ion-exchange chromatography technique offers far better separations in comparison with solvent extraction, as the number of theoretical plates in ion-exchange chromatography is high. In General, the ratio of column height to diameter should be 8:1. Higher ratios lead to reduced flow rate while the lower ratios might not provide effective separations [95].

The efficiency of the ion-exchange column is expressed in terms of ‘Height Equivalent to a Theoretical Plate’ (HETP) which is shown below

$$HETP = \frac{L}{N} \qquad (1.25)$$

where, N is the number of theoretical plates, L is length of the column. The efficient ion-exchange columns should have high N and low HETP. Each theoretical plate acts as an extraction system and multiple extractions take place along the length of the column and hence separation factors are higher compared to solvent extraction.

1.12.3. Extraction chromatography

Extraction chromatography is also termed as solid-phase extraction which generally refers to macro porous polymers that hold an organic complexing compound or extractant within the pore structure of the polymer. These materials can be called as extraction chromatography resins or solvent-loaded resins or ligand-immobilized resins or solvent-impregnated resins. The solid-phase extraction resins combine the metal selectivity of liquid-liquid solvent extraction with the operational benefits of better separation efficiency of the packed bed ion exchange into the conventional polymeric adsorbent material. They combine not only the advantages of ion exchange for processing dilute solutions but also with the simplicity of equipment and operational characteristics of solid ion-exchange technology [96]. Separations based on solid phase extractants (SPE) are promising because of the inherent advantages such as (a) any ligand can be immobilized into the form of a solid phase extractant (b) no issue of third phase formation (c) less waste generation (d) disposal of the extractant is relatively easier as compared to solvent extraction techniques and (e) the requirement of relatively less amount of the extractant which is cost efficient while handling expensive extractants like some crown ethers [97]. Extraction chromatography has wide applications in pharmaceutical, analytical organic chemistry and nuclear industry. Extractant molecules are adsorbed through interactions between the resin surface and hydrophobic regions of the extractant molecules. An extraction chromatography resins comprises three major components: a solid support or substrate (typically inert polymer), a stationary extractant phase, and a mobile fluid phase (e.g., conditioning, feed, wash, or eluent).

1.12.4. Precipitation and Co-precipitation

The most common and classical methods for the separation and purification of ions in radioanalytical chemistry are precipitation and co-precipitation [95]. These separation methods are used when the method deals only with trace levels. Precipitation may occur if the concentration of a compound exceeds its solubility level. On the other hand in the analysis of trace elements, co-precipitation is the important way of separating an element. Since the trace element is too dilute as often the case in radiochemistry, it is typically co-precipitated with a carrier, a substance which has similar crystalline structure that can incorporate the desired element. Typical co-precipitation method is employed for micro as well as nano-level quantities. Often, undesired impurities also get co-precipitated along with the analyte of interest is the major draw-back of this separation method.

1.12.5. Distillation

Differences in vapour pressures of elements or their compounds can be exploited for the separation of radionuclides. The distillation process is therefore, essentially takes advantage of the differences in the boiling points of the constituents to separate a mixture into its individual components. The distillation process is very selective and yields clear separations. Generally, in a batch distillation, the sample solution containing volatile components with widely varying boiling points is placed in a distillation chamber, heated to boiling, and the vapours are then continuously removed, condensed and collected into another chamber. Mixtures containing multiple volatile components require fractional distillation, which employs repeated vaporization-condensation cycles for separation, and is commonly performed in a fractionation column. Another important distillation process is vacuum distillation which is used for compounds that have very high boiling points. Lowering the pressure reduces the boiling point of the component and is often more effective for high boiling point substances, which otherwise need rise to a high temperature [94].

1.13. Scope of the present study

The Pneumatic Fast Transfer Facility (PFTS) of KAMINI reactor is being used to study the irradiation effects of various materials. Characterization of such neutron irradiation facility is mandatory requirement for the accurate evaluation of the experimental results involving the irradiation of materials. Characterization of the neutron source needs the establishment of neutron energy spectrum and determination of reactor parameters such as sub-cadmium to epithermal neutron flux ratio (f) and epithermal neutron flux shape factor (α). f and α are the two important parameters required for the single-comparator (Au) based k_0-neutron activation analysis, a radioanalytical technique for the estimation of the elemental profile of a sample. Neutron energy spectrum is very useful for the determination of various reactor characteristics like reactivity, burn-up, nuclear reaction rates, temperature distribution etc.

Fast reactors are the part of the Indian nuclear power program and studies involving fast neutron as projectile is the mandate of the department. In order to gain the experience in operating fast reactors, FBTR was commissioned in IGCAR, Kalpakkam. A new irradiation location called Fast Flux Experimental Facility (FFEF) is installed in FBTR which opens up of opportunity for research with fast neutrons in India. In other words, this facility is envisaged to carry out research on several fields like fast neutron induced fission studies, fast neutron activation analysis, minor actinide transmutation, studies on threshold nuclear reaction etc. The establishment of this facility required the selection of appropriate material for the construction which should cause less radiation dose to reactor operators due to the irradiation inside the reactor. Therefore, the material needed to be assayed for the various impurities and computations for radiation dose from the matrix material as well as impurities due to irradiation is needed to be carried out.

The societal benefits of FBTR are the production of radioisotopes which are used extensively in medical field. Production of high specific active radioisotopes such as ^{89}Sr and ^{32}P are feasible in fast reactors through the (n,p) reactions. These isotopes required to be high pure, before administering into human body. Radiochemical purification methods play an important role to obtain the radioisotopes with desire purity. Simple purification methods needed to be standardized for the separation of ^{89}Sr and ^{32}P from the respective irradiated targets, and the purified sources are to be assayed for the production yields as well as for the presence of other impurities. Similarly, a rapid purification method needed to be established for the separation of ^{144}Ce from the in-grown daughter ^{144}Pr and from other fission products which is required for the demonstration of radioactive secular equilibrium concept.

Studies carried out on the above related activities form the basis of this thesis as given in the following chapters.

1.14. References

1. H. Becquerel, Emission des radiations nouvelles par l'uranium metallique, Comt. rend. 122 (1896) 1086-1088.
2. M. Curie, Rayons emis par les composes de l'uranium et du thorium, Comt. rend. 126 (1898) 1101-1103.
3. P. Curie, Sur une nouvelle substance fortement radioactive, contenue dans la pechblende, Comt. rend. 127 (1898) 1215-1217.
4. P. Curie, Sur une substance nouvelle radioactive, contenue dans la pechblende, Comt. rend. 127 (1898) 175-178.
5. E. Rutherford, LXXIX. The scattering of α and β particles by matter and the structure of the atom, The London, Edinburgh, and Dublin Philos. Mag. and J. of Sci., 21 (1911) 669-688.
6. E. Rutherford, Collision of α particles with light atoms. IV. An anomalous effect in nitrogen, Philos. Mag. 90 (2010) 31-37.
7. E. Rutherford, Bakerian lecture, nuclear constitution of atoms, Proc. Royal Soc. London. Series A, Containing Papers of a Mathematical and Physical Character, 97 (1920) 374-400.
8. J. Chadwick, The existence of a neutron, Proc. Royal Soc. London A: Math. Phys. Eng. Sci. The Royal Society (1932) 692-708.
9. E. Fermi, E. Amaldi, O. D'Agostino, F. Rasetti, E. Segrè, Artificial radioactivity produced by neutron bombardment, Proc. Royal Soc. London. Series A, Containing Papers of a Mathematical and Physical Character 146 (1934) 483-500.

10. E. Amaldi, O. d'Agostino, E. Fermi, B. Pontecorvo, F. Rasetti, E. Segrè, Artificial radioactivity produced by neutron bombardment. II, Proc. Royal Soc. London. Series A, Mathematical and Physical Sciences 149 (1935) 522-558.
11. E. Fermi, Possible production of elements of atomic number higher than 92, Nature 133 (1934) 898-899.
12. O. Hahn, F. Strassmann, Über die Entstehung von Radiumisotopen aus Uran durch Bestrahlen mit schnellen und verlangsamten Neutronen, Naturwissenschaften 26 (1938) 755-756.
13. O. Hahn, F. Strassmann, Über den Nachweis und das Verhalten der bei der Bestrahlung des Urans mittels Neutronen entstehenden Erdalkalimetalle, Naturwissenschaften 27 (1939) 11-15.
14. O. Hahn, F. Strassmann, Nachweis der Entstehung aktiver Bariumisotope aus Uran und Thorium durch Neutronenbestrahlung; Nachweis weiterer aktiver Bruchstücke bei der Uranspaltung, Naturwissenschaften 27 (1939) 89-95.
15. L. Meitner, O. Frisch, When Man Became God, Nature 143 (1939) 239-240.
16. L. Meitner, O.R. Frisch, Products of the fission of the uranium nucleus, Nature, 143 (1939) 471-472.
17. N. Bohr, J. A. Wheeler, The mechanism of nuclear fission, Phys. Rev. 56 (1939) 426-450.
18. A. Lorenz, Survey of neutron sources and their applications, California Univ., Livermore Lab. (1972) UCRL No. - 51298.
19. M. Arai, K. Crawford, Neutron sources and facilities, Neutron imaging and applications, Springer US (2009) 13-30.

20. D. Reilly, N. Ensslin, H. Smith Jr, S. Kreiner, Passive nondestructive assay of nuclear materials, Nuclear Regulatory Commission, Washington, DC (US), Office of Nuclear Regulatory Research; Los Alamos National Lab. NM (US) (1991).
21. J. Hoste, Isotopic neutron sources for neutron activation analysis, International Atomic Energy Agency (1988).
22. A.V.R. Reddy, Nuclear Reactors, IANCAS, 1 (2002).
23. D.D. Sood, A.V.R. Reddy, N. Ramamoorthy, Fundamentals of radiochemistry. 4, (2010).
24. B. Watt, Energy spectrum of neutrons from thermal fission of U-235, Phys. Rev. 87 (1952) 1037.
25. DOE Fundamentals Handbook, Nuclear physics and reactor theory, Washington DC: Department of Energy, Volume 1 of 2 (1993).
26. G.F. Hewitt, J.G. Collier, Introduction to nuclear power, CRC Press (2000).
27. W. Marshall, Nuclear power technology, Volume 1, Reactor technology, United Kingdom Atomic Energy Authority, (1983).
28. K. S. Kumar, A. Babu, B. Anandapadmanaban, G. Srinivasan, Twenty five years of operating experience with the fast breeder test reactor, Energy Procedia, 7 (2011) 323-332.
29. Research Reactors: Purpose and Future, IAEA 60 years, Atoms for Peace and Development (2016) Vienna, Austria.
30. A. Vértes, S. Nagy, Z. Klencsár, R. G. Lovas, F. Rösch, Handbook of Nuclear Chemistry: Vol. 1: Basics of Nuclear Science; Vol. 2: Elements and Isotopes: Formation, Transformation, Distribution; Vol. 3: Chemical Applications of Nuclear Reactions and Radiation; Vol. 4: Radiochemistry and

Radiopharmaceutical Chemistry in Life Sciences; Vol. 5: Instrumentation, Separation Techniques, Environmental Issues; Vol. 6: Nuclear Energy Production and Safety Issues, Springer Science & Business Media (2010).

31. N. B. Prasad, A. S. Rao, The Swimming Pool Reactor, Apsara, Second United Nations International Conference on the Peaceful Uses of Atomic Energy, Genf, (1958) 13.
32. S. Sankar, Planning and management of refurbishment work of Cirus, IAEA-SM-360/45 (1960).
33. K. Rao, Dhruva reactor - a high flux facility for neutron beam research, Indian J. Pure Appl. Phys. 27 (1989) 548-553.
34. S. Usha, R. Ramanarayanan, P. Mohanakrishnan, R. Kapoor, Research reactor KAMINI, Nucl. Eng. Des. 236 (2006) 872-880.
35. Department of Atomic Energy, India, Annual Report, (2011) 4, dae.nic.in/writereaddata/ar2012_0.pdf, (2011-12).
36. F. Sokolov, K. Fukuda, H. Nawada, Thorium fuel cycle-potential benefits and challenges, IAEA-TECDOC, 1450 (2005) 45.
37. H. J. Bhabha, The role of atomic power in India and its immediate possibilities, in: Proceedings of the International Conference on the Peaceful Uses of Atomic Energy, United Nations, Geneva (1955) 103-109.
38. http://www.npcil.nic.in/main/AllProjectOperationDisplay.aspx, (April, 2017).
39. M. Ramkumar, On a sustainable future of Earth's natural resources, Springer (2013).
40. B. Raj, S. Mannan, P.R.V. Rao, M. Mathew, Development of fuels and structural materials for fast breeder reactors, Sadhana 27 (2002) 527-558.

41. S. Banerjee, H. Gupta, The evolution of the Indian nuclear power programme, Progress in Nuclear Energy (2017).
42. B. Bhattacharjee, An overview of R and D in fuel cycle activities of AHWR, Nuclear fuel cycle technologies: closing the fuel cycle, (2003).
43. S. Agrawal, A. Chauhan, A. Mishra, The VVERs at KudanKulam, Nucl. Eng. Des. 236 (2006) 812-835.
44. D. Mohapatra, C. S. Sunny, P. Mohanakrishnan, K. Subbaiah, Monte Carlo modeling of KAMINI, Ann. Nucl. Energy 31 (2004) 2185-2194.
45. D. Mohapatra, E. Radha, P. Mohanakrishnan, Theoretical and experimental investigations of reactor parameters in a U-233 fuelled research reactor, Ann. Nucl. Energy 31 (2004) 197-212.
46. D. Mohapatra, P. Mohanakrishnan, Measurement and prediction of neutron spectra in the Kalpakkam mini reactor (KAMINI), Appl. Radiat. Isot. 57 (2002) 25-33.
47. R. Indira, R. S. Keshavamurthy, Neutron Flux Profiles and Heating in Axial Shields of FBTR, Activity Report of Reactor Physics Division (1993), TRN-IN9600327, IGC-157, IGCAR, Kalpakkam, India.
48. B. Anandapadmanaban, A. Babu, B. Babu, K. Dinesh, V. Ramanathan, G. Srinivasan, Life Extension of the Fast Breeder Test Reactor, 18th Internatl. Conf. Nucl. Eng. American Society of Mechanical Engineers (2010) 97-102.
49. B. Babu, V. Ramanathan, B. Rajendran, P. Ramalingam, B. Raj, Proposed modernization and refurbishment of instrumentation and control systems of the FBTR and KAMINI reactors in India, Modernization and Refurbishment (2009) 95.

50. D. Saha, J. Vithya, G.V.S. Ashok Kumar, K. Swaminathan, R. Kumar, C.R. Venkatasubramani, P.R. Vasudeva Rao, Feasibility studies for production of ^{89}Sr in the Fast Breeder Test Reactor (FBTR), Radiochimca Acta 101 (2013) 667-673.
51. L. Hamidatou, H. Slamene, T. Akhal, B. Zouranen, Concepts, Instrumentation and Techniques of Neutron Activation Analysis, Imaging and Radioanalytical Techniques in Interdisciplinary Research-Fundamentals and Cutting Edge Applications, InTech (2013).
52. O. T. Hogdahl, Neutron absorption in pile neutron activation analysis, Univ. of Michigan, (1962).
53. F. De Corte, A. Simonits, A. De Wispelaere, J. Hoste, Accuracy and applicability of the k_0-standardization method, J. Radioanal. Nucl. Chem. 113 (1987) 145-161.
54. F. De Corte, A. Simonits, k_0-Measurements and related nuclear data compilation for (n, γ) reactor neutron activation analysis: IIIb: Tabulation, J. Radioanal. Nucl. Chem. 133 (1989) 43-130.
55. H.L. Atkins, Overview of nuclides for bone pain palliation, Appl. Radiat. Isot. 49 (1998) 277-283.
56. W. A. Volkert, T. J. Hoffman, Therapeutic radiopharmaceuticals, Chem. rev. 99 (1999) 2269-2292.
57. H. Dung, S. Cho, A simple method for a determination, J. Radioanal. Nucl. Chem. 257 (2003) 573-575.
58. M. Dias, V. Cardoso, M. Koskinas, I. Yamazaki, R. Semmler, M. Moralles, G. Zahn, F. Genezini, M. deMenezes, A. Figueiredo, Measurements of k_0 and Q_0 values for ^{64}Zn(n,γ)^{65}Zn and ^{68}Zn(n,γ)^{69m}Zn reactions with covariance analysis, Appl. Radiat. Isot. 69 (2011) 960-964.

59. F. De Corte, L. Moens, A. Simonits, K. Sordo-El Hammami, A. De Wispelaere, J. Hoste, The effect of the epithermal neutron flux distribution on the accuracy of absolute and comparator standardization methods in (n, γ) activation analysis, J. Radioanal. Nucl. Chem. 72 (1982) 275-286.
60. H. Dung, F. Sasajima, Determination of α and f for k_0-NAA in irradiation sites with high thermalized neutrons, J. Radioanal. Nucl. Chem. 257 (2003) 509-512.
61. F. De Corte, K. Hammami, L. Moens, A. Simonits, A. De Wispelaere, J. Hoste, The accuracy and precision of the experimental α-determination in the $1/E^{1+\alpha}$ epithermal reactor-neutron spectrum, J. Radioanal. Nucl. Chem. 62 (1981) 209-255.
62. S. Sen, S. Bagchi, R. Prasad, D. Venkatasubramanian, P. Mohanakrishnan, R. Keshavamurty, A. Haridas, A.J. Arul, P. Puthiyavinayagam, Determination of neutron energy spectrum at KAMINI shielding experiment location, Appl. Radiat. Isot. 115 (2016) 165-171.
63. A. Seghour, F. Seghour, Neutron energy spectra unfolding from foil activation detector measurements with minuit, Nucl. Instr. Meth. Phys. Res. A: Accelerators, Spectrometers, Detectors and Associated Equipment, 555 (2005) 347-355.
64. B. d'Utra, Ulysses, P.G.M. Fernando, J. Rogerio, Measurements of the neutron spectrum energy in the IPEN/MB-01 reactor core, Braz. J. Phys, 39 (2009) 39-43.
65. J. Marques, M. Sousa, J. Santos, A. Fernandes, Characterization of the fast neutron irradiation facility of the Portuguese Research Reactor after core conversion, Appl. Radiat. Isot. 69 (2011) 1128-1130.
66. E. Szondi, E. Zsolnay, Documentation of the Code SANDBP: Report, Institute of Nuclear Techniques, Technical University of Budapest, Budapest, (1992).

67. C. Greer, J. Halbleib, J. Walker, Technique for Unfolding Neutron Spectra from Activation Measurements, Sandia Corp., Albuquerque, N. Mex. (1967).
68. J. Graham, S. Landsberger, P. Ferreira, J. Ihlefeld, G. Brennecka, Neutron flux characterization techniques for radiation effects studies, J. Radioanal. Nucl. Chem. 291 (2012) 503-507.
69. T. England, B. Rider, Evaluation and compilation of fission product yields, ENDF-349, LA-UR-94-3106, Los Alamos National Laboratory, (1994).
70. J. Rein, Status of burn-up measurement methodology, Analytical methods in the nuclear fuel cycle (1972).
71. S. Prakash, S. Manohar, Radiochemical methods of measurements of fission products yields, J. Radioanal. Nucl. Chem. 142 (1990) 119-133.
72. J.M. Crook, Radiochemical studies of some pile-neutron fission yields of thorium-232, (1962).
73. H. Jain, M. Ramaniah, Fission yields in the thermal neutron fission of plutonium-239, Radiochimica Acta 37 (1984) 63-68.
74. H.J. Arnikar, Isotopes in the atomic age, Wiley Eastern Ltd., New Delhi (1989).
75. G. Hardarson, Use of nuclear techniques in studies of soil-plant relationships, International Atomic Energy Agency Vienna, Austria, (1990).
76. Therapeutic applications of radiopharmaceuticals, IAEA-TECDOC-1228 (2001) Vienna.
77. Manual for Reactor Produced Radioisotopes, IAEA-TECDOC-1340, Vienna (2003).
78. S. Banerjee, M. R. A. Pillai, N. Ramamoorthy, Evolution of Tc-99m in diagnostic radiopharmaceuticals, Seminars in nuclear medicine, Elsevier (2001) 260-277.

79. G. B. Saha, Fundamentals of nuclear pharmacy, Springer Science & Business Media (2010).
80. D. Hnatowich, Recent developments in the radiolabeling of antibodies with iodine, indium, and technetium, Seminars in nuclear medicine, Elsevier (1990) 80-91.
81. S. J. DeNardo, L. A. Kroger, G. L. DeNardo, A new era for radiolabeled antibodies in cancer?, Current opinion in immunology 11 (1999) 563-569.
82. S. D. Sharma, S. Kumar, P. Srinivasan, G. Chourasiya, Establishment of air kerma reference standard for low dose rate Cs-137 brachytherapy sources, J. Appl. Clin. Med. Phys. 12 (2011) 275-285.
83. W. Schulz, L. Bray, Solvent extraction recovery of by product ^{137}Cs and ^{90}Sr from HNO_3 solutions-a technology review and assessment, Sep. Sci. Technol. 22 (1987) 191-214.
84. W. Semmelrogge, F. Sicilio, A study of secular equilibrium using Ce^{144}-Pr^{144}, J. Chem. Educ, 42 (1965) 427.
85. V. O. Zilio, O. P. Joneja, Y. Popowski, F. O. Bochud, R. Chawla, ^{144}Ce as a potential candidate for interstitial and intravascular brachytherapy, Int. J. Radiat. Oncol. Biol. Phys. 62 (2005) 585-594.
86. J. Douglas, M. Goss, D. Hill, Measurements of pore characteristics in a clay soil under ploughing and direct drilling, including use of a radioactive tracer (^{144}Ce) technique, Soil Tillage Res. 1 (1980) 11-18.
87. S. Jerome, Preparation of calibrated reference sources containing fresh fission products, J. Radioanal. Nucl. Chem. 264 (2005) 517-522.

88. F. R. Knapp, S. Mirzadeh, A. Beets, M. O'doherty, P. J. Blower, E. Verdera, J. Gaudiano, J. Kropp, J. Guhlke, H. Palmedo, Reactor-produced radioisotopes from ORNL for bone pain palliation, Appl. Radiat. Isot. 49 (1998) 309-315.
89. A. Zvonarev, ^{89}Sr production in fast reactor, Atomnaya Ehnergiya 82 (1997) 396-399.
90. V. N. Agent, Health Effects of Project Shad Chemical Agent (2004).
91. N. Nair, Relative efficacy of ^{32}P and ^{89}Sr in palliation in skeletal metastases, J. Nucl. Med. 40 (1999) 256.
92. D. Schlyer, P. Van den Winkel, T. Ruth, M. Vora, M. R. A. Pillai, M. Haji-Saeid, Cyclotron produced radionuclides: Principles and practice, Technical Reports Series No. 465, Vienna, (2008).
93. J. Rydberg, Solvent extraction principles and practice, revised and expanded, CRC Press (2004).
94. D. A. Skoog, D. M. West, F. J. Holler, S. Crouch, Fundamentals of analytical chemistry, Nelson Education, 2013.
95. C. T. Whitman, D. G. Whitman, EPA-SAB-RAC-03-009 (2003).
96. E. Philip Horwitz, R. Chiarizia, M. L. Dietz, A novel strontium-selective extraction chromatographic resin, Solvent Extr. Ion Exch. 10 (1992) 313-336.
97. I. Villaescusa, N. Miralles, J. De Pablo, V. Salvado, A. Sastre, Extraction of Gold(III) from hydrochloric acid solutions by tri-n-dodecylammonium chloride in toluene, Estimation of the interaction coefficient between $AuCl_4$ and H^+, Solvent Extr. Ion Exch. 11 (1993) 613-626.

CHAPTER 2

Chapter 2: Experimental

This chapter deals with the details on various activation foils, chemicals, extractants, instruments and analytical techniques used for the studies on neutron spectrum characterization of KAMINI and FBTR and radiochemical purification of various radioisotopes. This chapter also includes the experimental details on neutron spectrum unfolding technique, neutron activation analysis, fission product yield measurements and purification of radioisotopes using various radiochemical separation techniques. It also describes the experimental details on foil activation method for neutron spectrum characterization as well as radiochemical separations involving solvent extraction, ion-exchange chromatography, selective precipitation, distillation and extraction chromatography. This chapter in addition, furnishes the details on the analysis of activated foils, fission products etc. accomplished using radioanalytical techniques such as gamma spectrometry by using HPGe detector as well as NaI(Tl) detector, liquid scintillation counter (LSC) and Cerenkov counting.

The experimental details described in this chapter facilitated the accomplishment of the following studies i.e.

1. Determination of sub-cadmium to epithermal neutron flux ratio (*f*) and epithermal neutron flux shape factor (α) at Pneumatic Fast Transfer System (PFTS) position of KAMINI reactor which are useful in standardising the composite nuclear constant (k_0) based neutron activation analysis (NAA).
2. Neutron spectrum characterization of PFTS of KAMINI reactor using foil activation technique.

3. Design and installation of Fast Flux Experimental Facility (FFEF) in Fast Breeder Test Reactor (FBTR) followed by the measurement of its associated neutron flux.
4. Determination of fission yields of KAMINI-irradiated uranium foil as well as FBTR-irradiated PuO_2-ZrO_2 targets.
5. Radiochemical purification of ^{144}Ce-^{144}Pr pair from FBTR irradiated $(U,Pu)O_2$ fuel dissolver solution by using solvent extraction and ion-exchange & extraction chromatographic techniques.
6. Radiochemical purification of ^{90}Sr from fission products by ion-exchange chromatography using tri-Sodium tri Meta Phosphate (SMP), and its extended application for the purification of ^{89}Sr from FBTR irradiated yttria target.
7. Radiochemical purification of ^{32}P from various sulphur bearing targets irradiated in KAMINI reactor.

2.1. Activation foils, tracers, chemicals and reagents

2.1.1. Activation foils

The following activation foils were procured from M/s Good Fellow Cambridge Limited, England with their associated purities and thickness as given in the parentheses. i.e. Au (99.99% & 100 µm), Al (99.999% & 30 µm), Zr (99.8% & 75 µm), Fe (> 99.99% & 125 µm), Ti (> 99.99% & 125 µm), Co (> 99.99% & 125 µm), Mo (99.9% & 100 µm), Zn (> 99.99% & 1 mm), In (99.999% & 125 µm), Ni (99.9% & 100 µm), and Cd (> 99.99% & 125 µm). Similarly, Au-0.1 wt%Al alloy wire with 1 mm diameter was procured from M/s European Reference Materials, Belgium.

The standard stock solution of gold was prepared by dissolving a known amount of gold foil in dilute nitric acid and made up to the concentration of 1 mg/mL.

An aliquot of the standard solution was evaporated on a tissue paper and double sealed with sealing machine for irradiation.

2.1.2. Radioactive tracers

Standard Radioactive source

Standard radioactive gamma sources such as ^{152}Eu tracer solution, ^{60}Co, ^{133}Ba and ^{137}Cs point sources were procured from Amersham, Inc., USA. Further, the point standard source as well as the 5 mL liquid standard solution in a vial were prepared using the standard stock solution of ^{152}Eu.

Standard sources of pure beta emitter viz. ^{3}H, ^{99}Tc, ^{208}Tl, ^{89}Sr, ^{32}P and ^{90}Sr-^{90}Y were procured from M/s Cerca LEA, France and were used for the efficiency calibration of HIDEX 300SL liquid scintillation counting system for both LSC as well as Cerenkov counting modes of measurements.

Stock dissolver solutions of FBTR irradiated targets

The stock fuel dissolver solution was prepared by dissolving the FBTR irradiated (U,Pu)O_2 pellets with burn-up of 112 GWd/t in 12M nitric acid and used for the studies on radiochemical separation of Ce and Sr. Similarly, yttria stock solution was prepared by dissolving FBTR irradiated yttria pellets in 9M nitric acid and the same was used for the studies on radiochemical purification of strontium.

2.1.3. Chemicals and Reagents

All the chemicals and reagents used in this study were of analytical grade and were used without further purification unless mentioned otherwise.

The concentrated HNO_3 and HCl acids of ACS reagent grade were procured from M/s Merck Specialities Private Limited, Mumbai, India. The different concentrations of acid solutions were prepared by diluting these concentrated acids with Millipore water and were standardized by using standard acid-base titration methods with standard NaOH solution and phenolphthalein as indicator.

NaOH of AR grade was procured from M/s Hi-Pure Fine Chem industries, Chennai, India. Phenolphthalein was procured from M/s Merck Specialities Private Limited, Mumbai, India and its solution was prepared by dissolving ~ 500 mg in 100 mL of distilled water and ethanol mixture corresponding to 1:1 ratio. Ethylenediaminetetraacetic acid (EDTA), tri-sodium tri-meta phosphate (SMP) of 95% purity and copper sulphate ($CuSO_4$) of > 99% purity were obtained from M/s Sigma Aldrich Chemie GmbH, Steinheim, Germany.

Potassium bromate ($KBrO_3$) of 99.8% purity of AR grade was procured from M/s S. D. Fine-Chem Limited, Mumbai, India. Yttria (Y_2O_3) of 99.999% purity was procured from M/s Alfa-aeser, USA. Magnesium sulphate ($MgSO_4.7H_2O$), strontium sulphate ($SrSO_4$) and Sulphur powder each of 99% purity and 30% hydrogen peroxide (H_2O_2) were obtained from M/s MERCK Specialities Private Limited, Mumbai, India. Ammonium hydroxide (NH_4OH) and sodium carbonate (Na_2CO_3) were procured from M/s Loba Chemie, Mumbai, India.

2.1.4. Organic materials and Solvents

While, amberlite XAD-7 (20-60 mesh) and Dowex 50WX8 (100–200 mesh) resins were procured from M/s Sigma Aldrich Chemie GmbH, Steinheim, Germany, the solvents, n-hexane and n-heptane, were from M/s Loba Chemie, Mumbai, India. However, the solvent cyclo-hexane of 99.9 % purity of HPLC grade was procured from M/s Spectrochem Pvt. Ltd., Mumbai, India. While Di-(2-ethylhexyl) phosphoric acid (HDEHP) was procured from M/s BDH chemical Ltd., England, the MAXILIGHT scintillation cocktail was from M/s HIDEX, Finland.

2.2. Instrumentation

2.2.1. HPGe detector for high resolution gamma spectrometry

Radioactive assay of activation foils and fission products was accomplished by high resolution gamma spectrometry technique using 30% HPGe detector (co-axial) of Canberra Eurisys make from Canberra Industries, Inc., USA with its resolution of 1.9 keV at 1332 keV of ^{60}Co. The HPGe detector was connected to 8k multichannel analyser (MCA) system with Aptec spectra software. Energy as well as efficiency calibration of the HPGe detector were carried out using the standard gamma sources of ^{137}Cs, ^{60}Co, ^{133}Ba and ^{152}Eu. Gamma peak fitting was accomplished using PHAST software developed by Bhabha Atomic Research Centre (BARC), Mumbai, India [1].

2.2.2. NaI(Tl) detector for gamma assay

The gamma assay of ^{144}Ce-^{144}Pr was accomplished using a well-type NaI(Tl) scintillation detector with its associated photomultiplier tube (PMT) unit, a single channel analyser (SCA) and a timer-scalar module. While, the NaI(Tl) - PMT integral assembly was procured from M/s The Harshaw Chemical Co., Division of Kewanee Co., U.S.A., the other associated electronic modules were obtained from M/s Electronic Corporation of India Limited (ECIL), Hyderabad, India.

2.2.3. Liquid Scintillation Counter (LSC) for beta detection

Hidex 300 SL Automatic Triple to Double Coincidence Ratio (TDCR) LSC system was procured from Finland. This detector has efficiencies of 50% for Cerenkov mode and 100 % for LSC mode for the $\beta^{-}_{\max}$ energy of 1.5 MeV corresponding to ^{89}Sr source. The efficiency calibration of the LSC detection system in the Cerenkov mode was carried out using the standard sources such as ^{3}H, ^{14}C, ^{99}Tc, ^{89}Sr, ^{32}P, ^{204}Tl and ^{90}Sr-^{90}Y.

2.2.4. pH meter

All pH measurements were carried out using Cyberscan 500 pH, Metrohm which was calibrated using standard buffers of pH 4, 7 and 10 at 298 K.

2.2.5. Rotary evaporator

A rotary evaporator (model R-3000) was procured from M/s Buchi Laboratory Technique AG, Switzerland and used for distilling off the volatile solvents during the preparation of impregnated resins for the extraction chromatographic studies.

2.2.6. Inductively coupled plasma-optical emission spectrometer (ICP-OES)

Ultima C spectroanalyser (M/s JobinYvon, France) equipped with Inductively Coupled Plasma (ICP) excitation source was used for various inactive elemental analysis required in this study. The spectrometer provides a resolution of 0.015 nm with a polyscan facility of ± 2 nm. RF generator of 40.68 MHz with a maximum output power of 1550 W was used for plasma generation. Samples were injected by the in-built peristaltic pump with its associated flow rate of 1 mL/min. The most sensitive emission lines were chosen for the given element that had no interference from other elements in the group.

2.2.7. SEM-EDX

While the Field Emission Gun-Scanning Electron Microscopy (FEG-SEM) images were obtained using TESCAN MIRA 3 model at 15 kV, the Energy Dispersive X-ray spectral analysis (EDX) image was recorded using an Oxford instrument for the surface morphology as well as for the elemental composition of the materials.

2.2.8. XRD

The X-ray diffraction (XRD) pattern of the materials was obtained using a Philips 1011 X-ray diffractometer that operated at 40 kV and 45 mA with Cu K_α (1.5406 Å) radiation.

2.2.9. Rotospin

A rotospin was procured from M/s Tarsons Products Pvt. Ltd., Kolkatta, India and was used in batch studies for the determination of distribution ratio values.

2.3. Experimental procedures

2.3.1. Characterization of PFTS at KAMINI reactor - Determination of the parameters f & α

Considering the wide variation of their resonance energies, the flux monitors Al-0.1%Au wire, Zr and Zn foils were chosen for the study of the determination of parameters f and α [2]. The foils were cleaned with alcohol and the bare as well as cadmium covered foils were doubly sealed in polythene bags. The bare and cadmium covered flux monitors were irradiated at PFTS position of KAMINI reactor at 20 kW power for 2 h and 4.2 h, respectively. The thickness of the cadmium (Cd) foil was restricted to 0.5 mm even though 1.0 mm thickness was preferable because of the limited permissibility of Cd mass in the reactor [3]. After the irradiation, the foils were sufficiently cooled to bring down the initial radiation dose to an acceptable level before its transfer to Radiochemistry Laboratory (RCL) for the subsequent analysis of their activation products.

2.3.1.1. Assay of flux monitors

All the irradiated foils were assayed using HPGe detector at a reproducible geometry with its pre-determined detection efficiency. The efficiency of the HPGe detector was calibrated using ^{152}Eu standard point source. The detector has a 30% relative efficiency with a resolution of 1.9 keV at 1332 keV of ^{60}Co. The peak areas were evaluated using the peak fitting software PHAST. The specific count rates (A_{sp}) of the activated products ^{198}Au, ^{95}Zr and ^{65}Zn were used to evaluate the f and α values. The nuclear data of the above flux monitors are presented in Table 2.1.

Table 2.1. The nuclear data used in the determination of *f* and *α* values [3]

Target	Q_0	$\bar{E}_r$ (eV)	Corresponding activation product	$T_{1/2}$ (d)	E_γ (keV)	$k_{0,Au}$ (% uncertainty)
^{197}Au	15.71	5.65	^{198}Au	2.695	411.8	1
^{64}Zn	1.908	2560	^{65}Zn	244.3	1115.5	5.72E-3 (0.4)
^{94}Zr	5.31	6260	^{95}Zr	64.02	724.2	8.90E-5 (1.3)
					756.7	1.10E-4 (1.3)

2.3.2. Foil activation method

Multi-foil activation method [4,5] was employed for the characterization of the neutron energy spectrum at the PFTS of KAMINI reactor. The PFTS is the position, mostly used for NAA with its associated neutron spectrum of thermal, epithermal and fast neutron components. Thus, the above mentioned foils were chosen for the present study, in order to investigate the sensitivities of the entire energy of the spectrum from thermal to fast neutron region.

All the activation foils used in the present study with their natural compositions are presented in Table 2.2 along with their irradiation details and activation data. The foils were weighed accurately, sealed placed in polypropylene containers and irradiated in PFTS position at 20 kW power. The irradiation period (T_{irr}) was chosen based on the half-lives of their corresponding activated products and their associated cross-sections for activation.

Table 2.2. Nuclear reaction characteristics of the various foils used in this study

Foil	**Associated Nuclear Reaction**	**Irradiation Period (h)**	**Reaction cross Section (b)**	**$E_{threshold}$ (MeV)**	**$t_{1/2}$**	**Mass of the Foil (mg)**
0.1% Au-Al	$^{197}Au(n,\gamma)^{198}Au$	2	98.8	$2.5*10^{-8}$	2.69 d	5.65
Co	$^{59}Co(n,\gamma)^{60}Co$	2	37.4	$2.5*10^{-8}$	5.27 y	1.43
Fe	$^{58}Fe(n,\gamma)^{59}Fe$	6	1.28	$2.5*10^{-8}$	45.1 d	15.6
Mo	$^{98}Mo(n,\gamma)^{99}Mo$	6	0.13	$2.5*10^{-8}$	67 h	10.6
In	$^{115}In(n,n')^{115m}In$	2	0.17	1.2	4.5 h	5.18
Ni	$^{58}Ni(n,p)^{58}Co$	2	0.109	2.8	72 d	7.9
Fe	$^{54}Fe(n,p)^{54}Mn$	2	0.078	3.1	310 d	10.82
Al	$^{27}Al(n,p)^{27}Mg$	0.5	$4.1x10^{-3}$	4.4	9.5 m	2.13
Ti	$^{48}Ti(n,p)^{48}Sc$	2	$3.0x10^{-4}$	7.6	44 h	9.65
Y_2O_3	$^{89}Y(n, 2n)^{88}Y$	6	$1.5x10^{-4}$	11.7	106 d	11.25

After irradiation, the foils were sufficiently cooled to bring down the radiation dose to the accepted level before taking up their assay by high resolution gamma ray spectrometry. The short-lived nuclides were assayed at the Neutron Activation

Analysis Laboratory – KAMINI (NAAL - KAMINI) and long lived nuclides were analyzed at RCL using the HPGe detector with resolution of 1.9 keV at 1332 keV of ^{60}Co. The activation foils were assayed at suitable distances from detector depending upon the observed dead time as well as the required count rate. All the foils were assayed for sufficiently long time to achieve a good counting statistics. The assay was repeated several times for each activation foil to evaluate the error propagation. The detection efficiency was established previously using ^{152}Eu standard source before the assay of the activated foil in the reproducible geometry. All the peak areas were evaluated using the peak fitting software PHAST.

2.4. Installation of Fast Flux Experimental Facility (FFEF) at FBTR

Development of a FFEF with a sample holder [6] was envisaged to carry out the studies on fast neutron activation analysis, fission studies and minor actinide transmutation studies in FBTR. The above studies were expected to be carried out at 400 kW power of the reactor with liquid sodium temperature being around 400 ^{o}C. The rod attached to the bottom of the central canal plug itself could undergo all possible nuclear reactions and hence it was necessary to compute the dose due to this rod under various irradiation conditions. As titanium was chosen as the material of construction for this facility, the computations of the radiation dose for titanium due to its irradiation in FBTR was taken up.

2.4.1. Analysis of the impurities in titanium

The radiation dose due to the continuous irradiation of the lengthy titanium rod along with its sample holder was measured. The location of the sample holder was assumed to be 28.5 cm above the top of the central subassembly while the corresponding neutron flux in this location was assumed to be 1.16E+13 $cm^{-2}.s^{-1}$. Computations of the radiation dose were carried out using Ti as the matrix material for its associated natural isotopic composition (Table 2.3).

The two major sources of activation reactions are (i) the nuclear reactions occurring in the matrix material (Ti) and (ii) the activation of the impurities present in the matrix.

Table 2.3. Natural isotopic composition of Ti

Ti - Isotope	Abundance (%)
^{46}Ti	8.25
^{47}Ti	7.44
^{48}Ti	73.72
^{49}Ti	5.42
^{50}Ti	5.15

The elemental impurities present in the titanium material were analysed by both relative as well as k_o-based internal mono-standard neutron activation analysis (IM-NAA) methods. High purity titanium strips along with the reference materials (IAEA Reference Materials, SL-1) were irradiated for the analysis. The titanium samples were irradiated for a period of 7 h in self-serve position of CIRUS reactor, Bhabha Atomic Research Centre (BARC) at a neutron flux of $3x10^{13}$ $cm^{-2}.s^{-1}$ to profile the activated products of long and medium half-lives. Ti samples of 10 mg were also irradiated for a short period of 1 min at pneumatic carrier facility (PCF), Dhruva reactor, BARC with its associated neutron flux of $5x10^{13}$ $cm^{-2}.s^{-1}$ to profile the short lived activation products. The irradiated samples were assayed for the estimation of the short-lived activation products. Radiometric assay of all the activation products was carried out using HPGe detector and the spectra were analyzed using PHAST software.

2.4.2. Radiation dose computations

The following nuclear reactions were considered for the computation of radiation dose due to the irradiation of the titanium matrix, and the activated products produced there on with reasonable half-life as well as significant gamma intensities i.e. $^{46\text{-}50}$Ti(n, p), ^{48,50}Ti(n, α), ^{46}Ti(n, 2n) and ^{50}Ti(n, γ). However, the radiation dose due to the impurities present in the titanium matrix was considered only through (n, γ) reaction and the contribution to the overall dose due to other particle emission reactions from these impurities was expected to be negligible owing to their trace level quantity as well as the nature of the threshold activation reactions.

Considering a typical operation cycle in FBTR, a conservative irradiation period of 10 days followed by an hour of cooling was assumed to compute the activity induced per unit volume under these conditions. Assuming the dimensions of the rod being 1.1 m length and 12 mm diameter, the total activities and the gamma emission rates were calculated. The corresponding dose was computed by assuming the activated rod being a line source.

2.4.3. Simulation run with aluminium foils

A simulation study was carried out at RCL to evaluate the stability and phase changes of the Al foil during its usage as the catcher foil at the typical operational temperature of FBTR at 400 kW. Two Al foils of similar dimensions were matched over each other and wrapped the same again with another Al foil simulating the actual sample prepared for the irradiation. The above Al foil was heated in a furnace for 6 h in air ambience at the conservative temperature of 450 ^oC, even though FBTR operational temperature is only around 400 ^oC at 400 kW power. The foil was allowed to cool to room temperature and the changes, if any, in the surface morphology and phase of the heat treated Al foils were evaluated with reference to the fresh Al foil by analysing them both using SEM coupled with EDX and XRD techniques.

2.4.4. Neutron flux measurement studies at FFEF

A gold foil weighing 10.01 mg with 0.1 mm thickness was cleaned with alcohol and wrapped in an aluminium foil of 14.22 mg weight. The wrapped foil was loaded into the titanium sample holder which was attached to the bottom of the lengthy titanium rod. This was again inserted into the reactor core from top of reactor core building (RCB) and was positioned just above the top of the central fuel subassembly. The reactor was operated at a power of 25 kW for an irradiation period of 4 h. At the end of the irradiation, the sample holder was cooled for an hour so that the radiation dose due to the short lived activation products was brought down. The titanium rod was lifted completely with the help of a mechanical crane and the sample holder was removed into a tastena meant exclusively for the containment of sample holder [7]. The measurement of the radiation dose of the sample holder as well as the surface contamination tests were carried out by the health physicist. The sample holder along with the foil was transferred to RCL. The irradiated foil was taken out from the sample holder and the gold foil was removed from the aluminium wrapper and the same was transferred into a polythene bag. The induced radioactivity was measured by using high resolution gamma-ray spectrometry. The irradiated gold foil was assayed at a geometrical position whose efficiency was pre-calibrated using ^{152}Eu standard source. The spectra were analysed for the peak areas using the peak fitting software, PHAST.

2.5. Studies on the determination of fission yields at KAMINI and FBTR

2.5.1. Irradiation of uranium foil at KAMINI reactor

Recoil catcher technique was used to trap the recoiled fission products covering 2π solid angle of their emission from the irradiated target [8]. A uranium foil of 169 mg with 0.1 mm thickness was cleaned with alcohol and dried. The foil was then sandwiched between two aluminium (Al) catcher foils in order to facilitate the capture of the recoil fission products from the nuclear fission of the uranium foil. The above sample was wrapped further with an Al foil and the same was irradiated in KAMINI reactor for a period of 6 h.

2.5.2. Analysis of catcher foils and uranium target

The irradiated uranium foil along with the catcher foils were transferred to RCL and separated from each other. The catcher foils and the uranium foil were counted individually by high resolution gamma-ray spectrometry using HPGe detector and the spectra were analysed.

2.5.3. Irradiation of PuO_2-ZrO_2 targets at FBTR

The fissile targets of 15 wt% PuO_2-ZrO_2 with 2 μm thick nickel coating were prepared and fixed in foil holders. The foil holders were loaded again vertically in two different capsules which were loaded into different subassemblies called ISZ-100. These subassemblies were finally loaded at centre and third ring of FBTR core. The irradiation of the foils was carried out for 4 h at the reactor operating power of 25 kW.

The isotopic composition of plutonium and masses of PuO_2-ZrO_2 targets employed are presented in Table 2.4 and 2.5, respectively.

Table 2.4. Isotopic composition of Plutonium used for FBTR irradiation

Isotope	Composition (%wt)
^{238}Pu	0.0226
^{239}Pu	93.33
^{240}Pu	6.108
^{241}Pu	0.509
^{242}Pu	0.0275

Table 2.5. Masses of PuO_2-ZrO_2 targets irradiated in FBTR

Core Centre		Third Ring	
Foil ID	**Weight (mg)**	**Foil ID**	**Weight (mg)**
FH28	136.78	FH25	124.73
FH32	138.85	FH74	134.56
FH49	144.4	FH47	136.11
FH51	125.45	FH40	116.23
FH59	141.56	FH60	147.31
FH27	129.50	FH38	129.97
FH63	131.87	FH43	138.84

2.5.4. Analysis of PuO_2-ZrO_2 targets by HPGe detector

The irradiated foils were sufficiently cooled in order to facilitate their handling with the permissible levels of radiation dose. They were unloaded from the foil holders, sealed in polythene bags and assayed by high resolution gamma spectrometry using HPGe detector. The foils were conveniently assumed to be point sources in order to use the efficiency calibration obtained using ^{152}Eu point standard source. The reaction rates were calculated using reactor physics codes and used them for the estimation of fission yields of various fission products along the length of the capsule. The fission yields were compared for the targets irradiated in core centre and third ring of the reactor.

2.6. Radiochemical purification studies of ^{144}Ce-^{144}Pr

2.6.1. Batch studies

Batch studies were carried out for the determination of distribution ratio values of fission products with Dowex 50WX8 (100-200) resin as a function of nitric acid concentration. A simulated fission product solution was prepared using the corresponding radioactive tracers such as ^{141}Ce, ^{137}Cs, $^{85+89}$Sr, ^{58}Co and ^{54}Mn. The simulated solution was used to determine the distribution ratios of some of the long lived fission products (^{144}Ce, ^{137}Cs, ^{90}Sr) and activation products (^{60}Co, ^{54}Mn) in Dowex resin. Equilibration tubes with known amount of Dowex 50WX8 (100-200) resin and different concentrations of HNO_3 i.e. 0.5, 1, 2, 4 and 6M were taken with the required amount of simulated fission product solution. The tubes were properly sealed and equilibrated continuously for a period of 4 h using a roto-spin. The contents of the tube were allowed to settle after which it was centrifuged. An aliquot of the centrifuged solution was sampled and assayed by high resolution gamma ray spectrometry.

2.6.2. Purification of ^{144}Ce-^{144}Pr from dissolver solution by ion-exchange chromatography

An aliquot of irradiated (U,Pu)O_2 fuel dissolver stock solution was taken and dried under IR lamp. The input feed for ion-exchange chromatography was thus prepared by dissolving the above residue in 0.001M nitric acid. 1 g of Dowex 50W×8 (100-200) resin was kept for overnight soaking in 0.001M HNO_3 which was made into a slurry form. The resin was loaded into a glass column of dimensions of 25 cm length and 8 mm ID. After loading, the resin bed height was found to be about 4 cm. The column was conditioned with the nitric acid concentration of the feed solution i.e. 0.001M. The feed solution of irradiated (U,Pu)O_2 dissolver solution was introduced into the column and the elution was started initially using 1M nitric acid (0-80 mL) followed by 6M nitric acid (80-100 mL). The flow rate was maintained at 0.4-0.5 mL/min throughout the elution. The fractions of 10 mL each were collected every time in a glass vial and the assay of the same was carried out by using high resolution gamma ray spectrometry.

2.6.3. Purification of HDEHP

Di-(2-ethylhexyl) phosphoric acid (HDEHP) was used as an extractant in the present study to purify the parent (^{144}Ce) from its in-grown daughter product (^{144}Pr), as well as from the other radioactive impurities in the fraction collected from ion-exchange chromatography. Initially, purification of HDEHP was carried out by the selective precipitation of the copper-HDEHP salt [9]. Approximately 1M HDEHP in cyclohexane was saturated with copper (II) for the effective precipitation by adding NaOH to an aqueous solution of $CuSO_4$ which was in contact with the organic phase. After removal of the aqueous phase, acetone was added slowly into the well stirred organic phase that precipitated Cu-HDEHP complex. The precipitate was filtered subsequently, washed with acetone, air dried and contacted with 0.5M hydrochloric acid and Millipore water. Further, the HDEHP was heated to about 60 °C at reduced pressure using a rotary evaporator. The above purified HDEHP was used for the subsequent separation studies.

2.6.4. Purification of the parent ^{144}Ce by solvent extraction

The purified ^{144}Ce-^{144}Pr sample fraction with the trace level of fission product impurities (^{154}Eu) obtained from the above procedure was evaporated to dryness under IR lamp. The residue was dissolved in 5 mL of concentrated nitric acid. 30 mL of 1M potassium bromate in 9M HNO_3 was added to this solution. 10 mL of the solution was taken into a separating funnel to which a freshly prepared 5 mL of 1M $KBrO_3$ was added again [10]. 0.7M HDEHP in n-heptane was added to the separating funnel and the mixture was equilibrated for a period of 5 minutes. The mixture was allowed to settle down for a minute for effective phase separation. A 2 mL fraction of the organic phase was assayed for its total activity using NaI(Tl) as well as HPGe detector.

2.6.5. Secular equilibrium

The sample was assayed by a well-type NaI(Tl) scintillation detector in an integral mode where the lower level discriminator (LLD) and shaping time were set to 0/50 and 1 μs, respectively in the single channel analyser (SCA). The coarse and fine gains were fixed at 200 and 9/60, respectively in spectroscopy amplifier. The total activity of the sample was recorded by counting it in regular intervals for two hours duration using NaI(Tl) detector. The counting was carried out for 30 sec duration with an interval of equal duration of 30 sec between the countings for the initial 20 minutes and later the counting duration was maintained same i.e for 30 sec while the interval between the successive countings was increased to 5 minutes for the next 100 min duration. The sample was assayed again by high resolution gamma spectrometry using HPGe detector. The decay curve was profiled by plotting the total activity against the time of counting on a semi-log graph paper.

2.6.6. Preparation of HDEHP impregnated Amberlite XAD-7 resin

The Amberlite XAD-7 beads were washed with 4M nitric acid, distilled water and acetone in the same order and dried at 40 °C [11]. The purified and accurately weighed XAD-7 resin was mixed with appropriate amount of HDEHP in a reagent bottle corresponding to 40% (w/w) HDEHP coated XAD7 resins. *n*-hexane, a diluent was added to this mixture and the same was equilibrated for 2 h using a mechanical stirrer to facilitate an uniform distribution of HDEHP on to the resin. After the equilibration, the diluent n-hexane was evaporated using a rota-evaporator and the resin was dried at 60 °C for about an hour.

2.6.7. Purification of the daughter nuclide ^{144}Pr by using extraction chromatography

About 5 g of 40% (w/w) HDEHP-XAD-7 resin was made into its slurry form using 0.1M HNO_3 and the same was loaded into a glass column of 25 cm length and 1 cm ID resulting into a resin bed height of 10 cm. The column was conditioned with 1M $KBrO_3$ solution prepared using 9M HNO_3. The tracer mixture of ^{144}Ce-^{144}Pr in 1M $KBrO_3$ was loaded on to the column. The elution was initially started with 1M $KBrO_3$ at its corresponding flow-rate of 0.8-0.9 mL/min. Sample fractions of 15 mL were collected every time and the same were assayed using HPGe detector. At the end of the elution, the chromatographic column was washed using 9M HNO_3 in order to maintain the column free from the eluent, 1M $KBrO_3$. Periodical assay of the purified sample of ^{144}Pr was carried out for a duration of 100 min to establish the decay profile of ^{144}Pr followed by the determination of its half-life graphically.

2.7. Radiochemical purification studies of ^{90}Sr and ^{89}Sr

2.7.1. Elution profile of fission products in FBTR irradiated $(U,Pu)O_2$ fuel dissolver solution using Dowex resin with the eluent SMP

A small fraction of 0.25 mL of the irradiated (U, Pu)O_2 fuel dissolver stock solution was taken in a glass vial and dried under IR lamp. The residue was taken into 0.1M SMP solution which became feed solution for the ion-exchange chromatography. The behaviour of ^{90}Sr, a pure beta emitter was followed through gamma assay by adding its gamma emitting tracer $^{85+89}$Sr. 2 g of Dowex 50Wx8 (100-200) resin was kept for overnight soaking in 0.1M SMP which was later made into a slurry form to load into a glass column of the dimensions of 25 cm length and 8 mm ID. The glass column was tapped during the loading of the resin for ensuring the efficient filling of the resin particles. The resultant resin bed height in the column was found to be about 8 cm. The column was conditioned initially using 0.1M SMP and the feed solution was transferred into the column gradually. The elution was initiated using 40 mL of 0.05M SMP followed by 60 mL of 0.1M SMP. The elution flow rate was maintained at 0.4-0.5 mL/min throughout the experiment. The samples of 5 mL fractions were collected in gamma vials during the elution and the same were assayed using HPGe detector.

2.7.2. Distribution ratio measurement

From the elution behavior studies of irradiated fuel solution in Dowex resin with SMP, it was observed that the long lived fission products such as ^{137}Cs and ^{90}Sr were held strongly in the column. Hence, this novel eluent was proposed for the separation of ^{89}Sr from the FBTR irradiated yttria solution as well.

The distribution ratios of the various radioisotopes present in FBTR irradiated yttria dissolver solution containing SMP in 0.1M HNO_3 of different strengths were evaluated through batch method for the Dowex 50WX8 (100-200) resin. Equilibration tubes with known amount of Dowex resin, different concentrations of SMP i.e. blank, 0.025, 0.05, 0.075, 0.1, 0.3, 0.5M and the required amount of each tracer such as $^{85+89}$Sr, ^{54}Mn, ^{60}Co, ^{88}Y and ^{65}Zn in μCi range were equilibrated for 4 hours using a roto-spin. The centrifuged samples were assayed for their gamma contents using HPGe detector.

2.7.3. Separation profiles for the simulated sample

A simulated sample as that of the FBTR irradiated yttria dissolver solution containing the radioactive tracers $^{85+89}$Sr, ^{54}Mn, ^{60}Co, ^{88}Y, ^{139}Ce, ^{65}Zn etc. in the μCi range was prepared in 0.1M SMP solution [12]. 1 g of Dowex resin was loaded in its slurry form into a glass column of the dimension of 0.5 cm ID and 25 cm of length that resulted into a resin bed height of 9 cm. The column was conditioned initially using 0.1M SMP. The simulated feed solution was passed through the Dowex resin with the flow rate of 0.1-0.15 mL/min. Elution started initially using 0.1M SMP followed by 4M nitric acid. Sample fractions of 5 mL size were collected every time and were assayed by high resolution gamma spectrometry.

2.7.4. Purity evaluation of ^{89}Sr source from the possible contamination of the eluent SMP

During the purification of ^{89}Sr source from the irradiated dissolver solution, the various impurity elements such as Y, Zn, Mn, Co, Eu, Ce and Tb were complexed and eluted using 0.1M SMP whereas the pure Sr fraction was subsequently eluted from the column using 4M HNO_3. However, an investigation was carried out to establish that the pure Sr fraction obtained by the above method was free from the possible residual impurities of sodium ions and its anionic moiety of SMP.

Thus an experiment was carried out using SMP containing radioactive tracers ^{24}Na and ^{32}P for sodium and phosphorous, respectively. On irradiation in KAMINI reactor at Kalpakkam, the Na and P present in SMP were activated to ^{24}Na and ^{32}P via ^{23}Na (n, γ) ^{24}Na and ^{31}P (n, γ) ^{32}P, respectively. The above purification experiment was repeated using 20 mL of 0.1M SMP but containing 0.5 mL of the activated SMP as well as 25 µL of $^{85+89}$Sr tracer, all of them being in µCi range. The same was passed through the blank Dowex 50WX8 column which was earlier conditioned using 0.1M SMP as earlier. The column was later washed with 50 mL of distilled water followed by elution using 50 mL of 0.5M HNO_3. After ensuring the complete elution of Na and P from their respective tracers in the samples, the column was further eluted using 20 mL of 4M HNO_3 to collect the Sr fraction. The eluted fractions were collected in 5 mL lots and were analyzed both by gamma spectrometry using HPGe detector for $^{85+89}$Sr and ^{24}Na as well as Cerenkov counting for the assay of pure beta emitter of ^{32}P. The elution procedure followed in this experiment was basically identical as that of the one standardized for Sr purification described in the previous section but for the washing of the column with distilled water and 0.5M nitric acid just before collecting the Sr fraction in 4M HNO_3.

2.7.5. Purification of ^{89}Sr from the irradiated yttria dissolver solution

^{89}Sr, a medically useful radioisotope was produced via ^{89}Y(n, p)^{89}Sr using yttria target irradiation in FBTR. The radiochemical processing of irradiated yttria pellets was already established previously [13]. The sintered yttria pellets were packed into a quartz tube and was accommodated into a stainless tube again. The same was irradiated in FBTR with its flux of ~ 10^{15} n.cm^{-2}.s^{-1}. The 114 days-irradiated yttria pellets of 62 numbers each weighing about ~0.35 g were dissolved in hot quartz distilled 9M nitric acid. The bulk target yttrium in the dissolver solution was removed using TBP by solvent extraction technique. The aqueous phase obtained after the separation of bulk yttrium contained Sr along with other radionuclidic impurities including a trace amount of Y.

Known amount of the above aqueous phase containing Sr and trace impurities was evaporated to dryness under IR lamp and the residue was taken into 0.1M SMP to which added further the tracer $^{85+89}$Sr. The addition of the tracer $^{85+89}$Sr with its gamma signature became necessary to monitor the separation of ^{89}Sr, a pure beta emitter produced during the irradiation. This became the feed solution for the subsequent purification of ^{89}Sr source by ion exchange chromatography. The conditioned feed solution was introduced into 1 g of Dowex 50WX8 (100-200 mesh) resin packed in the glass column which was already previously conditioned using 0.1M SMP. Purification of ^{89}Sr from the various other impurities such as ^{60}Co, ^{65}Zn, ^{54}Mn, ^{192}Ir, ^{86}Rb, ^{113}Sn, ^{103}Ru, ^{58}Co, ^{88}Y etc was achieved using the standardized procedure as described in the previous section. Initial elution was started using 40 mL of 0.1M SMP followed by i) 10 mL of distilled water, ii) 40 mL of 0.5M HNO_3 and finally, iii) 10 mL of 4M HNO_3 in the same order. The flow rate was maintained in the range of 0.1 to 0.15 mL/min throughout the experiment. All the samples of 5 mL size were collected every time and assayed using HPGe detector.

The same experiment was repeated using 2 g of Dowex 50WX8 (100-200 mesh) but using 4M HCl as medium of elution in place of HNO_3 and a column of different size i.e. 8 mm ID and 25 cm length in order to obtain directly the ^{89}Sr source in the HCl medium as required in its final use [14]. This reduces the burden of nitrate impurity, the requirement for the quality control of ^{89}Sr source even though nitric acid medium was preferred over hydrochloric acid to minimize the acid corrosion of hot cell facility during the chemical processing of the irradiated yttria pellets. Final experiment was carried out with the dissolver solution but without addition of the tracer $^{85+89}$Sr to obtain pure ^{89}Sr source from the irradiated yttria target. The eluted Sr fraction containing ^{89}Sr alone was quantified using Cerenkov counting as well as liquid scintillation counting. The same was confirmed again by long counting of the weak gamma signature (909.0 keV with intensity of 0.00956 %) of ^{89}Sr using HPGe detector.

2.7.6. Quantification of ^{89}Sr

The pure ^{89}Sr fraction obtained from the above separation was quantified using M/s HIDEX 300 SL liquid scintillation counting (LSC) system by both LSC as well as Cerenkov counting modes. Efficiency of the LSC system was calibrated for LSC and Cerenkov assay using standard sources of pure beta emitters such as ^{3}H, ^{99}Tc, ^{204}Tl, ^{89}Sr, ^{32}P and ^{90}Sr-^{90}Y (Table 2.6). The standards were taken into a liquid scintillation counting vial in 0.1M HNO_3 medium for Cerenkov counting and in MAXILIGHT cock-tail medium for liquid scintillation counting. All of them were assayed using HIDEX LSC system. The purified ^{89}Sr fraction was assayed by both LSC and Cerenkov counting techniques using HIDEX beta counting instrument and its yield was established using the efficiency calibration.

Table. 2.6. β^-_{max} energies of standard radioactive sources

S.No	Beta Standard	β^-_{max} (keV)
1	^{3}H	18.6
2	^{99}Tc	293.8
3	^{204}Tl	763.7
4	^{89}Sr	1495
5	^{32}P	1710
6	^{90}Sr-^{90}Y	2280

2.8. Radiochemical Processing of ^{32}P from irradiated sulphur bearing targets

2.8.1. Processing of irradiated Magnesium sulphate target

10 g of magnesium sulphate was doubly sealed in a polythene cover and irradiated in KAMINI reactor for 4 h 22 min at south thimble position which has the thermal neutron flux of $3.6\text{x}10^{8}$ cm^{-2}.s^{-1}. The stock solution of the irradiated target was prepared by dissolving it in 25 mL of 10^{-4} M nitric acid. An aliquot of 5 mL of the stock solution was used to standardize the method of purification of ^{32}P source from the irradiated target. 0.5 mL of 3% H_2O_2 was added to the aliquot of 5 mL dissolver solution and the same was heated to 70 ^{o}C for few minutes. This step was repeated with addition of another 0.5 mL of 3% H_2O_2. Addition of H_2O_2 ensured all ^{32}P was converted into its phosphate form. The solution was agitated for 30 minutes with a

magnetic stirrer. Required amount of 25% ammonium hydroxide was added to the above solution till phosphate was precipitated as magnesium ammonium phosphate (Struvite) at the pH of 8-10 [15].

The supernatant was assayed by Cerenkov counting technique to estimate the ^{32}P that remained un-precipitated in the solution. The suspension was filtered through a sintered glass of medium porosity and the filtered precipitate was taken into solution by dissolving it in 5 mL of 0.5M HCl. The solution was evaporated to dryness with an IR-lamp and the residue was taken into a 5 mL of 10^{-3}M HCl. This became the feed solution for the subsequent purification of the source by ion-exchange chromatography technique. A small fraction of this feed solution i.e. 0.5 mL was analysed for its ^{32}P and Mg content by Cerenkov counting technique and Ethylene di-amine tetra-acetic acid (EDTA) titration, respectively

The slurry form of the cationic resin Dowex 50WX8 (100-200 mesh) weighing about 2 g was packed in a glass column having dimensions of 8 mm ID, 21 cm length and resulted into a bed height of 9 cm. The column was initially conditioned using 10^{-3}M HCl. The feed solution conditioned in HCl medium of the same concentration was loaded into the column and the elution was started using 10^{-3}M HCl solution. The sample fractions collected every time were of 5 mL size with a flow rate maintained about 0.5 mL/min. After eluting with the initial 30 mL, the eluent was changed from 10^{-3}M to 1:1 HCl to remove Mg from the column. The eluted sample fractions were analysed for ^{32}P content using Cerenkov counting and Mg content by complexometric titration using EDTA.

2.8.2. Processing of irradiated Strontium sulphate target

About 1 g of $SrSO_4$ was doubly sealed in a polythene cover and irradiated for 6 h in KAMINI reactor at PFTS, the available irradiation position of maximum thermal neutron flux of 1.6×10^{11} $cm^{-2}.sec^{-1}$.. A fraction of the irradiated $SrSO_4$ target was dissolved in water and precipitated by adding sodium carbonate with heating and stirring for about 2 hours. The strontium carbonate precipitate was filtered using Whatman-42 filter paper and the residue and filtrate were treated by cation-exchange chromatography to purify the ^{32}P, as indicated below.

The residue was dissolved in HCl medium followed by the addition of ferric chloride and ammonium hydroxide to scavenge the ^{32}P as its ferric phosphate into the ferric hydroxide precipitate. The precipitate was washed with Millipore water and was taken into 1M HCl. This solution was evaporated to dryness and conditioned to 0.1M HCl. Similarly the ^{32}P content from the filtrate was also collected as ferric phosphate using ferric hydroxide precipitate and the same was brought into 0.1M HCl medium as described above.

The conditioned solutions from residue and filtrate were mixed and taken as feed for the purification of its ^{32}P content by cationic exchange chromatography using Dowex 50WX8 (100-200) resin. The feed solution was passed through a glass column containing 2 g of Dowex resin which was pre-conditioned using 0.1M HCl. Elution was started with 0.1M HCl to wash ^{32}P in its phosphate form followed by 3M HCl to wash off Sr and Fe content from the column. The eluted samples were collected in 5 mL size and ^{32}P was quantified by Cerenkov counting. The elution profile of ^{89}Sr and ^{85}Sr produced during the irradiation were also established by the assay of ^{85}Sr by gamma spectrometry using HPGe detector and ^{89}Sr by Cerenkov counting. Fe content of the samples was profiled using inductively coupled plasma - optical emission spectroscopy (ICP-OES).

5 mL of the purified ^{32}P source from both the processed targets i.e. magnesium sulphate and strontium sulphate was assayed by Cerenkov counting to quantify its ^{32}P yield and also by high resolution gamma spectrometry using HPGe detector to determine the presence of any other gamma emitting impurities.

2.8.3. Processing of irradiated Sulphur powder – Leaching method

About 5 g of sulphur powder was irradiated in thimble position of KAMINI reactor for 6 h with its associated flux of about 10^8 n.cm^{-2}.s^{-1}. The irradiated target was treated with 10 mL of glacial acetic acid and heated on a hot plate to the boiling point of the medium i.e. 120 ^{o}C for 20 min. During this process the sulphur was melted releasing the ^{32}P as phosphate into the acetic acid medium [16]. The mixture was allowed to cool to room temperature and the sulphur was solidified. The supernatant containing ^{32}P was filtered and collected using Whatman 542 filter paper. This process was repeated four times with the filtered solid sulphur using fresh acetic acid every time and collected the filtrates containing ^{32}P. The filtrates added together contained the total ^{32}P produced in the target and was assayed by Cerenkov counting. The above procedure was repeated with a slight modification in cooling process i.e. the cooling of the mixture was made rapid by adding cold water instead of natural cooling in the fume hood. The fraction containing total ^{32}P was conditioned into 0.1M HCl medium and the same was purified from any other impurities, if present by cationic exchange chromatography using DOWEX 50WX8 (100-200) resin.

About 5 g of Dowex 50WX8 (100-200 mesh) resin was washed with Millipore water as well as 0.1M HCl and kept for overnight soaking in the same medium. The resin in its slurry form was filled into a glass column of the dimensions of 1 cm ID and 30 cm length and the bed height was about 9 cm. The column was conditioned with 40 mL of 0.1M HCl. An aliquot of the ^{32}P feed solution from natural cooling method was introduced into the column. The column was eluted with 0.1M HCl followed by 6M HCl. The source ^{32}P was collected as phosphoric acid in dilute HCl medium. The same procedure was repeated for the radiochemical processing of ^{32}P for the sample obtained from the rapid cooling method also. The analysis of the eluted samples for ^{32}P was accomplished by Cerenkov counting. The decay process of the purified ^{32}P source was profiled using Cerenkov counting and the determination of its half-life graphically from the decay curve so obtained helped in ascertaining its purity against other beta impurities, if any.

2.8.4. Processing of irradiated Sulphur powder – Distillation method

About 300 mg of sulphur powder was doubly sealed and irradiated in PFTS position of KAMINI reactor for 6 h with a flux of about $1.6x10^{11}$ $n.cm^{-2}.s^{-1}$. The irradiated target was transferred to a distillation chamber which was connected to a series of bubblers to trap the hazardous sulphur vapours from its release to atmosphere. The distillation chamber with sulphur powder was heated to the temperature of 250 ^{o}C - 300 ^{o}C [17]. After complete distillation of sulphur powder, the distillation chamber was allowed to cool to room temperature. The ^{32}P residue in the distillation chamber was leached out in 10 mL of 0.1 M HCl at 60-70 ^{o}C.

The leached ^{32}P was purified from cationic impurities, if any using Cation-exchange chromatographic technique (Dowex 50WX8 (100-200). The resin was made into slurry form using 0.1M HCl and transferred to glass column of the dimensions of 1 cm ID and 30 cm length and the resultant resin bed length was about 9 cm. The column was conditioned using 50 mL of 0.1M HCl. The feed solution of ^{32}P was added to the column and the elution of ^{32}P was started with 0.1M HCl followed by 6M HCl to remove any other cationic impurities, if present in the resin. The samples were collected in 15 mL size and assayed by Cerenkov technique.

The results obtained using all the experiments described here are discussed in the subsequent chapters.

2.9. References

1. P. K. Mukhopadhyay, The operating software of the PHAST PC-MCA Card, Proceedings of the Symposium on Intelligent Nuclear Instrumentation (INIT-2001), Bhabha Atomic Research Centre, Mumbai, India (2001) pp. 307–310.
2. F. De Corte, A. Simonits, A. De Wispelaere, J. Hoste, Accuracy and applicability of the k_0-standardization method, J. Radioanal. Nucl. Chem. 113 (1987) 145-161.
3. J. S. Brahmaji Rao, E. Senthilvadivu, N. P. Seshadreesan, R. Acharya, C. R. Venkatasubramani, A. V. R. Reddy, Characterization of pneumatic fast transfer system irradiation position in KAMINI reactor for k_0-based NAA, J. Radioanal. Nucl. Chem. 294 (2012) 137-141.
4. A. Seghour, F. Z. Seghour, Neutron energy spectra unfolding from foil activation detector measurements with MINUIT, Nucl. Instrum. Methods. Phys. Res. A 555 (2005) 347-355.
5. L. Yuan-Hao, N. Sander, L. Hong-Ming, M. Ray, J. Shiang-Huei, Monte Carlo determined self-shielded group-wise cross-sections for the activation foil stack applied in the epithermal neutron spectrum adjustment, Nucl. Instrum. Methods. Phys. Res. A 602 (2009) 557-563.

6. K. V. Suresh Kumar, A. Babu, B. Anandapadmanaban, G. Srinivasan, Twenty five years of operating experience with the Fast Breeder Test Reactor, Energy Procedia 7 (2011) 323-332.
7. M. T. Jose, T. Ravi, V. Meenakshisundaram, V. M. Raghunath, Primary sodium component contamination measurements at FBTR by gamma spectrometry, Internatl. Conf. on Radiat. Prot. measurements and dosimetry: Current practices and future trends, Mumbai, India, 20-23 Feb (2001).
8. H. Naik, G. N. Kim, R. Schwengner, K. Kim, R. John, R. Massarczyk, A. Junghans, A. Wagner, A. Goswami, Fission product yield distribution in the 12, 14 and 16 MeV bremsstrahlung-induced fission of ^{232}Th, Eur. Phys. J. A 51 (2015) 150.
9. J. A. Partridge, R. C. Jensen, Purification of Di-(2-ethylhexyl) phosphoric acid by precipitation of copper(II) di-(2-ethylhexyl) phosphate, J. Inorg. Nucl. Chem. 31 (1969) 2587-2589.
10. A.R. Landgrebe, R.H. Rodriguez-Pasques, F.J. Schima, The Rapid Radiochemical separation of Radioactive Praseodymium from Radioactive Cerium, Int. J. Appl. Radiat. Isot. 19 (1968) 147-149.
11. R. Kumar, N. Sivaraman, A. Thiruvenkadasamy, C. R. Venkatasubramani, P. R. Vasudeva Rao, Carrier-free separation of ^{22}Na from magnesium by chromatographic techniques, J. Radioanal. Nucl. Chem. 251 (2002) 21–24.
12. A. Akseli, S. Kutun, Separation and determination of various elements by cation-exchange chromatography with sodium trimetaphosphate as the eluent, J. Chromatogr. A 847 (1999) 245–250.

13. D. Saha, J. Vithya, G. V. S. Ashok Kumar, K. Swaminathan, R. Kumar, C. R. Venkatasubramani, P. R. Vasudeva Rao, Feasibility studies for production of ^{89}Sr in the Fast Breeder Test Reactor (FBTR), Radiochim. Acta 101 (2013) 667-673.
14. C. Z. Deptula, T. Kempisty, A. Markiewicz, R. Mikolajczak, S. Stefancyk, T. Terlikowska, W. Zulczyk, Quality control methods of strontium chloride $^{89}SrCl_2$, radiopharmaceutical for palliative treatment of bone metastases, Second Internatl. Conf. Isot. Sydney, NSW, Australia, 12-16 Oct (1997) 195-199.
15. F. W. Lima, A. Abrao, L. Atalla, Production of Carrier-free Phosphorus-32 by Using Sulphates as Material for Irradiation, Third Inter-American Symp. Peac. Appl. Nucl. Energ., Petrópolis, Brazil, July 16-23 (1960) I.E.A, NO. 37.
16. B. A. Hadfield, Separation of phosphorus, Patent No. US 2552032A, May 8, (1951).
17. M. Ananthakrishnan, Phosphorus-32 ($^{32}P_{15}$), Manual for Reactor Produced Radioisotopes, Radioisotope Centre, Poland, IAEA TECDOC-1340 (2003) 158.

CHAPTER 3

Chapter 3: Studies on the Characterization of Neutron Spectrum at Pneumatic Fast Transfer System (PFTS) of KAMINI Reactor

This chapter presents the results of the studies on characterization of neutron energy spectrum along with the determination of the reactor parameters called sub-cadmium to epithermal neutron flux ratio (f) and the epithermal neutron flux shape factor (α) at pneumatic fast transfer system (PFTS) of KAMINI reactor, which is used extensively for the neutron activation analysis (NAA). The study involves the (i) determination of f and α using Cd-ratio and Cd-covered methods, (ii) estimation of reaction rates using multi-foil activation method and (iii) unfolding of the neutron spectrum from the computed guess spectrum based on the least square minimization approach.

3.1. Introduction

Neutron spectrum characterization of a neutron source like nuclear reactor is a mandatory requirement for the accurate evaluation of the experimental results involving the irradiation of materials in these facilities. The type and extent of reaction that takes place during the irradiation highly depend on the neutron energy spectrum of the particular irradiation facility [1]. The neutron spectrum characterization is very useful for the determination of various reactor characteristics like reactivity, burn-up, nuclear reaction rates, temperature distribution etc. [2]. In addition, characterization is also mandatory in order to interpret the experimental results accurately for the studies in nuclear and radiochemistry, radioanalytical chemistry, radiation physics, radiobiology and the radiation damage in the materials due to the bombardment of neutrons of different energies [3].

Further, the determination of the reactor parameters, f and α is needed for the single-comparator (Au) based k_0-NAA, a radioanalytical technique for the estimation of the elemental profile of a sample [4]. The epithermal neutron flux distribution in a nuclear reactor is theoretically proportional to 1/E, but in real cases, it is proportional to $1/E^{1+\alpha}$. The non-ideal epithermal neutron flux distribution (α) depends on the reactor and irradiation position. The most frequently used relative NAA method requires a priori knowledge of elements present in the sample. Individual elemental standards or suitable multi-elemental standards like Certified Reference Materials (CRM) are used in relative NAA for an accurate estimation of elements present in the sample. In the case of k_0-based NAA method, a single comparator such as gold (^{197}Au) is being used widely for various radioanalytical applications [4]. Another method of similar nature is k_0-based internal mono-standard instrumental NAA (IM-INAA) in which an isotope present in the sample itself is used as mono standard for the analyses of small as well as large-sized samples of ~mg and ~kg levels, respectively [5,6].

Several samples are being studied using the k_0 based NAA by irradiating them in the PFTS location of KAMINI reactor [7-9] and this requires the knowledge of both f and α values [10]. The characterization of neutron energy spectrum at PFTS is also essential as the same is being used for analyzing the irradiated samples. The f and α values, established already, were only relevant to the subassemblies containing ^{233}U. However, recently the KAMINI reactor core was modified, i.e. one of the ^{233}U fuel subassemblies was replaced by a ^{239}Pu based subassembly and hence there existed a need for re-establishing these values for the modified core. The present study involves the redetermination of f and α values for the modified core.

In the present work, the initial guess neutron spectrum was calculated for the neutron energy group 175 using Monte Carlo code. The spectrum unfolding was accomplished by applying the least square minimization approach using saturated activity and the nuclear reaction rates obtained experimentally. Activation cross section data were obtained from JENDL-96A library. Therefore, the present work discusses the determination of f and α along with the characterization of neutron energy spectrum at PFTS position of KAMINI reactor by using the multi-foil activation method.

3.2. Characterization of PFTS at KAMINI reactor

3.2.1. Determination of f and α

The α value was estimated using Cd-ratio and Cd-covered triple monitor methods as per the equations 3.1 and 3.2, respectively shown below [4,11,12]. The relevant nuclear data of the monitors used for f and α determination are furnished in Table 2.1 in the section 2.3.1.1.

$$Cd - Ratio\ method: \ T_i = \frac{(\bar{E}_{r,i})^{-\alpha}}{(F_{Cd,i}R_{Cd,i} - 1).Q_{0,i}(\alpha).G_{e,i}/G_{th,i}} \tag{3.1}$$

$$Cd - covered \quad method: \ T_i = \frac{(\bar{E}_{r,i})^{-\alpha}(A_{sp,i})_{Cd}}{k_{0,Au}(i).\varepsilon_{P,i}.F_{Cd,i}.Q_{0,i}(\alpha).G_{e,i}} \tag{3.2}$$

where T_i represents a value for an isotope i,

F_{Cd} - cadmium transmission factor for epithermal neutrons [9],

$\bar{E}_{r,i}$ - effective resonance energy in eV,

$Q_0(\alpha)$ - ratio of infinite dilute resonance integral to thermal n-capture cross-section

R_{Cd} - cadmium ratio of activities,

$(A_{sp})_{Cd}$ - specific count rate of Cd-cover irradiation,

ε_p - full-energy peak detection efficiency and

G_{th} and G_e represent the correction factors for thermal and epithermal neutron self-shielding, respectively.

The specific count rates of the activated monitors i.e. ^{198}Au, ^{95}Zr and ^{65}Zn of gold, zirconium and zinc, respectively were calculated using the photo peak areas obtained from the gamma-ray spectrometry. In both Cd-ratio & Cd-covered methods, calculation of T_i needed the input parameter $Q_0(\alpha)$.

The determination of α-value was carried out using Microsoft-Excel spread sheet [12]. The α value was obtained using iteration procedure in both Cd ratio and Cd covered methods. A graph of log (T_i) vs $\log(\bar{E}_{r,i})$ was plotted and the α value was obtained from the slope $(-\alpha)$ of the fitted straight line [11-13]. Initially, the value of α was assigned to be zero and the slope $(-\alpha)$ obtained from the plot of $\log(T_i)$ versus $\log(\bar{E}_{r,i})$ was used in the subsequent iterations. The iteration continued till a constant α value was obtained.

The plots of the final iterations obtained with constant α value for both Cd-ratio and Cd-covered methods are shown in Figure 3.1 and 3.2, respectively. The α values obtained finally were $-5.01\text{x}10^{-02} \pm 0.02\text{x}10^{-02}$ and $-4.01\text{x}10^{-02} \pm 0.36\text{x}10^{-02}$ using Cd-covered and Cd-ratio triple monitor methods, respectively, yielding an average α value of $-4.5\text{x}10^{-02} \pm 0.2\text{x}10^{-02}$. The negative sign indicates the presence of hard neutron spectrum at PFTS position of KAMINI reactor.

The sub-cadmium to epithermal flux ratio (*f*) value was also determined in the Cd ratio method using the following equation [12].

$$f = (F_{Cd} R_{Cd} - 1).Q_0(\alpha).G_e / G_{th} \qquad (3.3)$$

The *f*-value was computed using the α value and found to be 27.8 ± 0.3. The *f* and α values for the initial and modified core are presented in Table 3.1. These values suggest that there is no significant change in the reactor parameters i.e. *f* and α after the modification of the core configuration i.e. replacement of one of the ^{233}U-Al sub-assemblies with ^{239}Pu-Al fuel.

Table 3.1. *f* and α values at PFTS for the old and modified core of the KAMINI reactor

Reactor Parameter	Old Core	Modified Core
Sub-cadmium to epithermal flux ratio (*f*)	25.1 ± 0.4	27.8 ± 0.3
Epithermal neutron flux shape factor (α)	$-4.0\text{x}10^{-02} \pm 0.3\text{x}10^{-02}$	$-4.5\text{x}10^{-02} \pm 0.2\text{x}10^{-02}$

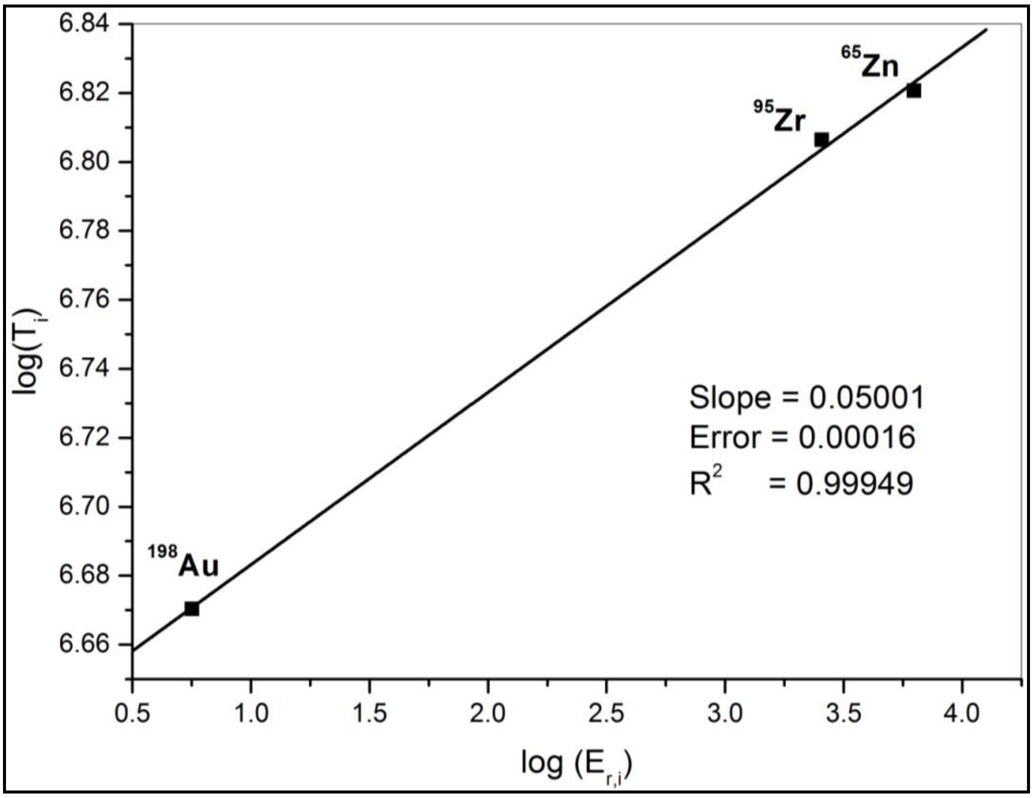

Figure 3.1. Log(T_i) vs Log($\bar{E}_{r,i}$) using Cd-covered method.

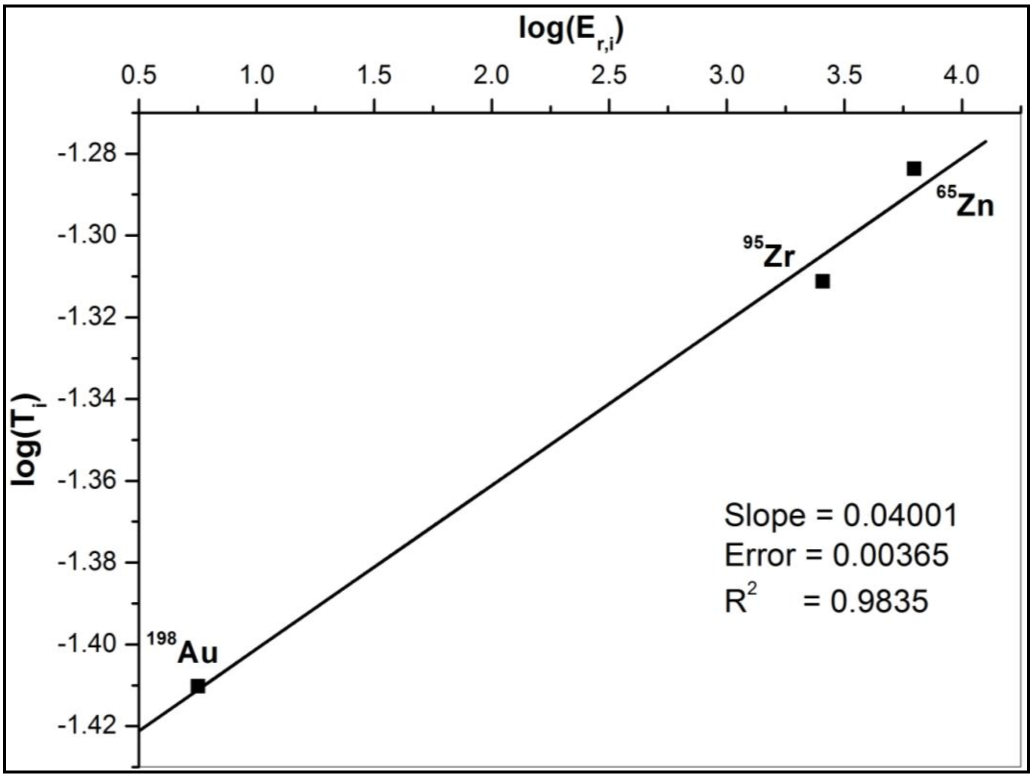

Figure 3.2. Log(T_i) vs Log($\bar{E}_{r,i}$) using Cd-ratio method.

3.2.2. Neutron spectrum characterization - Multi-foil activation method

The multiple foil activation approach is an established technique for characterizing the neutron field in a reactor owing to its simplicity. However, there exists a possibility of several potential sources of errors getting into the numerical estimation of the neutron spectrum, such as inaccurate description of material composition, geometric details, fuel compositions of various burn-up, cross sections etc. Foil activation method validates, not only the computational estimation of neutron spectrum, but also, mostly is useful for minor adjustment of the estimated spectrum obtained under constrained conditions.

The set of foils, sensitive to different energies were irradiated in the reactor with its associated neutron flux till their activities reached almost to their saturated levels. The characteristic gammas emitted from the activated foils were counted in a high resolution HPGe detector to arrive at the saturated activities / reaction rates with the due corrections incorporated for the delays in measurements as per the equation 3.4 given below [14]. The net peak areas of the photo peaks were obtained by analyzing the spectra with PHAST peak fit software.

$$\text{Measured Reaction rate} = \frac{C_{peak}.\lambda}{N.y.\varepsilon_{peak}.\exp(-\lambda T_d).[1-\exp(-\lambda T_c)].[1-\exp(-\lambda T_{irr})]} \quad (3.4)$$

where, C_{peak} - net peak area of full energy photo peak (total counts),

λ – decay constant (sec^{-1}),

N - number of target atoms in the foil,

y - gamma intensity (gammas/decay),

T_d – decay time (sec),

T_c - counting time (sec),

T_{irr} – irradiation duration (sec) and

ε_{peak} – the detector efficiency for the gamma ray of interest.

Efficiency of HPGe detector was obtained as a function of gamma-ray energy from 244 to 1408 keV using ^{152}Eu standard point source (Figure 3.3).

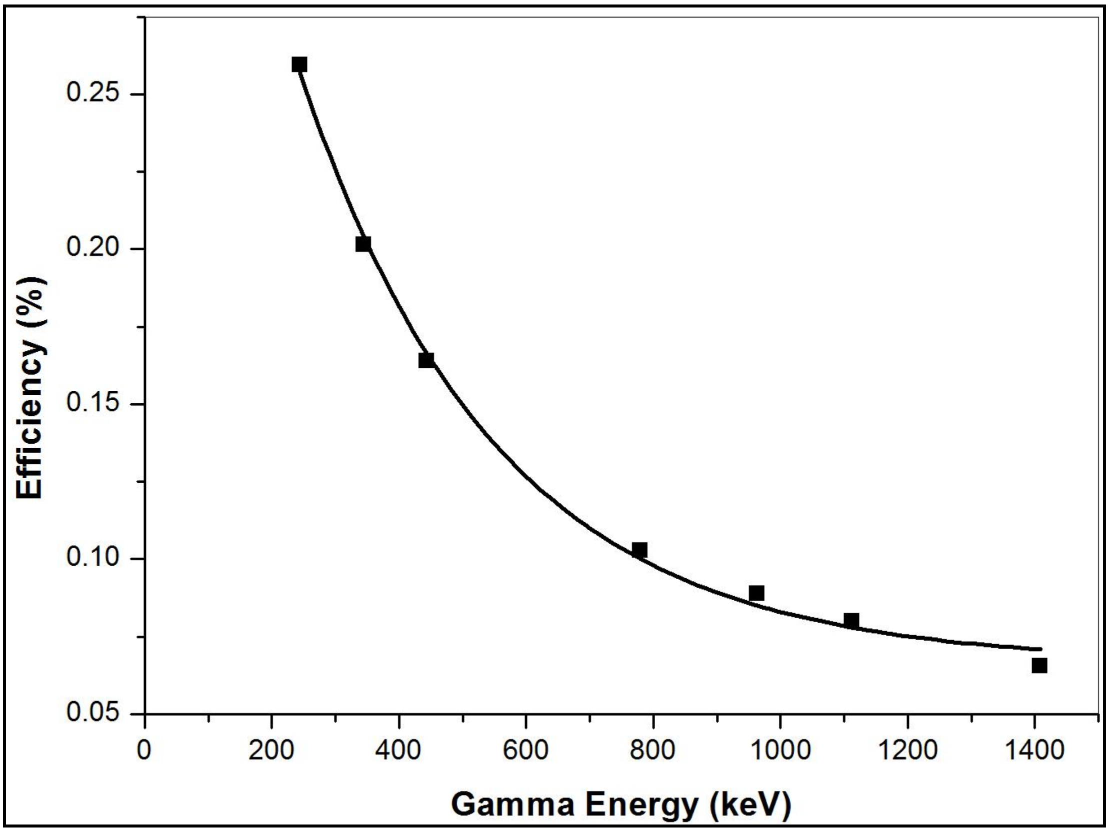

Figure 3.3. Efficiency of HPGe detector (10 cm away) for ^{152}Eu standard point source as a function of gamma energy from 244 to 1408 keV.

The details of the activation foils with their associated nuclear reactions and the various nuclear and irradiation parameters are presented in Table 2.2 of the section 2.3.2. A total of 10 nuclear reactions were evaluated and the spectrum unfolding was thus accomplished using these reactions. The nuclear reactions studied in the present work include both threshold as well as non-threshold reactions covered up to the neutron energy of 11.7 MeV. While, the threshold reactions are only sensitive to the neutrons of energy higher than their threshold energy, typically in MeV ranges, the non-threshold reactions are generally triggered by thermal neutrons themselves. The threshold nuclear reactions studied in the present work included (n, p), (n, n') and (n, 2n) reactions whereas the non-threshold nuclear reactions included radiative capture reactions i.e. (n, γ).

3.3. Theoretical prediction of the spectrum

A guess spectrum in a spectrum unfolding problem is an estimated input spectrum from a numerical model; in this case it is Monte Carlo computed spectrum. The purpose of spectrum unfolding is to derive a suitable spectrum based on foil activation measurements with close proximity to the computed or guess spectrum which makes the unfolded spectrum physically acceptable.

The guess neutron spectrum calculation presented in this work was carried out using Transport Monte Carlo Code and ENDF/B-VII.0 cross sections [15] for the core configuration with 9 U-Al fuel subassemblies, adjustable reflector blocks (ARB1) with no top axial reflector. Beam tubes were modeled up to the height of the reactor vessel whereas the PFTS was modeled up to a height of 81 cm from the core centre. Safety Control Plates (SCP) were placed at positions corresponding to the state of criticality (SCP-1: 300 mm and SCP-2: 210 mm) observed in the calculation. The neutron spectrum at the irradiation location of PFTS was calculated for 175 energy group structure.

3.4. Spectrum unfolding

The estimation of neutron spectrum was based on the computational model of the reactor in Monte Carlo Neutral Particle (MCNP) [16]. Estimated fluxes were determined in 175-groups Vitamin-J structure [17]. The chosen group structure represented the thermal, intermediate and fast regions appropriately. Activities under the saturated condition are given below in equation 3.5.

$$A_i = \int R_i(E)\varphi(E)dE, \quad \text{I = 1 to m,} \tag{3.5}$$

where R_i – the detector response function [18] for the ith foil,

φ – the neutron flux spectrum and

m – the number of different foils.

The continuous energy response function for the foils was approximated by average responses over the energy group limits as given below.

$$R_{i,g} = \int_{E_g}^{E_{g+1}} R_i(E)dE \,/ (E_{g+1} - E_g) \tag{3.6}$$

The computed reaction rates can thus be written as

$$A_i = \sum_{g=1}^{n} R_{i,g}\Phi_g \,, \qquad \text{where I = 1 to m and n >> m} \tag{3.7}$$

The computed reaction rates often deviated from the measured values which necessitated minor adjustments to be incorporated for a more accurate estimation of the spectrum, while retaining physical contents of the computed one. Condition of n >> m in equation 3.7 leads to a system of linear equations with non-unique solution which facilitated the arrival at a solution under constrained condition. The unfolding method used the numerical estimate as the initial guess spectrum, adjusted it iteratively and finally converged to a solution to the linear system in equation 3.6. Constraint function optimization technique used here constituted least square deviation between calculated and measured reaction rates, measure of sharp variation in flux with energy and least-squared deviation between the calculated and adjusted spectrum as given in equations 3.8 and 3.9. The components of the constraint function were weighted to ensure a satisfactory solution commensurate to all the requirements described above. The use of relative deviation in place of actual deviation was to ensure uniform weightage across all the reactions and logarithmic deviations were used for the other constraints.

$$F(\Phi) = \chi^2(\Phi) + \lambda_c C(\Phi) + \lambda_s S(\Phi) \tag{3.8}$$

where,

$$\begin{aligned} \chi^2 &= \sum_i \left(\frac{A_i^{mes} - \sum_g \sigma_{ig} \Phi_g}{A_i^{mes}} \right)^2, \\ C &= \sum_g \left(\frac{\log \frac{\varphi_{g-1}\varphi_{g+1}}{\varphi_g^2}}{\log \frac{E_{g+1}}{E_g}} \right)^2, \\ S &= \sum_g \left(\log \frac{\varphi_g}{\varphi_g^0} \right)^2 \end{aligned} \tag{3.9}$$

The spectrum generated using Monte Carlo method at PFTS was used as the initial guess spectrum. The input guess spectrum was adjusted iteratively such that the constraint function gradually approached a minimum in the neighborhood of the guess spectrum. The minimization algorithm used here makes use of the steepest descend method built in *fminunc* of *octave* [19]. The weights λ_s and λ_c used here corresponded to the values of 10^{-3} and 10^{-4}, respectively. The transformation $\Phi_g \longrightarrow \Phi_g^2$ ensured positive definite solution of flux. In this study, 10 activation reactions were chosen, that the response functions of these reactions roughly spanned the energy range of interest i.e. thermal to the fast energies (Figure 3.4 and 3.5). In the intermediate region, where foil had low responses, the unfolding procedure attempted to retain the calculated shape of the guess spectrum by use of shape constraint.

The deviations of the measured reaction rates from that of the calculated were found to exceed the experimental tolerances (Table 3.2). The unfolding procedure attempted to adjust the calculated spectrum such that the deviation between measured and evaluated spectrum could be minimized. An adequate shape of neutron energy spectrum was thus obtained using the constraint function minimization approach as presented in Figure 3.6. The spectrum reproduced the measured reaction rates within 10% errors, which can be attributed to the several sources of errors that are inherent with the foil activation measurements. The major sources of errors arose from the counting statistics variations observed during the detector efficiency calibration. The deviations from the measured reaction rates in the adjusted spectrum suggest that the actual flux does not greatly vary from the calculated flux. Therefore, the least square minimization approach used for the spectrum unfolding is proved to be satisfactory as well as appropriate.

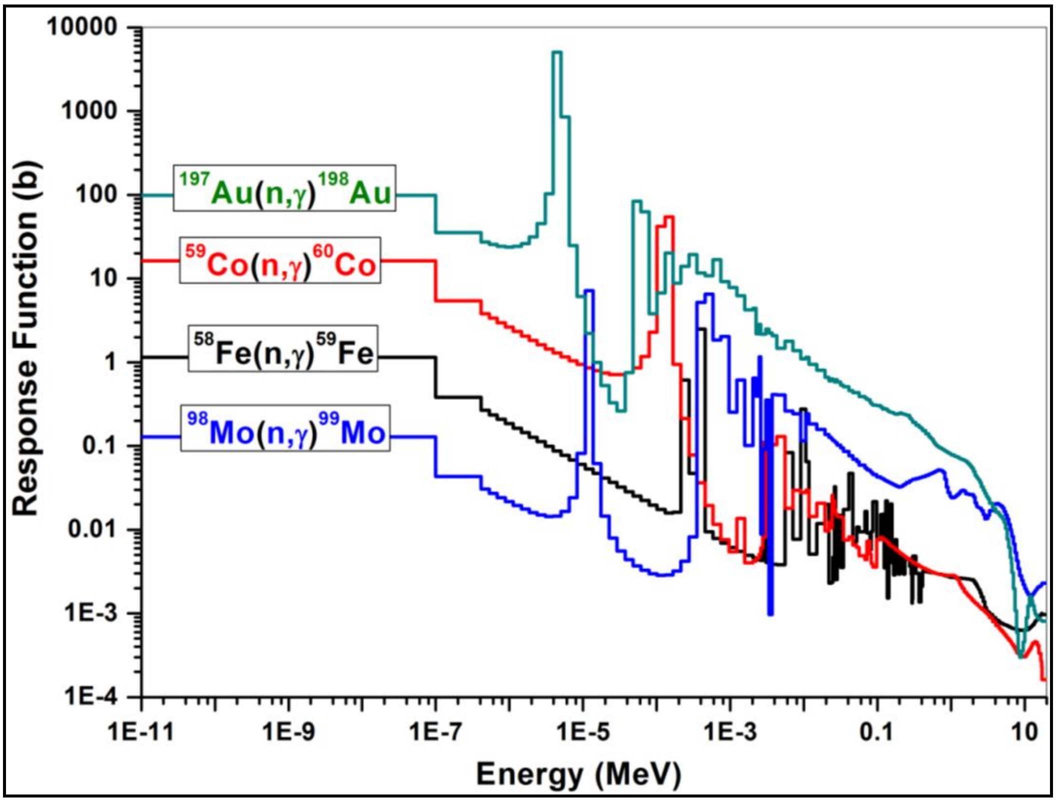

Figure 3.4. 175-group response function from JENDL-96A for non-threshold reactions.

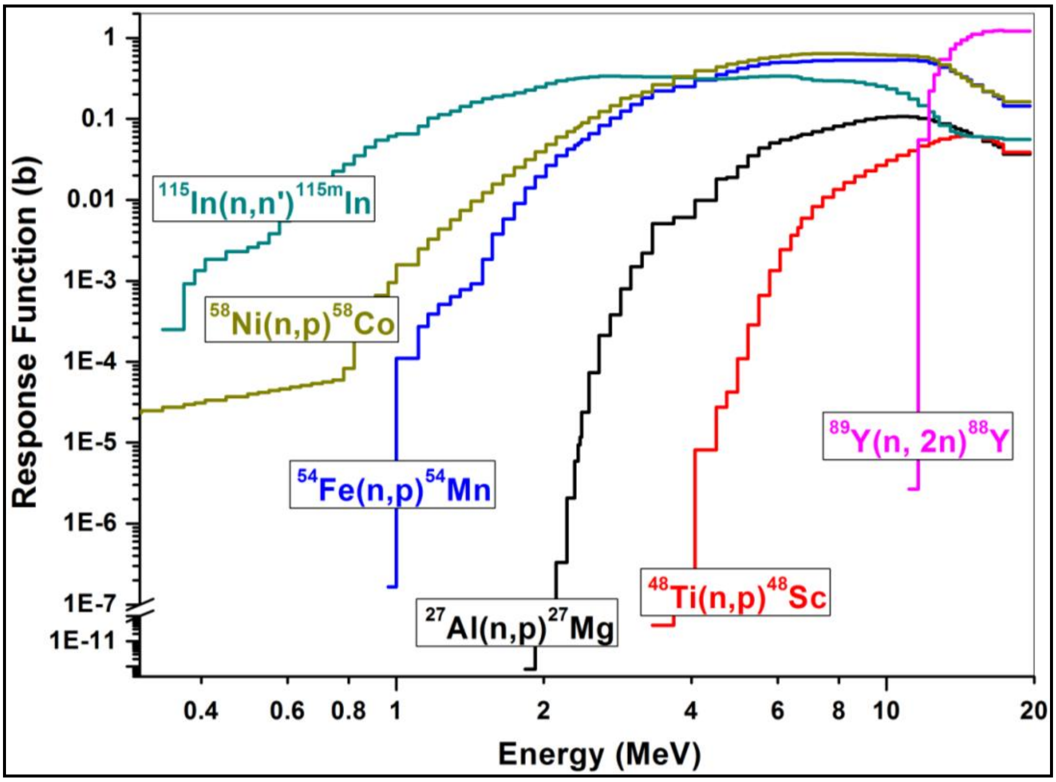

Figure 3.5. 175-group response function from JENDL-96A for threshold reactions.

Table 3.2. Measured Saturated Activity and reaction rates along with their deviations from guess spectrum and adjusted spectrum

Foil	**Activated Product**	**Gamma Energy (keV)**	**Measured Saturated Activity (dps/nucleus)**	**Measured Reaction Rate (per sec)**	**Deviation from measured reaction rates (%)**	
					MCNP Spectrum	**Adjusted Spectrum**
Al	^{27}Mg	843.8	$4.2\text{x}10^{-16} \pm 1.36\%$	$4.71\text{x}10^{-16}$	-50.68	4.28
Ti	^{48}Sc	1037.5	$1.5\text{x}10^{-18} \pm 1.56\%$	$4.82\text{x}10^{-17}$	-61.61	-3.52
Fe	^{54}Mn	834.8	$2.6\text{x}10^{-18} \pm 1.88\%$	$1.37\text{x}10^{-14}$	-69.97	-8.66
Fe	^{59}Fe	1099.2	$1.3\text{x}10^{-16} \pm 2.9\%$	$3.33\text{x}10^{-14}$	89.96	1.80
Co	^{60}Co	1332.5	$4.6\text{x}10^{-16} \pm 2.76\%$	$1.53\text{x}10^{-11}$	-92.95	-3.05
Ni	^{58}Co	810.8	$13.6\text{x}10^{-18} \pm 1.87\%$	$1.68\text{x}10^{-14}$	-67.86	0.75
Mo	^{99}Mo	739.5	$7.5\text{x}10^{-15} \pm 2.3\%$	$1.23\text{x}10^{-13}$	-37.20	-0.04
In	^{115m}In	336.3	$9.0\text{x}10^{-15} \pm 1.6\%$	$3.41\text{x}10^{-14}$	-72.72	3.20
Au	^{198}Au	411.8	$1.5\text{x}10^{-12} \pm 1.49\%$	$7.12\text{x}10^{-11}$	-81.85	0.07
Y	^{88}Y	1836.05	$3.9\text{x}10^{-20} \pm 0.99\%$	$2.40\text{x}10^{-17}$	-18.10	0.10

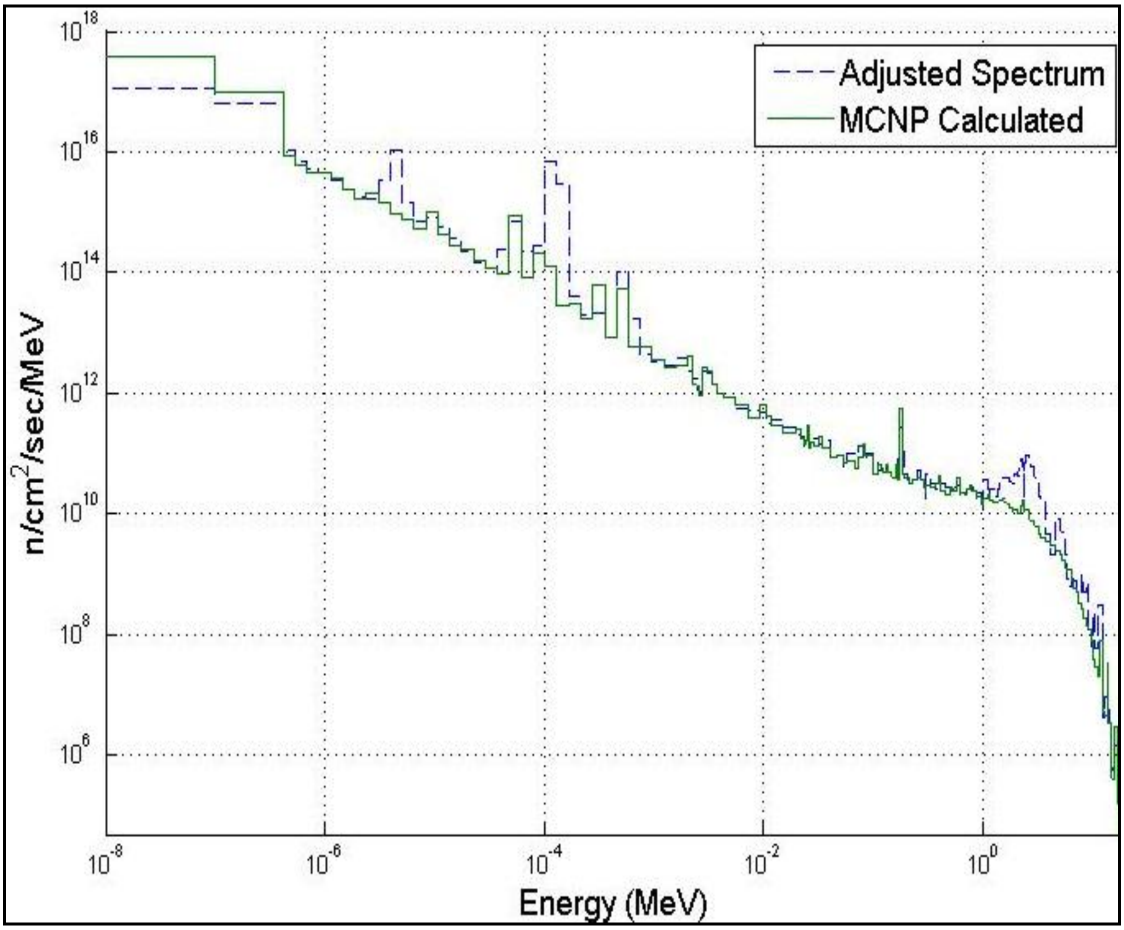

Figure 3.6. Neutron spectrum at Pneumatic Fast Transfer System of KAMINI reactor.

The neutron spectrum shape exhibits distinct regions of thermal – Maxwellian, 1/ε (epithermal) and a watt distribution (fission neutrons) which are generally the characteristics of a thermal reactor. The integral neutron flux obtained was found to be 6.01×10^{11} cm^{-2}.s^{-1}. The neutron energy flux was split into 3 energy groups [2] i.e. thermal (below 0.56 eV), intermediate (0.56 eV – 0.5 MeV) and fast (above 0.5 MeV) and the integral neutron flux inside each energy group is presented in the Table 3.3. The results suggest that the neutron spectrum at PFTS has the thermal, epithermal and fast neutron components corresponding to 5.8%, 71.5% and 22.7%, respectively. The epithermal neutron component is found to be predominant in the neutron spectrum which may have significant effect on the materials during irradiation [5]. The higher epithermal neutron component also suggests that the spectrum at PFTS is hard and is in good agreement with the epithermal neutron flux shape factor (α) that has a negative sign. The effects of the epithermal neutron component on the irradiation of materials at PFTS form a part of our future investigations.

Table 3.3. Neutron fluxes at PFTS

Neutron Energy Region	Flux(Φ) (n.cm^{-2}.sec^{-1})	
Thermal neutron	3.45×10^{10}	[Φ_{Thermal}]
Intermediate neutron	4.30×10^{11}	[$\Phi_{\text{Intermediate}}$]
Fast neutron	1.36×10^{11}	[Φ_{Fast}]
Integral neutron	6.01×10^{11}	[Φ_{Total}]

3.5. Conclusion

The pneumatic fast transfer system (PFTS) of KAlpakkam MINI (KAMINI) reactor is being used extensively for irradiation studies towards the neutron activation analysis, shielding experiments, neutron detector testing etc. The k_0 - based neutron activation analysis is being utilized at KAMINI reactor to determine the elemental profile of a sample which requires the knowledge of the reactor parameters such as sub-cadmium to epithermal neutron flux ratio (f) and epithermal neutron flux shape factor (α). The f and α values were determined using Cd-ratio and Cd-covered triple monitor methods using Zr, Au and Zn foils and found to be 27.8 ± 0.3 and $-4.5\text{x}10^{-02} \pm 0.2\text{x}10^{-02}$, respectively suggesting that there is no remarkable change in these reactor parameters for the modified core configuration i.e. replacing one of the ^{233}U-Al sub-assemblies with ^{239}Pu-Al fuel. The negative sign of the α value indicates that the neutron spectrum present at PFTS position of KAMINI reactor is hard in nature.

The neutron spectrum characterization at PFTS position was accomplished using multi-foil irradiation method that included both threshold as well as non-threshold nuclear reactions and covered the neutron energy spectrum up to 11.7 MeV. The saturated activities as well as their associated nuclear reaction rates of various irradiated activation foils were determined. The estimated guess neutron spectrum for 175 energy group structure was generated using the theoretical model of the reactor with the transport Monte Carlo Code and ENDF/B-VII.0 cross sections for the core configuration with 9 U-Al fuel subassemblies.

Neutron spectrum unfolding was accomplished using the least square minimization approach. The associated deviations from the reaction rates of the adjusted spectrum were observed to be within the experimental tolerance. The integral flux resulted from the study was found to be about $6.01\text{x}10^{11}$ n.cm^{-2}s^{-1}. The shape of neutron spectrum at PFTS showed distinct regions of thermal – Maxwellian, $1/\varepsilon$ (epithermal) and a watt fission spectrum; the thermal, epithermal and fast neutron components corresponding to 5.8%, 71.5% and 22.7%, respectively. The neutron energy spectrum is also useful for testing and validating the reactor physics codes and different nuclear data libraries.

3.6. References

1. J. Graham, S. Landsberger, P. J. Ferreira, J. Ihlefeld, G. Brennecka, Neutron flux characterization techniques for radiation effects studies, J. Radioanal. Nucl. Chem. 291 (2012) 503–507.
2. U. D.U. Bitelli, F. P. G. Martins, R. Jerez, Measurements of the Neutron Spectrum Energy in the IPEN/MB-01 Reactor Core, Braz. J. Phys. 39 (2009) 39-43.
3. D. K. Mohapatra, P. Mohanakrishnan, Measurement and prediction of neutron spectra in the Kalpakkam mini reactor (KAMINI), Appl. Radiat. Isot. 57 (2002) 25-33.
4. F. De Corte, A. Simonits, A. De Wispelaere, J. Hoste, Accuracy and applicability of the k_0-standardization method, J. Radioanal. Nucl. Chem. 113 (1987) 145-161.
5. F. De Corte, L. Moens, A. Simonits, K. S. Hammami, A. de Wispelaere, J. Hoste, The effect of the epithermal neutron flux distribution on the accuracy of absolute and comparator standardization methods in (n, γ) activation analysis, J. Radioanal. Chem. 72 (1982) 275–286.
6. R. Acharya, A. G. C. Nair, K. Sudarshan, A. V. R. Reddy, A. Goswami, Development and applications of the k_0-based internal mono standard INAA method, Appl. Radiat. Isot. 65 (2007) 164-169.
7. A. Simonits, F. De Corte, J. Hoste, Single-Comparator methods in reactor neutron activation analysis, J. Radioanal. Chem. 24 (1975) 31-46.
8. O. T. Hogdahl, Neutron Absorption in Pile Neutron Activation Analysis, Report MMPP-226-1, Phoenix Memorial Laboratory, The University of Michigan, Michigan (1962).

9. F. De Corte, A. Simonits, k_0-measurements and related nuclear data compilation for (n, γ) reactor neutron activation analysis, J. Radioanal. Nucl. Chem. 133 (1989) 43-130.
10. Ho M. Dung, Y. Cho Seung, A simple method for α determination, J. Radioanal. Nucl. Chem. 257 (2003) 573–575.
11. Ho M. Dung, F. Sasajima, Determination of α and f for k_0-NAA in irradiation sites with high thermalized neutrons, J. Radioanal. Nucl. Chem. 257 (2003) 509–512.
12. J. S. Brahmaji Rao, E. Senthilvadivu, N. P. Seshadreesan, R. Acharya, C. R. Venkatasubramani, A. V. R. Reddy, Characterization of pneumatic fast transfer system irradiation position of KAMINI reactor for k_0-based NAA, J. Radioanal. Nucl. Chem. 294 (2012) 137–141.
13. M. S. Dias, V. Cardoso, M. F. Koskinas, I. M. Yamazaki, Determination of the neutron spectrum shape parameter α in k_0 NAA methodology using covariance analysis, Appl. Radiat. Isot. 68 (2010) 592-595.
14. Y. H. Liu, S. Nievaart, H. M. Liu, R. Moss, S. H. Jiang, Monte Carlo determined self-shielded group-wise cross-sections for the activation foil stack applied in the epithermal neutron spectrum adjustment, Nucl. Instrum. Methods. Phys. Res. A 602 (2009) 557-563.
15. A. Lopez, A. L. Nichols, ADS-2.0: “A Test Library for Accelerator Driven Systems and New Reactor Designs”. INDC(NDS)-0545, IAEA, Wagramer Strasse 5, A-1400 Vienna, Austria (2008).
16. J. K. Shultis, R. E. Faw, An MCNP Primer, Manhattan, KS 66506 (2011).

17. R. Macfarlane, D. W. Muir, R. M. Boicourt, A. C. Kahler III, J. L. Conlin, The NJOY Nuclear Data Processing System, Version 2016 (No. LA-UR-17-20093). Los Alamos National Laboratory (LANL) (2017).
18. Reference neutron activation library, IAEA-TECDOC-1285, ISSN 1011–4289, Vienna, Austria (2002).
19. J. W. Eaton, D. Bateman, S. Hauberg, R. Wehbring, GNU Octave - A high-level interactive language for numerical computations, Edition - 3 for Octave version 3.8.0 (2011).

CHAPTER 4

Chapter 4: Design and Installation of Fast Flux Experimental Facility (FFEF) at FBTR and neutron flux Measurement

This chapter deals with the various experiments and calculations involved in the design and installation of Fast Flux Experimental Facility (FFEF) at FBTR as well as neutron flux measurement in FFEF at 25 kW power [1]. Development of FFEF with a sample holder was envisaged to carry out the studies on characterization of neutron spectrum, fission systematics, determination of reaction cross sections, fast neutron activation analysis and minor actinide transmutation [2,3]. The development of the facility, FFEF involved the modification of the already-existing-auxiliary shield plug of the central canal plug, by attaching a long titanium rod along with a sample holder to its bottom. The modification was done in such a way that the sample holder was positioned just above the head of the central subassembly. The facility is meant only for the irradiation of the samples which are stable at FBTR operating temperature.

The present chapter describes the modification details, impurity profile of the construction material (Ti) by neutron activation analysis and the calculation of the radiation dose burden due to the activation of the construction materials and its associated impurities themselves, if any. This chapter also presents the determination of neutron flux at FFEF in FBTR using foil activation method.

4.1. Computations

The radiation dose generated due to the irradiation of titanium in FFEF of FBTR was computed. The calculations considered both the matrix material (titanium) along with its associated impurities. The isotopic composition of titanium is shown in Table 2.3 of section 2.4.1. The elemental impurities present in the titanium were established by instrumental neutron activation analysis (INAA).

4.1.1. Analysis of titanium for impurities

The irradiated titanium samples and standards were assayed, one at a time by using HPGe detector. The impurities in Ti were quantified using relative NAA method by comparing the activities of elements in samples and standards. Using the mass of the element in standard ($m_{x,std}$) and activities of standard ($cps_{x,std}$) and sample ($cps_{x,sample}$), the mass of the element in the sample ($m_{x,sample}$) was determined using the following equation [4].

$$m_{x,sample} = m_{x,std} \cdot \frac{cps_{x,sample}}{cps_{x,std}} \cdot \frac{D_{std}}{D_{sample}} \cdot \frac{C_{std}}{C_{sample}} \tag{4.1}$$

where D is the decay correction factor, C is the counting correction factor.

Another method of analysis, namely, Internal Mono-standard NAA (IM-NAA) was also employed to determine the elemental concentration ratios of impurities present in the titanium sample by applying the following equation [5].

$$\frac{m_x}{m_y} = \frac{(S.D.C)_y}{(S.D.C)_x} \cdot \frac{P_{Ax}}{P_{Ay}} \cdot \frac{\varepsilon_y}{\varepsilon_x} \cdot \frac{(f+Q_0(\alpha))_y}{(f+Q_0(\alpha))_x} \cdot \frac{k_{0,Au}(y)}{k_{0,Au}(x)} \tag{4.2}$$

where P_A is the net peak area under the gamma peak of interest,

S is the saturation factor,

ε is the in-situ relative detection efficiency,

$Q_0(\alpha)$ is the ratio of $I_0(\alpha)$ to σ_0, where, $I_0(\alpha)$ is infinitely dilute resonance integral corrected for α, σ_0 is the (n,γ) cross-section at 2200 m.s^{-1} and

$k_{0,Au}$ is the literature k_0-factor of an isotope with respect to gold.

Gamma spectrum of a titanium sample irradiated at CIRUS reactor, BARC, Mumbai is shown in Figure 4.1. The in-situ relative detection efficiency was obtained by using the following equation [6,7].

$$\ln \varepsilon_\gamma = k_j + \sum_{i=0}^{m} a_i (\ln E_\gamma)^i \tag{4.3}$$

where a_i is the coefficient of the polynomial of order m,

k_j is a constant characteristic of the jth nuclide.

The present analysis used a second order polynomial (m=2) for the calculation of the in-situ relative detection efficiency. A typical in-situ relative detection efficiency plot obtained for titanium sample is shown in Figure 4.2. This plot covers gamma energies range from 134 to 2754 keV using the activation nuclides such as ^{187}W, ^{140}La and ^{24}Na. The f and α values used in the calculation were 80 and 0.011, respectively for the self-serve position of CIRUS reactor [8].

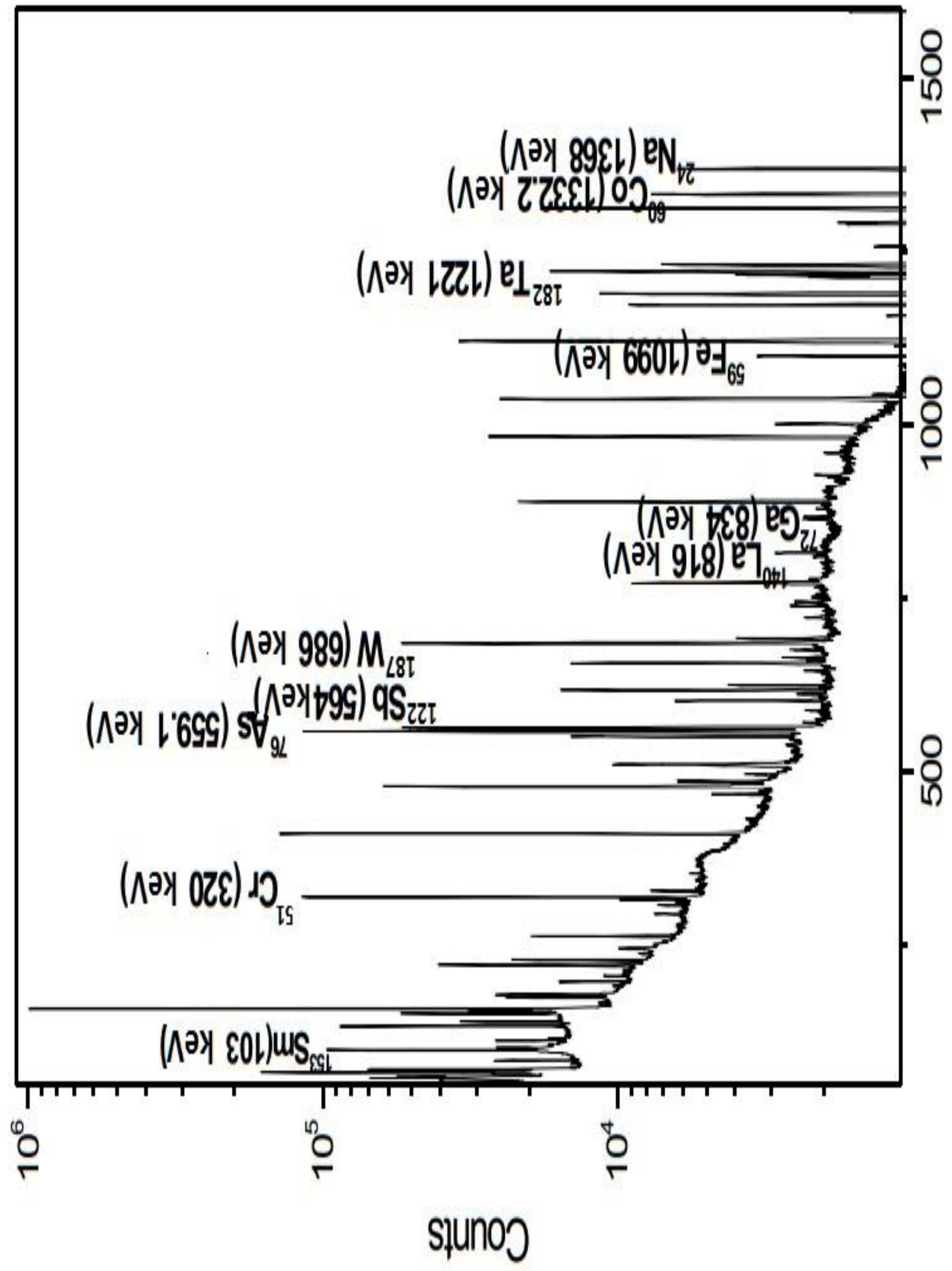

Figure 4.1. Gamma ray spectrum of neutron activated Ti sample in CIRUS reactor.

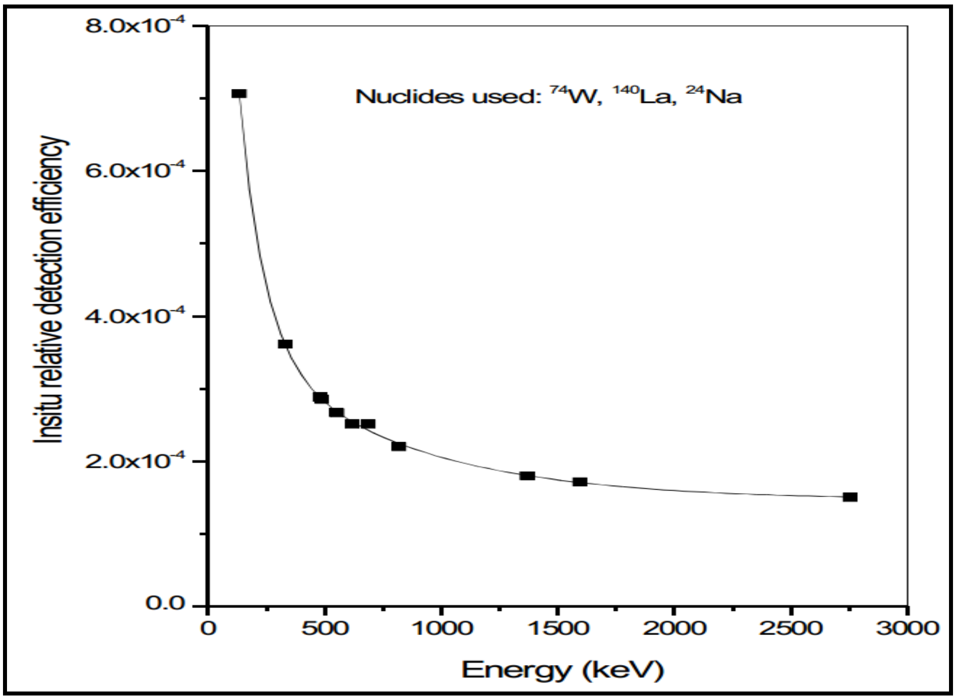

Figure 4.2. Insitu relative detection efficiency of neutron irradiated titanium sample.

Table 4.1 shows the various elemental impurities present in the titanium as obtained by NAA. A total of 14 elemental impurities i.e. Na, K, Cl, Sc, Fe, Mn, As, W, Co, Cr, Sb, La, Ta and Sm were determined by both relative as well as IM-NAA methods. Among them, the concentrations of Fe and Cr were found to be high i.e. 483 ppm and 147 ppm, respectively. The remaining impurities were at trace level and fell in the range of 0.1 to 40 ppm. The estimated concentration of Sc being 0.37 ppm through the nuclear reaction ^{45}Sc(n,γ)^{46}Sc may be possibly and slightly, overestimated because of its production from the threshold nuclear reaction of ^{46}Ti(n,p)^{46}Sc as well [9].

These elemental impurities were categorized into two types, (i) elements associated with short-lived activation products such as Na, K, Cl, Mn, As, La and Sm and (ii) elements associated with long-lived activation products such as Sc, Fe, W, Co, Cr, Sb and Ta. The half-lives of the activation products of these impurities are shown in Table 4.1. In General, the impurities associated with short-lived activation products do not lead to the radiation dose burden as they decay fast to the background level. However, the impurities associated with long-lived activation products are not desirable and is a matter of concern in titanium as they lead to the increased radiation dose burden after the irradiation of titanium material [10].

Table 4.1. Impurities present in titanium

Impurity Element	Corresponding Activation Product	Half-life	Concentration (ppm)
As	^{76}As	1.07 d	9.2 ± 0.1
Na	^{24}Na	14.95 d	10 ± 1
W	^{187}W	23.8 h	8.14 ± 0.04
Sb	^{122}Sb	2.72 d	1.52 ± 0.01
La	^{140}La	1.67 d	0.133 ± 0.004
Ta	^{182}Ta	115 d	6.9 ± 0.1
Fe	^{59}Fe	44.5 d	483 ± 6
Co	^{60}Co	5.27 y	3.94 ± 0.03
Sm	^{153}Sm	46.3 h	0.15 ± 0.01
K	^{42}K	12.36 h	32.7 ± 1.3
Cr	^{51}Cr	27.1 d	147 ± 4
Mn	^{56}Mn	46.7 m	21.5 ± 0.3
Cl	^{38}Cl	37.3 m	36.0 ± 1.7
Sc*	^{46}Sc	83.7 d	0.370 ± 0.002

*Sc is slightly overestimated due to its formation from Ti (n,p) as well.

4.1.2. Radiation dose computations

The rod attached to the bottom of the central canal plug can undergo all possible nuclear reactions, i.e. (n, γ), (n, p), (n, 2n), (n, α) etc. on its exposure to neutrons in FBTR and hence it is necessary to compute the dose due to the activation of this rod under typical operational conditions of FBTR [11]. The radiation dose needs to be within the permissible limits to avoid the man-rem problems. Hence, the radiation dose computations were carried out for the matrix material (titanium) as well as the associated impurities, profiled by NAA. The dose computations considered that the location of the sample holder was 28.5 cm above the central subassembly top and the neutron flux encountered in this location was assumed to be $2.57\text{X}10^{11}$ $\text{cm}^{-2}.\text{sec}^{-1}$ at 400 kW power of FBTR [1].

Since the neutron flux seen by the rod during its exposure inside FBTR decreases along its length from bottom to the top, the degree of activation is also expected to vary accordingly. Therefore, the titanium rod was divided into three equal portions having a length of about 1.1 m each and the reaction rates were computed at these three locations, i.e. bottom, middle and top portions of the titanium rod. The microscopic reaction rates for the various possible nuclear reactions, leading to the activated products of Ti matrix material and the associated impurities are presented in Table 4.2 and Table 4.3, respectively. Since the impurities associated with the titanium matrix are being at very low concentration, the activated products due to the radiative capture alone are expected to contribute significantly to the dose in the Ti matrix. Hence, the activation due to the radiative capture alone was considered in the radiation dose calculations for the impurities present in titanium.

Table 4.2. Microscopic reaction rates of Titanium for various nuclear reactions

Nuclear Reaction	**$t_{1/2}$ of product**	**Microscopic Reaction Rate (sec^{-1})**		
		Bottom	**Middle**	**Top**
$^{46}Ti(n,2n)^{45}Ti$	3.08 h	2.64E+05	7.85E+02	9.70E-02
$^{46}Ti(n,p)^{46}Sc$	83.79 d	5.43E+08	1.07E+06	2.00E+02
$^{47}Ti(n,p)^{47}Sc$	3.35 d	1.25E+09	1.95E+06	1.77E+02
$^{48}Ti(n,p)^{48}Sc$	1.82 d	1.29E+07	2.72E+04	4.84E+00
$^{49}Ti(n,p)^{49}Sc$	0.96 h	3.48E+07	6.35E+04	8.76E+00
$^{50}Ti(n,p)^{50}Sc$	0.028 h	3.24E+05	7.43E+02	1.00E-01
$^{50}Ti(n,\gamma)^{51}Ti$	0.096 h	3.25E+10	1.67E+09	1.96E+02
$^{48}Ti(n,\alpha)^{45}Ca$	162.6 d	1.49E+04	4.11E+01	5.51E-03
$^{50}Ti(n,\alpha)^{47}Ca$	4.536 d	2.55E+03	7.74E+00	9.62E-04

Table 4.3. Microscopic reaction rates for impurities in Titanium

Nuclear Reaction	$t_{1/2}$ of product	Microscopic Reaction Rate (sec^{-1})		
		Bottom	**Middle**	**Top**
$^{75}As(n,\gamma)^{76}As$	1.08 d	4.81E+13	1.5E+12	5.74E+5
$^{37}Cl(n,\gamma)^{38}Cl$	37.2 m	6.79E+10	4.0E+09	4.29E+2
$^{59}Co(n,\gamma)^{60}Co$	5.27 a	5.26E+13	1.9E+12	7.00E+5
$^{50}Cr(n,\gamma)^{51}Cr$	27.7 d	2.27E+12	1.4E+11	1.63E+4
$^{58}Fe(n,\gamma)^{59}Fe$	44.4 d	1.34E+12	2.9E+10	1.42E+4
$^{139}La(n,\gamma)^{140}La$	1.68 d	6.08E+12	2.8E+11	7.47E+4
$^{55}Mn(n,\gamma)^{56}Mn$	2.58 h	8.45E+12	2.4E+11	8.89E+4
$^{23}Na(n,\gamma)^{24}Na$	15.0 h	8.73E+10	5.1E+09	1.42E+3
$^{121}Sb(n,\gamma)^{122}Sb$	2.72 d	7.40E+13	4.7E+12	5.71E+5
$^{45}Sc(n,\gamma)^{46}Sc$	83.7 d	3.38E+12	2.4E+11	2.01E+4
$^{152}Sm(n,\gamma)^{153}Sm$	46.2 h	7.72E+14	6.7E+13	3.24E+6
$^{181}Ta(n,\gamma)^{182}Ta$	114.4d	2.48E+14	1.5E+13	1.88E+6
$^{186}W(n,\gamma)^{187}W$	23.72 h	2.03E+14	1.3E+13	1.84E+6

From the data presented in Table 4.2 and 4.3, it is observed that the reaction rates are considerably higher for the bottom portion of the rod i.e. ~ orders of magnitude higher than that of the middle portion, which again in turn, is higher than the top portion. Since the dose due to the activated products at middle and top portions are relatively negligible in comparison with that of bottom portion, it suffices to consider only the activation products at the bottom for dose calculation.

Taking into the account of the typical operation cycle of FBTR, the dose computation was carried out at 400 kWt power for a typical irradiation period of 10 days with an hour of cooling time. Assuming a length of 1.1 m and a diameter of 12 mm for the titanium rod, the gamma emission rate (N_γ) was calculated using the following equation.

$$N_\gamma = N\sigma\phi.[1-\exp(-\lambda t_{irr})].\exp(-\lambda t_d).a_\gamma \qquad (4.4)$$

where, N refers to number of target atoms, $\sigma\phi$ refers to reaction rate (sec^{-1}), λ refers to decay constant (sec^{-1}), a_γ refers to gamma abundance, t_{irr} and t_d refers to duration of irradiation and decay time, respectively.

The gamma emission rates due to the different nuclear reactions in the matrix titanium as well as its associated impurities are presented in an ascending order of the gamma energies, originated from the activation products formed at the bottom portion of the titanium rod (Table 4.4). The titanium rod is conveniently assumed to be a line source and the radiation dose due to this line source was computed [12] at a distance of 2 cm as well as 100 cm from the rod. The obtained results are presented in Table 4.5.

Table 4.4. Gamma emission rate from the bottom portion of the Titanium rod with a length of 1.1 m & dia of 12 mm (T_{irr} = 10 days, t_{cool} = 1 h, 400 kW power)

Nuclear Reaction	E_γ (keV)	Intensity (%)	Gammas / s
$^{152}Sm(n,\gamma)^{153}Sm$	103.2	29.19	4.14E+05
$^{47}Ti(n,p)^{47}Sc$	159.38	68.1	8.73E+06
$^{51}Ti(n,\gamma)^{51}Ti$	320.1	93.1	1.72E+05
$^{50}Cr(n,\gamma)^{51}Cr$	320.08	9.89	4.72E+04
$^{186}W(n,\gamma)^{187}W$	479.5	21.8	3.87E+06
$^{139}La(n,\gamma)^{140}La$	487	46.1	1.89E+04
$^{50}Ti(n,p)^{50}Sc$	523.8	88.7	5.99E-08
$^{75}As(n,\gamma)^{76}As$	559.08	45	1.93E+07
$^{121}Sb(n,\gamma)^{122}Sb$	564.3	70.55	2.55E+06
$^{186}W(n,\gamma)^{187}W$	685.7	27.3	4.85E+06
$^{50}Ti(n,\alpha)^{47}Ca$	807.85	6.8	1.06E+00
$^{139}La(n,\gamma)^{140}La$	815.78	23.7	9.71E+03
$^{55}Mn(n,\gamma)^{56}Mn$	846.8	98.85	1.87E+07
$^{46}Ti(n,p)^{46}Sc$	889.25	99.98	5.79E+05
$^{45}Sc(n,\gamma)^{46}Sc$	889.25	99.98	1.64E+04
$^{50}Ti(n,\gamma)^{51}Ti$	928.64	6.9	1.27E+04
$^{48}Ti(n,p)^{48}Sc$	983.5	99.9	1.43E+06
$^{48}Ti(n,p)^{48}Sc$	1037.49	97.6	1.39E+06
$^{58}Fe(n,\gamma)^{59}Fe$	1099.25	56.5	1.91E+04

Continued ……

Nuclear Reaction	E_γ (keV)	Intensity (%)	Gammas / s
^{46}Ti(n,p)^{46}Sc	1120.51	99.97	5.79E+05
^{45}Sc(n,γ)^{46}Sc	1120.51	99.97	1.64E+04
^{50}Ti(n,p)^{50}Sc	1121.1	99.5	6.71E-08
^{181}Ta(n,γ)^{182}Ta	1121.3	35.17	1.44E+06
^{59}Co(n,γ)^{60}Co	1173.23	99.85	9.45E+04
^{181}Ta(n,γ)^{182}Ta	1189	16.58	6.87E+05
^{181}Ta(n,γ)^{182}Ta	1221	27.27	4.84E+05
^{58}Fe(n,γ)^{59}Fe	1291.59	43.2	1.46E+04
^{50}Ti(n,α)^{47}Ca	1297	75	1.15E+01
^{48}Ti(n,p)^{48}Sc	1312.04	99.9	1.43E+06
^{59}Co(n,γ)^{60}Co	1332.5	99.98	9.46E+04
^{23}Na(n,γ)^{24}Na	1368.6	99.99	2.72E+05
^{50}Ti(n,p)^{50}Sc	1553.78	100	6.75E-08
^{139}La(n,γ)^{140}La	1596.5	95.4	3.93E+04
^{37}Cl(n,γ)^{38}Cl	1642.7	31.9	1.22E+04
^{55}Mn(n,γ)^{56}Mn	1810.8	26.9	5.15E+06
^{55}Mn(n,γ)^{56}Mn	2113.19	14.2	2.71E+06
^{37}Cl(n,γ)^{38}Cl	2167.7	42.4	1.65E+04
^{23}Na(n,γ)^{24}Na	2753.99	99.86	2.71E+05

The total radiation dose due to the activation of the titanium rod at 400 kW in FBTR for 10 days with a cooling period of 1 h was found to be 125 mR/h and 0.8 mR/h at a distance of 2 cm and 1 m, respectively. These computations assumed that the reaction rates at the bottom of the titanium rod are valid for the entire 1.1 m length of the bottom portion. However, in the actual case, the reaction rates might be much smaller as shown in Table 4.2 and 4.3. Thus, the computed conservative radiation dose rates are presented in Table 4.5, even though the actual dose rate is expected to be much smaller. The fact that favours titanium being the material of choice for the intended application includes that (i) the activated products due to (n, γ) reactions are found to be stable ones which do not hence contribute to the actual dose and also (ii) the only radioactive isotope (^{51}Ti) formed during the irradiation happens to be relatively a short-lived nuclide with its associated half-life of only 5.74 min [13].

Table 4.5. Dose computations for bottom portion of the titanium rod

S.No	Distance from rod (cm)	Total dose (R/h)*
1	2.0	0.125
2	100.0	0.819E-03

(* Cooling: 1 h; Power operated at: 400 kW; t_{irr} = 10 d)

Thus, the above computations establish that the titanium is the most suitable choice of material for this particular application. Therefore, a titanium extension rod of length 3252.5 mm and a diameter of 14.0 ± 0.1 mm was attached to the bottom end of the shield plug. A schematic of titanium extension rod along with the sample holder is depicted in Figure 4.3. A titanium sample holder of length 50 mm and diameter 12 mm was attached to the bottom of this rod by a screw joint (Figure 4.4). The bottom of the sample holder was made to be a solid hexagon with a diameter of 12.12 mm across the flat surface.

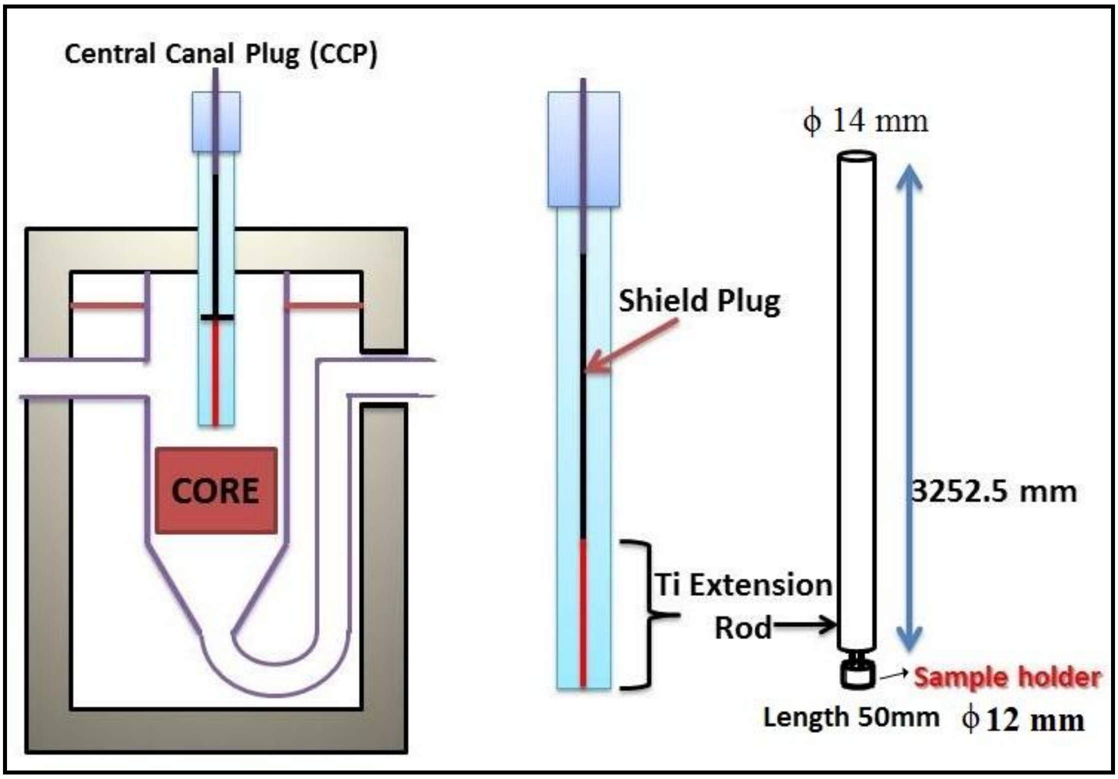

Figure 4.3. Ti extension rod with sample holder.

Figure 4.4. Titanium sample holder.

4.1.3. Simulation studies with aluminum foil as a catcher foil in FBTR

Aluminium foil was chosen as the catcher foil for the irradiation studies at FBTR, since it produces only a short-lived activation product from the radiative-capture reaction, i.e. $^{27}Al(n,\gamma)^{28}Al$ with its associated short half-life of only 2.24 min [14]. However, the stability of aluminium foils with respect to the morphology and phase changes need to be evaluated at the ambient temperature inside FBTR.

In order to evaluate the effect of heating on the aluminium catcher foils to the temperature of FBTR core, the same was heated in air to the temperature of 450 ^{o}C for 6 h and allowed to cool to room temperature. The Al foil was found to be (i) thermally stable and (ii) easily detachable mutually or separable from each other. The micro-structures obtained from scanning electron microscope (SEM) for the study of surface morphological changes, if any, for both heated and normal foils are shown in Figure 4.5. These images confirmed that there is no morphological change in the heated Al foil compared to the Al foil before heating. Further, the x-ray diffraction patterns of these foils (Figure 4.6) confirmed that there is no phase transformation as well, in aluminium due to the heating.

Coker studied the oxidation behaviour of high pure aluminium foils at various temperatures up to 1550 ^{o}C; and reported that, between 650-750 ^{o}C, a very little or no oxidation observed in Al foils even after the exposure for 12 h in air [15]. Thus, in the present case, the Al foil was exposed to a temperature of 450 ^{o}C only for a period of 6 h and hence no oxidation (passivation) or phase changes observed in the foil. The same results are confirmed in SEM and XRD results as well, shown in the Figure 4.5 and 4.6., respectively. The overall study confirmed that the aluminium foil could be conveniently used as the catcher foil for the irradiation studies at 400kW power in FBTR.

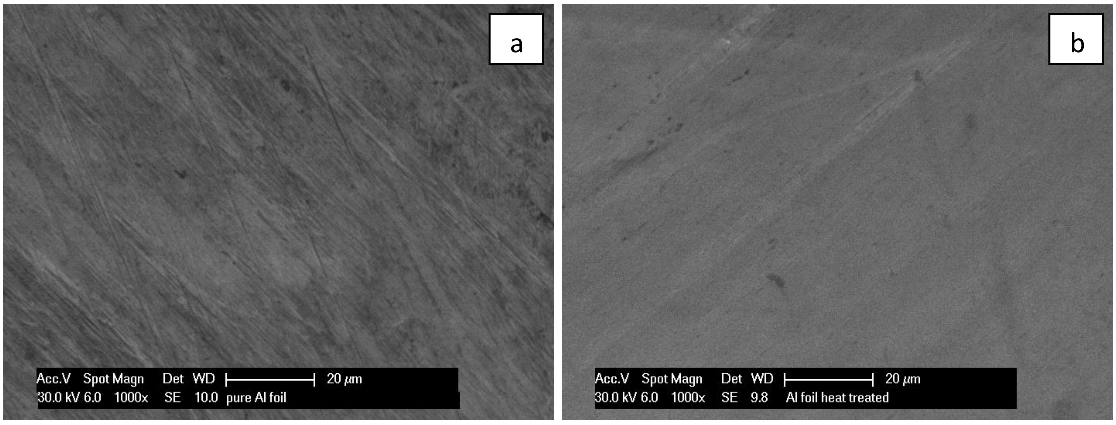

Figure 4.5. SEM micro-structures of Al foil (a) before & (b) after heating.

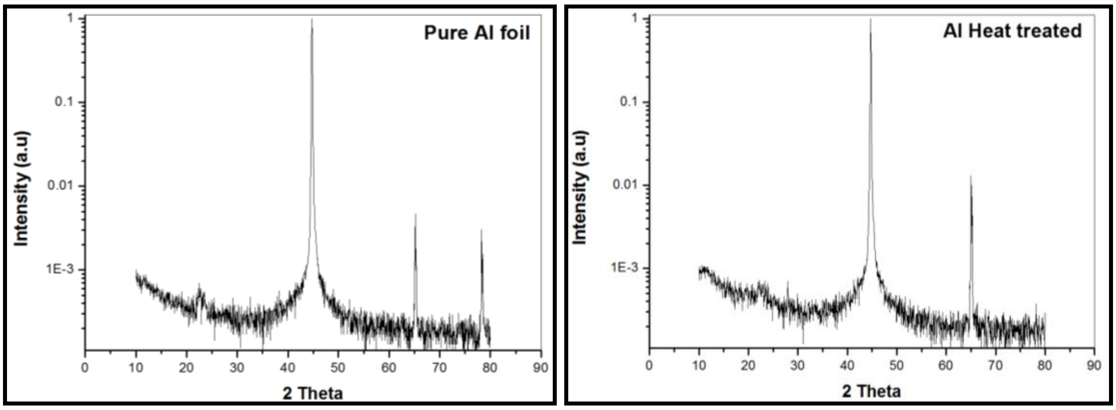

Figure 4.6. XRD profiles of pure and heat treated Al foils.

4.2. Neutron flux measurement studies at FFEF of FBTR

A gold foil was irradiated in FFEF of FBTR at 25 kW power for 4 h. The irradiated Au foil was assayed for its activation using HPGe detector at 30 cm distance and the peak areas were obtained using peak fitting software, PHAST [16]. The gamma spectrum of the irradiated gold foil in FBTR is shown in Figure 4.7. The peak area was facilitated the evaluation of the Au equivalent neutron flux using the following equation [17],

$$\phi_{Au} = \frac{\left(\frac{PA_{Au}}{LT}\right)}{N.\sigma.S.D.C}.a_{\gamma}.\varepsilon \tag{4.5}$$

where PA – photo peak area corresponds to 411.8 keV of ^{198}Au, LT – live time (sec), a_γ – absolute gamma intensity, ε – absolute detector efficiency for 411.8 keV of ^{198}Au, N – number of ^{197}Au atoms that are irradiated, σ – thermal neutron capture cross section for ^{197}Au (99.8 b). The detector efficiency was calibrated using the calibration source ^{152}Eu for the gamma energy from 244 to 1408 keV using the equation 4.6. However, the energy range did not include 121 keV of ^{152}Eu owing to its vulnerability to the large fluctuations of the efficiency.

$$\%Efficiency = \frac{cps.(100).(100)}{dps.\%a_{\gamma}} \tag{4.6}$$

The efficiency of HPGe detector for a point source as a function of gamma energy from 244 to 1408 keV is shown in the Figure 4.8. The calibration source ^{152}Eu and the sample Au foil were assayed in the reproducibly same position with respect to the detector in order to maintain the calibrated geometrical efficiency valid. The Au equivalent neutron flux (ϕ_{Au}) at FFEF was found to be 2.54x10^{9} cm^{-2}.s^{-1} at 25 kW power of FBTR.

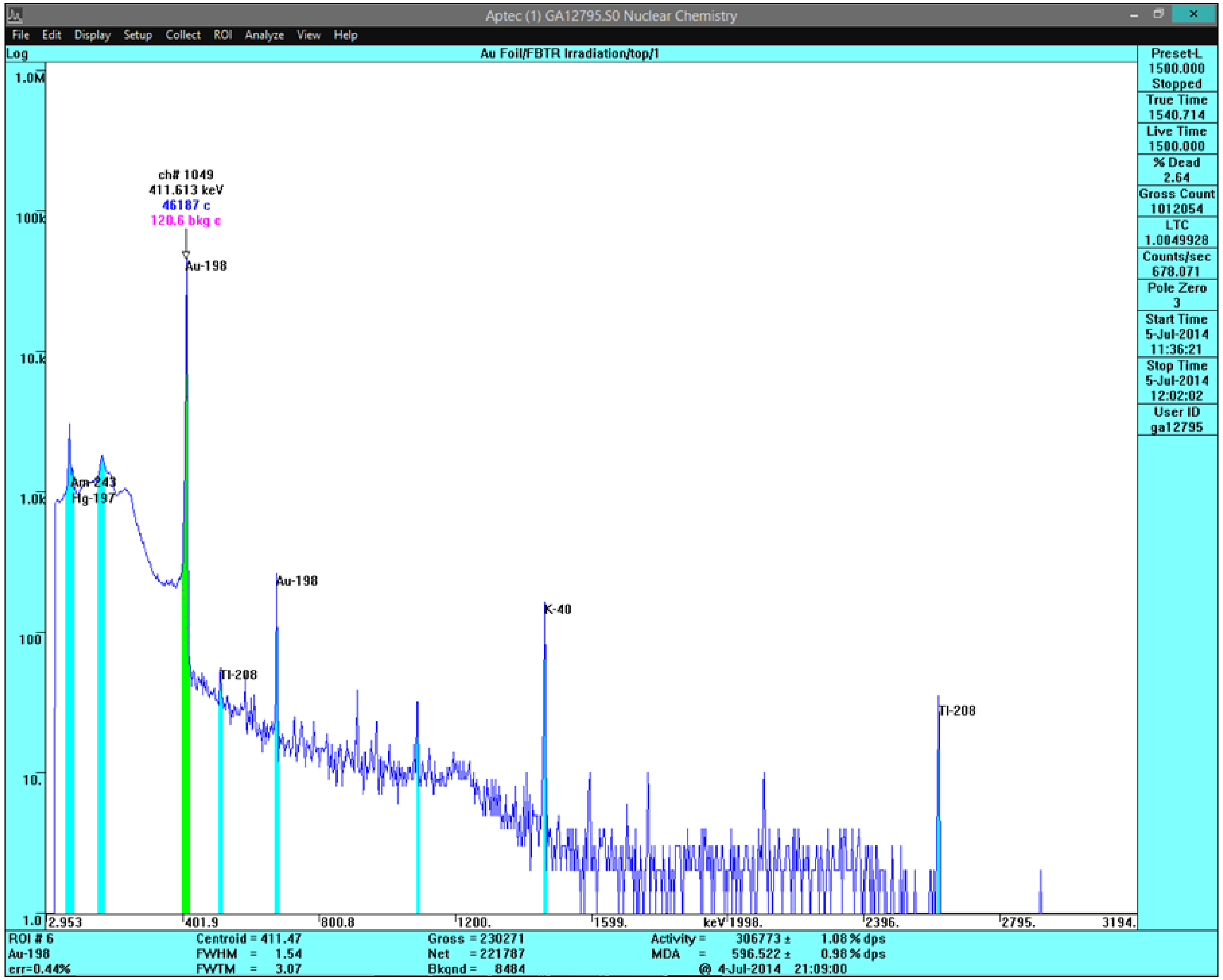

```
ch# 1049
411.613 keV
46187 c
120.6 bkg c
```

```
Preset-L
1500.000
Stopped
True Time
1540.714
Live Time
1500.000
% Dead
2.64
Gross Count
1012054
LTC
1.0049928
Counts/sec
678.071
Pole Zero
3
Start Time
5-Jul-2014
11:36:21
Stop Time
5-Jul-2014
12:02:02
User ID
ga12795
```

```
ROI # 6        Centroid = 411.47    Gross  = 230271    Activity =    306773 ±    1.08 % dps
Au-198         FWHM   =   1.54      Net    = 221787    MDA      =    596.522 ±   0.98 % dps
err=0.44%      FWTM   =   3.07      Bkgnd =    8484               @ 4-Jul-2014   21:09:00
```

Figure 4.7. A typical gamma spectrum of Au foil irradiated at FFEF of FBTR.

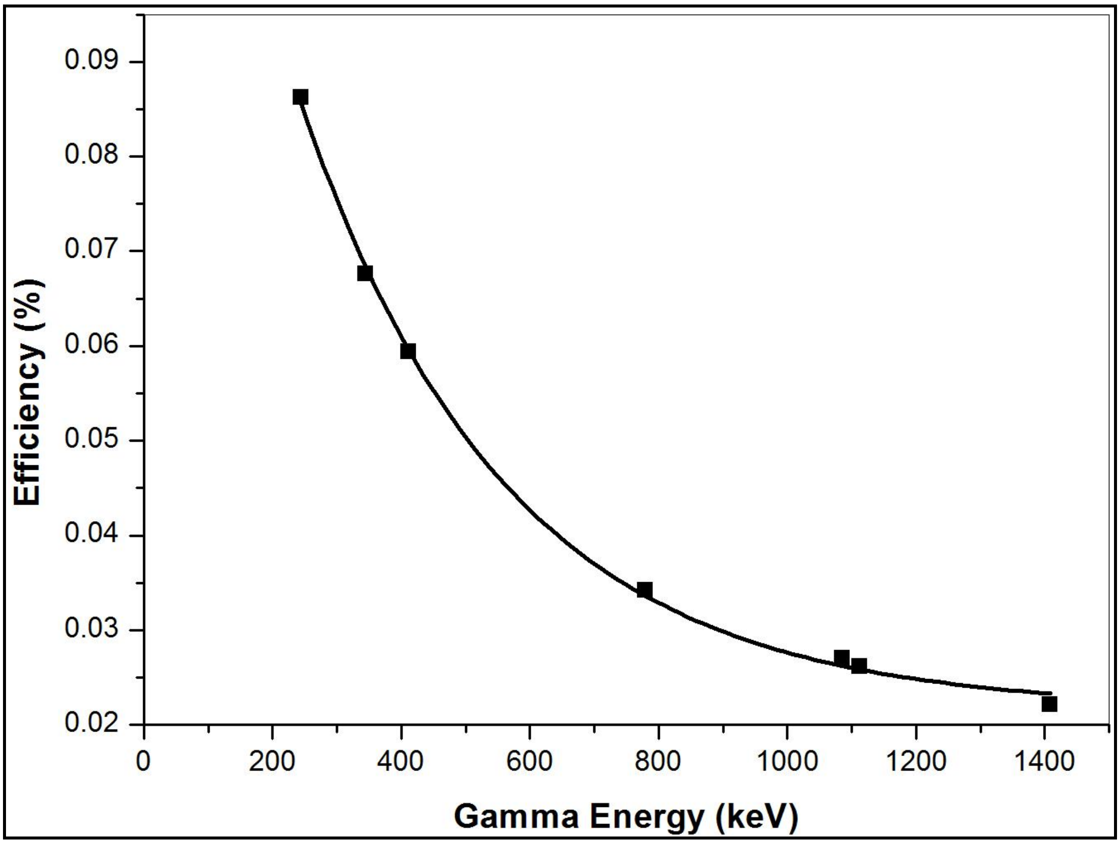

Figure 4.8. Efficiency of HPGe detector (30 cm away) for a point source as a function of gamma energy from 244 to 1408 keV.

4.3. Conclusion

Titanium has been chosen as the material of construction for the sample holder system to establish the FFEF at FBTR, because of its availability and better stability towards neutron irradiation. Radiation dose computations were carried out for both the matrix material (titanium) and its associated impurities present as well. The elemental impurities present in the titanium rod were established using the neutron activation analysis techniques (relative as well as IM-NAA). A total impurities of 14 elements i.e. Na, K, Cl, Sc, Fe, Mn, As, W, Co, Cr, Sb, La, Ta and Sm were found and quantified, except Fe and Cr, while all the other impurities were below 50 ppm. The concentration of Sc impurity has been slightly over estimated owing to the possible contribution from the other threshold nuclear reaction from titanium. The radiation dose due to the titanium and other impurities was evaluated corresponding to the 10 d irradiation at 400 kW power of FBTR and was found to be 125 mR/h and 0.8 mR/h at 2 cm and 1 m distance, respectively. The radiation dose values are highly conservative as the cross-sections considered at the sample location were much higher than the actual values. The radiation dose computations detailed above established that the most suitable choice of material for this purpose is titanium. Hence, a titanium extension rod of length 3252.5 mm and a diameter of 14.0 ± 0.1 mm is attached to the bottom end of the shield plug, while a titanium sample holder of length 50 mm and diameter 12 mm is attached to the bottom of this rod by screw joint. The bottom of the sample holder is in the form of a solid hexagon with a diameter of 12.12 mm across the flats.

Catcher foil technique is to be used for the irradiation studies at FFEF of FBTR. Aluminum was chosen as the catcher foil material and thermal stability of Al was evaluated to be favorable at ambient temperature in FFEF of FBTR towards the morphology and phase changes. The gold equivalent neutron flux was measured in this location at 25 kW power of FBTR using foil irradiation method and the same was found to be 2.54×10^{9} $cm^{-2}.s^{-1}$.

4.4. References

1. K. V. Suresh Kumar, A. Babu, B. Anandapadmanaban, G. Srinivasan, Twenty five years of operating experience with the Fast Breeder Test Reactor, Energy Procedia 7 (2011) 323-332.

2. Use of fast reactors for minor actinide transmutation, Proc. of a Specialists Meeting held in Obninsk, Russian Federation, 22-24 September (1992) IAEA-TECDOC-693,
3. T. Wakabayashi, K. Takahashi, T. Yanagisawa, Feasibility Studies on Plutonium and Minor Actinide Burning in Fast Reactors, Nucl. Technol. 118 (1997) 14-25.
4. D. I. Coomber, Radiochemical methods in analysis, Plenum press, New York and London, DOl: 10.1007/978-1-4613-4401-8 (1975).
5. K. K. Swain, R. Acharya, A. V. R. Reddy, Analysis of SMELS by k_0-based IM-NAA method using PFTS position of KAMINI reactor for quality control exercise, J. Radioanal. Nucl. Chem. 300 (2014) 33–37.
6. B. P. Singh and H. C. Evans, Relative efficiency of Ge(Li) gamma ray detectors from 0.5 to 12 MeV, Nucl. Instr. and Meth. 97 (1971) 474-482.
7. W. R. Kane and M. A. Mariscotti, An empirical method for determining the relative efficiency of a Ge(Li) Gamma-ray Detector, Nucl. Instr. and Meth. 56 (1967) 189-196.
8. R. Acharya, A. G. C. Nair, K. Sudarshan, A. Goswami, A. V. R. Reddy, Development and applications of k_0 based NAA and prompt gamma-ray NAA methods at BARC, J. Radioanal. Nucl. Chem. 278 (2008) 617–620.
9. D. M. Kemp, A. A. Smales, The determination of Scandium in rocks and meteorites by neutron-activation analysis, Anal. Chim. Acta. 23 (1960) 410-418.
10. S. G. Hutchison, F. I. Hutchison, Radioactivity in Everyday Life, J. Chem. Educ. 74 (1997) 501-505.
11. R. Acharya, K. B. Dasari, S. Sodaye, P. K. Pujari, C. R. Venkatasubramani, Determination of Trace Element Impurities in High Purity Titanium by INAA

Methods, Proc. Nucl. Radiochem. Symp. (NUCAR-2011), (Ed) R. M. Sawant, S. K. Sali, Meera Venkatesh and V. Venugopal, BRNS, Visakhapatnam (2011) 170.

12. H. Cember, T. E. Johnson, Introduction to Health Physics, Fourth Edition, he McGraw-Hill Companies, Inc., (2009).
13. C. K. Kim, W. W. Meinke, Thermal neutron-activation analysis of titanium using 5.8-minute titanium-51 and rapid radiochemical separation, Talanta 10 (1963) 83-89.
14. H. Naik, G. N. Kim, R. Schwengner, K. Kim, R. John, R. Massarczyk, A. Junghans, A. Wagner, A. Goswami, Fission product yield distribution in the 12, 14, and 16 MeV bremsstrahlung-induced fission of ^{232}Th, Eur. Phys. J. A 51 (2015) 150.
15. E. N. Coker, The oxidation of aluminum at high temperature studied by Thermogravimetric Analysis and Differential Scanning Calorimetry. Sandia National Laboratories(SNL-NM), Albuquerque NM, United States (2013).
16. P. K. Mukhopadhyay, The operating software of the PHAST PC-MCA Card, Proceedings of the Symposium on Intelligent Nuclear Instrumentation (INIT-2001), Bhabha Atomic Research Centre, Mumbai, India (2001) 307–310.
17. G. Steinhauser, S. Merz, F. Stadlbauer, P. Kregsamer, C. Streli, M. Villa, Performance and comparison of gold-based neutron flux monitors, Gold Bull. 45 (2012) 17-22.

CHAPTER 5

Chapter 5: Measurement of Relative Fission Yields for Actinide Targets at KAMINI and FBTR

The present chapter describes the results obtained from the irradiation of uranium foil and PuO_2-ZrO_2 targets at KAMINI and FBTR irradiation facilities, respectively [1,2]. The yields of several fission products were determined in both the irradiated targets. The data on fission product yields were an essential requirement to appreciate various phenomenon of nuclear physics and fission theory [3,4]. Studies on mass and charge distribution in the thermal and fast fission is necessitated for the investigation on the nuclear shells closure effects, nucleon pairing effects and the mechanism of fission process [5,6]. Further, the yield data for some of the fission products are still in ambiguity and need to be evaluated accurately [7]. The fission yield data were also needed at various stages of nuclear fuel cycle in order to optimize several factors in reactor design and operation, reprocessing of spent fuel, management of nuclear waste etc. [7-10].

5.1. Introduction

This chapter describes the irradiation studies of actinide targets carried out at Kalpakkam MINI (KAMINI) reactor and Fast Breeder Test Reactor (FBTR) with their associated characteristic neutron energy spectra. The catcher foil technique using aluminum foil was employed for the irradiation of natural uranium foil in KAMINI reactor [11]. The ratio of the cumulative yields of the various fission products with respect to one among them were determined and compared with literature reported values for the fission of ^{235}U. This chapter also provides various isobaric chains of the fission products studied along with their gamma emissions. The 15 wt% PuO_2-ZrO_2 targets were irradiated in a vertical stack of the FBTR. The cumulative yields of the several fission products for the fission of Pu were established along the axial length of the FBTR core, are reported here.

5.2. Irradiation of Uranium at KAMINI reactor

Ultra high pure aluminum was used as the catcher foil for capturing the recoiled fission products from the nuclear fission of uranium foil irradiated in KAMINI reactor with its neutron fluence of 7.8 x 10^{12} cm^{-2}. A typical gamma spectrum of Al catcher foil with fission products is shown in Figure 5.1 which was analyzed using PHAST peak fitting software [12]. The peak areas of various fission products were utilized to determine the relative fission yields with respect to one of the yields of the fission products using the following equation [13].

$$Y_i = Y_s \frac{A_i}{A_s} \frac{[(1-e^{-\lambda_s T_{irr}})e^{-\lambda_s T_d}]}{[(1-e^{-\lambda_i T_{irr}})e^{-\lambda_i T_d}]} \tag{5.1}$$

where 'Y_i' and 'Y_s' are the yields of the fission products of 'interest' and 'standard' that was used as reference, respectively. 'A' refers to the activity of the fission product which was calculated by equation 5.2 [14].

$$A = \frac{PA.(100).(100)}{LT.\%\varepsilon.a_\gamma} \tag{5.2}$$

where %ε refers to the efficiency of the HPGe detector,

PA refers photo peak area,

LT refers live time (sec) and

a_γ refers to the abundance of gamma ray from fission product.

The efficiency of HPGe detector was evaluated using ^{152}Eu standard point source as a function of gamma energy and is shown in the Figure 3.3 of section 3.2.2. The reported photon energies with their associated abundances are given in Table 5.1 for important gamma rays of different fission products encountered in this work [15]. Various isobaric chains of different low and high mass fission products observed in this study are given in Figure 5.2 and 5.3, respectively [4].

5.3. Relative yield measurements

The cumulative yields of all the fission products were determined with respect to the cumulative yield of the reference fission product ^{135}I chosen as suggested by IAEA [7]. The fission product ^{135}I is chosen as reference because all the precursors of the same are short-lived and hence its cumulative yield is expected to be associated with minimum error.

The relative yields with respect to ^{135}I obtained in the present study were compared with the reported values of CROUCH [16] and T.R. England & B.F. Rider from ENDF-349 [17] (Table 5.2). Percentages of deviations from the reported values in this study are also presented here. From the table, it is clear that the observed experimental fission yields ratios with respect to ^{135}I are in good agreement with the reported values for the fission in ^{235}U. The variations of fission yields in this study with respect to the reported values may be attributed to the nature of the neutron energy spectrum that may be different from the one corresponding to the reported values.

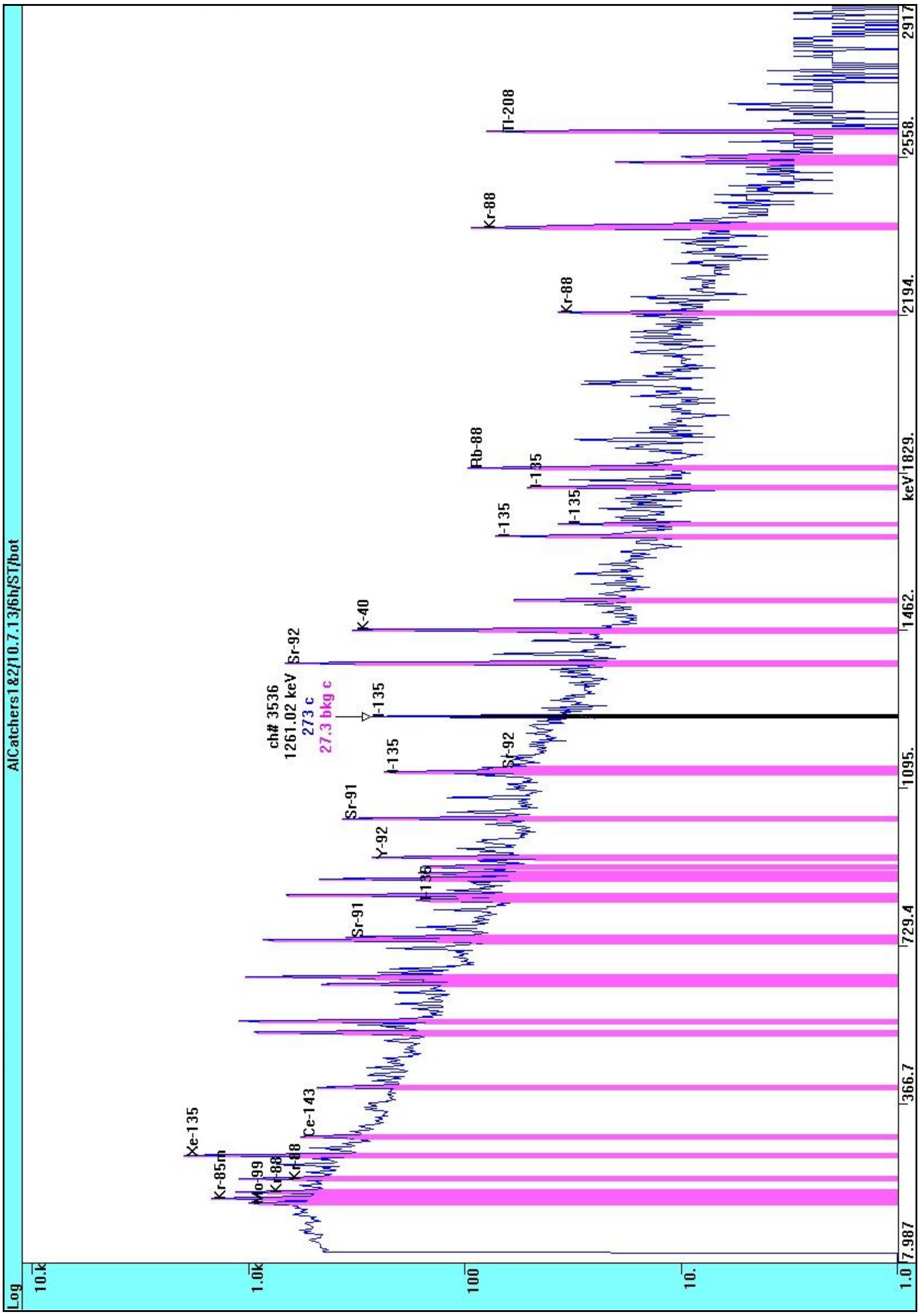

Figure 5.1. Gamma spectrum of Al catcher foil irradiated with natural uranium in KAMINI reactor.

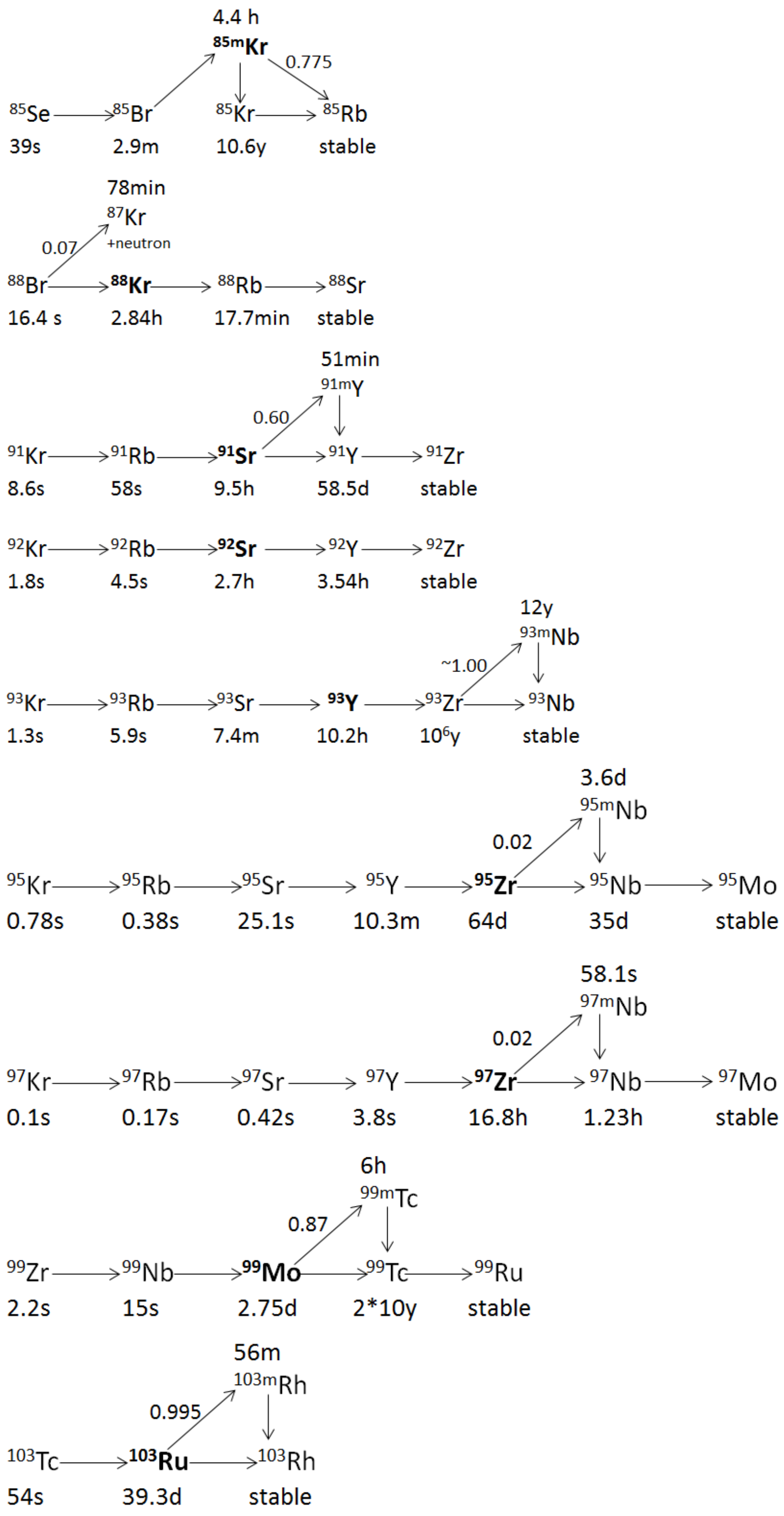

Figure 5.2. The isobaric chains for lower mass fission products [4] (The fission product for which cumulative yields were determined are shown bold).

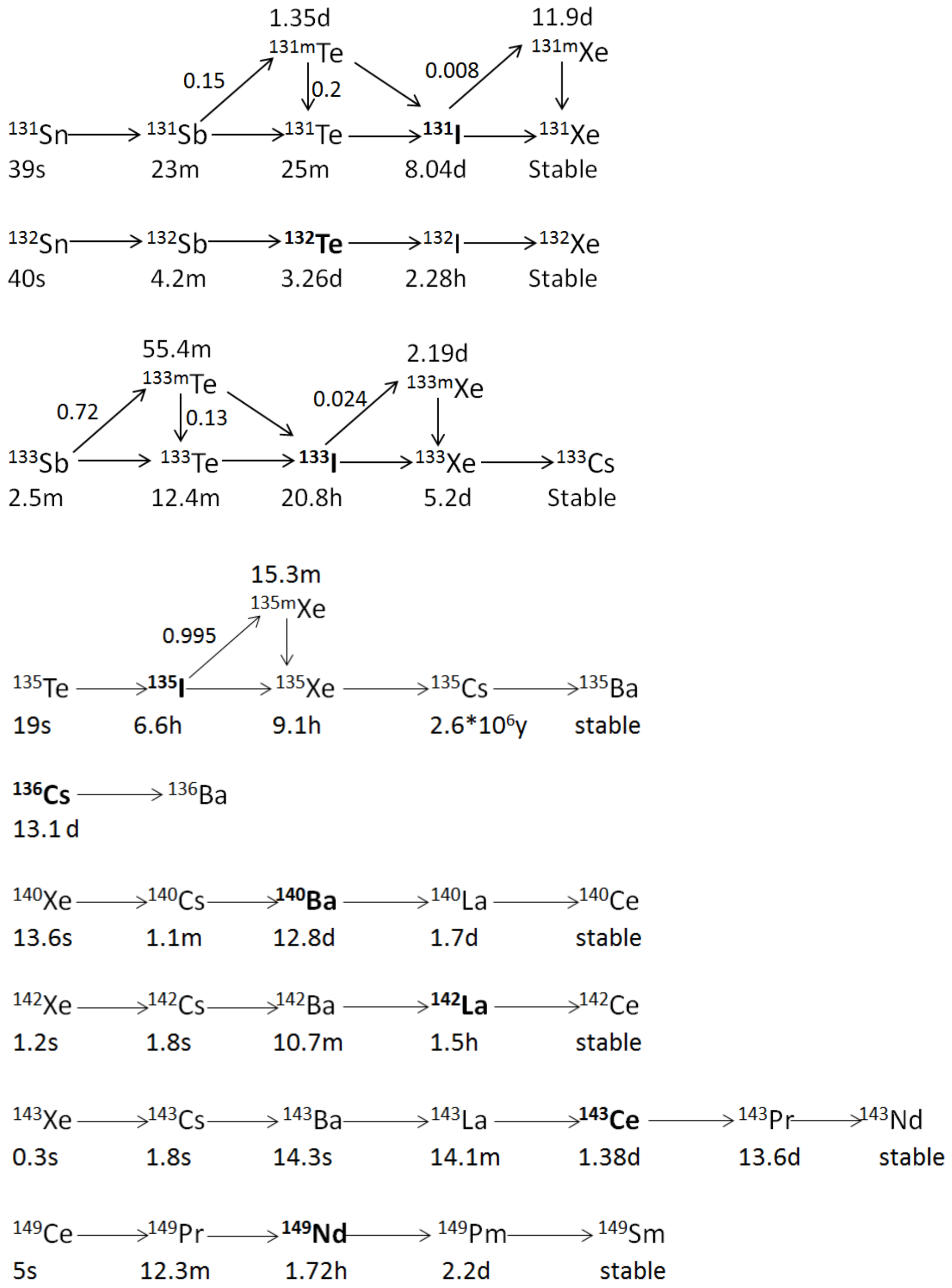

Figure 5.3. The isobaric chains for higher mass fission products [4] (The fission product for which cumulative yields were determined are shown bold).

Table 5.1. Nuclear Properties of fission products [15] observed in the present study

Fission Product	Gamma Energy (keV)	Intensity (%)
^{85m}Kr	151.2	75
^{88}Kr	2195.8	13.2
	2392.1	34.6
^{91}Sr	555.6	62
	749.8	23.7
	1024.3	33.5
^{92}Sr	1384.9	90.0
^{93}Y	266.9	7.3
^{95}Zr	724.2	44.3
	756.7	54.4
^{97}Zr	743.4	94.8
^{99}Mo	140.5	89.6
^{103}Ru	739.5	12.1
^{131}I	364.5	81.2
^{132}Te	228.2	88.1
^{133}I	529.9	86.3
^{135}I	1260.4	28.7
	1457.6	8.7
	1678.0	9.6
^{140}Ba	537.3	24.6
^{142}La	641.3	47
^{143}Ce	293.3	42.8
^{149}Nd	211.3	27.3

Table 5.2. Comparison experimentally observed relative fission yields by fission of ^{235}U with respect to ^{135}I with reported values

Fission Product	T.R. England & B.F. Rider [ENDF-349]	E. A. C. CROUCH	Experimental (Present Study)	Differences (%)	
				ENDF	Crouch
^{85m}Kr	0.2054	0.2195	0.2220	7.492	1.166
^{88}Kr	0.5653	0.5609	0.6173	8.419	9.124
^{91}Sr	0.9283	0.9815	0.9737	4.654	-0.8048
^{92}Sr	0.9459	0.9713	1.0093	6.282	3.763
^{93}Y	1.0111	1.0590	1.0541	4.076	-0.4655
^{95}Zr	1.0350	1.0819	1.1342	8.742	4.610
^{97}Zr	0.9522	1.0010	1.0123	5.931	1.110
^{99}Mo	0.9729	1.0205	0.9639	-0.9332	-5.869
^{103}Ru	0.4825	0.5237	0.4628	-4.255	-13.16
^{131}I	0.4602	0.4621	0.4504	-2.181	-2.616
^{132}Te	0.6847	0.7040	0.6735	-1.659	-4.518
^{133}I	1.0669	1.1180	1.0185	-4.750	-9.766
^{135}I	1	1	1	-	-
^{140}Ba	0.9889	1.0476	0.9708	-1.862	-7.915
^{142}La	0.9315	0.9818	0.9319	0.0348	-5.359
^{143}Ce	0.9490	0.9871	0.7854	-20.82	-25.67
^{149}Nd	0.1720	0.1796	0.1719	-0.0397	-4.451

It is also understood that the fission of ^{235}U with thermal neutrons is asymmetric in nature and the associated deviations are positive for lower mass fission products and negative for higher mass fission products with respect to the reported values. This observation can be attributed to the recoiling nature of fission products towards the Al catcher foil. The lower mass fission products easily recoil towards the catcher foil because of their long recoil range and higher recoil energy, whereas the higher mass fission products recoil relatively less readily due to their heavy mass with less recoil range and energy [18,19]. This leads to the positive deviation for almost all lower mass fission products as the reference fission product ^{135}I happens to be a higher mass fission product.

Figure 5.4 shows the comparison of cumulative yield ratios with respect to ^{135}I as a function of mass number (A). From the figure, it is observed that the cumulative mass – yield graph is incomplete at the valley and wings. This may be attributed to the fact that the fission products at valley (mass number, A, around 117) and at wings (mass number, A, near 75 and 155) are too low to be observed by gamma spectrometry. The gamma rays from these low yielded fission products were masked by the gamma rays of high intensity and high fission yields [20]. Hence, the radiochemical separation of either the fission products with high yield and high intense gamma fission products or low yield fission products specifically results into making the corresponding gamma spectrum less complex. This exercise also facilitated the identification and quantification of low yielded fission products at valley and wings by gamma spectrometry [20].

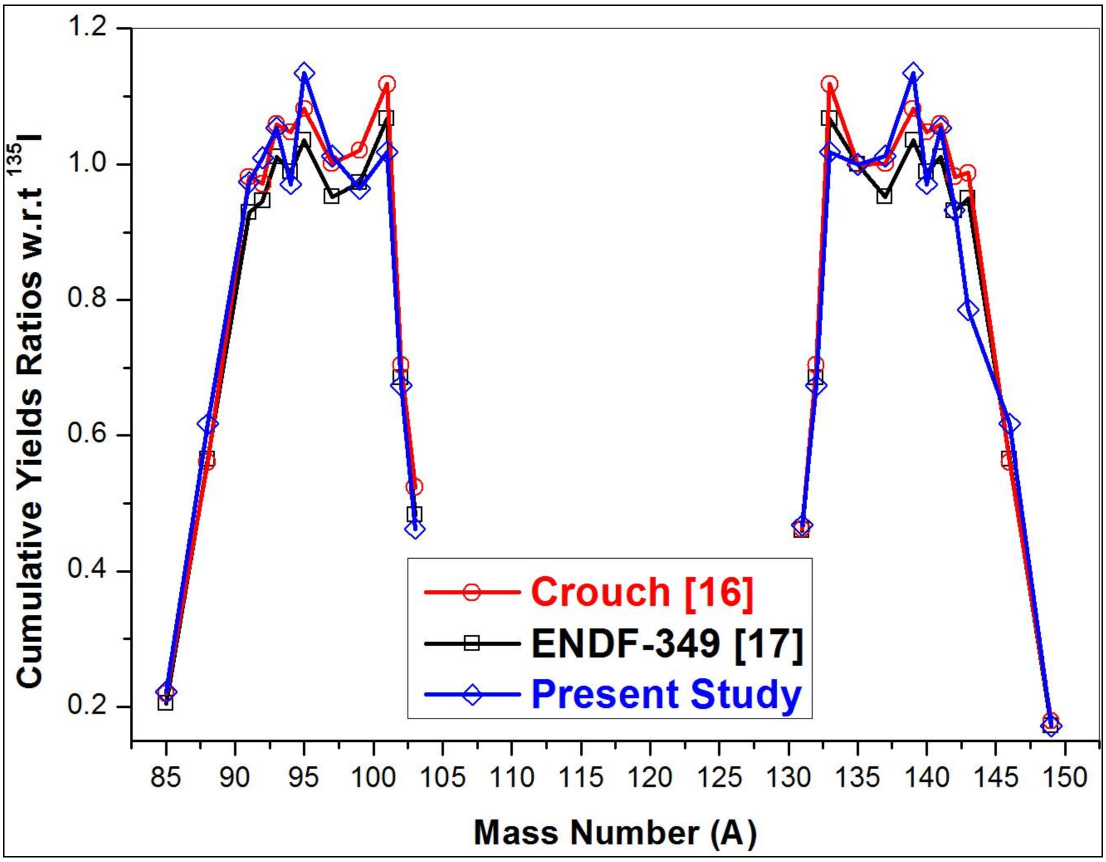

Figure 5.4. Mass-Cumulative yield ratios curve for the fission of ^{235}U comparing with literature values.

5.4. Irradiation of PuO_2-ZrO_2 targets at FBTR

The FBTR irradiated PuO_2-ZrO_2 targets at core centre and third ring were assayed by HPGe detector and the gamma spectra were analyzed using PHAST peak fit software. A typical gamma spectrum of irradiated target of PuO_2 -ZrO_2 with its associated fission products is shown in Figure 5.5. The activities of fission products were determined using their peak areas as per the equation 5.2 and the yields were calculated using the following equation [13].

$$Y = \frac{A}{N.\sigma.\phi.(1-e^{-\lambda T_{irr}}).e^{-\lambda T_d}} \tag{5.3}$$

where N is the number of target ^{239}Pu atoms,

σ is reaction cross section (cm^2) and

ϕ is neutron flux ($n.cm^2.s^{-1}$)

Remaining terms (λ, T_{irr} and T_d) are similar to the ones described in section 3.2.2.

The fission reaction rates for ^{239}Pu at core centre and third ring with respect to the stack height were theoretically calculated by Monte Carlo neutral particle simulations and presented in Table 5.3. The reaction rates were used to measure the yields of various fission products at core centre and third ring which are again presented in Table 5.4. It is observed from the table that the chain yields of all the fission products at third ring were higher than the corresponding yields at core centre. This may be due to the relatively higher thermal component at third ring than that of the core centre which thus reflects into higher fission cross sections at third ring.

Table 5.3. Fission reaction rates of ^{239}Pu at Core centre and third ring calculated by Monte Carlo simulations

Core Centre		**Third Ring**	
Target ID	**Fission Reaction Rate (s^{-1})**	**Target ID**	**Fission Reaction Rate (s^{-1})**
28	2.96E-12	25	2.36E-12
32	3.26E-12	74	2.58E-12
49	4.53E-12	47	3.34E-12
51	5.31E-12	40	3.89E-12
59	4.86E-12	60	3.74E-12
27	4.03E-12	38	3.31E-12
63	3.93E-12	43	3.32E-12

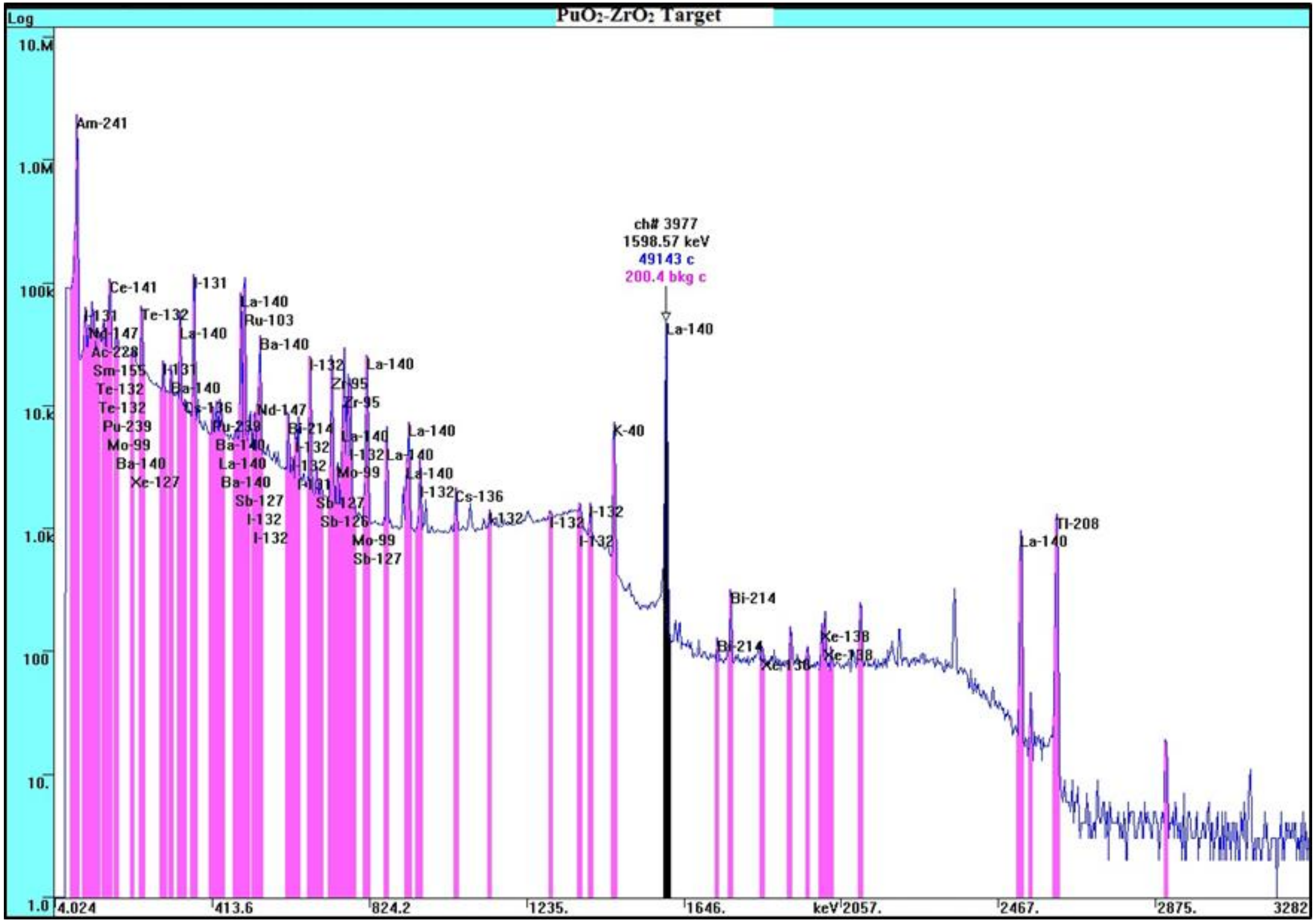

Figure 5.5. A typical gamma spectrum of one of the PuO_2-ZrO_2 targets irradiated at Fast Breeder Test Reactor.

Table 5.4. Yields of various fission products of ^{239}Pu at Core centre and third ring

Target No	^{103}Ru	^{136}Cs	^{99}Mo	^{140}Ba	^{132}Te	^{131}I
% Yields at Core centre						
28	6.45	0.0719	7.65	4.97	3.81	3.88
32	7.09	0.0989	8.01	5.35	4.25	4.13
49	4.85	0.0796	5.59	3.97	3.45	3.28
51	4.58	0.0698	4.84	3.49	3.27	2.84
59	4.43	0.0725	4.91	3.70	3.04	3.04
27	3.95	0.0540	4.94	3.29	2.91	2.50
63	4.88	0.067	6.34	3.83	3.03	3.08
% Yields at Third Ring						
25	10.45	0.130	8.78	7.66	5.16	5.33
74	10.53	0.115	8.93	7.77	5.04	5.56
47	8.37	0.119	7.98	6.69	4.42	4.53
40	8.44	0.110	7.28	6.24	4.30	4.62
60	7.66	0.102	6.64	5.72	3.64	3.78
38	8.57	0.096	7.49	6.23	4.16	4.60
43	8.10	0.085	7.34	5.76	4.04	4.15

5.5. Conclusion

Irradiation of uranium foil along with the Al catcher foils was carried out at KAMINI reactor and fission products were assayed by HPGe detector. The role of the catcher foils attached to uranium was to capture the recoiled fission products. The peak areas obtained from the gamma spectrometric analysis of the catcher foils were used to find out the activities of various fission products. The cumulative yields of various fission products were determined with respect to the cumulative yield of the reference fission product, ^{135}I. Thus, the relative cumulative yields were compared with the Crouch and ENDF-349 reported values and the same was found to be in good agreement. The minor deviations from these reported values were positive for lower mass fission products where as it was negative for higher mass fission products. This may be attributed to the relatively higher recoiling nature of lower mass fission products towards the catcher foil in comparison with ^{135}I.

PuO_2-ZrO_2 targets were irradiated at Fast Breeder Test Reactor by loading them vertically into a special subassembly (ISZ-100). The activities of different fission products were determined by high resolution gamma-ray spectrometry. The reaction rates for the fission of ^{239}Pu at the irradiation location were calculated using Monte Carle simulations. The activities and reaction rates were utilized to determine the yields of various fission products. The yields of the fission products at third ring were found to be higher compared to the yields at core centre. The possible explanation for this observation may be the presence of higher thermal component of neutrons at third ring than the one at core center resulting into higher reaction rates at third ring.

5.6. References

1. S. Usha, R. R. Ramanarayanan, P. Mohanakrishnan, R. P. Kapoor, Research reactor KAMINI, Nucl. Eng. Des. 236 (2006) 872-880.
2. K. V. Suresh Kumar, A. Babu, B. Anandapadmanaban, G. Srinivasan, Twenty five years of operating experience with the Fast Breeder Test Reactor, Energy Procedia 7 (2011) 323-332.
3. R. Vandenbosch, J. R. Huizenga, Nuclear Fission, Academic Press, INC. New York, (1973).
4. E. K. Hyde, The Nuclear Properties of the Heavy Elements, III, Fission Phenomena, Dover Publications, INC., New York, (1971).
5. A. C. Wahl, Nuclear-charge distribution near symmetry for thermal-neutron-induced fission of ^{235}U, Phys. Rev. C 32 (1985) 184.
6. A. C. Wahl, Nuclear Charge Distribution in Fission, New Directions in Physics, N. Metropolis, D. M. Kerr, G. C. Rota, (Eds.), Academic Press, INC., San Diego (1987) 163.
7. Compilation and evaluation of fission yield nuclear data, IAEA-Vienna (2000) IAEA-TECDOC-1168.
8. K. Kern, M. Becker, C. Broeders, K. C. Nord, Assessment of fission product yields data needs in nuclear reactor applications, PHYSOR 2012 Advances in Reactor Physics Linking Research, Industry, and Education, Knoxville, Tennessee, USA, April 15-20 (2012).
9. F. L. Lisman, W. J. Maeck, J. E. Rein, Determination of Nuclear Fuel Burnup from Fission Product Analysis, Nucl. Sci. Eng. 42 (1970) 215-219.

10. J. E. Rein, Status of Burn-up Measurement Methodology, IAEA-SM-149/40, Proc. of Symp. on Anal. Meth. Nucl. Fuel cycle, 29 November-3 December (1971) Vienna, 449-471.
11. H. Naik, G. N. Kim, R. Schwengner, K. Kim, R. John, R. Massarczyk, A. Junghans, A. Wagner, A. Goswami, Fission product yield distribution in the 12, 14, and 16 MeV bremsstrahlung-induced fission of ^{232}Th, Eur. Phys. J. A 51 (2015) 150
12. P. K. Mukhopadhyay, The operating software of the PHAST PC-MCA Card, Proceedings of the Symposium on Intelligent Nuclear Instrumentation (INIT-2001), Bhabha Atomic Research Centre, Mumbai, India (2001) pp. 307–310.
13. S. Prakash, S. B. Manohar, Radiochemical Methods of Measurements of Fission Products Yields, J. Radioanal. Nucl. Chem. 142 (1990) 119-133.
14. D. D. Sood, A. V. R. Reddy, N. Ramamoorthy, Fundamentals of Radiochemistry, 4 Eds., Indian Association of Nuclear Chemists and Allied Scientists; Mumbai, India (2010).
15. E. Browne, R. B. Firestone, Table of Radioactive Isotopes, V. S. Shirley (eds.) John Wiley & Sons, Inc., U.S.A. (1986).
16. E. A. C. Crouch, Fission-Product Yields From Neutron-Induced Fission, Atomic Data and Nuclear Data Tables 19 (1977) 417-532.
17. T. R. England and B. F. Rider, Evaluation and Compilation of Fission Product Yields, LA-UR-94-3106, ENDF-349, Los Alamos National Laboratory, October (1994).
18. R. B. Evans III, J. L. Rutherford, and R. B. Perez, Recoil of Fission Products in Homogeneous Carbon Structures, J. Appl. Phys. 38 (1967) 3127.

19. R. B. Evans III, J. L. Rutherford, and R. B. Perez, Recoil of Fission Products. II. In Heterogeneous Carbon Structures, J. Appl. Phys. 39 (1968) 3253.
20. D. E. Dry, E. Bauer, L. A. Petersen, Rapid separation of fresh fission products, J. Radioanal. Nucl. Chem. 236 (2005) 19-22.

CHAPTER 6

Chapter 6: Radiochemical Separation Studies of ^{144}Ce-^{144}Pr from fission products

This chapter deals with the radiochemical separation studies of ^{144}Ce-^{144}Pr pair from fission product solution using ion-exchange chromatography and solvent extraction techniques followed by demonstration of radioactive equilibrium phenomenon more particularly secular equilibrium using ^{144}Ce-^{144}Pr pair.

In radioactive decay, secular equilibrium is one of the most interesting phenomena in which a steady-state condition of equal activities occurs between a long-lived parent radionuclide and its short-lived daughter. The concept of radioactive equilibrium can be demonstrated using the ^{144}Ce-^{144}Pr pair. However, the experiment needs the pure source of parent ^{144}Ce, which demands a rapid and practically simple chemical method of separation. Separation of ^{144}Ce-^{144}Pr pair form fission products and activation products was achieved by ion-exchange chromatography followed by the separation of pure parent ^{144}Ce by solvent extraction method using di-(2-ethylhexyl)phosphoric acid (HDEHP) as the extractant. Assay of the separated pure ^{144}Ce fraction was carried out by NaI(Tl) detector and the total activity due to both parent (^{144}Ce) and in-grown daughter (^{144}Pr) was monitored continuously to profile the secular equilibrium. Half-life of ^{144}Pr was determined from secular equilibrium plot and compared with the half-life value obtained from the decay curve of pure ^{144}Pr fraction obtained from ^{144}Ce-^{144}Pr pair using extraction chromatographic technique.

6.1. Introduction

Radioactive equilibrium is a condition in which the ratio of the parent and its daughter activities remains constant whenever the daughter’s half-life is shorter than that of the parent. However, there is no possibility of achieving the equilibrium condition if the daughter half-life is longer than that of the parent. Further, there exists two types of equilibria i.e. secular and transient. A radioactive equilibrium between the parent and the daughter is referred as either transient or secular equilibrium, depending upon the relative half-lives of the parent and daughter in the pair. For a secular equilibrium, $T_{½}$ of the parent is greater than $T_{½}$ of daughter by at least an order of magnitude. However, for a transient equilibrium, the ratio of the half-life of the parent to that of the daughter is about or less than 10. Various parent-daughter pairs which are in radioactive equilibrium are shown in the Table 6.1 [1-7].

Table 6.1. Parent-Daughter pairs which are in radioactive equilibrium [1-7]

Type of equilibrium	Parent-Daughter pair	Half-life of Parent	Half-life of Daughter	Ratio $T_{1/2(P)} / T_{1/2(D)}$
Secular	^{137}Cs-^{137m}Ba	30 y	2.55 min	6.2x10^{6}
	^{144}Ce-^{144}Pr	285 d	17.3 min	2.37x10^{4}
	^{90}Sr-^{90}Y	28.8 y	2.7 d	3.9x10^{2}
Transient	^{99}Mo-^{99m}Tc	2.75 d	6.0 h	11.0
	^{166}Dy-^{166}Ho	3.4 d	1.117 d	3.04
	^{72}Se-^{72}As	8.4 d	1.08 d	7.77

In a radioactive equilibrium, the daughter always appears to decay with the half-life of the parent as long as it is present in the mixture but decays with its own half-life when separated from its parent. This observation is explained from the fact that the daughter is continuously produced from the parent when it is in equilibrium with the latter. In the case of secular equilibrium, the activity ratio of parent to daughter tends towards a constant value i.e. unity in this case. Further, the activity of parent remains apparently constant over the period of measurement because of its relatively very long half-life and hence its activity shows no significant or negligible change during the period of measurement. However, the activity of the daughter increases continuously until the rate of formation of the daughter equals to the rate of decay of the parent. Hence, the secular equilibrium phenomenon can be defined as a condition in which the ratio of activities of the parent and daughter radionuclides becomes a constant i.e unity with no significant or observable change in the parent activity during the period of observation [8]. Similarly, the ratio in the transient equilibrium is also a constant, but less than unity depending upon the decay constants of parent and daughter nuclides.

Among them, the pair ^{144}Ce-^{144}Pr was chosen to demonstrate the concept of radioactive equilibrium in general and secular equilibrium in particular in this work, for a practical convenience even though some of the other pairs also can be used for the same. Among the known pairs which are in secular equilibrium as shown in Table 6.1, the ^{90}Sr-^{90}Y has the disadvantage of having relatively a long lived daughter with a half-life of 2.7 d, which demands the observation period of more than about two weeks for the convenient demonstration of the phenomenon of secular equilibrium. The other pair ^{137}Cs-^{137m}Ba has a relatively short half-life for its daughter i.e. 2.55 min which is convenient to establish the secular equilibrium phenomenon in a relatively short observation time, but limits the accuracy in the measurement of the half-life of the daughter nuclide owing to the practical delay between the purification of the parent nuclide and the starting of the assay of the total activity using a detector. However, the pair ^{144}Ce-^{144}Pr which is in secular equilibrium has reasonable half-lives providing a practically convenient observation time of establishing the secular equilibrium phenomenon (~ 2 hours) as well as the accurate measurement of half-life.

In order to profile the growth of the daughter with a better accuracy, in a demonstration experiment, it is necessary to have a pure source of the parent, ^{144}Ce, free from its in-grown daughter of ^{144}Pr. The only viable source for the production of ^{144}Ce is the nuclear fission. The chain yields of the mass number 144 are 5.38% and 3.82% for the thermal neutron induced fission of ^{235}U and ^{239}Pu, respectively; but the same are 5.34%, 4.65% and 3.73% for the fast fission of ^{235}U, ^{238}U and ^{239}Pu, respectively [9]. The decay chain for the isobaric series corresponding to the mass number 144 is as follows.

$$^{144}Xe \xrightarrow{\beta^-(1.2s)} {}^{144}Cs \xrightarrow{\beta^-(1.01s)} {}^{144}Ba \xrightarrow{\beta^-(11.4s)} {}^{144}La \xrightarrow{\beta^-(40.7s)}$$

$$^{144}Ce \xrightarrow{\beta^-(284.9d)} {}^{144}\mathrm{Pr} \xrightarrow{\beta^-(17.29m)} {}^{144}Nd \xrightarrow{\alpha(2.29*10^{15}y)} {}^{140}Ce$$

The decay chain rapidly accumulates into the long-lived ^{144}Ce. Thus the presence of ^{144}Ce and its daughter (^{144}Pr) are the only observable radionuclides practically because of the fact that all the precursors of ^{144}Ce are short-lived. Decay schemes of ^{144}Ce and^{144}Pr are depicted in Figure 6.1 [10,11]. The parent nuclide ^{144}Ce decays into its daughter nuclide ^{144}Pr through β^- emission which decays again into ^{144}Nd by a beta emission. The half-lives of ^{144}Ce and ^{144}Pr are 284.9 d and 17.29 minutes, respectively. Some of the important decay characteristics of the parent ^{144}Ce and its daughter ^{144}Pr are shown in the Table 6.2.

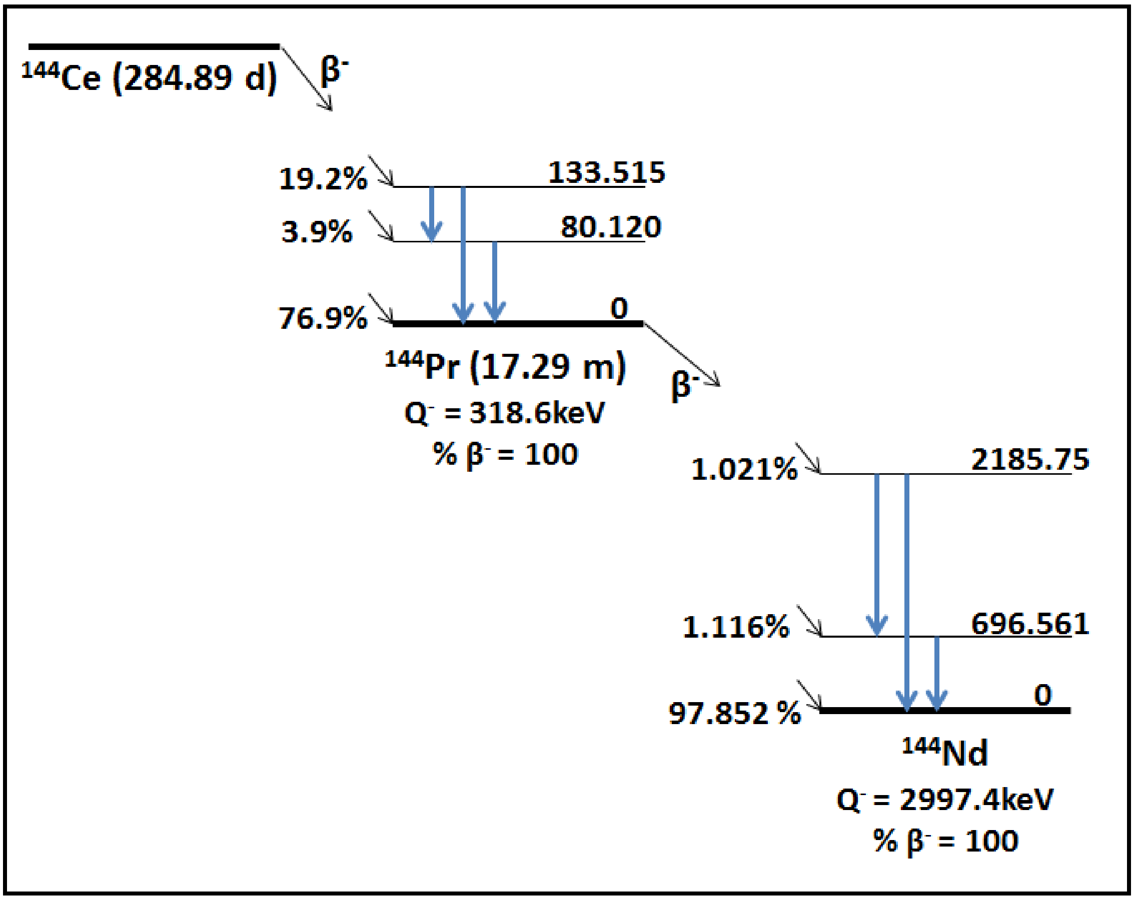

Figure 6.1. Decay scheme of ^{144}Ce and ^{144}Pr; Based on data from [10,11].

Table 6.2. Decay characteristics of the parent (^{144}Ce) and daughter (^{144}Pr)

	Gamma energy (keV)	**% Intensity**	$\beta^{-}_{\max}$ **(keV)**	**% Intensity**
^{144}Ce	133.5	10.83	185.1	19.2
	80.1	1.4	238.5	3.9
	53.4	0.1	318.6	76.9
^{144}Pr	696.5	1.4	811.8	1.02
	1489.2	0.28	2301	1.12
	2185.7	0.73	2997.5	97.85

In order to demonstrate the secular equilibrium behaviour using ^{144}Ce-^{144}Pr, it is preferred to start with a pure parent ^{144}Ce followed by assaying it by a suitable counting technique and thus the in-growth of daughter with the parent is profiled until the equilibrium or steady state is reached. Several methods were reported for the separation of ^{144}Pr from ^{144}Ce, particularly towards the development of its radio nuclide generator [1,4]. However, reports on the source preparation of ^{144}Ce for the demonstration of secular equilibrium concept were limited.

Walter et al. studied the absorption of ^{144}Ce from ^{144}Pr on manganese dioxide coated alumina and elution of ^{144}Pr under different conditions [4]. Semmelrogge et al. carried out the studies on secular equilibrium of ^{144}Ce-^{144}Pr in which ^{144}Ce was separated by solvent extraction followed by its precipitation on a planchet [1]. Tompkins et al. studied the separation of ^{144}Pr from ^{144}Ce using a cation-exchange resin, Dowex 50 with a 5% citrate complexing solution (pH=3.0) as the eluent [12]. But McDonald et al. studied the same using an anion exchange resin, Dowex l (100-200), and 9N HNO_3 containing 0.5N $NaBrO_3$ as an eluting agent [13]. Bradley et al. separated ^{144}Ce from ^{144}Pr as an insoluble iodate salt of cerium in the oxidation state of +4 [14].

All these methods describe either the separation of ^{144}Pr from ^{144}Ce, or precipitation of ^{144}Ce, a time consuming and a relatively clumsy process which is a matter of concern especially while demonstrating the secular equilibrium concept in a normal chemistry laboratory where the radiochemical processing is carried out very carefully observing all the safety precautions to avoid contamination. In order to establish the secular equilibrium and to determine the half-life of daughter nuclide, it is important to obtain a sample of parent nuclide ^{144}Ce with as much purity as possible, so that the profiling of daughter nuclide before reaching the radioactive equilibrium can be accomplished conveniently as accurately as possible. To follow the kinetics more proficiently, the time gap between the separation of ^{144}Ce and its counting should be as short as possible. Hence, a rapid solvent extraction method was demonstrated in this work in which the pure parent (^{144}Ce) was obtained and assayed immediately after its separation.

Extraction chromatographic studies were also carried out to separate pure ^{144}Pr and subsequently follow its half-life, by which its purity was ascertained clearly and indirectly, for reporting its half-life unambiguously. The present work describes a simple and rapid separation procedure to obtain a pure ^{144}Ce by using solvent extraction and pure ^{144}Pr by using extraction chromatography. This procedure is established to be a simple and a practically convenient technique for a demonstration experiment in any educational institution which is not qualified to handle radioactive materials with negligible or no possibility of any spread of contamination.

6.2. Separation of ^{144}Ce-^{144}Pr from the fuel dissolver solution by using ion-exchange chromatography

6.2.1. Batch studies with fission product solution

All the equilibrated samples from batch studies were assayed by HPGe detector and the distribution ratios (D_M) were calculated using the following equation.

$$D_M = \frac{(A_0 - A)V}{AM} \qquad (6.1)$$

where A_0 and A are the activities (cps) of the elements in the aqueous phase before and after equilibration with the resin, respectively; V is the volume of the solution kept for equilibration (mL) and M is weight of the resin (g).

The distribution ratios for the different radio tracers, representing various fission and activated products present in the dissolver solution were determined as a function of nitric acid concentration for the Dowex resin. The data obtained are plotted as shown in Figure 6.2. It is observed from the graph that the D_M values of all the tracers decreased nearly exponential with the increased concentration of nitric acid in the range of study. It was also observed that the D_M values of Ce were always much higher than that of the other tracers over a range of nitric acid concentration i.e. up to 4M nitric acid.

This behaviour may be attributed to the relatively stronger interaction of Ce with cation-exchange resin in comparison with the other fission products in the simulated solution owing to its relatively higher ionic potential i.e. charge to radius ratio. Even though, the distribution ratio and the separation factor were observed to be higher and comparable for Ce at both 0.5M as well as 1M HNO_3, the latter concentration was chosen because of the fact that it yielded a baseline separation of Ce from other fission products by ion-exchange chromatography, in a relatively less volume of eluent.

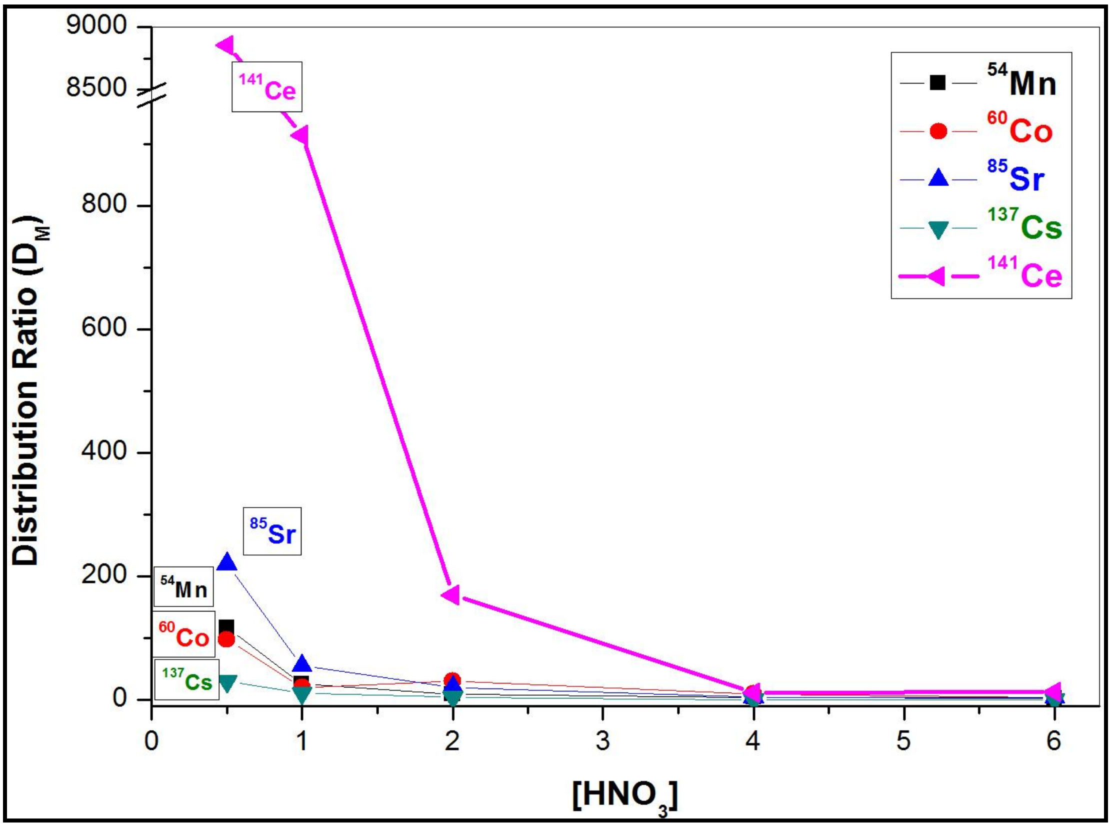

Figure 6.2. Variation of the distribution ratios with the nitric acid concentration in the DOWEX 50W×8 (100–200 mesh) resin (Amount of resin in each tube: 50 mg; Volume of the HNO_3 solution: 5 mL; Equilibration time: 4 h; Assay: Gamma Spectrometry using HPGe detector).

6.2.2. Separation of ^{144}Ce-^{144}Pr from fuel dissolver solution

The separation profile for the fission products using Dowex resin column was established and the elution profile is shown in Figure 6.3. It is observed that the fission products such as ^{137}Cs, ^{134}Cs, ^{125}Sb, ^{106}Ru-^{106}Rh and more importantly the activation products ^{54}Mn and ^{60}Co were all eluted in the initial fractions with 1M nitric acid as the eluting agent. This can be attributed to the lower distribution ratio values of these metal ions at the eluent concentration of 1M HNO_3. Cerium was eluted last owing to its very high distribution ratio and collected in a small fraction using 6M

HNO_3 along the other lanthanides i.e. in-grown ^{144}Pr and traces of ^{154}Eu impurity. Thus, a lanthanide group separation from other fission products was performed initially followed by a specific isolation of cerium from the lanthanide group was carried out to demonstrate the secular equilibrium behaviour subsequently.

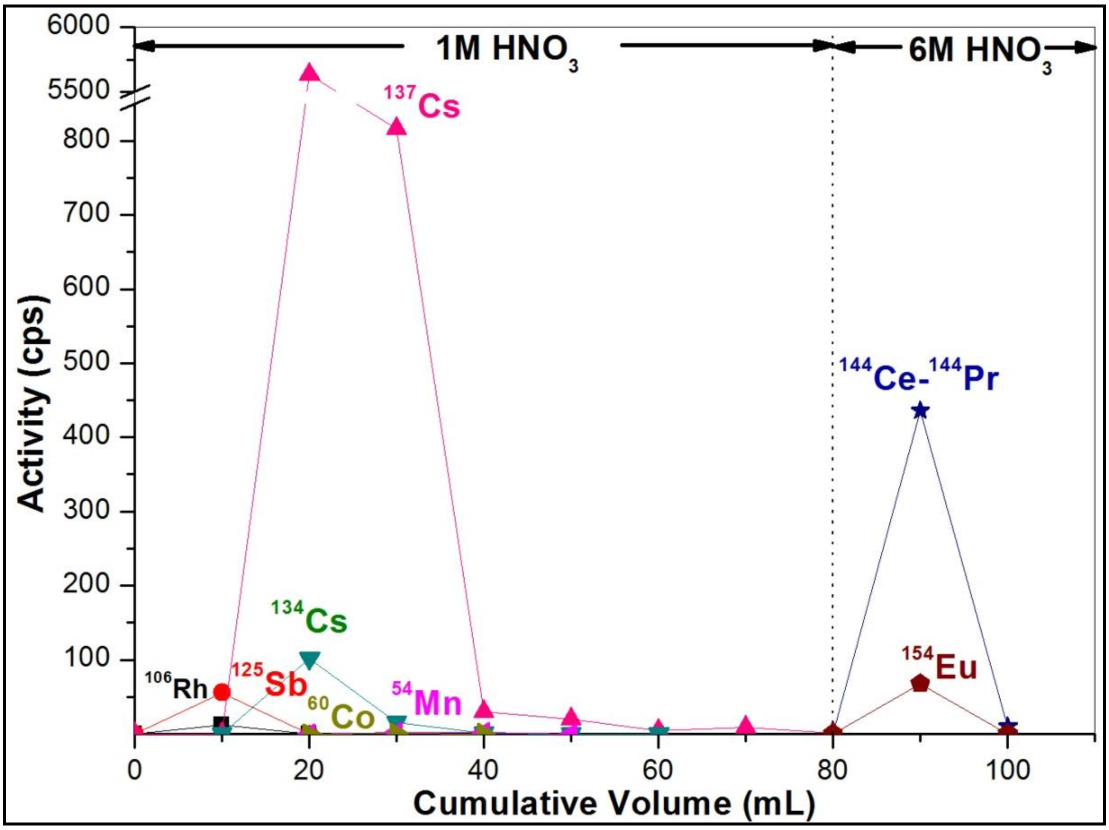

Figure 6.3. Elution profile for the separation of ^{144}Ce from fission and activation products using cation exchange chromatography (Amount of Dowex resin: 1 g; Column Dimensions: 8 mm ID, 25 cm Length and 4 cm bed height; Conditioning: 0.001M Nitric acid; Feed: Fission product solution in 0.001M HNO_3; Flow rate: 0.4-0.5 mL/min; Assay: Gamma Spectrometry using HPGe detector).

6.3. Purification of ^{144}Ce from its in-grown-daughter-in-equilibrium ^{144}Pr by using solvent extraction

6.3.1. Purification of HDEHP

The pure HDEHP (Figure 6.4) is a clear colourless solvent, it is amber in colour in case of commercial HDEHP. The purification of the commercial HDEHP was accomplished through the precipitation of its copper complex [15] i.e.

$$Cu(OH)_2 + 2HDEHP_{(org)} \Leftrightarrow Cu(DEHP)_{2_{(org)}} + 2H_2O \qquad (6.2)$$

The $Cu(DEHP)_2$ precipitate was converted into the pure HDEHP by contacting it with dilute HCl. The acid washings were repeated with HCl to remove all the copper from the HDEHP phase. The clear HDEHP phase was contacted with Millipore water to remove the dissolved acid and the water was evaporated off using a rotary evaporator. The purified HDEHP was used for the subsequent separation studies.

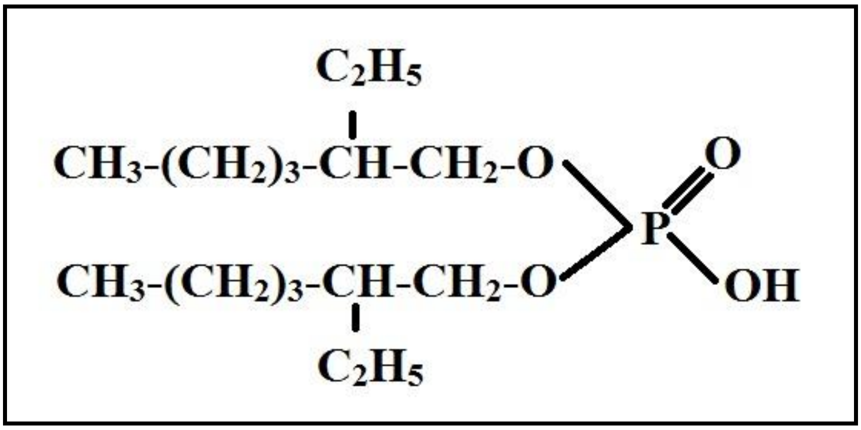

Figure 6.4. Structure of di-(2-ethylhexyl)phosphoric acid (HDEHP).

6.3.2. Purification of ^{144}Ce from ^{144}Pr

The secular equilibrium phenomenon was demonstrated conveniently using the pure fraction of ^{144}Ce including its purification from its in-grown daughter product ^{144}Pr. The variation in the total counts of the pure ^{144}Ce fraction was profiled using NaI (Tl) detector that included the associated growth of the daughter product ^{144}Pr there on. Purification of ^{144}Ce from its in-grown daughter product, ^{144}Pr is a challenging task owing to the fact that they both belong to the same lanthanide series and their separation is made difficult by the nature of their inherent complicated separation chemistry owing to the similar oxidation state of +3 as well as their similar chemical behaviour due to the phenomenon of lanthanide contraction. However, cerium also has another stable oxidation state of +4 which facilitates its separation both from the other lanthanides as well as the fission products [16,17]. Initially, the lanthanides i.e. ^{144}Ce-^{144}Pr and ^{154}Eu were separated from the other fission products by ion-exchange chromatography as described earlier in this chapter followed by the separation of ^{144}Ce(IV) from the lanthanide fraction using solvent extraction technique. Separated fraction of pure ^{144}Ce(IV) gets quickly contaminated with its in-grown daughter nuclide ^{144}Pr and hence requires fresh purification every time to obtain a pure fraction of the parent nuclide ^{144}Ce. The purification of the parent fraction from its daughter ^{144}Pr is carried out by adding 1M $KBrO_3$ solution that converts all the Ce(III) into a single and uniform oxidation state of Ce(IV) and facilitates its efficient extraction by the extractant HDEHP from the other lanthanides as well [16,17], as shown below.

$$KBrO_3 + 6Ce(NO_3)_3 + 6HNO_3 \rightleftharpoons 6Ce(NO_3)_4 + KBr + 3H_2O \qquad (6.3)$$

$$KBrO_3 + 5KBr + 6HNO_3 \rightarrow 3Br_2 \uparrow + 3H_2O + 6KNO_3 \qquad (6.4)$$

^{144}Ce was extracted into the organic phase (HDEHP) while the daughter product ^{144}Pr was retained in the aqueous phase. HDEHP exists as a dimer in dilute organic medium, i.e. $(HDEHP)_2$. The nature of the extracted species depends on the nature of the acid in the aqueous phase and its concentration [18]. The extraction of cerium(IV) from nitric acid medium to the organic phase is represented as follows [19,20].

$$Ce^{4+} + 4(HDEHP)_2 \rightleftharpoons Ce(H[DEHP])_4 + 4H^+ \qquad (6.5)$$

The purified ^{144}Ce in the organic phase was assayed by using a NaI(Tl) detector to demonstrate the secular equilibrium phenomenon.

6.4. Demonstration of secular equilibrium behaviour of ^{144}Ce-^{144}Pr

The time interval between the end of separation of pure ^{144}Ce and to the beginning of assay in the experiment must be as short as possible, to precisely profile the variation of the total activity as well as the growth of the daughter ^{144}Pr. The pure parent sample was counted by well type NaI(Tl) scintillation detector and the total activity there on was monitored periodically for a period of about two hours as shown in Table 6.3. The initial delay of seven minutes to assay the purified fraction was due to the minimum time required to bring the sample to the detector immediately after its separation. The total activity was observed to increase initially that remained apparently constant after some time. The initial increase in the total activity was attributed to the in-growth of the daughter nuclide ^{144}Pr from its pure parent ^{144}Ce. The total activity remained apparently constant due to the subsequent achievement of radioactive equilibrium (Table 6.3).

Table 6.3. Activity profiles of parent (^{144}Ce) and daughter (^{144}Pr) used for the demonstration of secular equilibrium phenomenon (Sample: 2 mL of pure ^{144}Ce; Assay: NaI(Tl) detector)

Time (min)	**Total Activity (cps) [$^{144}Ce+^{144}Pr$] (Experimental)**	**Parent decay (cps) (Calculated)**	**Daughter growth in Parent (cps) (Calculated)**	**Daughter Decay (cps) (Calculated)**
7.0	356.7	285	71.7	213.3
8.0	367.2	285	82.2	202.9
9.0	374.5	285	89.5	195.5
10.0	382.8	285	97.8	187.3
11.0	389.1	285	104.1	180.9
12.0	394.1	285	109.1	175.9
13.0	406.5	285	121.5	163.6
14.0	408.7	285	123.7	161.3
15.0	410.6	285	125.6	159.4
16.0	422.2	285	137.2	147.8
17.0	431.7	285	146.7	138.3
18.0	432.5	285	147.5	137.5
19.0	433.6	285	148.6	136.4
20.0	445.0	285	160.0	125.0
25.0	467.8	285	182.8	102.2
30.0	485.2	285	200.2	84.8
35.0	501.9	285	216.9	68.1
40.0	514.3	285	229.3	55.7
45.0	522.2	285	237.2	47.8
50.0	531.9	285	246.9	38.2
55.0	540.8	285	255.8	29.3
60.0	542.1	285	257.1	27.9
65.0	553.9	285	268.9	
70.0	555.4	285	270.4	
75.0	553.5	285	268.5	
80.0	563.0	285	278.0	
85.0	562.7	285	277.7	
90.0	560.1	285	275.1	
95.0	563.8	285	278.8	
100.0	563.0	285	278.0	
110.0	567.7	285	282.7	
120.0	575.0	285	290.0	

The total activity of ^{144}Ce-^{144}Pr pair from the NaI (Tl) detector was plotted as a function of time *(curve a)* using a semi-log graphical pattern as shown in Figure 6.5 [21]. As there was some short time delay between the separation of pure ^{144}Ce and its initial counting, the missing data points during this period were obtained by back-extrapolating the total activity data to the Y-axis. By using this plot, individual profiles i.e. profiles of the parent decay, daughter growth in parent and daughter decay were resolved (Figure 6.5.).

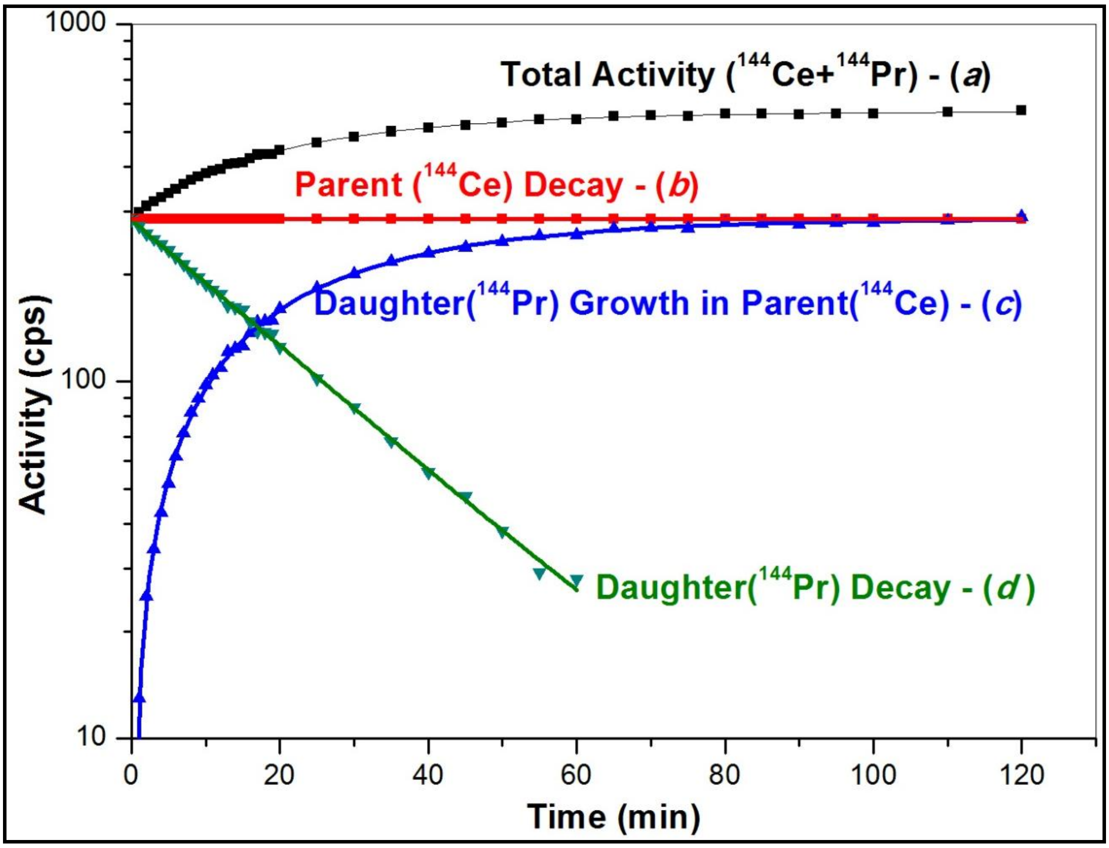

Figure 6.5. Demonstration for secular equilibrium using ^{144}Ce-^{144}Pr pair (Sample details: 2 mL of pure ^{144}Ce fraction separated by solvent extraction using HDEHP & the total activity assay by using NaI(Tl) scintillation detector).

‘Parent decay’ profile *(curve b)* was obtained by drawing a straight line parallel to the linear portion of the total activity curve from the point of total activity at zero time. ‘Daughter growth in parent’ *(curve c)* line was obtained by subtracting parent activity curve (*b*) from the ‘Total activity’ *(curve a)*. ‘Daughter decay’ *(curve d)* was profiled by subtracting daughter growth in parent curve *(curve c)* from parent activity curve *(b)*. This corresponds to the independent decay profile of daughter activity, separated from the parent in-equilibrium. The half-life of the daughter ^{144}Pr was determined using its decay curve which was found to be 17.14 ± 0.17 min and agreed well with the reported value of 17.29 min [10,11].

The ^{144}Ce-^{144}Pr pair which is in secular equilibrium was analysed by HPGe detector. The gamma spectrum of the same sample is shown in Figure 6.6. The spectrum indicated the presence of parent ^{144}Ce which was extracted in its pure form into organic phase and the in-grown daughter ^{144}Pr from the same. The long lived ^{144}Ce parent shows no significant change in decay rate except the variation due to the statistics during the period of experiment, while the daughter ^{144}Pr grows into a constant value. The rate at which the daughter ^{144}Pr grows to this constant value depends on its half-life and not on that of parent ^{144}Ce. This experiment demonstrates the parent-daughter relationship in the phenomenon of secular equilibrium satisfactorily.

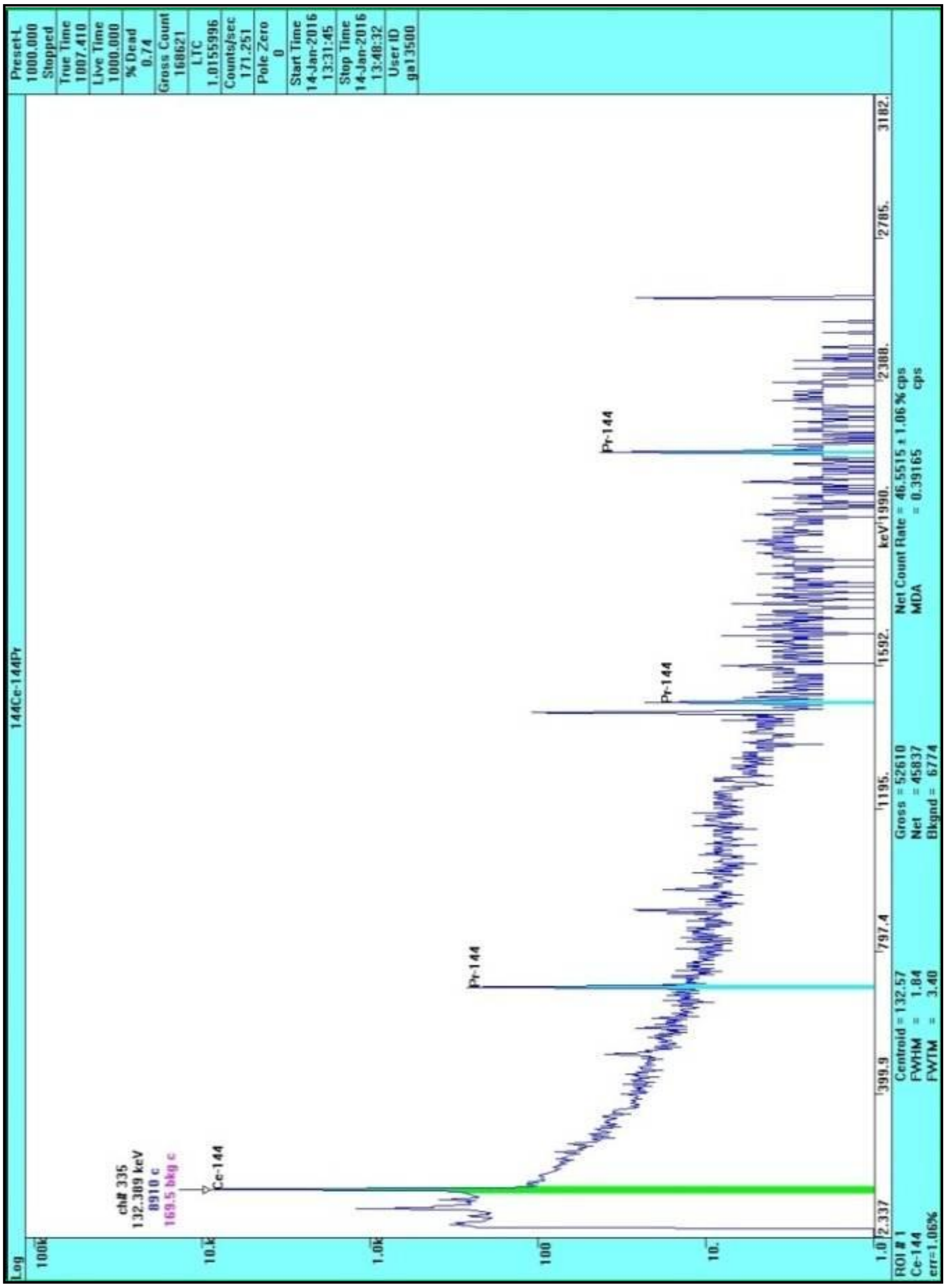

Figure 6.6. Gamma spectrum of ^{144}Ce-^{144}Pr secular equilibrium pair by HPGe detector.

6.5. Determination of half-life using the pure fraction of ^{144}Pr obtained by extraction chromatography

The extraction chromatographic studies for the purification of ^{144}Pr were carried out using 40% w/w HDEHP-XAD7 resin. The column was conditioned using $KBrO_3$ to maintain the Ce oxidation state in +4, so that it binds more strongly to the resin. The gamma spectrometric analysis of the eluted fractions in the medium of 1M $KBrO_3$ in 9M HNO_3 showed the presence of ^{144}Pr only, indicating that all the ^{144}Ce was held strongly with the resin. The decay curve of the purified fraction of ^{144}Pr was established by assaying it continuously using HPGe detector over a period of time.

The pure ^{144}Pr fraction was assayed continuously, periodically by high resolution gamma ray spectrometry using HPGe detector for a period of 75 min and obtained its corresponding decay profile (Figure 6.7). The half life obtained from the decay profile was found to be 17.32 ± 0.64 min which was again in good agreement with the reported value i.e. 17.29 min [10,11]. The half-life value of the daughter nuclide ^{144}Pr obtained from the pure fraction yielded a more accurate value compared to the value (17.14 min) obtained by secular equilibrium graph as discussed earlier, which in turn ascertains the purity of the daughter nuclide. This may be due to the fact that the half-life value is obtained directly from the decay of the pure daughter nuclide ^{144}Pr.

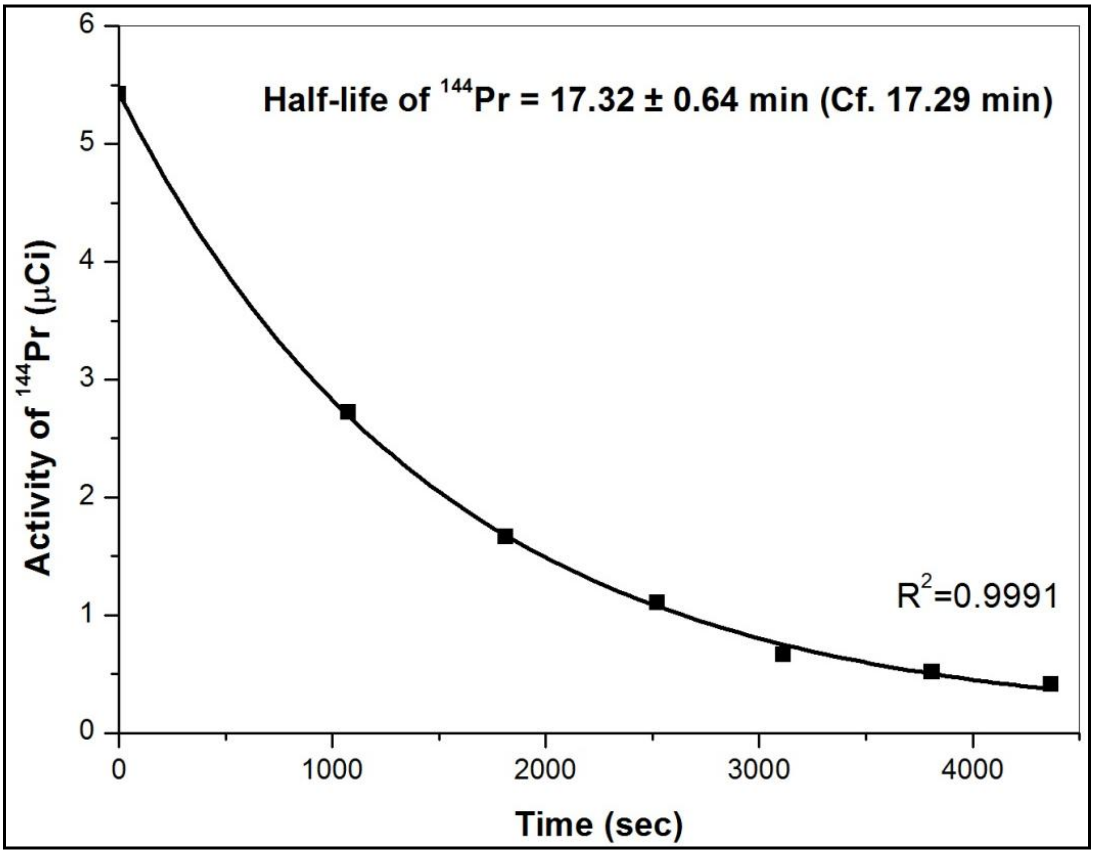

Figure 6.7. Decay profile of ^{144}Pr (Amount of resin: 5 g of 40% w/w HDEHP coated XAD7; Column Dimensions: 10 mm ID, 25 cm Length and 10 cm bed height; Conditioning: 1M $KBrO_3$ in 9M HNO_3; Feed: tracer mixture (^{144}Ce-^{144}Pr) in 1M $KBrO_3$/9M HNO_3; Flow rate: 0.8-0.9 mL/min; sample volume: 15 mL; Assay: Gamma Spectrometry using HPGe detector).

6.6. Conclusion

Batch studies were performed to determine the distribution ratio values of simulated fission products solution in Dowex 50Wx8 (100-200 mesh) resin as a function of nitric acid concentration. Cerium exhibited higher distribution ratio and separation factors than the other radionuclides at all concentrations of nitric acid. The purification of ^{144}Ce-^{144}Pr pair by ion-exchange chromatography involved the initial elution of all the other fission products by 1M HNO_3 and subsequent elution of ^{144}Ce-^{144}Pr pair from the column using 6M HNO_3 in a single fraction.

The solvent, di-(2-ethylhexyl)phosphoric acid (HDEHP) was purified by precipitation method with $Cu(SO_4)_2$ and used for the subsequent studies. The separation of pure parent (^{144}Ce) from the ^{144}Ce-^{144}Pr pair was achieved by solvent extraction method using 0.7M HDEHP/n-heptane as an extractant. The pure fraction of ^{144}Ce was assayed using a well type NaI(Tl) detector and the total activity of the pure ^{144}Ce and its in-grown daughter nuclide ^{144}Pr thereon was also monitored as a function of tie. The graph of total activity versus time was plotted in a semi log graph paper, to establish the secular equilibrium. The plot was resolved for its individual components i.e. parent decay, daughter growth in parent and daughter decay.

The daughter nuclide ^{144}Pr was purified from its parent in-equilibrium ^{144}Ce by extraction chromatographic technique using 40% w/w HDEHP impregnated XAD7 resin with 1M $KBrO_3$- 9M HNO_3 as the eluent. Half-life of ^{144}Pr was obtained from this graph and found to be 17.32 ± 0.64 min which is in agreement with the value obtained from the secular equilibrium graph i.e. 17.14 ± 0.17 min. Thus the half-life values obtained from pure fraction ^{144}Pr as well as equilibrium curve were in agreement with the reported value, namely, 17.29 min. Thus the phenomenon of secular equilibrium was demonstrated using the pure fraction of ^{144}Ce satisfactorily.

6.7. References

1. W. F. Semmelrogge, Fred Sicilio, A Study of Secular Equilibrium using ^{144}Ce-^{144}Pr, J. Chem. Educ. 42 (1965) 427-428.
2. G. R. Choppin, Carson L. Nealy, Demonstration of a parent-daughter radioactive equilibrium using ^{137}Cs-^{137m}Ba, J. Chem. Educ. 41 (1964) 598-600.
3. H. Arino, H. H. Kramer, A new ^{137}Cs/^{137m}Ba Radioisotope generator system, Int. J. Appl. Radiat. Isot. 24 (1973) 197-200.

4. J. S. Walter, H. Arino, K. H. Herman, A New ^{144}Ce-^{144}Pr Radioisotope Generator System, Int. J. Appl. Radiat. Isot. 29 (1978) 575-578.
5. M. F. L'Annunziata, Birth of an Unique Parent-Daughter Relation: Secular Equilibrium, J. Chem. Educ. 48 (1971) 700-703.
6. V. P. Chechev, M. M. Bé, Radioactive equilibrium: ^{99}Mo/^{99m}Tc decay characteristics, Appl. Radiat. Isot. 87 (2014) 132–136.
7. Production of Long Lived Parent Radionuclides for Generators: ^{68}Ge, ^{82}Sr, ^{90}Sr and ^{188}W; IAEA Radioisotopes and Radiopharmaceuticals Series No. 2; International Atomic Energy Agency, Vienna, (2010).
8. J. R. Prince, Comments on Equilibrium, Transient Equilibrium, and Secular Equilibrium in Serial Radioactive Decay, J. Nucl. Med. 20 (1979) 162-164.
9. E. A. C. Crouch, Fission-product yields from neutron-induced fission, At. Data Nucl. Data Tables, 19 (1977) 417-532.
10. B. V. N. Rao, G. N. Rao, Decay of ^{144}Ce to levels in ^{144}Pr and ^{144}Nd, J. Phys. Soc. Jpn. 40 (1976) 1-5.
11. S. Raman, Decay of ^{144}Pr to levels in ^{144}Nd, Nucl. Phys. A, 107 (1968) 402-410.
12. E. R. Tompkins, S. W. Mayer, Ion Exchange as a Separations Method. III. Equilibrium Studies of the Reactions of Rare Earth Complexes with Synthetic Ion Exchange Resins, J. Am. Chem. Soc. 69 (1947) 2859–2865.
13. D. MacDonald, Carrier-Free Separation of Praseodymium-144 from Cerium-144 by Anion Exchange, Anal. Chem. 33 (1961) 1807.
14. A. Bradley, M. Adamowicz, Separation of Ce^{144} from Pr^{144}, J. Chem. Educ. 36 (1959) 136-138.

15. J. A. Partridge, R. C. Jensen, Purification of Di-(2-ethylhexyl) phosphoric acid by precipitation of copper(II) di-(2-ethylhexyl) phosphate, J. Inorg. Nucl. Chem.31 (1969) 2587-2589.
16. Radiotracer Generators for Industrial Applications, IAEA Radiation Technology Series No. 5, International Atomic Energy Agency, Vienna, (2013) 124-134.
17. A.R. Landgrebe, R.H. Rodriguez -Pasques, F.J. Schima, The Rapid Radiochemical separation of Radioactive Praseodymium from Radioactive Cerium, Int. J. Appl. Radiat. Isot. 19 (1968) 147-149.
18. V. K. Manchanda, P. N. Pathak, P. K. Mohapatra, New Developments in Thorium, Uranium, and Plutonium Extraction, Bruce A Moyer (Eds.), Ion Exchange and Solvent Extraction, A Series of Advances, CRC Press, 19 (2009) 65–118;DOI: 10.1201/9781420059700-c2.
19. R. Lundqvist, L. U. Jiu-Fang, I. Svantesson, Hydrophilic Complexes of the Actinides. II. Comparison of TBP, HTTA and HDEHP Liquid-Liquid Distribution Systems, Acta. Chem. Scand. A 37 (1983) 743-753.
20. T. S. Grimes, P. R. Zalupski, L. R. Martin, Features of the Thermodynamics of Trivalent Lanthanide/Actinide Distribution Reactions by Tri-n-octylphosphine Oxide and Bis(2-ethylhexyl) Phosphoric Acid, J. Phys. Chem. B. 118 (2014) 12725−12733.
21. P.M. Edwards, Origin 7.0: scientific graphing and data analysis software, J. Chem. Inform. Comput. Sci. 42 (2002) 1270-1271.

CHAPTER 7

Chapter 7: Studies on Radiochemical Separation of Sr from fission products and from irradiated yttria dissolver solution using tri-Sodium tri-Meta Phosphate

This chapter deals with the radiochemical separation studies of Sr from the (U,Pu)O_2 fuel dissolver solution as well as from the yttria target, both irradiated in FBTR. The process of radiochemical purification of Sr has several useful applications in various fields. The ^{90}Sr ($t_{1/2}$ = 30 years) is one of the long lived fission products and its removal from the other fission products is necessary for a better radioactive waste management protocol [1]. ^{90}Sr is a pure beta emitters and can thus be used as beta standard for the efficiency calibration studies for beta counting systems such as liquid scintillation counter and Cerenkov counting technique [2,3]. The ^{90}Sr-^{90}Y pair is in secular equilibrium and hence the radionuclidic generator ^{90}Sr-^{90}Y is useful source of ^{90}Y to produce labeled compounds (^{90}Y- hydroxyapatite) for radiation synovectomy [4].

^{89}Sr as $SrCl_2$ in dilute HCl medium is being used as a pain palliative care for metastatic bone cancer [5,6]. ^{89}Sr was produced through the nuclear reaction, ^{89}Y (n, p) ^{89}Sr with a threshold energy of 660 keV using yttria as the target in FBTR. A flow-sheet has been standardized for the radiochemical separation and purification of ^{89}Sr from the irradiated yttria target using solvent extraction followed by ion-exchange chromatography [7]. The solvent extraction step involves the separation of bulk yttrium, and the subsequent step involving ion-exchange chromatography using Dowex 50WX8 (100-200) ensures the purification of ^{89}Sr source. The present study establishes the method of purification of ^{89}Sr source from the other radioactive impurities like ^{88}Y, ^{65}Zn, ^{54}Mn, ^{60}Co, ^{86}Rb, ^{192}Ir, ^{103}Ru, ^{113}Sn, ^{139}Ce ^{160}Tb,^{154}Eu etc. produced during the irradiation of yttria, using tri-Sodium tri-Meta Phosphate (SMP) as eluent in an ion-exchange chromatographic technique. The purification was achieved by using 0.1M SMP as complexing agent which was optimized based on the distribution ratio data. The final elution of pure Sr fraction was obtained in nitric acid medium. This procedure resulted into a faster purification of ^{89}Sr source and also the collection of the purified fraction of ^{89}Sr in a relatively smaller volume of eluent in comparison with the technique reported earlier [7]. Purity of Sr source from the residual contamination of the complexing agent (SMP) was also confirmed experimentally.

7.1. Introduction

The present study involves (i) the investigation of a complexing agent which can be used for the separation of ^{90}Sr and ^{137}Cs from $(U,Pu)O_2$ dissolver solution and (ii) to separate the rare earths effectively to purify the ^{89}Sr from FBTR irradiated yttria with minimum amount of eluent and faster processing time, compared to other conventional eluents such as nitric acid and hydrochloric acid.

Separation of long-lived fission products such as ^{137}Cs and ^{90}Sr from nuclear waste streams is an important environmental concern in nuclear waste management. The removal of Cs and Sr from the fission product solutions is generally achieved by physico-chemical processes such as solvent extraction, ion exchange, coagulation, co-precipitation, electrochemical processes and membrane processes [1]. The separation of these fission products is necessary to handle the fission products present in high level liquid waste (HLLW) solution with the reduced radiation dose.

^{89}Sr (half-life: 50.53 d), a pure beta emitter with β^{-}_{max} of 1.46 MeV is being used as pain palliative care for bone metastatic cancer [8]. The radioactive strontium isotope, ^{89}Sr being an alkaline earth metal, is a biological analogue of calcium which gets localized in bone as calcium hydroxyapatite and provides pain relief due to constant irradiation of the bone with its beta energy of 1.46 MeV [9-12]. Since the cancer cells are more active than normal cells, the uptake is ten times greater for metastatic tumor lesions than for healthy bone [13]. $^{89}SrCl_2$ is commercially available under the brand name of “METASTRON” in USA and Canada [11,13,14] and a typical activity of 148 MBq is required per dose [9,11,12]. ^{89}Sr can be produced either through ^{89}Y (n, p) ^{89}Sr reaction in fast reactors or ^{88}Sr (n, γ) ^{89}Sr reaction in thermal reactors. However, the former route is preferred over the latter, as it results into ^{89}Sr source of higher specific activity [15] due to the fact that the target element Y is chemically separable from the ^{89}Sr source and thus the ^{89}Sr is obtained as carrier-free source. ^{89}Sr was produced by irradiating yttria target through (n,p) reaction in FBTR [7] as depicted in Figure 7.1.

Even though the direct purification of ^{89}Sr source using Sr- specific crown ether such as di-tertiary butyl di-cyclohexano 18-Crown-6 is preferable [16-18], the method still has some drawbacks such as high cost and possible cross contamination of chemically hazardous and carcinogenic crown ether into ^{89}Sr source which is meant for human injection. It, therefore, demands the separation of ^{89}Sr without cross contamination from crown ether. A method of purification has been standardized in our laboratory that involved i) removal of bulk target Y by solvent extraction technique using TBP extractant and ii) final purification of ^{89}Sr from the target yttrium and various other activated impurities by cation-exchange chromatography using Dowex 50WX8 resin with nitric acid as eluting agent [7].

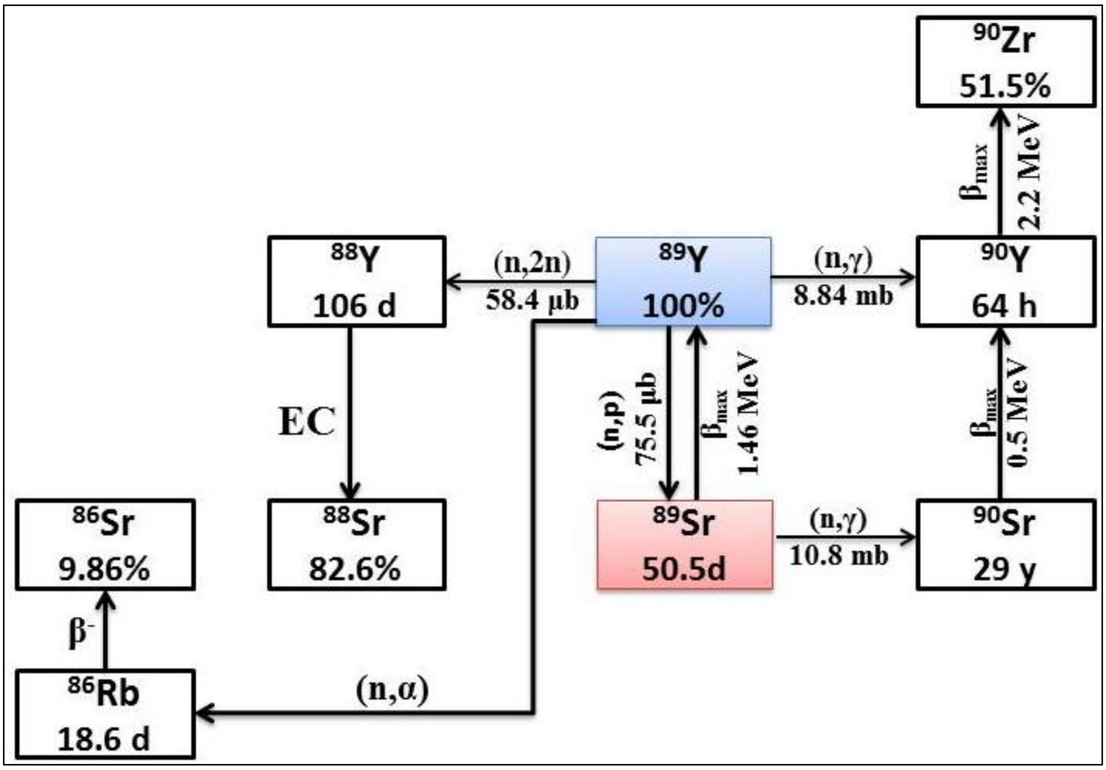

Figure 7.1. Production Route of ^{89}Sr from ^{89}Y via (n,p) reaction.

The various complexing reagents used for the separation of rare earths include lactates, citrates, aminopolyacetic acids, α-hydroxy isobutyrate (α-HIBA), etc [19-21]. Most of the separation procedures for rare earths use extensively the complexing reagent, α-HIBA i.e. the separation of light rare earth elements using α-HIBA as eluting agent with Dowex-50 ion exchange column [22,23] and carrier-free separation of the individual rare earths by cation-exchange chromatography or by pressurised ion-exchange chromatography [24-25]. Other complexing reagents used for the separation of various metal ions such as Co and Ni include ethylene diaminetetraacetic acid (EDTA), nitrile tri-acetic acid (NTA), imino di-acetic acid (IDA) and citrate [26]. Similarly Sr and Ba were separated by cation-exchange chromatography using 2-hydroxyl ethylethylene diaminetriacetic acid (HEDTA) and diethylenetriaminepentaacetic acid (DTPA) as eluents [27]. Various metal ions such as Ce, Al, Fe, Bi, Ca and Pd were separated by cation-exchange resin Purlite C100 using different chelating agents such as sodium nitrate, citric acid and EDTA [28].

Another important rare earth specific complexing reagent, SMP (Figure 7.2) is used as an eluent in chromatographic separation and has certain inherent advantages as an eluent such as: (i) being relatively economical; (ii) yielding fast elution; (iii) yielding sharp peaks with minimum tailing effects and (iv) importantly pH independent [29]. Separation of various elements such as Al, Fe, Mn, Ca, Be, Cu, Mg, V, Mo, Sn and Th were accomplished using ion-exchange resin Dowex 50WX8 with SMP as an eluent [29]. Similarly separation of rare earths from thorium using Dowex 1X4 [30] and Dowex 50WX8 [19] as well as mutual separation of rare earths with Dowex 2X8 resin [31] were also achieved using SMP as an eluting agent.

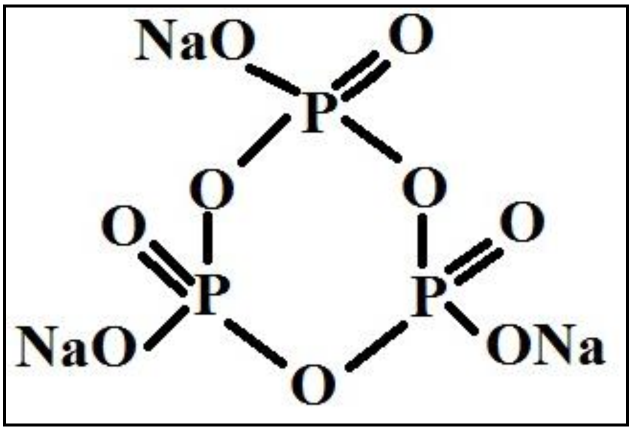

Figure 7.2. Structure of tri-Sodium tri-MetaPhosphate (SMP).

The present study involves the purification of ^{89}Sr source from other impurities including the trace amount of the matrix element Y by cationic exchange chromatography using Dowex 50WX8 (100-200) resin with the complexing agent

SMP in nitric acid medium as an eluent. This procedure resulted a faster separation with the purified Sr fraction in a relatively less volume of the eluent in comparison with the acid alone as the eluent.

7.2. Elution profiles of fission products from FBTR irradiated (U,Pu)O_2 fuel dissolver solution in Dowex resin using SMP as an eluent

The (U,Pu)O_2 fuel dissolver solution containing various fission products was loaded on to the column containing Dowex 50WX8 (100-200) resin conditioned appropriately and the elution was carried out using SMP reagent. The activity in the eluted fractions were assayed by HPGe detector and plotted as a function of cumulative volume of the eluting agent. The separation profile for the fission products was established as shown in Figure 7.3. The profile shows that the fission products such as ^{144}Ce, ^{125}Sb, ^{106}Rh, ^{155}Eu and ^{154}Eu and the activation products such as ^{60}Co and ^{54}Mn were eluted with 0.05M SMP as these elements have low distribution ratio values in Dowex 50WX8 (100-200) resin [19,30]. The fission products such as ^{137}Cs, ^{134}Cs and ^{90}Sr loaded with ^{85}Sr radio-tracer were eluted with 0.1M SMP. Thus, a base line separation of the long lived fission products (^{90}Sr and ^{137}Cs) was established using SMP as an eluent in the Dowex resin. Removal of these long-lived fission products i.e. ^{90}Sr and ^{137}Cs make the handling of the fuel dissolver solution for the subsequent studies easier owing to the reduced radiation dose.

The above results enabled the expansion of this procedure to the purification of ^{89}Sr from the irradiated yttria dissolver solution along with its associated radionuclidic impurities as shown in Table 7.1 [7]. As most of these impurities are either of transition metals or of rare earths, the purification of ^{89}Sr from these impurities seems to be feasible by ion-exchange chromatography using SMP as eluting agent. Distribution ratio (D_M) measurement followed by the ion-exchange separation of ^{89}Sr from the rest of the impurities was carried out and the results are presented here.

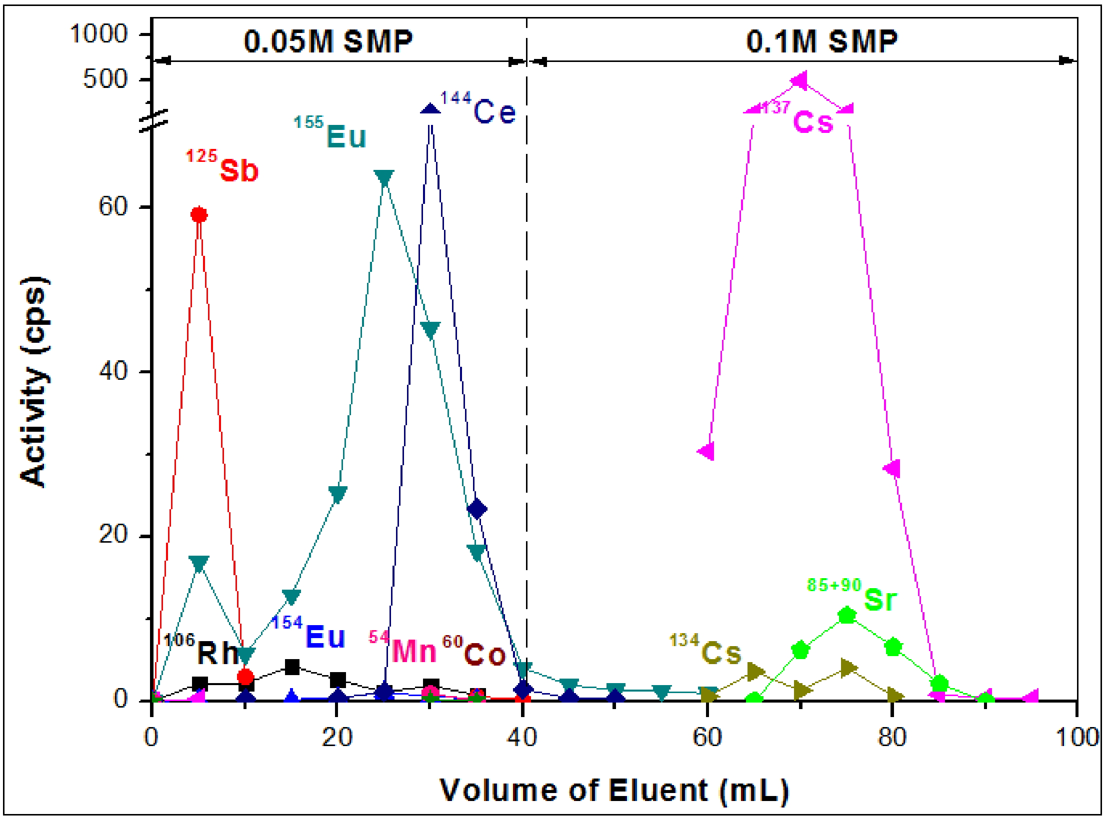

Figure 7.3. Elution profile of various fission products in Dowex 50WX8 (100-200) resin (Amount of Dowex 50WX8 resin: 2 g, Column Dimensions: 8 mm ID, 25 cm Length and 8 cm bed height; Conditioning: 0.1M SMP; Feed: FBTR irradiated (U,Pu)O_2 fuel dissolver solution in 0.1M SMP; Flow rate: 0.4-0.5 mL/min; Assay: high resolution gamma spectrometry using HPGe detector).

Table 7.1. Production routes for various radionuclidic impurities produced during the irradiation of yttria in FBTR [7]

S.No.	Isotope	Production Route
1	^{65}Zn	^{64}Zn(n, γ)^{65}Zn
2	^{54}Mn	^{54}Fe(n, p)^{54}Mn
3	^{60}Co	^{59}Co(n, γ)^{60}Co
4	^{58}Co	^{58}Ni(n, p)^{58}Co
5	^{192}Ir	^{191}Ir(n, γ)^{192}Ir
6	^{113}Sn	^{112}Sn(n, γ)^{113}Sn
7	^{139}Ce	^{138}Ce(n, γ)^{139}Ce
8	^{103}Ru	^{102}Ru(n, γ)^{103}Ru
9	^{154}Eu	^{153}Eu(n, γ)^{154}Eu
10	^{160}Tb	^{159}Tb(n, γ)^{160}Tb

7.3. Distribution ratio (D_M) measurement

Batch studies were carried out to determine the distribution ratios of various radionuclides present in the FBTR irradiated yttria dissolver solution. The centrifuged samples from the batch experiment were assayed by HPGe detector to determine the initial and final activities and the D_M were calculated using the following equation.

$$D_M = \frac{(A_0 - A).V}{A.M} \tag{7.1}$$

where A_0 and A are the activities (cps) of the metal ions before and after equilibration with the resin, V is the volume of the solution (mL) kept for equilibration and M is weight of the resin (g) taken.

Distribution ratio (D_M) for the different radio tracers were plotted as a function of the SMP concentrations (Figure 7.4). From the figure, it is observed that the distribution ratios of all metal ions decrease with increased concentration of SMP in the given range. It is also observed that the distribution ratio value of Sr(II) is always relatively higher compared to the other elements in the dissolver solution at all concentrations of SMP. This may be attributed to the strong complexing behavior of all these metal ions (Y^{3+}, Co^{2+}, Mn^{2+} and Zn^{2+}) with SMP and hence less interaction with Dowex cation-exchange resin. 0.1M SMP was chosen for the subsequent elution in the ion exchange chromatographic separation of Sr from Y and other radionuclides present in the dissolver solution based on the optimized separation factor as well as the separation time from the distribution data.

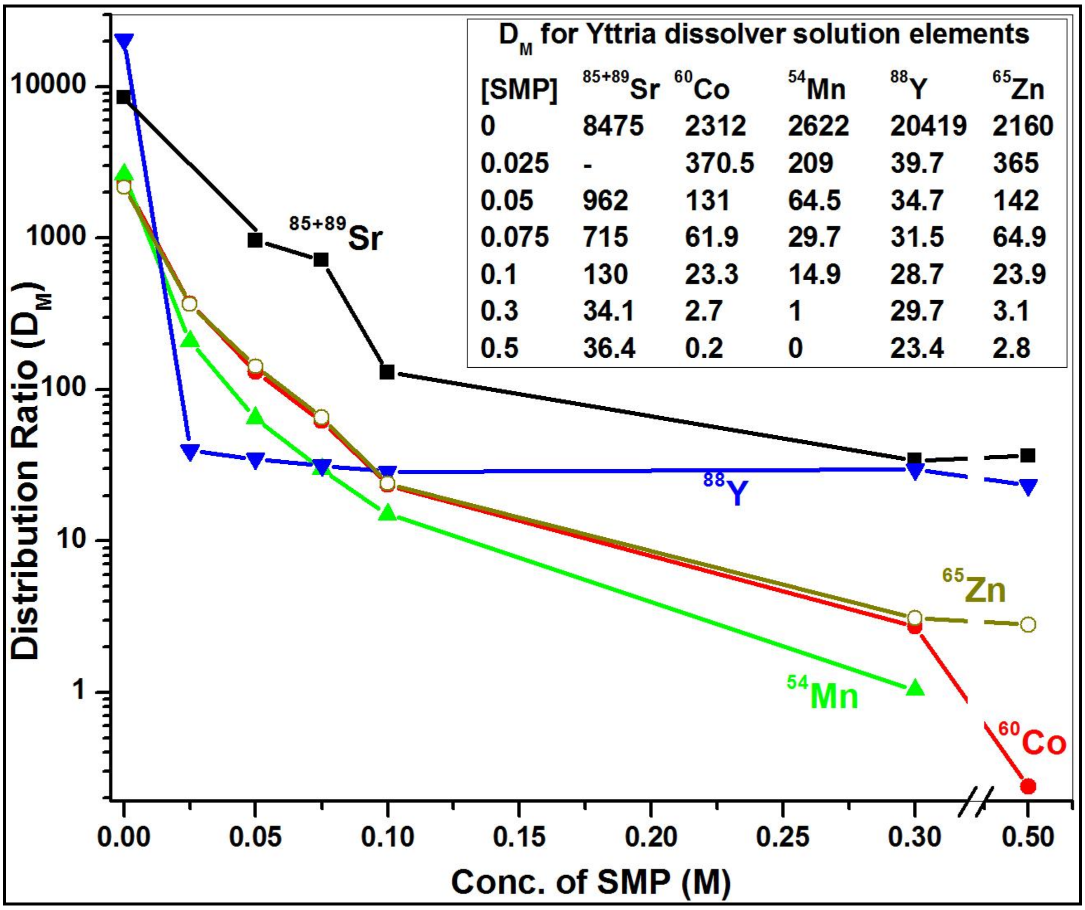

D_M for Yttria dissolver solution elements

[SMP]	$^{85+89}$Sr	^{60}Co	^{54}Mn	^{88}Y	^{65}Zn
0	8475	2312	2622	20419	2160
0.025	-	370.5	209	39.7	365
0.05	962	131	64.5	34.7	142
0.075	715	61.9	29.7	31.5	64.9
0.1	130	23.3	14.9	28.7	23.9
0.3	34.1	2.7	1	29.7	3.1
0.5	36.4	0.2	0	23.4	2.8

Figure 7.4. Distribution ratios of elements present in irradiated yttria dissolver solution measured using Dowex 50WX8 100-200 mesh as a function of SMP concentration (Amount of resin in each tube: 50 mg; Volume of SMP solution: 5 mL; Equilibration time: 4 h; Assay: Gamma spectrometry using HPGe).

7.4. Purification of Sr from the simulated sample of the FBTR irradiated yttria dissolver solution

From the distribution ratio values of Sr and other metal ions (Figure 7.4), it was chosen to use 0.1M SMP as an eluent to purify Sr from the other impurities. Separation was carried out in the Dowex resin packed glass column using simulated sample containing the tracers of Sr and other impurities as present in the actual dissolver solution of irradiated yttria target. Activities of the eluted fractions were assayed by HPGe detector and plotted as a function of cumulative volume of eluting agent. The elution profile using SMP as eluent in Dowex resin is shown in Figure 7.5.

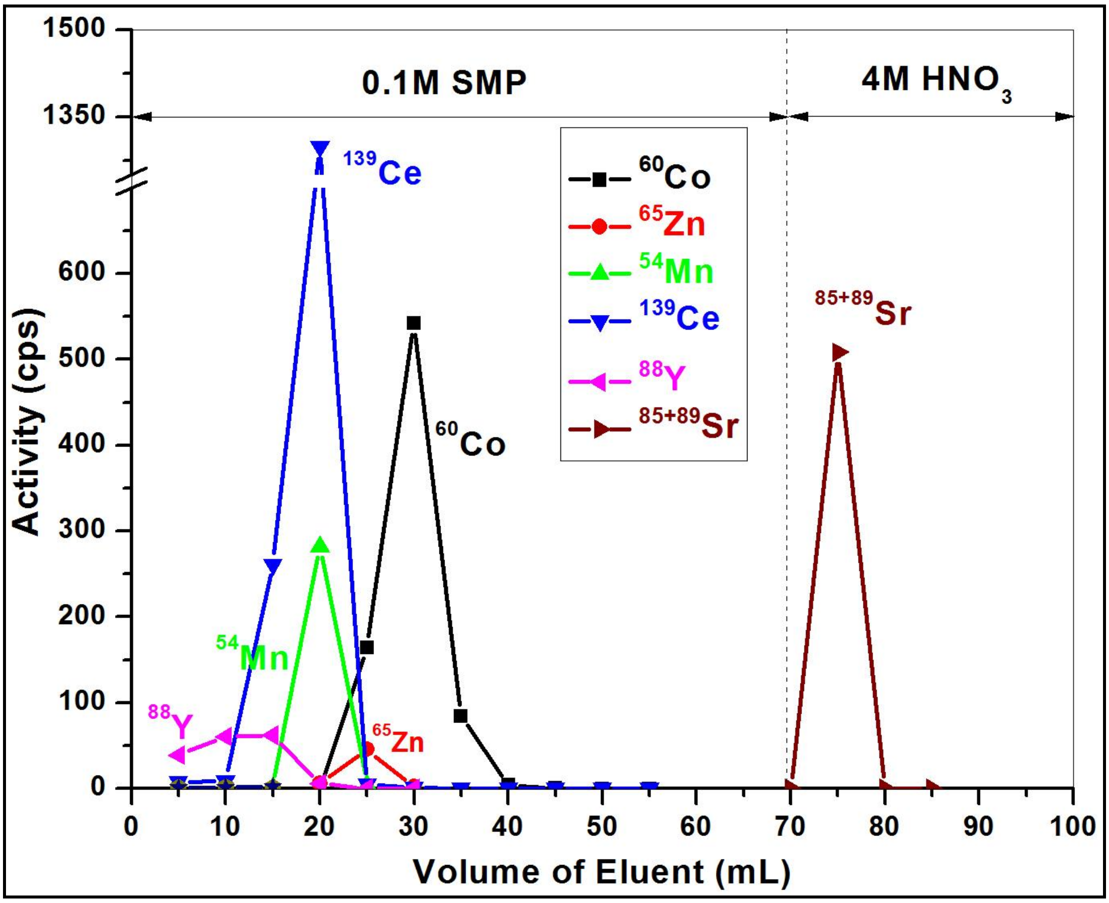

Figure 7.5. Elution profile of the various tracers in the simulated sample (Amount of Dowex resin: 1 g; Column Dimensions: 5 mm ID, 25 cm Length and 9 cm bed height; Conditioning: 0.1M SMP; Feed: Simulated sample in 0.1M SMP; Flow rate: 0.1-0.15 mL/min; Assay: Gamma spectrometry using HPGe).

All metal ions in the simulated sample solution i.e. ^{88}Y, ^{65}Zn, ^{54}Mn, ^{60}Co and ^{141}Ce other than $^{85+89}$Sr were eluted in the initial fractions i.e. in 50 mL of 0.1M SMP. This observation is attributed to the low distribution ratios of these elements for Dowex resin in SMP medium. Subsequently the eluting agent was changed from SMP to nitric acid to remove the Sr from the Dowex resin. All the $^{85+89}$Sr held in the column was thus eluted in a single fraction of 5 mL of 4M HNO_3 solution. The distribution data [7] supported the elution process of i) the washing off the residual SMP using a dilute acid of 0.5M nitric acid without losing the Sr held in the column and ii) the final washing using a high acidity medium i.e. 4M nitric acid to have Sr source in relatively low volume enabling the collection of Sr source in just one sample size used in the experiment. However, a lower acidity of the eluent than the one used above might result into the elution of the source spreading into more sample volume; while the use of a higher acidity of the eluent might not result into any proportional advantage other than the minimization of the elution time. A clear base line separation of $^{85+89}$Sr from the other radioactive impurities was achieved in this case. Before applying this elution profile to the actual yttria dissolver solution, another study was carried out to confirm that the pure ^{89}Sr source obtained from the above purification procedure is actually free from the residual contamination of Na and its associated anionic moiety of SMP.

7.5. Investigation for the residual cross contamination of ^{89}Sr fraction by Na and its anionic moiety of the eluent, SMP

Separation profiles of the simulated sample described above was repeated under similar conditions but with irradiated SMP containing the activated products of ^{24}Na and ^{32}P mixed with inactive SMP eluent to study the possibility of residual contamination of SMP in the final fraction of ^{89}Sr source. The activated SMP tracer was obtained by irradiating it in KAMINI reactor and the activation reactions of sodium and phosphorous in SMP are as follows.

$$^{23}\mathrm{Na} + {}^{1}\mathrm{n} \rightarrow {}^{24}\mathrm{Na} + \gamma \qquad (7.2)$$

$$^{31}\mathrm{P} + {}^{1}\mathrm{n} \rightarrow {}^{32}\mathrm{P} + \gamma \qquad (7.3)$$

The activities of ^{85}Sr and ^{24}Na present in the eluted samples obtained using gamma spectrometry and of ^{32}P by Cerenkov counting were plotted as a function of cumulative volume of the eluting agent (Figure 7.6).

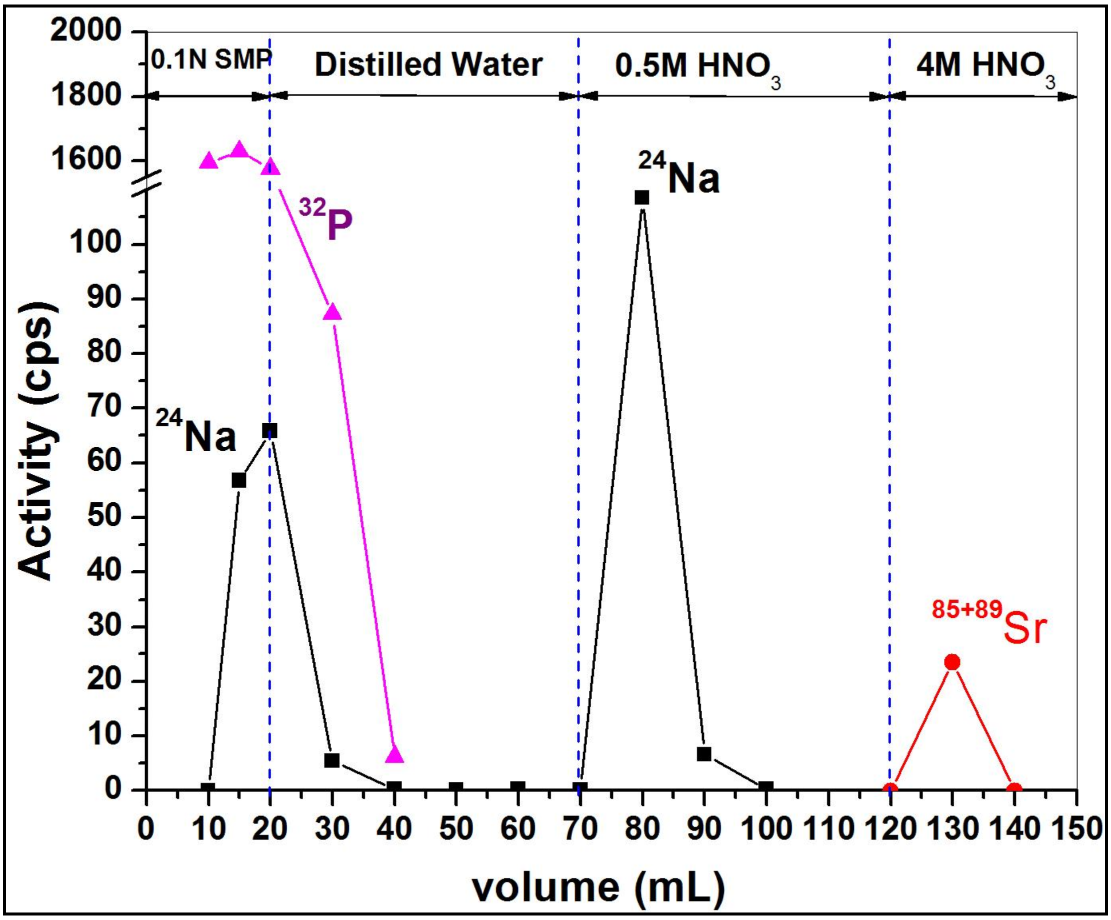

Figure 7.6. Elution profile of Sr, Na and P using SMP as eluent containing its radioactive tracers (Amount of Dowex resin: 1 g; Column Dimensions: 5 mm ID, 25 cm Length and 9 cm bed height; Conditioning: 0.1M SMP with irradiated SMP; Feed: Irradiated SMP with Sr tracer; Flow rate: 0.1-0.15 mL/min; Assay: Gamma spectrometry using HPGe).

It is established that the Sr fraction obtained using the above procedure was free from Na and anionic moiety of SMP containing P. However, it was interesting to observe that there were two ^{24}Na peaks which appeared in different volumes of the eluent due to i) the peak corresponding to the excess sodium from the counter ion of the anionic moiety containing P of SMP which occurred immediately after the saturation of the initial loading of sodium (cation of SMP) onto the column during passing of the 0.1M SMP and ii) another peak corresponding to the eluted fraction of the loaded sodium in 0.5M HNO_3 i.e. Na loaded initially onto the column but not washed along with the elution of 0.1M SMP. However, it was confirmed from the absence of ^{24}Na and ^{32}P activities in the pure Sr fraction that there was no residual cross contamination of either Na or the counter anionic moiety of SMP in the pure Sr fraction under these experimental conditions. The elution profile was applied to the separation of ^{89}Sr from the actual FBTR irradiated yttria target and the other associated impurities as described in the next section.

7.6. Purification of ^{89}Sr from the actual irradiated yttria dissolver solution sample

Under the experimental conditions discussed in the section 2.7.5., the separation profile obtained for the irradiated yttria dissolver solution is shown in Figure 7.7. The glass column contained 1 g of Dowex resin and the elution started with 0.1M SMP to remove all the radioactive impurities i.e. ^{60}Co, ^{65}Zn, ^{54}Mn, ^{192}Ir, ^{86}Rb, ^{113}Sn, ^{103}Ru, ^{58}Co, ^{88}Y etc. The elution was followed by washing the column with Millipore water to remove the traces of sodium and the anionic moiety of SMP from the column.

Even though the activities of the above radioactive impurities were much lower than the levels used in the simulated sample i.e. in the range of 10-700 times lower, still they were sufficiently high enough to be assayed using HPGe detector.

Subsequent elution using 0.5M HNO_3 removed all the residual sodium loaded onto the column during the initial elution with SMP. Finally pure ^{89}Sr fraction with the tracer $^{85+89}$Sr was eluted and collected in a 5 mL fraction of 4M HNO_3 which was well separated from all other impurities. The experiment took approximately 15 h to complete the elution process which was relatively faster than the other purification process in which nitric acid alone was used as the eluting agent that took about 25 h [7].

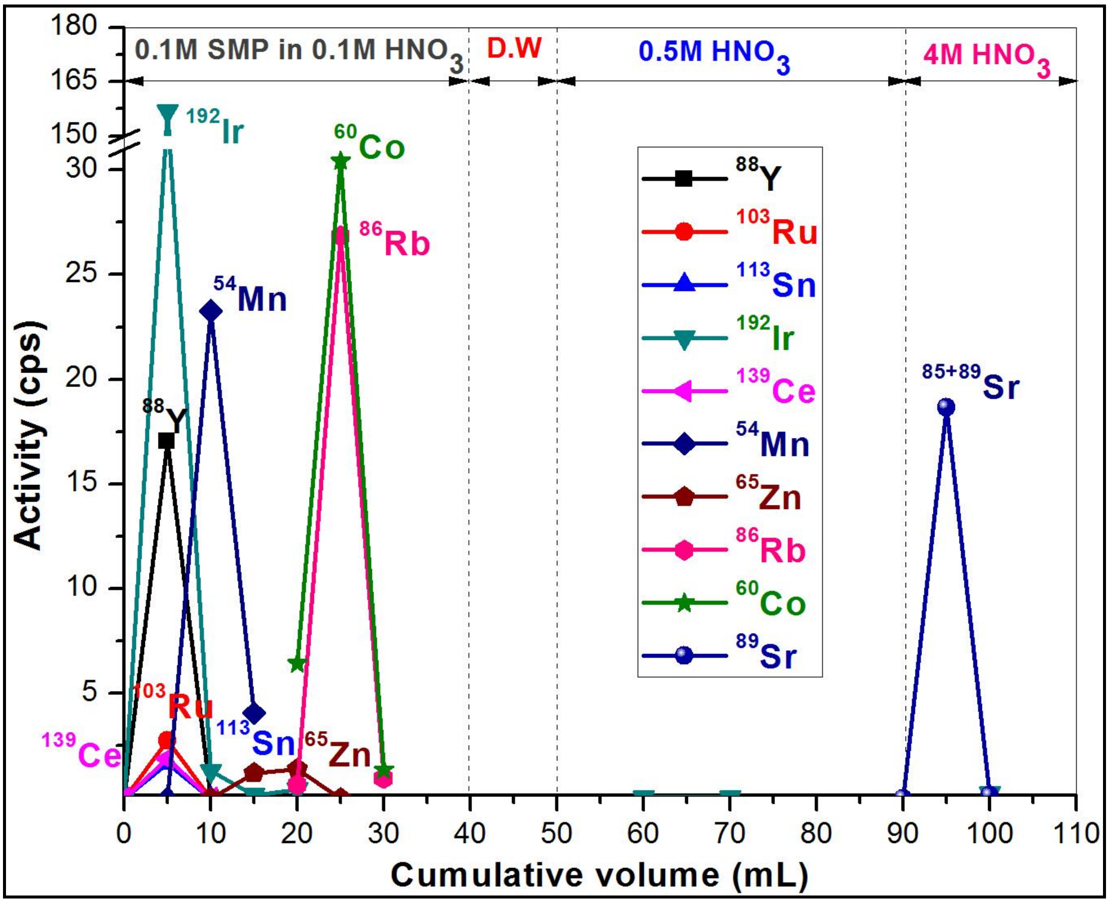

Figure 7.7. Purification profile of ^{89}Sr from the irradiated yttria dissolver solution (Amount of Dowex resin: 1 g; Column Dimensions: 5 mm ID, 25 cm Length and 9 cm bed height; Conditioning: 0.1M SMP; Feed: Solvent extracted irradiated yttria dissolver solution in 0.1M SMP with ^{85}Sr tracer added; Flow rate: 0.1-0.15 mL/min; Assay: Gamma spectrometry using HPGe).

However, when the experiment was repeated with different column size using higher amount of resin i.e 2 g Dowex resin that took only 9 hours, but required a larger volume of the eluent for the purification i.e. 70 mL of 0.1M SMP to remove the impurities and 10 mL of 4M HNO_3 to collect Sr fraction owing to the more amount of resin in larger diameter column. The experiment was repeated with 2 g resin to purify the ^{89}Sr source in aqueous phase, from which the bulk Y was already removed but without adding Sr tracer to get pure ^{89}Sr source. The elution profile is shown in Figure 7.8. Gamma activity of these samples was measured by HPGe detector and beta assay by HIDEX counting system using LSC and Cerenkov counting techniques. Thus, a base line separation of ^{89}Sr was achieved from the rest of the radionuclidic impurities.

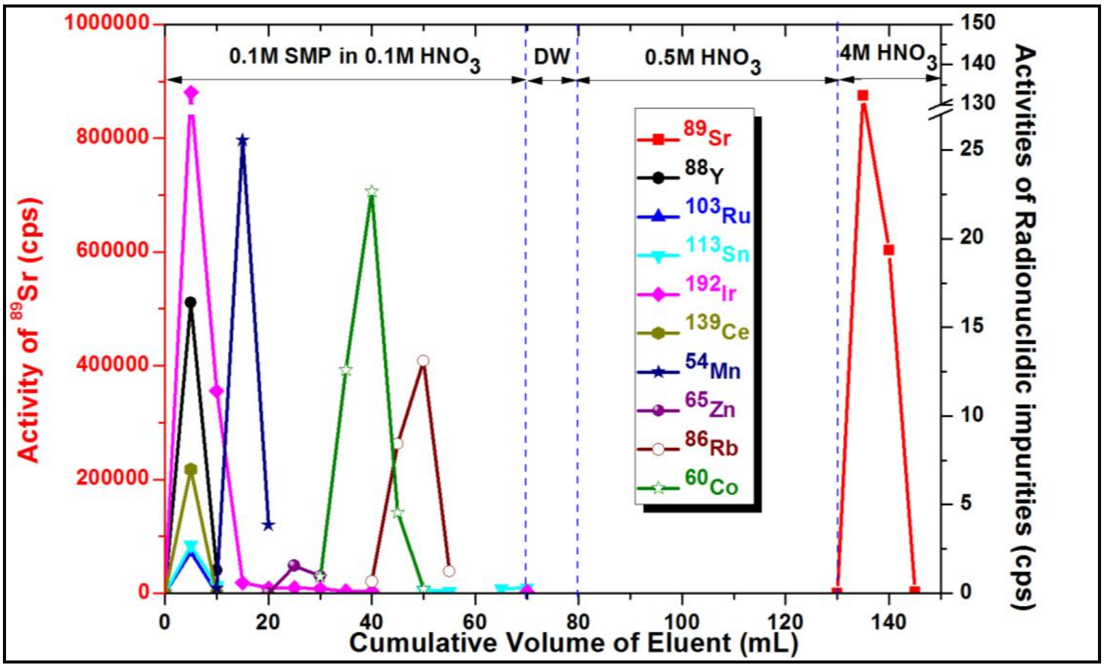

Figure 7.8. Purification profile of ^{89}Sr from the irradiated yttria dissolver solution (as indicated in Figure 7.7, but the amount of resin and column dimensions are different, Amount of Dowex resin: 2 g; Column Dimensions: 8 mm ID, 25 cm Length and 8 cm bed height; Feed: Solvent extracted irradiated yttria dissolver solution in 0.1M SMP without ^{85}Sr tracer; Assay: HPGe).

7.7. Quantification of ^{89}Sr

The efficiency of the HIDEX LSC system for the individual radioactive standard was determined using the following equation

$$Efficiency = \frac{PeakArea/LiveTime}{Becquerels} * 100 \qquad (7.4)$$

The efficiency of the HIDEX system for both LSC as well as Cerenkov counting methods was plotted as a function of β^{-}_{max} energy of the radioactive standards (Figure 7.9).

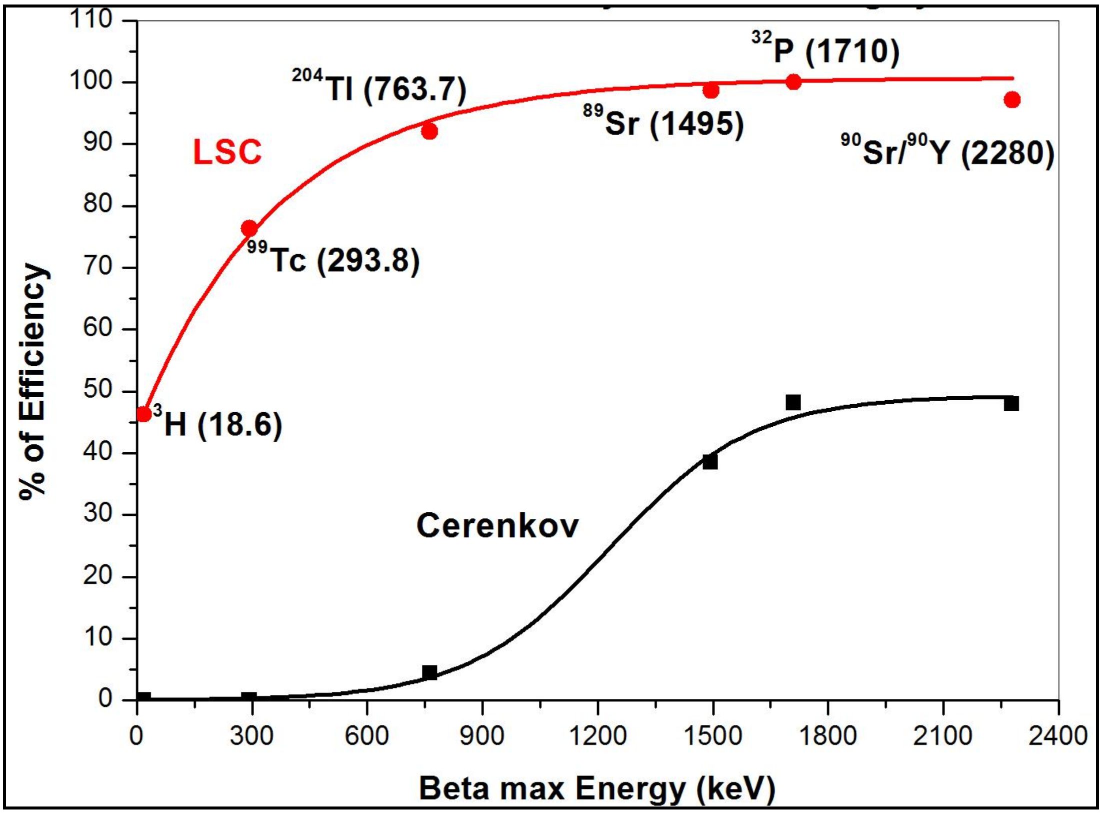

Figure 7.9. Efficiency Calibration of HIDEX LSC system for liquid scintillation counting and Cerenkov counting technique (Radioactive beta standards used for the calibration studies with 5 mL volume were ^{3}H (18.6 keV), ^{99}Tc (293.8 keV), ^{204}Tl (763.7 keV), ^{89}Sr (1495 keV), ^{32}P (1710 keV) and ^{90}Sr/^{90}Y (2280 keV) in cocktail for LSC and in 0.1M HNO_3 for Cerenkov counting, respectively).

From the figure, it is observed that the Cerenkov counting method exhibits a maximum efficiency of 50% for the β^-_{max} energy above 1700 keV, whereas LSC exhibits the efficiency of 100% for the β^-_{max} energy above 1500 keV. The pure ^{89}Sr fraction collected in the above experiment was quantified using the above beta counting methods and established the yield to be ~2 mCi/g of yttria target.

Thus the complexing agent SMP as eluent offers a faster base-line separation in a lower volume of the eluent in comparison with the process using nitric acid alone as the eluent for the purification of ^{89}Sr source during the chemical processing of the irradiated yttria target.

7.8. Conclusion

Radiochemical separation studies of ^{90}Sr from the FBTR irradiated (U,Pu)O_2 fuel dissolver solution was carried out. A base line separation of ^{90}Sr and ^{137}Cs from the host of remaining fission products was achieved by ion exchange chromatography using SMP as an eluting agent. The procedure is useful to handle the fission products present in its waste (HLLW) solution with the reduced radiation dose. The method was also extended for the purification of ^{89}Sr from the FBTR irradiated yttria dissolver solution as well.

The distribution ratio of the various metal ions present in the yttria dissolver solution was measured in Dowex resin as a function of SMP concentration. Distribution ratio of Sr was always relatively higher compared to the rest of the radioactive impurities present in the dissolver solution i.e. ^{88}Y, ^{65}Zn, ^{54}Mn, ^{60}Co etc. at all concentrations of SMP in nitric acid medium. The distribution ratio and separation factors suggested that 0.1M SMP was sufficient to separate ^{89}Sr from yttrium and other impurities. A base line separation of ^{89}Sr from all the impurities was established using simulated sample with radioactive tracers and the same was extended to the actual irradiated yttria dissolver solution. It was also established that the pure Sr fraction was obtained without the residual cross contamination from Na and anionic moiety of SMP, from the study carried out using activated SMP containing the radioactive tracers of ^{24}Na and ^{32}P. Final purification of ^{89}Sr source from the impurities present in the irradiated yttria dissolver solution was carried out by ion exchange chromatography without the addition of ^{85}Sr tracer using SMP as eluting agent. ^{89}Sr yields were established to be ~2 mCi/g of yttria by beta counting techniques (LSC and Cerenkov).

Thus the present study established that SMP is a potential eluting agent for a faster purification of ^{89}Sr source during the chemical processing of the bulk irradiated yttria target. The elution profiles with SMP were advantageous as it is less time consuming with minimum generation of radioactive waste in comparison with the procedure involving the elution using nitric acid alone.

7.9. References

1. M. V. Balarama Krishna, S. V. Rao, J. Arunachalam, M. S. Murali, Surendra Kumar, V. K. Manchanda, Removal of ^{137}Cs and ^{90}Sr from actual low level radioactive waste solutions using moss as a phyto-sorbent, Sep. Sci. Technol. 38 (2004) 149-161.
2. T. E. Sazonova, A. E. Kochin, N. I. Karmalitsyn, S. V. Sepman, A. V. Zanevsky, T. I. Shilnikova, Standardization of ^{204}Tl and ^{89}Sr at VNIIM. Appl. Radiat. Isot. 56 (2002) 453-456.

3. R. B. Randolph, Determination of Strontium-90 and Strontium-89 by Cerenkov and Liquid Scintillation Counting, Internatl. J. Appl. Radiat. Isot. 26 (1975) 9-16.
4. U. Pandey, A. Mukherjee, P. R. Chaudhary, M. R. A. Pillai, M. Venkatesh, Preparation and studies with ^{90}Y-labelled particles for use in radiation synovectomy, Appl. Radiat. Isot. 55 (2001) 471-475.
5. C. Z. Dickinson, Nancy S. Hendrix, Strontium-89 Therapy in Painful Bony Metastases, J. Nucl. Med. Technol. 21 (1993) 133-137.
6. E. K. Reddy, R. G. Robinson, C. M. Mansfield, Strontium-89 for Palliation of Bone Metastases, J. Natl. Med. Assoc. 78 (1986) 27-32.
7. D. Saha, J. Vithya, G. V. S. Ashok Kumar, K. Swaminathan, R. Kumar, C. R. Venkatasubramani, P.R. Vasudeva Rao, Feasibility studies for production of ^{89}Sr in the Fast Breeder Test Reactor (FBTR), Radiochim. Acta 101 (2013) 667–673.
8. J. Zweit, Radionuclides and carrier molecules for therapy, Phys. Med. Biol. 41 (1996) 1905–1914.
9. V. J. Lewington, Bone-Seeking Radionuclides for Therapy, J. Nucl. Med. 46 (2005) 38S–47S.
10. V. J. Lewington, Cancer therapy using bone-seeking isotopes, Phys. Med. Biol. 41 (1996) 2027–2042.
11. A. N. Serafini, Therapy of Metastatic Bone Pain, J. Nucl. Med. 42 (2001) 895–906
12. N. Pandit-Taskar, M. Batraki, C. R. Divgi, Radiopharmaceutical Therapy for Palliation of Bone Pain from Osseous Metastases, J. Nucl. Med. 45 (2004) 1358.
13. D. J. Hillegonds, S. Franklin, D. K. Shelton, V. Srinivasan, V. Vani, The Management of Painful Bone Metastases with an Emphasis on Radionuclide Therapy, J. Natl. Med. Assoc. 99 (2007) 785-794.

14. S. M. Larson, E. P. Krenning, A Pragmatic Perspective on Molecular Targeted Radionuclide Therapy, J. Nucl. Med. 46 (2005) 1S-3S.
15. Y. A. Karelin, V. N. Efimov, V. T. Filimonov, R. A. Kuznetsov, Y. L. Revyakin, O. I. Angreev, I. Y. Zhemkov, V. G. Bukh, V. M. Lebedev, Y. N. Spiridonov, Radionuclide production using a fast flux reactor, Appl. Radiat. Isot. 53 (2000) 825-827.
16. E. Blasius, W. Klein, U. Schön, Separation of strontium from nuclear waste solutions by solvent extraction with crown ethers, J. Radioanal. Nucl. Chem. 89 (1985) 389-398.
17. E. P. Horwitz, M. L. Dietz, D. E. Fisher, Extraction of Strontium from Nitric Acid Solutions using Dicyclohexano-18-Crown-5 and its Derivatives, Solvent Extr. Ion. Exch. 8 (1990) 557-572.
18. E. P. Horwitz, M. L. Dietz, D. E. Fisher, SREX: A New Process for the Extraction and Recovery of Strontium from Acidic Nuclear Waste Streams, Solvent Extr. Ion. Exch. 9 (1991) 1-25.
19. A. Akseli, S. Kutun, Distribution Coefficients and Cation-Exchange Separation of Rare Earths in Sodium Tri-metaphosphate Media and Application to Monazite, Sep. Sci. Technol. 35 (2000) 561–571.
20. M. Kubota, Separation of rare earths by an ion-exchange method, J. Radioanal. Nucl. Chem. 23 (1974) 73-82.
21. P. Karol, Chromatographic separation of rare-earths by cation exchange, J. Radioanal. Nucl. Chem. 24 (1975) 17-19.
22. M. M. Zeligman, Ion Exchange Separation of Fission Product Rare Earths with α-Hydroxyisobutyric acid, Anal. Chem. 37 (1965) 524-525.

23. L. Maoliang, L. Yongxiang, F. Jingyi, Ion exchange separation of light rare earths by gradient elution, J. Radioanal. Nucl. Chem. Articles 123 (1988) 613-617.
24. L. Wish, S. C. Foti, Carrier-free separation of the individual rare earth radionuclides from fission product mixtures, J. Chromatogr. A 20 (1965) 585-593.
25. D. O. Campbell, Rapid rare earth separation by pressurized ion exchange chromatography, J. Inorg. Nucl. Chem. 35 (1973) 3911-3919.
26. R. S. Juang, Y. C. Wang, Use of complexing agents for effective ion-exchange separation of Co(II)/Ni(II) from aqueous solutions, Water Res., 37 (2003) 845-852.
27. G. S. Wamanacharya, Separation of Strontium and Barium by Cation-exchange using Polyaminepolycarboxylic acids as eluants, Isotopes Development Center, ORNL, U. S. Atomic Energy Commission (1966) ORNL TM-1342.
28. S. A. Farha, N. A. Badawy, A. A. El-Bayaa, S. E. Garamon, The Effect of Chelating Agent on the Separation of Some Metal Ions from Binary Mixture Solution by Cation-Exchange Resin, Nature and Science 8 (2010) 16-25.
29. A. Akseli, S. Kutun, Separation and determination of various elements by cation-exchange chromatography with sodium trimetaphosphate as the eluent, J. Chromatogr. A 847 (1999) 245–250.
30. S. Kutun, A. Akseli, New elution agent, sodium tri-metaphosphate, for the separation and determination of rare earths by anion-exchange chromatography J. Chromatogr. A, 847 (1999) 261–269.
31. S. Kutun, A. Akseli, Separation and determination of rare earth elements by Dowex 2-X8 resin using sodium trimetaphosphate as elution agent, J. Chromatogr. A, 874 (2000) 311–317.

CHAPTER 8

Chapter 8: Radiochemical Processing of ^{32}P Produced via $^{32}S(n,p)^{32}P$ in KAMINI reactor

This chapter deals with the radiochemical processing of irradiated sulphur bearing targets to obtain carrier-free ^{32}P produced via ^{32}S(n,p)^{32}P using the small fast flux component available in KAMINI reactor. The flow-sheet has been established for the production of ^{32}P from the sulphur powder as well as other sulphate targets such as magnesium sulphate and strontium sulphate. The radiochemical processing involved (i) struvite precipitation method for the irradiated magnesium sulphate target, (ii) co-precipitation method with ferric hydroxide for the irradiated strontium sulphate target and (iii) leaching of ^{32}P into acetic acid and (iv) distillation of ^{32}P from irradiated sulphur powder target. In all these processes, the final purification of ^{32}P source was accomplished invariably using a cation-exchange chromatographic technique.

8.1. Introduction

Alpha or beta emitting radionuclides are playing a vital role in nuclear medicine [1]. Among them, ^{32}P (a pure β^- emitter with β^-_{max} of 1.7 MeV, $t_{1/2}$ = 14.29 d) is being used as a pain palliative care for metastatic bone cancer in the form of either $Na_3{}^{32}PO_4$ or $H_3{}^{32}PO_4$ and also tested for the treatment of arthritis of knee joints using the micro-particles of ^{32}P-labeled hydroxyapatite ($Ca_{10}(^{32}PO_4)_6(OH)_2$) [2,3]. ^{32}P labelled sodium phosphate tends to concentrate in the bone, liver and spleen, and has a whole body biological half-life of 39.2 d. ^{32}P as a radio-tracer has several other applications also in the field of plant physiology and soil chemistry [4].

8.1.1. ^{32}P production in KAMINI reactor

^{32}P can be produced either using the nuclear reaction $^{31}P(n, \gamma)^{32}P$ by irradiating phosphorous in a thermal reactor or using $^{32}S(n, p)^{32}P$ by irradiating sulphur with fast neutrons [5]. While the former method has a high yield but gives a product of low specific activity, the latter renders ^{32}P of high specific activity because of the possible and easy chemical separation of ^{32}P from the target sulphur [6]. Thus, ^{32}P can be produced with high specific activity using the fast neutron flux available in FBTR from elemental sulphur or sulphur bearing targets. Elemental sulphur is the most preferable choice of target material due to the highest sulphur content that makes possible the production of ^{32}P with high yield. However, use of this target is limited, since it has a very low melting point (120 ^{o}C) as well as low boiling point (444 ^{o}C) and it will be converted into liquid or gaseous state during its irradiation in FBTR because of the sodium coolant temperature being as high as 550 ^{o}C. Hence it was necessary to investigate the feasibility of the production of ^{32}P using sulphur compounds along with the sulphur powder as a target material. Among the various sulphur bearing compounds, sulphates are favoured as target materials because of their high melting points and also being stable at high temperatures. Among them, again, magnesium sulphate and strontium sulphate are chosen specifically as target materials owing to their relative advantages such as stability at high temperature and interference from the other activated products in the target during its irradiation in FBTR [6,7]. While magnesium sulphate has the advantage of having all of its activation products very short-lived, strontium sulphate has a better thermal stability. However, the drawback of sulphates as target material is its relative low yield of ^{32}P in comparison with sulphur powder due to the lower mass fraction of sulphur in the target compound. ^{32}S (n, p) ^{32}P is a nuclear reaction with a threshold energy of 0.9 MeV and a cross section of 68.4 mb [5]. The isotopic composition of natural sulphur and their associated nuclear reactions are shown in Figure 8.1. The other possible phosphorous radioisotope produced here, that may affect the radionuclidic purity of ^{32}P is ^{33}P which is formed through ^{33}S(n,p)^{33}P. But the yield of ^{33}P is fortunately low i.e. <1 % of ^{32}P [6], owing to its low cross section of the nuclear reaction and low abundance of the target ^{33}S which are being 1.6 mb and 0.75%, respectively [6,8].

The present chapter describes the investigation of the feasibility of ^{32}P production via ^{32}S (n, p) ^{32}P reaction using sulphate targets i.e. magnesium sulphate [7] and strontium sulphate [6] as well as sulphur powder [5] and the development of a flow sheet for the radio chemical processing of these targets using the small fast flux available in the research reactor KAMINI.

8.2. Radiochemical processing of ^{32}P

8.2.1. Magnesium sulphate

The separation and purification procedure for ^{32}P by the radiochemical processing from the irradiated magnesium sulphate target is shown schematically in Figure 8.2. ^{32}P produced during the irradiation of $MgSO_4.7H_2O$ target in KAMINI reactor was converted into its phosphate by addition of hydrogen peroxide and precipitated it subsequently as Struvite ($Mg(NH_4)PO_4.6H_2O$) using ammonium hydroxide at pH 8-10 [7,9,10].

$$Mg^{2+} + NH_4^+ + PO_4^{3-} \xrightarrow{6H_2O} Mg(NH_4)PO_4.6H_2O \downarrow (Struvite) \qquad (8.1)$$

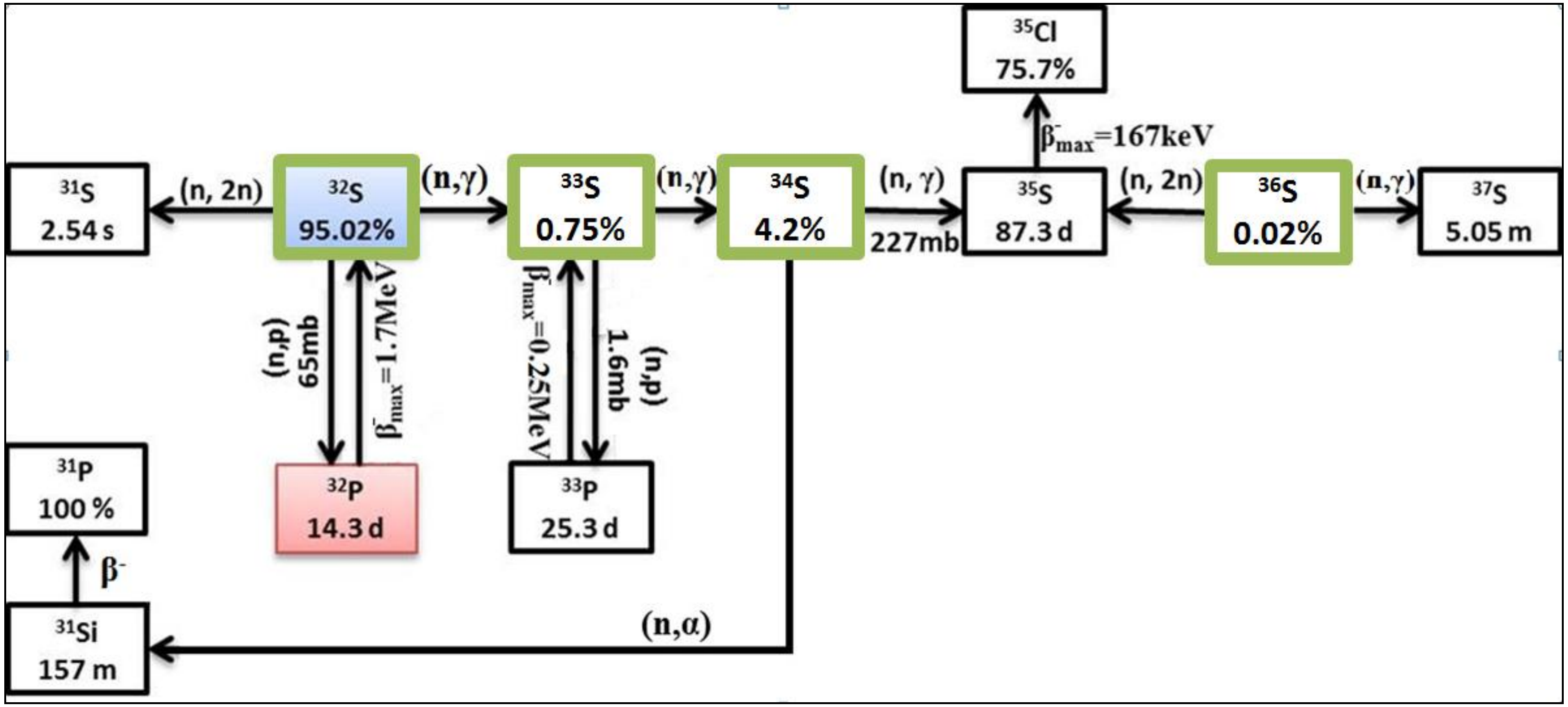

Figure 8.1. Production pattern of various P isotopes and other radionuclides from the sulphur target [5].

Radiometric assay of the supernatant using Cerenkov method showed that it contained about 20% of the ^{32}P and the remaining 80% of ^{32}P was precipitated as Struvite. The un-precipitated ^{32}P remained in the supernatant was also recovered subsequently by repeating the procedure.

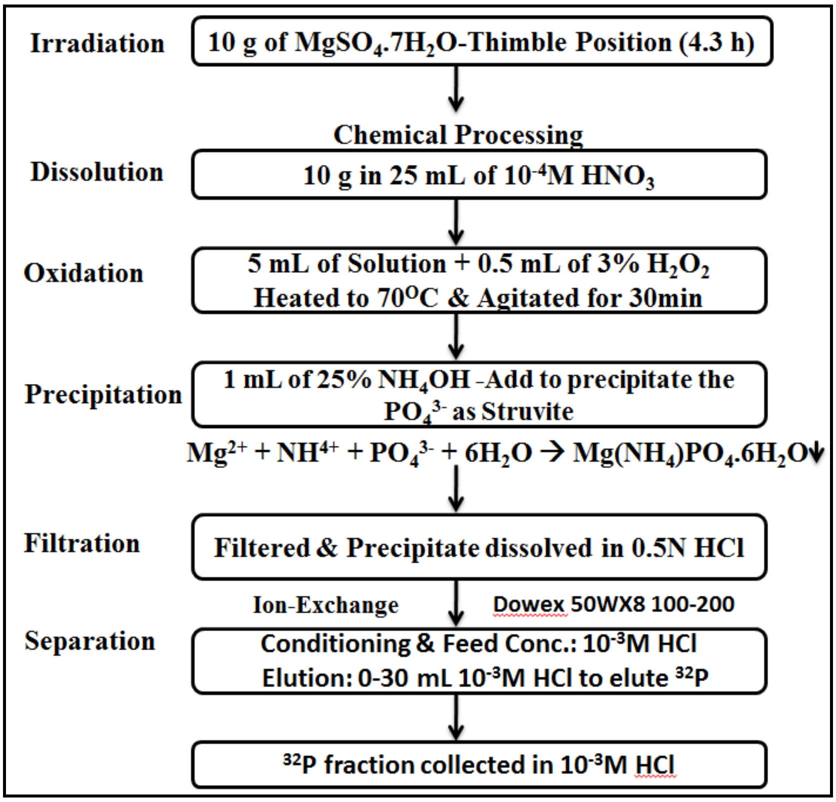

Figure 8.2. Flow-sheet for chemical processing of irradiated magnesium sulphate target.

The radiochemical purification of ^{32}P in its phosphate form from Mg in the dissolved struvite solution using cation-exchange chromatography with Dowex 50WX8 (100-200) resin resulted into its clear base line separation (Figure 8.3). The Mg was held in the resin during the elution with 0.001M HCl in which all the ^{32}P was eluted. Mg was subsequently eluted using 1:1 HCl. Over 99% of the initial total activity of 11.95 nCi of ^{32}P was eluted in the first 2 fractions of about 10 mL volume of 0.001M HCl itself. The separated ^{32}P from both struvite precipitate and the supernatant solution was quantified using Cerenkov detection method. About 83 nCi of ^{32}P was produced per 10 g of magnesium sulphate target irradiated in Thimble position of KAMINI reactor. The yield of ^{32}P from the radiochemical processing of the irradiated magnesium sulphate ($MgSO_4.7H_2O$) was found to be low as expected, owing to the fact that the sulphur content in the target is only ~13%.

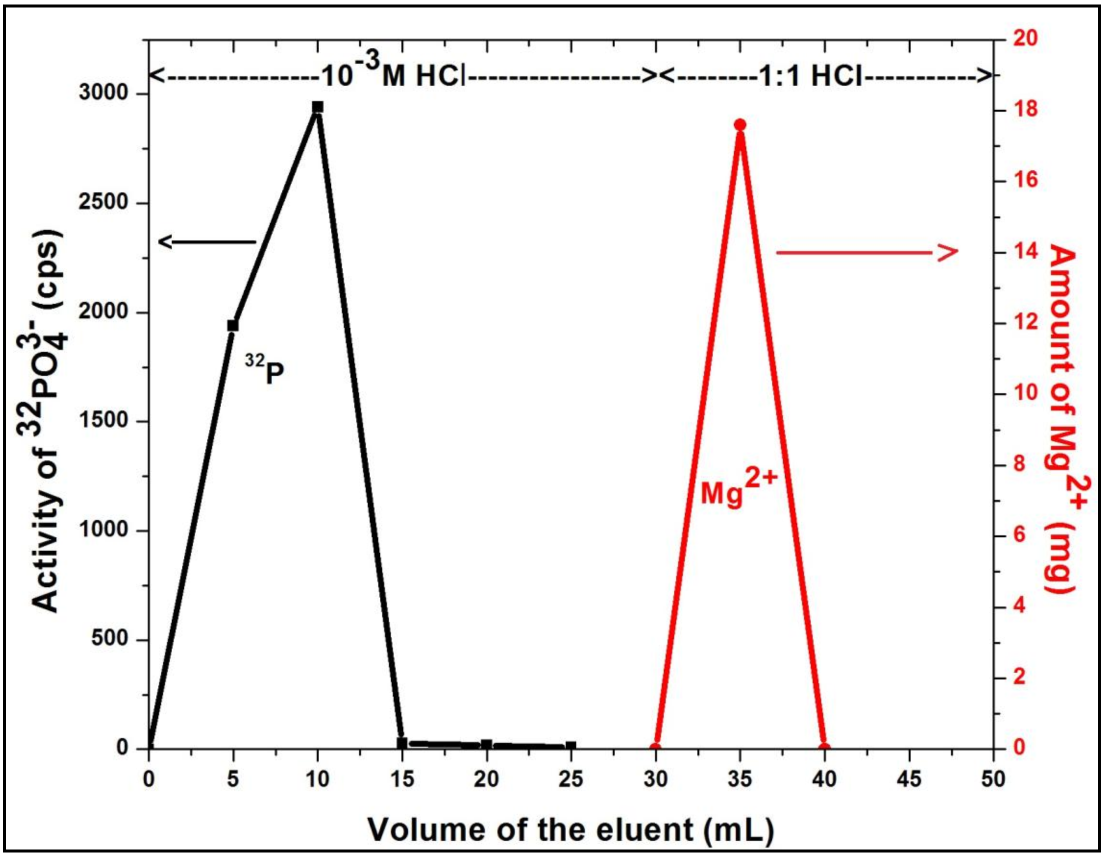

Figure 8.3. Elution profile of ^{32}P separated from Mg by cation-exchange chromatography (Amount of resin: 2 g of Dowex 50WX8 100-200 mesh; Column Dimensions: 8 mm dia, 25 cm Length and Bed height: 8 cm; Conditioning: 10^{-3}M HCl; Feed: Struvite solution in 10^{-3}M HCl; Flow rate: 0.3 mL/min; Assay: ^{32}P by Cerenkov and Mg by EDTA titration).

8.2.2. Strontium sulphate

The radiochemical purification of ^{32}P from the irradiated strontium sulphate target is shown schematically in Figure 8.4. The irradiation of $SrSO_4$ leads to the production of ^{32}P and $^{85+89}$Sr through the nuclear reactions $^{32}S(n,p)^{32}P$ and $^{84+88}Sr(n,\gamma)\,^{85+89}Sr$, respectively. The ^{32}P is separated from the bulk target matrix as well as from the other radioactive impurities by using the following radiochemical purification method.

The irradiated $SrSO_4$ target was converted into a precipitate of strontium carbonate by heating it with water and sodium carbonate [6]. The trace amount of ^{32}P (~pg) as phosphate was distributed in both precipitate as well as filtrate as shown in eqn 8.2.

$$\begin{array}{llcll} SrSO_4 + Na_2CO_3 & \xrightarrow{H_2O,\ \Delta,\ Stirring} SrCO_3\downarrow & + & Na_2SO_4 & (8.2) \\ \text{(Irradiated)} & \qquad\qquad\qquad + & & \quad + & \\ & \qquad\quad \{Sr_3(^{32}PO_4)_2\}_t\downarrow & & \{Na_3{}^{32}PO_4\}_t & \\ & \qquad\qquad\ \ \textbf{Residue} & & \ \textbf{Filtrate} & \end{array}$$

where ‘t’ indicates trace amounts. The residue and filtrate were treated to purify the ^{32}P as described below.

8.2.2.1. Residue

The filtered precipitate of strontium carbonate was dissolved in HCl medium. Ferric chloride and ammonium hydroxide were added to the solution to get the ferric hydroxide precipitate which also carried ^{32}P as ferric phosphate i.e.

$$FeCl_3 + 3NH_4OH \longrightarrow Fe(OH)_3\downarrow + 3NH_4Cl \qquad (8.3)$$

$$FeCl_3 + {}^{32}PO_4^{3-} \longrightarrow Fe^{32}PO_4\downarrow + 3Cl^- \qquad (8.4)$$

The above precipitate [$Fe(OH)_3$ and $FePO_4$] from eqn 8.3 and 8.4 was washed with Millipore water and taken into 1M HCl medium. This solution was evaporated to dryness under IR lamp and conditioned in 0.1M HCl medium.

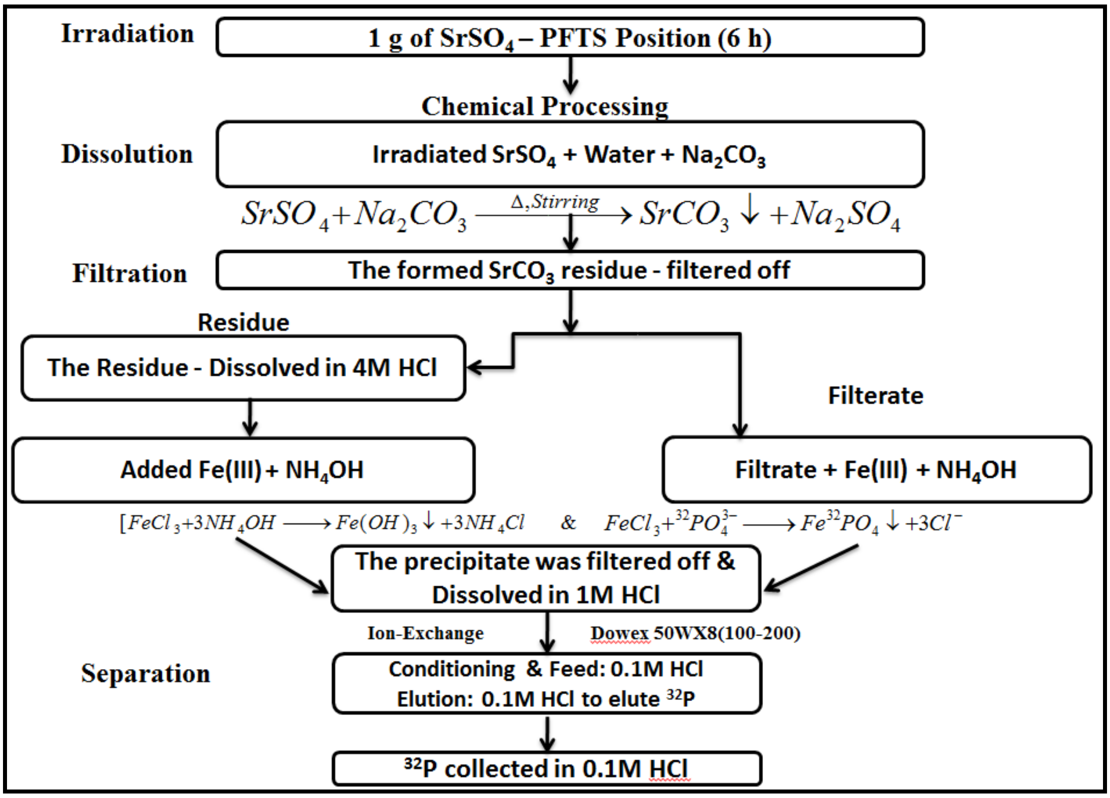

Figure 8.4. Flow sheet for the chemical processing of irradiated strontium sulphate target.

8.2.2.2. Filtrate

Similarly, the ^{32}P content that remained in the filtrate obtained from the eqn 8.2 in the above experiment was also co-precipitated as ferric phosphate by using ferric hydroxide and the same was brought into 0.1M HCl as described in the above residual part.

The conditioned solutions from the residue and filtrate were combined, and the same became the feed solution for the subsequent purification of ^{32}P from both Sr &

Fe by using cation exchange chromatographic technique. A clear base line separation of ^{32}P was achieved as shown in Figure 8.5. On the other hand, repeating the method separately for the residue alone and subsequently for the filtrate alone (eqn 8.2), it was found that the ^{32}P in the residue fraction was accounted for 75% of the total ^{32}P produced in the target; while the rest was present in the filtrate fraction. The amount of ^{32}P obtained together in both residue and filtrate by this method was 7.57μCi/g of target, accounting for 99.8% of the calculated yield of ^{32}P.

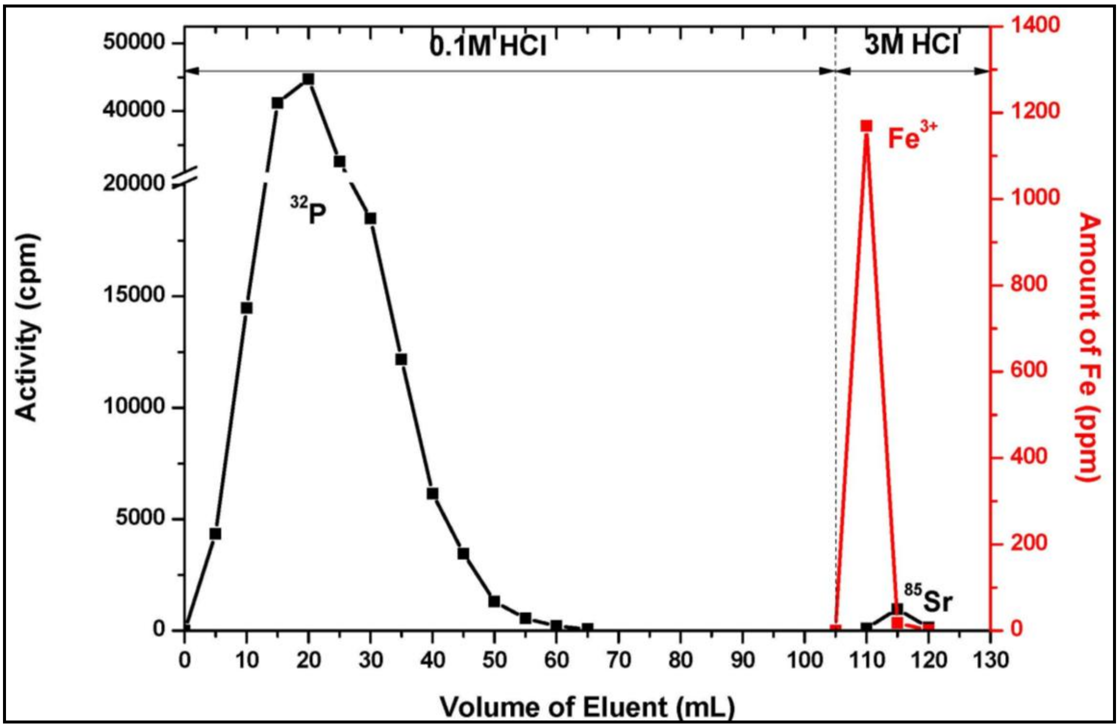

Figure 8.5. Elution profile of ^{32}P separated from Fe and Sr by cation-exchange chromatography (Amount of resin: 2 g Dowex 50WX8 100-200 mesh; Column Dimensions: 8 mm dia, 25 cm Length and Bed height: 8 cm; Conditioning: 0.1M HCl; Feed: Mixed solution of $SrCO_3$ and its filtrate; Flow rate: 0.3 mL/min; Assay: ^{32}P by Cerenkov; ^{85}Sr by Gamma spectrometry using HPGe and Fe(III) by ICP-OES).

The yield of ^{32}P was found to be higher in this case compared to the yield obtained by using magnesium sulphate as target. The major reason behind this is, that the strontium sulphate irradiation took place in PFTS position that is having 3-4 order higher neutron flux compared to the thimble position in which the other target magnesium sulphate was irradiated owing to the various logistic reasons. Otherwise, yields of ^{32}P are expected to be comparable in both the targets as the sulphur fractions in $MgSO_4.7H_2O$ and $SrSO_4$ are ~13% and ~17.4%, respectively which themselves were only almost comparable.

8.2.3. Sulphur powder - Leaching with glacial acetic acid

The flow-sheet for the separation of ^{32}P from the irradiated sulphur powder is shown schematically in Figure 8.6. ^{32}P produced in the target was leached into glacial acetic acid at the temperature of 120 ^{o}C [11]. The acid that was employed for the recovery of ^{32}P from the sulphur powder should only melt the sulphur but not dissolve it. Thus, the treatment of sulphur powder with alkyl mono carboxylic acids viz. glacial acetic acid, propionic acid or butyric acid was preferable as these acids do not dissolve sulphur powder and have the boiling point (acetic acid: 122 ^{o}C) slightly higher than the melting point of sulphur (119 ^{o}C).

The radiometric assay of leached ^{32}P in acetic acid medium by Cerenkov counting showed that the percentage of recovery was higher for the rapid cooling than the natural cooling method as shown in Figure 8.6 (Table 8.1). From the Figure 8.7, it is observed that the initial recovery of ^{32}P was found to be ~96% of the calculated amount produced in the target and the same was 99% when the natural cooling was replaced the rapid cooling.

The ^{32}P source was further purified using cation-exchange chromatography to collect the entire ^{32}P source in 20 mL of 0.1M HCl medium. The elution profiles are shown for natural and rapid cooled methods in Figure 8.8 and Figure 8.9, respectively. A clear base line separation of ^{32}P was achieved by ion-exchange chromatographic technique using Dowex 50WX8 (100-200) resin. The ^{32}P source was collected as phosphoric acid in dilute HCl medium. The amount of ^{32}P produced in this trial was found to be 0.43 µCi/g of sulphur powder irradiated in thimble position of KAMINI reactor. Thus, the feasibility of the production of ^{32}P from the sulphur target was established and its associated flow sheet for chemical processing was also standardized.

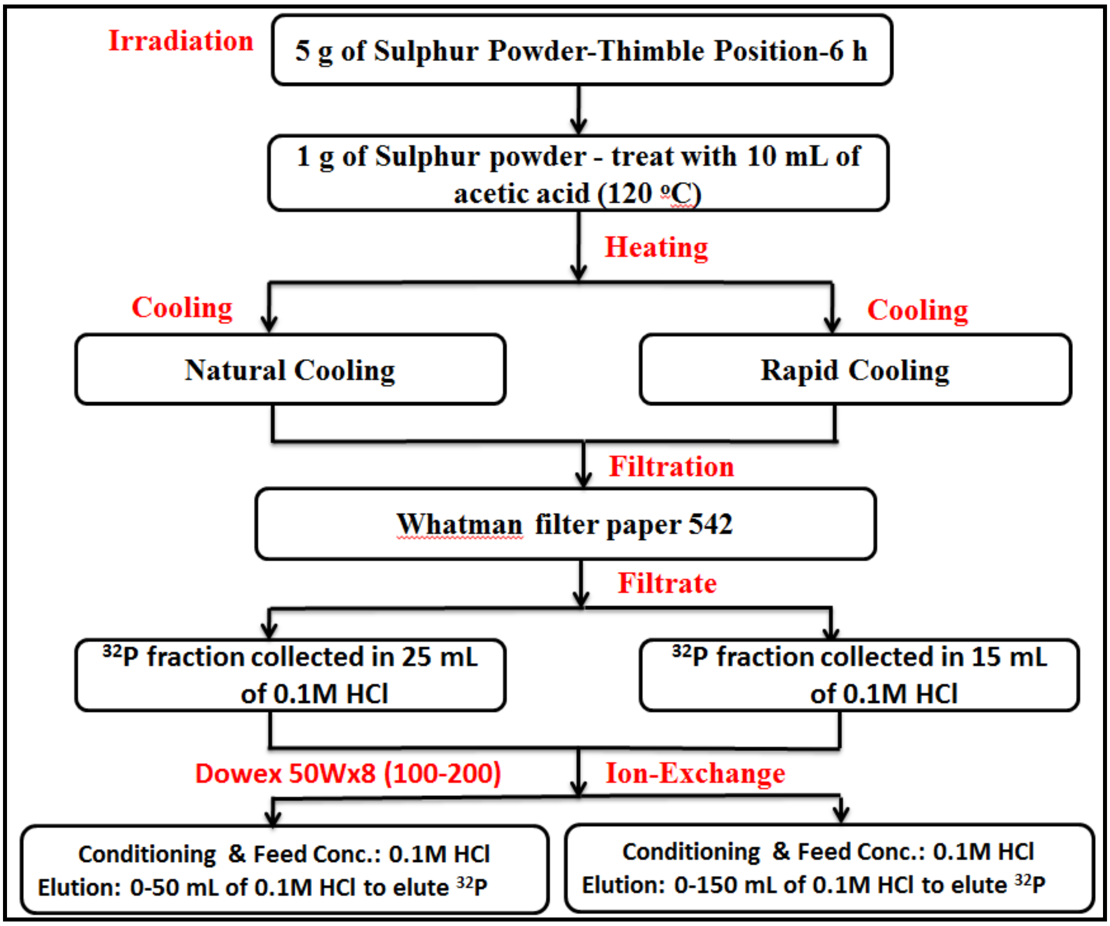

Figure 8.6. Flow-sheet for the separation of ^{32}P from Irradiated sulphur powder using Leaching method.

Table 8.1. Percentage of ^{32}P extraction with respect to two different cooling processes (as indicated in Figure 8.6)

Process No	**^{32}P extracted**	
	Natural Cooling	**Rapid Cooling**
1	42.8 %	74.1 %
2	35.9 %	17.5 %
3	11.8 %	5.1 %
4	5.9 %	2.3 %
Total Recovery	96.4 %	99 %

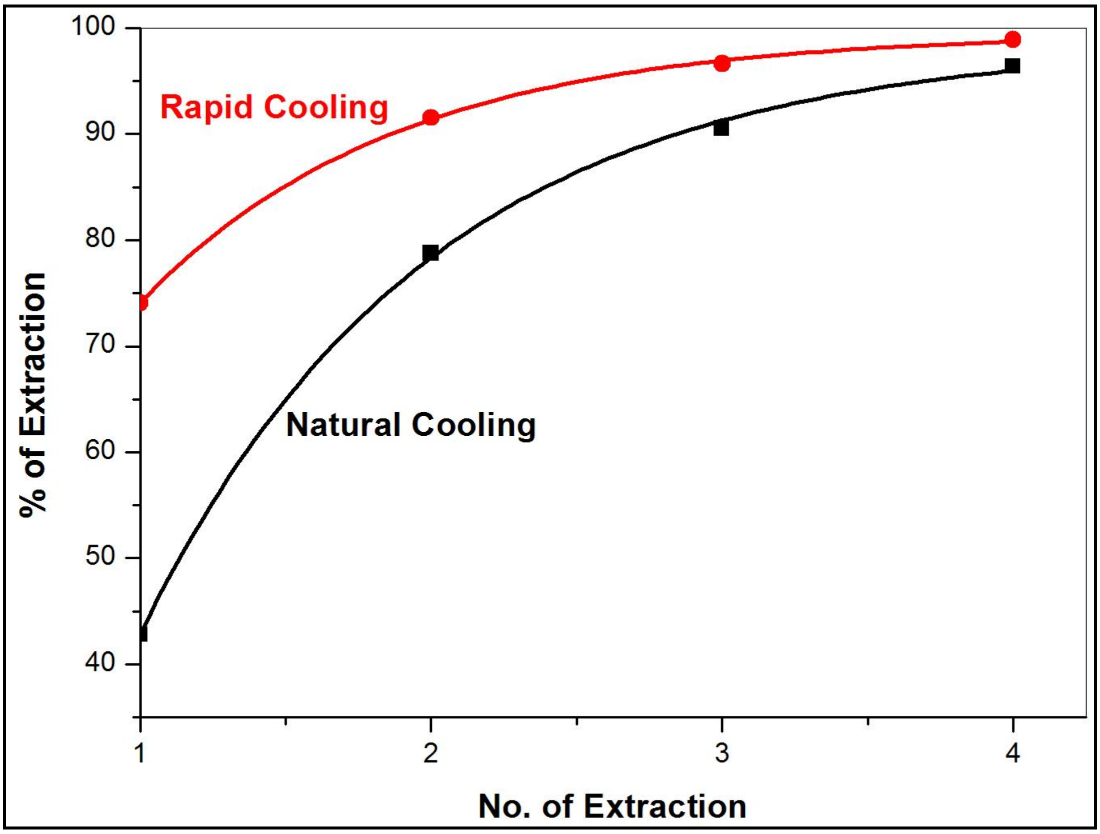

Figure 8.7. Extraction profile of ^{32}P with respect to number of extraction steps (Sample: 5 mL of ^{32}P leached into acetic acid medium; Assay: Cerenkov using HIDEX 300SL LSC system).

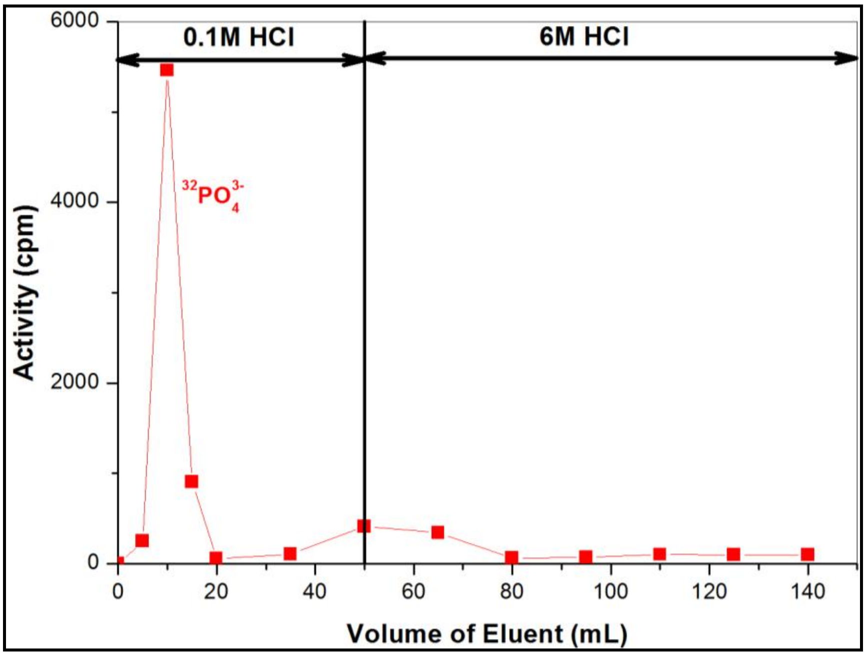

Figure 8.8. Elution Profile of ^{32}P obtained from natural cooling method (Resin: 5 g of Dowex 50WX8 (100-200); Column dimensions: 1 cm dia, 30 cm Length, Bed height: 9 cm; conditioning: 0.1M HCl; Feed: 5 mL of $^{32}PO_4^{3-}$ solution from natural cooling method; sample size & Assay: 5 mL fractions by Cerenkov method).

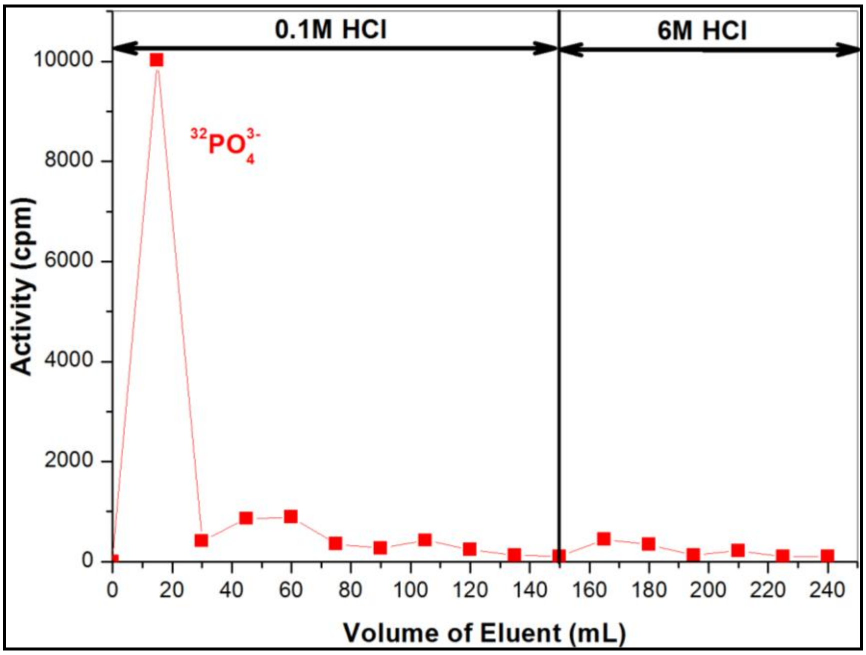

Figure 8.9. Elution Profile of ^{32}P obtained from rapid cooling method (Resin: 5 g of Dowex 50WX8 (100-200); Column dimensions: 1 cm dia, 30 cm Length, Bed height: 9 cm; conditioning: 0.1M HCl; Feed: 5 mL of $^{32}PO_4^{3-}$ solution from rapid cooling method; sample size & Assay: 15 mL fractions by Cerenkov method).

8.2.4. Sulphur powder – Distillation method

The flow sheet for the radiochemical processing of ^{32}P from the irradiated sulphur target using distillation method is shown in Figure 8.10. The flow-sheet describes the bulk separation of sulphur target using distillation method followed by the purification of ^{32}P from the cationic impurities using ion-exchange chromatographic technique by using Dowex 50WX8 (100-200) resin.

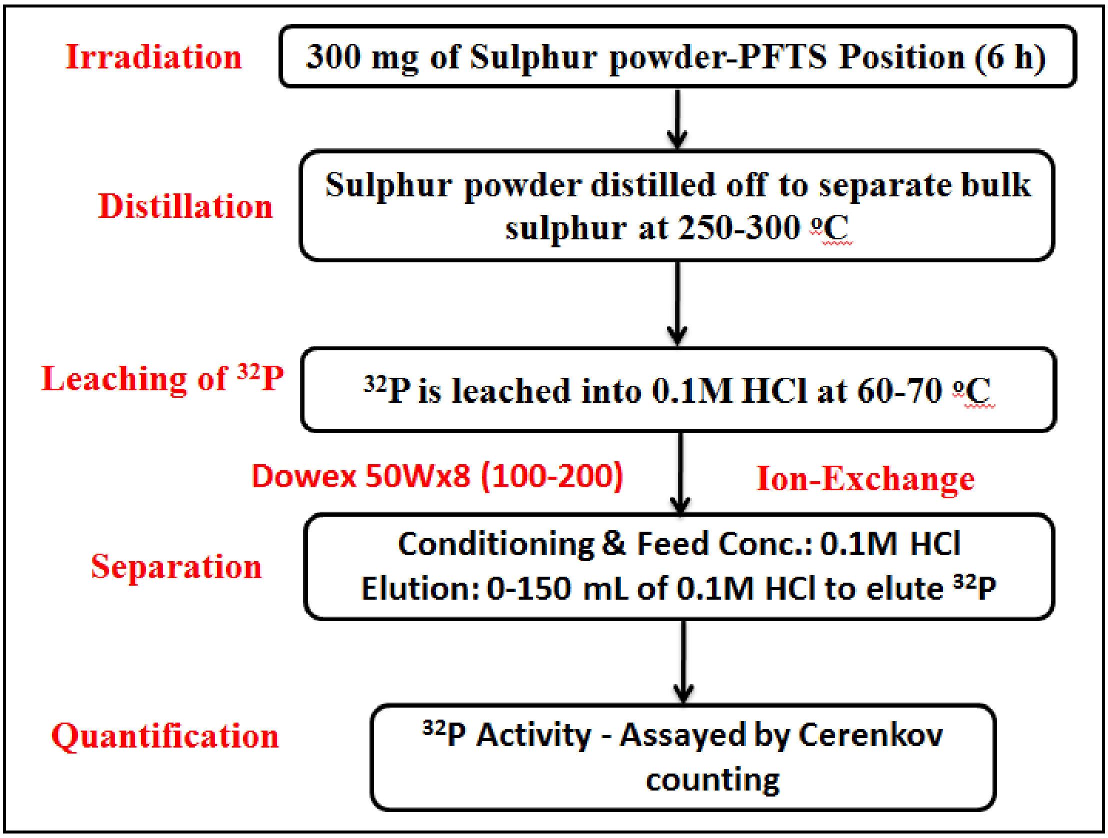

Figure 8.10. Flow-sheet for the separation of ^{32}P from Irradiated sulphur powder using distillation method.

The distillation process is the simplest and frequently used method among all the methods of purification of ^{32}P from bulk sulphur target [5]. The complete distillation of the irradiated sulphur took about 5 h by leaving ^{32}P in the residue of the distillation chamber. 10 mL of 0.1M HCl was used to leach out the ^{32}P activity from the chamber recovering about 99% of ^{32}P activity. Cation-exchange chromatography was used again to purify the ^{32}P from any other cationic impurities with the elution profile as shown in Figure 8.11. The figure shows that the entire ^{32}P was collected in just one fraction i.e. 15 mL of 0.1M HCl. Elution using 6M HCl was carried out subsequently to remove the other cationic impurities in the column. Pure ^{32}P source as phosphoric acid (H_3PO_4) was obtained in HCl medium. The activity of ^{32}P was quantified by using Cerenkov mode of counting and the yield was found to be ~39 μCi/g of sulphur powder irradiated in PFTS position of KAMINI reactor. A flow sheet was thus standardized for the purification of ^{32}P by the radiochemical processing of the irradiated sulphur powder using distillation method.

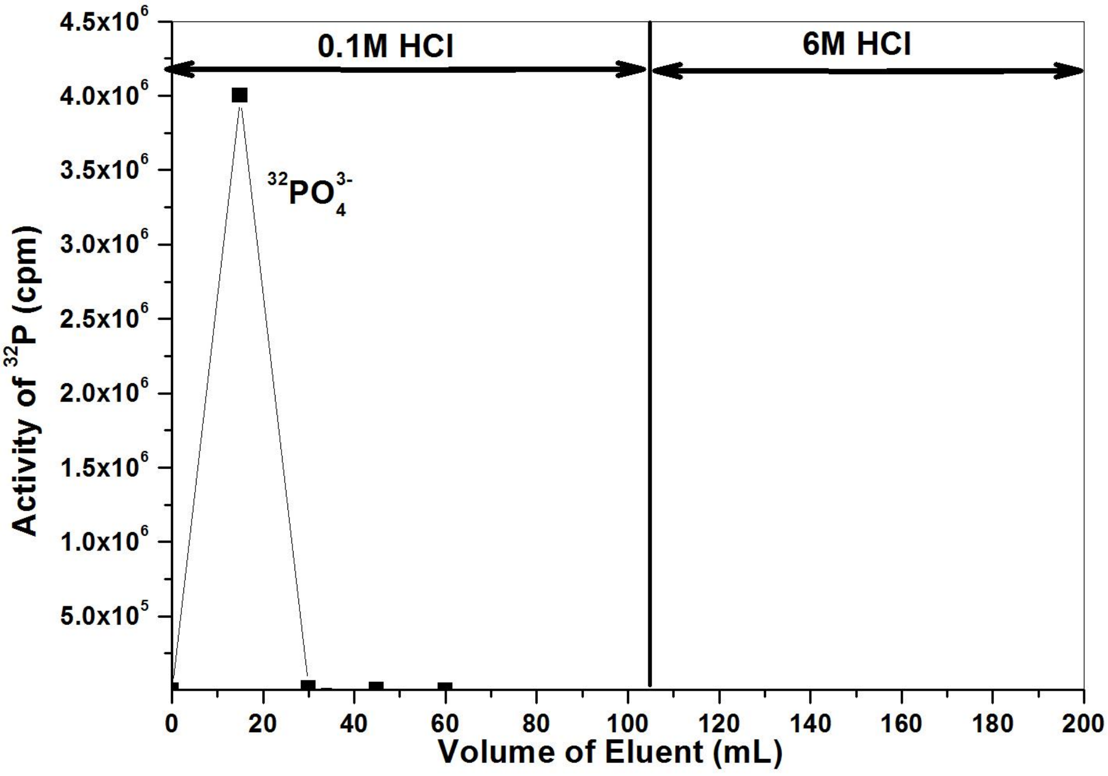

Figure 8.11. Elution Profile of ^{32}P obtained from distillation method (Resin: 5 g of Dowex 50WX8 (100-200); Column dimensions: 1 cm ID, 30 cm Length, Bed height: 9 cm; Conditioning: 0.1M HCl; Feed: 5 mL of $^{32}PO_4^{3-}$ solution; Sample size & Assay: 15 mL fractions by Cerenkov method).

The radiochemical purification of ^{32}P from the irradiated sulphur powder has been standardized using leaching as well as distillation methods. Between them, distillation process followed by ion-exchange chromatography is more preferable for the separation of ^{32}P, because of the method being simple and resulted into the complete recovery of ^{32}P. This method also requires application of minimum reagents and thus minimizing the possible chemical impurities in ^{32}P source. This method is adapted globally and thus is a well-accepted method for the purification of ^{32}P from the irradiated sulphur powder [5]. But the leaching method is however relatively complex with need for repetitive purification several times using external reagents.

8.3. Half-life determination

The purified fraction of ^{32}P obtained from all the targets as described above was analysed by gamma spectrometry using HPGe detector. The analysis confirmed the absence of any other gamma emitting impurities. The half-life estimation from the decay curve of ^{32}P obtained using Cerenkov counting also confirmed the absence of any other β^- emitting nuclide impurities. The ^{32}P fractions purified from each target were periodically assayed using Cerenkov counting for a period of about 6 weeks in order to profile its decay behaviour. The decay data of ^{32}P from the Cerenkov counting was plotted as ln(Activity) Vs time and the half-life was determined from the slope of the decay curve using the following equation

$$Slope = -decay \quad cons\tan t(\lambda) = -\frac{0.693}{t_{1/2}} \tag{8.5}$$

Half-life of ^{32}P obtained from the above plot is 14.4 d in the case of magnesium sulphate target (Figure 8.12) and 14 d and 14.4 d from the results of strontium sulphate and sulphur powder targets, respectively. The half-lives measured for each of the targets are in good agreement with its reported half-life of 14.29 d [5]. Thus, the half-life values obtained for the ^{32}P fraction from all the three targets were in good agreement with the reported value and hence indicating the purity of ^{32}P source obtained from all these methods.

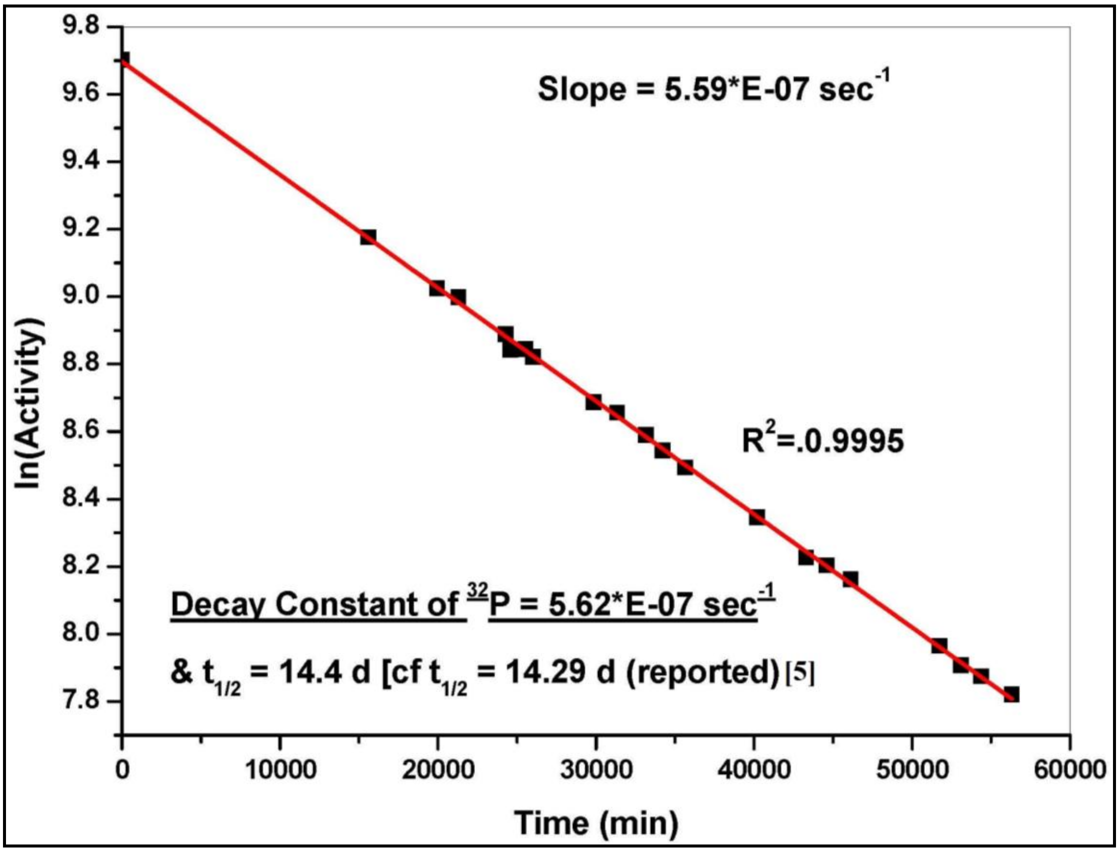

Figure 8.12. Decay profile of ^{32}P in the dissolver solution of the irradiated target magnesium sulphate (Sample: 5 mL of the purified ^{32}P fraction from irradiated magnesium sulphate target; Assay: Cerenkov Counting).

The irradiation details and corresponding results for each target are compared in Table 8.2. The table shows the comparison of all the three targets with respect to the various irradiation parameters, production yields etc. Among them, sulphur powder is preferred as the target because of its high yields. However, the irradiation of the sulphur powder as the target inside FBTR requires leak tight target holder pins because of the target getting converted into its liquid or vapour state owing to its low melting and boiling points of 120 ^{o}C and 444 ^{o}C, respectively; in comparison with the FBTR operational temperature being 550 ^{o}C. Distillation method followed by ion-exchange chromatography is preferred over the leaching method as the former is simple and well established.

Table 8.2. The irradiation data for sulphur containing targets in KAMINI reactor

Details	**$MgSO_4.7H_2O$**	**$SrSO_4$**	**Sulphur powder**	
			Leaching	**Distillation**
Amount irradiated	10 g	1 g	5 g	0.3 g
Amount of sulphur (% of S content)	1.298 g (12.98%)	0.174 g (17.42%)	4.75 g (94.99%)	0.285 g (94.99%)
Irradiation position	South thimble	PFTS	North thimble	PFTS
Irradiation duration	4 h 22 min	6 h	6 h	6 h
n-flux ($cm^{-2}.sec^{-1}$)	$3.6x10^{8}$	$6x10^{11}$	$1x10^{10}$	$6x10^{11}$
n-fluence (cm^{-2})	$5.66x10^{12}$	$1.3x10^{16}$	$2.16x10^{14}$	$1.3x10^{16}$
Activity produced (^{32}P/g of target)	*8.3 nCi/g*	*7.58 μCi/g*	*0.43 μCi/g*	*39.2 μCi/g*
Half-life determined (Cf. $T_{1/2}$: 14.29 d)	14.4 d	14.0 d	14.4 d	14.4 d

Between them, strontium sulphate is preferred over magnesium sulphate due to its relatively better thermal stability at high temperatures of FBTR operation as well as its relatively higher sulphur content. The major drawback of magnesium sulphate as the target is its hygroscopic behaviour, which demands an inert glove-box to handle and prepare these targets for the irradiation as the hygroscopic material is not permissible for the irradiation in the reactor. Thus, sulphur powder is the most preferable target provided the pressure increase due to its melting and boiling is addressed. Otherwise, strontium sulphate can be the choice of target material owing to its high thermal stability as indicated already.

8.4. Conclusion

The flow-sheet has been developed for the production of ^{32}P for the target materials such as magnesium sulphate, strontium sulphate and sulphur powder based on their test irradiation in KAMINI reactor at Kalpakkam.

The irradiated magnesium sulphate was processed by precipitating ^{32}P (~80%) as struvite followed by its purification using ion exchange chromatography. A clear base line separation of ^{32}P was achieved in the purification method by cation-exchange chromatography. The yield of ^{32}P was found to be 8.3 nCi/g of magnesium sulphate for the irradiation in south thimble position of KAMINI reactor. Similarly the irradiated strontium sulphate was processed by converting it into its corresponding carbonate followed by the co-precipitation of the phosphate ($^{32}PO_4^{3-}$) along with ferric hydroxide and further purification using ion exchange chromatography. The yield in this case was found to be 7.58 μCi/g of strontium sulphate for the irradiation this time in PFTS position of KAMINI reactor.

The radiochemical processing of irradiated sulphur powder was carried out by two methods i.e. (i) Leaching of ^{32}P as phosphate into the boiling glacial acetic acid followed by its purification using ion exchange chromatography and (ii) Distilling off the bulk sulphur target and the ^{32}P remains in the residue was taken into 0.1M HCl as phosphate followed by its purification by cation exchange chromatography. The yields for the irradiation of sulphur target were found to be 0.43 μCi/g and 39.2 μCi/g in thimble and PFTS positions, respectively in KAMINI reactor. In all the purifications, the final ^{32}P source was collected as phosphate form in dilute hydrochloric acid.

The gamma spectrometric analysis of the purified ^{32}P source from the above targets by HPGe detector indicated the absence of any gamma emitting impurity. The decay profile of the purified fraction of ^{32}P was obtained using Cerenkov counting technique and the half-life of ^{32}P was obtained from the decay curve. The half-life values of ^{32}P obtained from all the processed targets were found to be in good agreement with the reported value of 14.29 d indicating the purity of ^{32}P from any other high energy beta emitting impurities. Thus, the flow sheet developed for the production of ^{32}P from these targets as described above can be used in future endeavours in FBTR. However, the ^{32}P obtained from the irradiation in FBTR is expected to have higher yield owing to its corresponding higher flux of fast neutrons in comparison with the test irradiation carried out in KAMINI reactor. Among the various targets test reported here, sulphur powder is the most preferred one provided its problem of pressure increase during the irradiation in FBTR is addressed. Otherwise, strontium sulphate is the next preferable target material owing to its better thermal stability at the FBTR operational temperatures as described already.

8.5. References

1. H. L. Atkins, Overview of nuclides for bone pain palliation, Appl. Radiat. Isot. 49 (1998) 277-283.
2. A. Rajeswari, K. Vimalnath, H. Sarma, P. Shetty, S. K. Mohammed, J. Nuwad, S. Chakraborty, A. Dash, Hydroxyapatite (HA) microparticles labeled with ^{32}P - A promising option in the radiation synovectomy for inflamed joints, Appl. Radiat. Isot. 116 (2016) 85-91.
3. K. Vimalnath, P. Shetty, S. Chakraborty, T. Das, V. Chirayil, H. Sarma, K. Jagadeesan, P. Joshi, Practicality of production of ^{32}P by direct neutron activation for its utilization in bone pain palliation as $Na_3[^{32}P]PO_4$, Cancer Biother. Radiopharm. 28 (2013) 423-428.
4. D. Schlyer, P. Van den Winkel, T. Ruth, M. Vora, M. Pillai, M. Haji-Saeid, Cyclotron produced radionuclides: Principles and practice; Technical Reports Series-465 (2008).
5. M. Ananthakrishnan, Phosphorous-32 ($^{32}P_{15}$) in Manual for Reactor Produced Radioisotopes; IAEA-TECDOC-1340 (2003) 158.
6. A. Razbash, N. Nerozin, M. Panarin, Y. G. Sevast'yanov, O. Polyakov, D. Podsoblyaev, E. Y. Smetanin, T. Dubinkina, M. Nikulin, Winning ^{32}P in the BR-10 reactor, Soviet Atomic Energy 70 (1991) 333-335.
7. F. W. Lima, A. Abrao, L. Atalla, Production of Carrier-free Phosphorus-32 by Using Sulphates as Material for Irradiation, Sao Paulo, Brazil. Universidade. Instituto de Energia Atomica (1960).
8. K. F. M. Du, Phosphorus-33 ($^{33}P_{15}$) in manual for reactor produced radioisotopes; IAEA-TECDOC-1340, (2003) p 167.

9. M. Rahaman, N. Ellis, D. Mavinic, Effects of various process parameters on struvite precipitation kinetics and subsequent determination of rate constants, Water Science and Technology 57 (2008) 647-654.
10. V. Choudhary, S. Pataskar, M. Pandit, V. Gunjikar, Influence of precipitation conditions of magnesium hydroxide on its thermal decomposition in the preparation of active MgO, Thermochimica acta 194 (1992) 361-373.
11. B. A. Hadfield, Separation of phosphorus, Patent No. US2552032A, (1951).

CHAPTER 9

Chapter 9: Summary and Conclusions

This chapter summarizes the results of the following experiments i.e. (i) Characterization of neutron spectrum at PFTS of KAMINI reactor; (ii) Development of FFEF at FBTR; (iii) Determination of relative cumulative yields of fission products for actinides irradiated in KAMINI and FBTR; (iv) Radiochemical purification of ^{144}Ce-^{144}Pr; (v) Radiochemical purification of ^{90}Sr and ^{89}Sr from the irradiated (U,Pu)O_2 and yttria targets, respectively; (vi) Radiochemical purification of ^{32}P from irradiated sulphur bearing targets. The following sections describe the summary of the results of the above mentioned experiments.

9.1. Characterisation of n-spectrum at PFTS of KAMINI Reactor

Characterization of any neutron irradiation facility is a mandatory requirement to investigate the effect of irradiation on materials of interest accurately. The characterization of the neutron flux available at PFTS position in KAMINI reactor involves the evaluation of the reactor parameters such as 'thermal to epithermal neutron flux ratio' (f), epithermal neutron flux shape factor' (α) and the neutron spectrum. Assay of various samples by k_0 based NAA in KAMINI reactor needs the accurate values of these parameters and they were determined using Cd-ratio method and Cd-covered triple monitor methods using Zr, Au and Zn foils in this study. The values of f and α were estimated to be 27.8 ± 0.34 and $-4.5\text{x}10^{-02} \pm 1.8\text{x}10^{-03}$, respectively and they were re-estimated because of the modification of replacing one ^{233}U-Al subassembly with ^{239}Pu-Al fuel in KAMINI reactor. However, there were no significant changes observed in these values for the modified core. The negative sign of the α value indicated the presence of hard neutron spectrum at PFTS position.

The foil irradiation method was employed for the n-spectrum characterization of PFTS position, that covered the neutron energy spectrum up to 11.7 MeV. The guess n-spectrum for 175 energy group structure was generated using the theoretical model of the reactor with the transport Monte Carlo Code. The n-spectrum unfolding was accomplished using the least square minimization approach. The integral flux was found to be about 6.01×10^{11} $n.cm^{-2}s^{-1}$. The neutron energy spectrum is also useful for testing and validating the reactor physics codes and different nuclear data libraries.

9.2. Design and Installation of Fast Flux Experimental Facility (FFEF) at FBTR and neutron flux measurement at the location

Titanium was chosen as the material of sample holder system to establish the FFEF at FBTR owing to its easy availability and better stability towards neutron activation as well as thermal effects. Radiation dose computations were carried out for both the matrix material (Ti) as well as for its associated impurities. The elemental impurities present in the Ti rod were established using NAA which were found to be Na, K, Cl, Sc, Fe, Mn, As, W, Co, Cr, Sb, La, Ta and Sm. The radiation dose due to the activation of Ti and the other impurities in it was evaluated for 10 d irradiation at 400 kW power of FBTR and the same was found to be 125 mR/h and 0.8 mR/h at 2 cm and 1 m distance, respectively. The above described computations established that titanium was the most suitable choice of construction material for the development of the facility FFEF. Hence, a Ti extension rod of length 3252.5 mm and a diameter of 14.0 ± 0.1 mm was attached to the bottom end of the shield plug and a Ti sample holder of length 50 mm and diameter 12 mm was in turn attached to the bottom of this rod by screw joint. The gold equivalent neutron flux was measured at this location of

FBTR by using foil irradiation method which was found to be 2.54x10^9 $cm^{-2}.s^{-1}$ at 25 kW.

9.3. Measurement of relative fission yields for actinide targets irradiated in KAMINI and FBTR

The catcher foil technique was employed for the determination of relative fission yields of uranium irradiated in KAMINI reactor. The radiometric analysis of the irradiated catcher foil (Al) was carried out using HPGe detector and the peak areas were used to measure the activities of various fission products. The cumulative yields of various fission products were determined with respect to the reference fission product (^{135}I). The results were compared and found to be in good agreement in most of the cases with that of the reported values by Crouch and ENDF-349. However, the minor deviations observed in some cases are to be attributed to the extent or degree of recoiling of the fission products towards the catcher foil.

The PuO_2-ZrO_2 targets were irradiated in FBTR and the activities of the fission products formed thereon were measured using high resolution gamma spectrometry. The measured activities and MCNP calculated reaction rates were utilized to establish the yields of various fission products. The yields of the fission products from the target irradiated at third ring were found to be higher compared to that of the targets irradiated at core center. This observation may be attributed to the higher thermal neutron flux and hence higher cross sections at third ring in comparison with the core center.

9.4. Radiochemical purification of ^{144}Ce-^{144}Pr

The distribution ratios were determined for various fission products from $(U,Pu)O_2$ dissolver solution with Dowex 50WX8 (100-200) resin at different acidities and found that cerium showed a relatively higher distribution ratio than the other radionuclides at all concentrations of nitric acid. ^{144}Ce-^{144}Pr pair was purified from fission products as well as from the activation products by ion-exchange chromatography. The separation of pure parent (^{144}Ce) from the ^{144}Ce-^{144}Pr pair was also achieved by solvent extraction method using 0.7M HDEHP/n-heptane as the extractant. The separated pure ^{144}Ce fraction was assayed by well type NaI(Tl) solid scintillation detector and the total activity due to both parent ^{144}Ce and its in-grown daughter ^{144}Pr was profiled to establish the phenomenon of secular equilibrium. A plot was constructed on a semi-log graph by profiling the variation of the total activity as a function of time and the same was resolved into the individual components i.e. parent decay, daughter growth in parent and daughter decay. Extraction chromatographic studies were also carried out to purify ^{144}Pr from its parent-in-equilibrium ^{144}Ce by using HDEHP/XAD7 resin with 1M $KBrO_3$/9M HNO_3 as the eluent. The half-life for the daughter nuclide ^{144}Pr was obtained by both directly from the decay curve of the purified daughter ^{144}Pr as well as indirectly from the resolution of the equilibrium curve which was found to be 17.32 ± 0.64 min and 17.14 ± 0.17 min, respectively. They were found to be in good agreement with the reported half-life of 17.29 min.

9.5. Radiochemical purification of Sr from fission products as well as from irradiated yttria

Radiochemical separation studies of ^{90}Sr from the FBTR irradiated $(U,Pu)O_2$ fuel dissolver solution was carried out using ion exchange chromatography with SMP as an eluting agent. The method was applied to the separation of ^{89}Sr from the FBTR irradiated yttria dissolver solution as well as. The study on the distribution ratio of the various metal ions present in the irradiated yttria dissolver solution in Dowex resin suggested a relatively high D_M for Sr at all the concentrations of SMP studied. A base line separation of ^{89}Sr from all the impurities was established using simulated sample added with corresponding radioactive tracers. The same procedure was extended to the actual irradiated yttria dissolver solution also. It was also established that the pure Sr fraction was obtained in this case without the residual cross contamination from Na and anionic moiety of SMP. ^{89}Sr yields were established to be ~2 mCi/g of yttria by using beta counting techniques such as LSC and Cerenkov counting. Thus the eluent, SMP was established to be a desirable eluting agent for a faster purification of ^{89}Sr source during the radiochemical processing of the irradiated yttria target. The purification of Sr source using SMP, as an eluent in the ion exchange chromatography, offered the advantages of faster separation with generation of lesser radioactive wastes in comparison with the method where nitric acid was used as an eluent instead.

9.6. Radiochemical purification of ^{32}P

The flow sheet for the purification of ^{32}P from the KAMINI irradiated targets such as magnesium sulphate, strontium sulphate and sulphur powder was established. The flow sheet can however be extended to the targets irradiated in FBTR as well. Purification of ^{32}P was carried out from the irradiated magnesium sulphate target by precipitating it as struvite followed by its purification using ion exchange chromatography. The yield of ^{32}P in this case was found to be 8.3 nCi/g of magnesium sulphate when irradiated in south thimble position of KAMINI reactor. Similarly, the irradiated strontium sulphate was processed by the co-precipitation of phosphate ($^{32}PO_4^{3-}$) along with ferric hydroxide which was subsequently purified using ion exchange chromatography. The yield in this case was found to be 7.58 μCi/g of strontium sulphate when irradiated in PFTS position of KAMINI reactor. The radiochemical processing of irradiated sulphur powder was carried out by two methods, i.e. (i) Leaching of ^{32}P as phosphate into the boiling glacial acetic acid followed by its purification using ion exchange chromatography and (ii) Distilling off the bulk sulphur and purifying the residual ^{32}P in HCl medium by using ion-exchange chromatography. The yields from the sulphur target were found to be 0.43 μCi/g and 39.2 μCi/g in thimble and PFTS positions of KAMINI reactor using leaching and distillation methods, respectively.

The gamma spectrometric analysis of the purified ^{32}P source indicated the absence of any gamma emitting radionuclidic impurities. The decay curve of the purified ^{32}P fraction was profiled using Cerenkov counting technique. The half-life of ^{32}P was determined from the decay curve obtained above and was found to be in good agreement with the reported value, ascertaining its purity from any other high β^-_{max} emitting radionuclides. Thus the flow sheet for the processing of irradiated targets to obtain ^{32}P can be extended, to process the targets irradiated in FBTR as well to obtain ^{32}P source with a higher yield. Among the various targets used for the production of ^{32}P, sulphur powder was found to be most suitable, even though the use of the same demands a challenging leak tight container arrangement for its irradiation as it has low boiling point of 444 ^{o}C in comparison with the operational temperature of FBTR being 550 ^{o}C. Otherwise, the strontium sulphate was preferable as target due to its high thermal stability at high temperatures.

CHAPTER 10

Chapter 10: Scope of Future Studies

This chapter describes the scope for future work which will be the continuing efforts in the direction reported in this thesis.

10.1. Neutron activation analysis

KAMINI reactor is a research reactor and NAA is one of its main applications. The reactor parameters i.e. f and α corresponding to the irradiation position, PFTS of KAMINI reactor were evaluated. The accurate determination of these parameters contributes to the accuracy of the analysis by Internal Mono-standard NAA (IM-NAA) in the reactor. Further, in-situ detection efficiency using HPGe detector can also be evaluated for different matrices of interest. KAMINI reactor is at present being equipped with two additional irradiation facilities called Dry Tube-1 and Dry Tube-2. Thus the determination of the reactor parameters f and α for these new irradiation facilities can also be evaluated to facilitate the accurate analysis of the samples using these irradiation facilities similar to that of PFTS. Large Sample NAA (LS-NAA) is an important mode of analysis by NAA where the sample size (30 cm x 30 cm x 30 cm) can be as large as HEPA filters used in a glove box. While the conventional irradiation facility can generally handle only small size sample i.e. typically in 100's of mg levels, the requirement of analysis such as actinides in a HEPA filter of a radioactive glove box by NAA needs a large space for irradiation. Hence efforts can be made to develop a LS-NAA in these facilities where an element of impurity or element of contamination needs to be evaluated non-destructively in a large sample matrix.

10.2. Studies involving FFEF in FBTR

The FFEF has been established in FBTR. Future experiments using the fast neutron flux available in the reactor can be carried out for various studies involving Fast NAA, establishing fast fission systematics of actinides i.e. studies on mass and charge distribution of actinides and minor actinide transmutation towards a better nuclear waste management protocol. This facility is also useful to establish the feasibility studies of various radioisotope production as well as some fundamental studies on various threshold nuclear reactions of interest. The facility can also be utilized to study the effect of fast neutron irradiation on various materials.

10.3. Development of flow sheets for Radioisotope production

The work involving different radiochemical separations reported in this thesis has also facilitated in establishing the flow sheets for the production of various radioisotopes of societal applications. This is also one of the important components of the Department of Atomic Energy (DAE) for its obligation to the societal applications, apart from its mandatory objective of the power production technology. The flow sheets established so far are helpful for the production of ^{89}Sr and ^{32}P. Similarly, the radiochemical separations developed in this study can also be extended for the future endeavours on the production of various other radioisotopes of interest. There will be continuous efforts to make these radiochemical purification procedures reported hereby for various applications to be more adaptable for automation with the aim of reducing the man-rem problems as well as the minimization of the generation of radioactive wastes. Similarly these radiochemical separation methods can also be extended for the separation of many useful radioisotopes from the fission products of actinides.

Glossary

CRM	Certified Reference Material
D_M	Distribution Ratio of Metal ions
DT	Dead Time
DVB	Divinylbenzene
EDTA	Bis(ethylenediaminetetraacetic acid)
EDX	Energy Dispersive X-ray
eV	Electron volt
f	Sub-cadmium to epithermal neutron flux ratio
FBTR	Fast Breeder Test Reactor
F_{Cd}	Cadmium Transmission Factor for epithermal neutrons
FFEF	Fast Flux Experimental Facility
G_e	Correction Factor of epi-thermal neutron self-shielding
G_{th}	Correction Factor of thermal neutron self-shielding
HDEHP	Di-(2-ethylhexyl) phosphoric acid
HPGe	High Purity Germanium
HV	High Voltage
$I_0(\alpha)$	Infinite Dilute Resonance Integral corrected for α
ICP-OES	Inductively Coupled Plasma Optical Emission Spectroscopy
k_0	Composite Nuclear Constant
KAMINI	KAlpakkam MINI
kW	Kilo Watt
LLD	Lower Level Discriminator
Ln	Lanthanide

LSC	Liquid Scintillation Counter
LT	Live Time
MCNP	Monte Carlo Neutral Particle
MW	Mega Watt
NAA	Neutron Activation Analysis
NaI(Tl)	Sodium Iodide (Thalium) analyzer
PCF	Pneumatic Carrier Facility
PFTS	Pneumatic Fast Transfer System
PMT	Photo Multiplier Tube
$Q_0(\alpha)$	Ratio of $I_0(\alpha)$ to σ_0
R_{Cd}	Cadmium Ratio
SEM	Scanning Electron Microscope
SMP	tri-Sodium tri-Meta Phosphate
TBP	Tri-n-butyl phosphate
T_d	Decay Time
TDCR	Triple to Double Coincidence Ration
T_{irr}	Irradiation Time
ULD	Upper Level Discriminator
XRD	X-ray diffraction
α	Epithermal neutron flux shape factor
ε_p	Full energy Peak detection efficiency
σ_0	The (n, γ) cross-section at 2200 ms^{-1}